

CYCLIC DEFORMATION OF LOW-CARBON IRON

CYCLIC DEFORMATION OF LOW-CARBON IRON

By

NABIL ABDELFAHIM IBRAHIM (SAADEL-DIN)

A Thesis

Submitted to the School of Graduate Studies
in Partial Fulfilment of the Requirements
for the Degree
Doctor of Philosophy

McMaster University

November 1974

©

NABIL ABDELFAHIM IBRAHIM (SAADEL-DIN)

1977

DOCTOR OF PHILOSOPHY (1974)
(Metallurgy and Materials Science)

McMASTER UNIVERSITY
Hamilton, Ontario

TITLE: Cyclic Deformation of Low-Carbon Iron

AUTHOR: Nabil A. Ibrahim (Saadel-Din), B.Eng. (University of
Cairo, Egypt)

SUPERVISOR: Professor J. D. Embury

NUMBER OF PAGES: (x), 276

SCOPE AND CONTENTS:

The mechanical behaviour and the microstructural changes preceeding fatigue fracture have been investigated in ferrous systems subjected to controlled cyclic straining. Attention has been focussed on three basic aspects of the fatigue process:

(1) The Bauschinger Effect and the Polarisation of Plastic Flow in Single- and Two-Phase Iron-Based Alloys: the investigation involved the study of the influence of dislocation distribution on the magnitude of the Bauschinger effect, and the study of the Bauschinger effect in two phase materials as a function of both forward strain and volume fraction

(ii)

of particles. The results are interpreted in terms of some of the currently available theories for the deformation in plastically inhomogeneous materials.

(2) Fatigue Softening in Single-Phase Low-Carbon Iron: the investigation involved the study of the microstructural changes occurring in prestrained specimens during cyclic softening, and the influence of initial dislocation arrangement on the rate and extent of fatigue softening. Simple models were developed to rationalize the kinetics of fatigue softening.

(3) Instability of Plastic Flow in Quenched-Aged Armco Iron: the investigation involved the study of the influence of various particle dispersions on the stability of plastic flow in fatigue, and the detailed microstructural features developing in fatigue which lead to the localization of plastic flow and onset of fatigue cracks. The problem of instability has been rationalized, macroscopically, in terms of the mechanical equation of state, and microscopically, in terms of the detailed structure of the localized regions.

Structural changes were monitored by Transmission Electron Microscopy and ancillary techniques in order to provide a detailed characterisation of the fatigue state.

ACKNOWLEDGEMENTS

The author is sincerely grateful to Dr. J. D. Embury for his patient advice and guidance throughout the course of the present work.

The author wishes to thank Dr. L. M. Brown (Cambridge University) for valuable discussions and advice.

To Mr. C. M. Sargent and other members of the research group, the author would like to offer his thanks for useful discussions.

The author would further wish to acknowledge the assistance of Mr. F. Smith with the electron optical facilities, and to thank Ms. E. Long for rapidly and accurately typing the manuscript, and Mr. D. Hodgson for drafting the diagrams.

The author appreciates the work done on the micrographs by Mr. T. Bryner.

Financial support from the American Iron and Steel Institute is gratefully acknowledged.

TABLE OF CONTENTS

CHAPTER	PAGE
I INTRODUCTION	1
(a) The Bauschinger effect and the polarisation of plastic flow	2
(b) Fatigue softening in single-phase low-carbon iron	3
(c) Instability of plastic flow in fatigue	4
II THE BAUSCHINGER EFFECT AND THE POLARISATION OF PLASTIC FLOW	6
SECTION (1)	7
(1.1) Objectives	7
SECTION (2)	9
(2.1) Physical and Theoretical Aspects of the B.E.	9
(2.1.1) Back Stresses in Single-Phase Metals	9
(2.1.2) Back Stresses in Two-Phase Alloys	10
(2.1.3) Bauschinger Effect and Work-Hardening	11
(2.2) Factors Influencing the B.E.	19
(2.3) Methods of Measuring the B.E.	24
SECTION (3) - EXPERIMENTAL DETAILS	28
(3.1) Materials and Testing Procedure	28
(3.2) Measurements and Variables Investigations	32

TABLE OF CONTENTS & continued

CHAPTER		PAGE
	(3.2.1) The Bauschinger effect parameter	32
	(3.2.2) Method of measuring σ_R and σ_0	34
	SECTION (4) - EXPERIMENTAL RESULTS	37
	(4.1) B.E. in Single-Phase Armco Iron and Niobium	37
	(4.2) Effect of Second-Phase Particles on the B.E. in Steels	41
	SECTION (5) - DISCUSSION OF RESULTS	46
	(5.1) Summary of Experimental Results	46
	(5.2) The BEP in Single-Phase bcc Materials	47
	(5.3) The BEP in Steels Containing Strong Particles	52
	(5.4) Summary and Conclusions	58
III	FATIGUE SOFTENING IN LOW-CARBON IRON	60
	SECTION (1) - OBJECTIVES	61
	SECTION (2) - LITERATURE REVIEW	65
	(2.1) Effect of Deformation Temperature on Dislocation Distribution	65
	(2.2) Effect of Dynamic Strain Ageing	69
	(2.3) Cyclic Strain Softening	71
	(2.4) Cyclic Saturation Behaviour	75
	(2.5) Factor Influencing the Cyclic Saturation State	79
	SECTION (3) - EXPERIMENTAL RESULTS	83
	(3.1) Introduction	83

TABLE OF CONTENTS - continued

CHAPTER	PAGE
(3.2) Material Preparation	84
(3.3) Mechanical Testing	88
(3.3.1) Tensile testing	88
(3.3.2) Fatigue testing	90
(3.4) Transmission Electron Microscopy	94
(3.5) Laue Back-Reflection X-ray Photographs	96
(3.6) Thermal Recovery	96
SECTION (4) - EXPERIMENTAL RESULTS	97
(4.1) Introduction	97
(4.2) Overall Response	98
(4.3) Detailed Microstructural Changes	100
(4.3.1) Microstructural changes during softening	100
(4.3.2) The substructure at saturation	106
(4.4) Effect of Initial Dislocation Arrangements on the Kinetics of Cyclic Softening	114
(4.4.1) Initial dislocation arrangements	114
(4.4.2) Kinetics of cyclic softening	118
(4.5) Thermal Recovery of Fatigued Structure	126
(4.5.1) Thermal recovery of prestrained specimens	131
(4.5.2) Thermal recovery of fatigued specimens	133
SECTION (5) - DISCUSSION OF RESULTS	142
(5.1) Summary of Experimental Results	142

TABLE OF CONTENTS - continued

CHAPTER		PAGE
	(5.2) General Characteristics of the Fatigue Softening Process in Decarburised Iron	144
	(5.3) Kinetics of Fatigue Softening	147
	(5.4) Summary and Conclusions	156
IV	STABILITY OF PLASTIC FLOW IN FATIGUE	159
	SECTION (1) - OBJECTIVES	160
	SECTION (2) - EXPERIMENTAL DETAILS	164
	SECTION (3) - EXPERIMENTAL RESULTS	167
	(3.1) Initial Microstructure	167
	(3.2) Overall Mechanical Response	169
	(3.3) Microstructures After Fatigue	181
	(3.4) Comparison of Fatigue Data and Tensile Properties	193
	SECTION (4) - DISCUSSION OF RESULTS	198
	(4.1) Summary of Experimental Results	198
	(4.2) Nature of Localized Flow in Fatigue	200
	(4.3) The Mechanical Equation of State	204
	(4.3.1) Adiabatic heating effect	207
	(4.3.2) Development of instability and localization of strain rate	209
	(4.4) Microstructural Aspects of Instability	217
	(4.4.1) Mechanistic views on particle dissolution	218
	(4.4.2) Influence of second-phase particles on cyclic softening	222

TABLE OF CONTENTS - continued

CHAPTER	PAGE
(4.4.3) Particle coarsening under concurrent deformation	226
(4.5) Influence of Particle-Dissolution on Macroscopic Behaviour	230
(4.6) Summary	234
V CONCLUSIONS	237
APPENDIX	
A CYCLIC BEHAVIOUR IN QUENCH-TEMPERED VANADIUM STEEL	246
B SATURATION AND SUBSEQUENT HARDENING IN POLYCRYSTALS SUBJECTED TO CYCLIC STRAINING	255
(B.1) Relationship Between Saturation Stress and Cell Size	255
(B.2) Subsequent Hardening in Decarburised Iron	257
REFERENCES	269

CHAPTER I

INTRODUCTION

Structural components are often subject to forces which are time dependent and vary in amplitude with time. Progressive failure can occur under the action of such alternating or fluctuating stresses at a stress level well below that required for failure under static loading conditions. Such failures are usually termed fatigue failures.

The occurrence and prevention of fatigue failures are of great importance in modern transportation, structural and power generation equipment. In the past two decades much effort has been devoted to the development of techniques to improve the ability to predict fatigue life and failure stresses based on the use of cumulative damage theories, on the utilisation of the methods of linear elastic fracture mechanics and by the recognition of the statistical nature of fatigue failure; (for example, Frost and Dugdale 1958, Johnson 1964, Rice 1967, Tetelman and McEvily 1967 - for a brief review, see Barnby 1972).

These studies have led to improvements both in design from the viewpoint of ameliorating stress concentration effects and from the viewpoint of material selection. However, to date, the understanding of the detailed mechanism

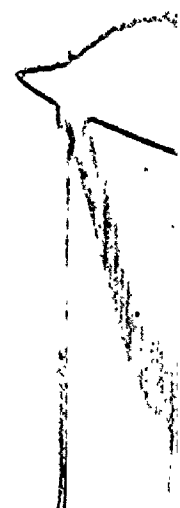
of fatigue failure does not enable us to understand the detailed processes of microstructural changes, associated with crack initiation and growth, in a quantitative manner.

The problem of fatigue is obviously a very broad and complex one, involving multidisciplinary studies in the areas of design and stress analysis as well as materials behaviour. In the present study attention has been focussed on the microstructural aspects of fatigue in some relatively simple bcc structures. This approach was chosen both in the hope that the study would prove applicable to the behaviour of more complex materials, such as a variety of structural steels, and that it would yield a more quantified view of the microstructural aspects of fatigue.

The study has been concerned predominantly with the microstructural changes preceeding fracture and thus attention has been focussed on three areas.

(a) The Bauschinger effect and the polarisation of plastic flow

The purpose of this investigation is to utilize the concept of the Bauschinger effect to study the accumulation of dislocations both in single-phase and two phase iron-based alloys. Such a study helps to predict the extent to which the structure is polarised with respect to the sense of deformation.



The investigation has two aspects: the study of the influence of dislocation distribution on the magnitude of the Bauschinger effect, and the study of the Bauschinger effect in two-phase materials as a function of plastic strain and volume fraction of second-phase particles.


The results are interpreted in terms of some of the currently available theories for the deformation in plastically inhomogeneous materials.

(b) Fatigue softening in single-phase low-carbon iron

An attempt is made, to characterize from a microstructural viewpoint the changes occurring in prestrained specimens of low carbon iron during cyclic softening and, to delineate the microstructural features which control the rate and extent of fatigue softening. The investigation involves a detailed study of the different structures developed by uniaxial and cyclic deformation.

Structural changes were monitored by transmission electron microscopy and ancillary techniques in order to provide a detailed characterisation of the fatigued state.

Simple models were developed, in an attempt to rationalize the kinetics of fatigue softening.




(c) Instability of plastic flow in fatigue

It is well established that local instabilities must arise from the nature of the microstructure at the onset of plastic strain localization. Thus, an important aspect of this investigation is to delineate the characteristic microstructural features developed in fatigue which lead to the condition where the work hardening characteristics of the material are unable to prevent localization and thus the onset of fatigue cracks.

The study was performed on low-carbon iron containing various dispersions of iron carbides. The experiments were designed to examine the influence of second-phase particles, on the dislocation accumulation and to delineate the stability of both the particle distribution and the dislocation structure during cyclic deformation.

The above three areas of study constitute the main contribution of this thesis to the understanding of the fatigue process, and can be correlated as follows: the role of microstructure in the fatigue process is in part concerned with the stability of the microstructure and the tendency to fatigue softening. This aspect is considered in both areas dealing with the Bauschinger effect and the fatigue softening.



In order to understand the detailed process of crack propagation it is necessary to recognise that the initiation of fatigue cracks is related to the concentration of plastic strain into narrow active regions. Thus the instability of plastic flow under cyclic deformation is an inherent part of the fracture process and this is the reason for the emphasis placed on this aspect in the present study.

CHAPTER II

THE BAUSCHINGER EFFECT AND THE


POLARISATION OF PLASTIC FLOW

SECTION (1)

(1.1) Objectives


Bauschinger (1882) was the first to report that a metal, after plastic deformation, has a higher yield stress in the direction of initial deformation than in the reverse direction. This phenomena has since been called the Bauschinger Effect.

The Bauschinger Effect (B.E.) illustrates the anisotropy of work hardening in materials. Materials showing no B.E. would be isotropic after unloading and would possess a compressive flow stress closely equal to that achieved in tension before unloading. A detailed knowledge of the microstructural features controlling the magnitude of the B.E. would be valuable in practice, specially for materials subjected to cyclic plastic strain reversals. Further, B.E. frequently occurs during the manufacture and processing of structural products, e.g., the U-ing and O-ing of steel pipe. The B.E. limits, for example, the possibility of workhardening steel rod by stretching, as it then becomes sensitive to bending. On the other hand, the action of the B.E. is desirable in cold rolling, as it produces less workhardening with multiple changes of direction during rolling than when



rolling in one direction only.

Though the existence of the B.E. has long been recognized, comparatively little work has been carried out to elucidate the effect in terms of basic microstructural aspects. It is the objective of this study to make a rather detailed investigation of some factors that influence the size of the B.E. in single and two phase iron-based alloys. The investigation has two aspects: the study of the influence of dislocation distribution on the magnitude of the B.E., and the study of the B.E. in two phase materials as a function both of forward plastic strain and volume fraction of second phase particles. The first aspect involved the study of the reverse flow behaviour in Armco iron and zone refined Niobium, while the second involved an analysis of existing data in the literature for a variety of carbon steels.



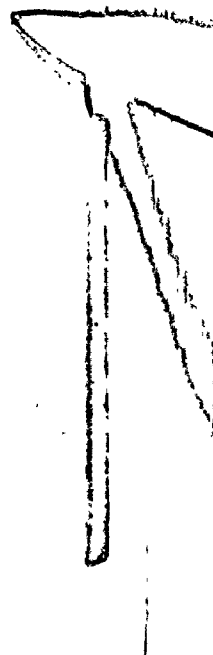
SECTION (2)

(2.1) Physical and Theoretical Aspects of the B.E.

During plastic deformation of metals and alloys, if the direction of straining is reversed, part of the work-hardening developed by the first mode of straining is lost in reversible straining. If, during prestraining, a pattern of elastic back stresses are developed due to plastic inhomogeneity, they will assist dislocation movement in reverse straining. The B.E. is generally explained in terms of the action of these residual back stresses remaining in the material after plastic deformation in one direction. The back stress is defined as the average elastic stress exerted by the obstacles on the matrix.

(2.1.1) Back Stresses in Single-Phase Metals

The origin of residual textural stresses developed by plastic deformation has been discussed by Greenough (1952) particularly in terms of intergranular stresses arising from the effects of anisotropy. However, during plastic deformation of a single-phase material the dislocations are moved through the "forest" of dislocations intersecting the slip planes, until they are stopped or locked by obstacles which are already present (as grain boundaries and inclusions), or which are formed during deformation (as cell walls). The repelling forces which exist between dislocations of the same



sign, and which can exist between obstacle and dislocation, act as residual elastic stresses which aid deformation in the reverse direction. Wilson and Konnan (1964) and Wilson's (1965) X-ray diffraction measurements of lattice strains on single-phase low carbon iron showed that such residual back stresses have an overall compressive component opposing the original extension and that their mean value is relatively small (5 - 10% of the flow stress). They have suggested that these compressive stresses could be balanced by relatively intense stresses of the opposite sign in small regions of high dislocation density such as cell walls.

Methods of measuring back stresses and their contribution to work-hardening ~~will be included~~ in Sections (2.1.3) and (3.2).

(2.1.2) Back Stresses in Two-Phase Alloys

In a plastically deformed matrix containing strong particles, which remain elastic rigid whilst the matrix is plastic, the particles act as a barrier to dislocations. During deformation, dislocation loops are built up around the particles which suffer purely elastic strain and a long range stress field will arise. The effect of removing the applied stress is to leave the material in a state in which there is a non-zero back stress within the matrix. This stress is, of course, in a sense to help the plastic



deformation of the matrix when a negative stress is externally applied.

Tanaka and Mori (1970) suggested that the back stress field is due to the difference of the amount of plastic deformation inside and outside the particles. Brown and Stobbs (1971) introduced a concept of image stress which is produced by misfits due to differences in the degree of deformation between the matrix and the particles and which is a result of the presence of the free boundary of a specimen (i.e., they have identified the image stress in Eshelby's theory of elastic inclusions with the back stress described and studied by Wilson). This image stress was considered to act as a general back stress of long range character.

Experimental data of Wilson (1965), Abel and Ham (1966), and Stoltz and Pelloux (1974) show that a large B.E. is generally associated with specimens containing undeformable particles.

(2.1.3) Bauschinger Effect and Work-Hardening

Theories advanced to explain work-hardening in single and two-phase materials have been of two main types. In one type, the flow stress is symmetrical with respect to the direction of straining and therefore does not predict a B.E. The other type predicts a decrease in the flow stress

when the sense of deformation is reversed and hence, a B.E. The latter type involves both relaxed and unrelaxed models of work-hardening. Some examples are briefly given in this section.


Ashby's Model of Symmetrical Hardening

Ashby (1970) has developed a simple theory of work-hardening in two-phase alloys in which he assumes that there is proportionality between the flow stress and the square root of the dislocation density. His theory predicts a relationship between the flow stress (τ) and the strain (ϵ) in the form:

$$\tau = \tau_0 + c' \mu \sqrt{\frac{b}{D}} \epsilon$$

where, τ_0 is a friction stress, c' is a constant, μ is the shear modulus, b is the burgers vector, ϵ is the strain, and D is the particle diameter.

The theory does not consider the detailed dislocation arrangement. It predicts a symmetrical behaviour with respect to the direction of deformation. It does not, therefore, make any prediction concerning the B.E. which clearly relies upon some characteristic asymmetry in the dislocation arrangement.



Orowan's Approach

Orowan (1959) invoked his loop-hardening theory in which a rather specific obstacle distribution with regions of both high and low obstacle density will accumulate dislocation loops on stressing in one direction. On removing the stress local adjustment takes place, so that on reapplying the stress in the reversed direction segments are propelled under both the back stress of the loop accumulations, and the applied stress, which will therefore be lower than in the forward direction. McClintock and Argon (1966) showed that a certain amount of permanent softening is obtained by further deformation in the reverse direction. This implies that part of the initial work-hardening is permanently removed by reverse straining.


Orowan has also discussed the problem of back stresses in terms of the effects of two generalized types of obstacles to slip namely, strong barriers and permeable obstacles. The build-up of loops around permeable obstacles results in continued hardening but at a much lower rate than for strong barrier hardening. Grain boundaries and cell walls may be considered as weak obstacles in single-phase metals, compared to strong particles in two-phase alloys. It is generally true that the permanent softening effects observed in most single-phase metals are much smaller than those observed in dispersion hardened alloys.

Fisher et al.'s Model

Fisher et al. (1953) have treated the work-hardening problem for a simple case, that of a random distribution of rigid obstacles of circular section in two dimensions. The passage of each dislocation leaves behind an Orowan dislocation loop round each particle intersecting the glide plane. Fisher et al. have pointed out that such loops will exert a shear stress on the matrix opposing further slip. Assuming the spacing of dislocation sources to be large compared to the spacing of accumulated loops, a uniform distribution of particles was shown to give rise to a hardening stress increment ($\Delta\tau_H$) so that,

$$\Delta\tau_H = 3 \frac{n}{R} f^{3/2}$$

where, n = number of loops per particle, R = particle radius, and f = volume fraction of particles. This stress field is reversible and is considered as a back stress which assists deformation in the reverse direction. Fisher et al.'s model neglects the possibility of cross slip and therefore the relaxation of highly developed back stresses around particles. Thus, it overestimates the B.E. in the two-phase alloys.



Tanaka and Mori's Model

Tanaka and Mori (1970) have developed a theory to explain the work-hardening behaviours of crystals with non-deforming particles or fibers. The theory is based on the stability of a material with the consideration of Gibbs free energy under the applied stress. Internal stresses are built-up around the particles because of the constraining effect on them by the uniformly deformed matrix. The theory predicts a linear hardening in the form:

$$\sigma = \sigma_0 + \frac{2\gamma f \mu \epsilon_p}{1-f} *$$

where, σ = applied stress, σ_0 = initial yield stress, and γ is a geometrical term = $\frac{7-5\nu}{15(1-\nu)}$ for spherical particles where ν is the Poisson's ratio.

The theory predicts an elastic back stress of $\frac{2\gamma f \mu \epsilon_p}{1-f}$ which acts to help deformation in the reverse direction. Brown and Stobbs (1971) have indicated that Tanaka and Mori's theory provides a lower bound for the strength because any additional heat production will increase the flow stress.

* The equation is a simplified form of Tanaka and Mori's original equation and assumes the same shear modulus for the particles and the matrix.

Hirsch's Theory for Single-Phase Metals (1963)

In Hirsch's theory of work-hardening the internal stresses from piled-up groups help to activate secondary sources causing hardening and changing the pile-ups into complex dislocation arrangements. When the internal stress exceeds a certain value a secondary source operates and stops the source nearby. Thus, secondary slip provides a mechanism for plastic relaxation. The theory predicts the formation of non-uniform structure so that, regions of high dislocation density trap more dislocations and a uniform cell structure is developed. The theory does not explicitly predict the relative contributions due to back stress, forest hardening, etc. to the flow stress.

Brown and Stobbs' Models

Brown and Stobbs (1971) have developed two models to account for work-hardening behaviour in copper containing spherical particles of silica. The first model (elastic model) assumes no plastic relaxation around the particles while the second one takes into account the role of plastic relaxation at the particles.

(a) The elastic model: If plastic relaxation does not occur, every Orowan loop remains as a shear loop around the particles. Brown and Stobbs showed that, if a volume fraction f of the material is only elastically strained then a uniform back stress of magnitude $\sim \mu \epsilon_p f$ exists together

with locally fluctuating, inhomogeneous stresses of both signs. In the linear hardening region the flow stress is given as:

$$\sigma = \mu \epsilon_p f + \sqrt{\frac{6}{\pi}} \mu \epsilon_p f^{3/2} + 2\sigma_0$$

which shows that for small volume fractions, the image stress is primarily responsible for the hardening. Brown and Stobbs showed that the work-hardening predicted by this model is about three times larger than that experimentally observed because of the hypothetical assumption of no plastic relaxation. They have also emphasized that the work-hardening described by the model is unstable with respect to unloading, and that reverse plastic flow will occur as long as the image stress is greater than the Orowan stress, so that a very large proportion of plastic strain is reversible.

(b) A model accounting for plastic relaxation: The Orowan loops around the particles act together to produce large stresses in the neighbourhood of the particles. In order to lower these elastic stresses plastic relaxation may take place by local climb of dislocation loops, or the screw segments can cross slip, as proposed by Hirsch, to produce prismatic loops; also various processes involving secondary slip can occur as proposed by Ashby. All these processes of plastic relaxation lower the work-hardening rate by lowering the local stresses at the barriers.



Brown and Stobbs have emphasized that at small strains and small particles only primary dislocations are involved in the stress-relief process by Hirsch's mechanism (1957) which proposes that when the cross-slip occurs, a shear loop is converted into two equal and opposite prismatic loops, and the line length of dislocation is increased.

Brown and Stobbs also showed that at large particles and large strains the stress-relief mechanism involves the generation of secondary dislocations and a plastic zone containing a high density of forest dislocations builds up in the neighbourhood of the particles. The plastic zones have two effects: to harden the matrix directly, and to inhibit the local slip which is required to relieve the elastic stresses. Thus, the presence of plastic zone prevents full plastic relaxation, and gives rise to a localized elastic stress field, with its accompanying image stress which acts as a back stress.

With the simple assumption that the flow stress consists of three additive components: an Orowan stress (σ_0), a Forest hardening, and a back stress. Brown and Stobbs' treatment predicts a flow stress in the form:

$$\sigma = \sigma_0 + \sqrt{3} \alpha \mu f^{1/2} \sqrt{\frac{8b\epsilon_p}{\pi R}} + \alpha \mu f \left(\frac{8\pi b}{\alpha^2 \epsilon_p R} \right)^{\frac{1}{8}} \sqrt{\frac{8b\epsilon_p}{\pi R}}$$

where α is a constant ($\frac{1}{3} \sim \frac{1}{5}$).

This model provides the most quantitative treatment to the problem of work-hardening in two-phase alloys. It predicts a strength in one direction of about $2f^{1/2}$ that in the opposite direction. The theory treats the problem of spherical hard particles in a soft matrix and does not account for the effect of particle shape.

It is clear from the above section that work-hardening of both single and two-phase alloys consists of two components: A reversible component due to a back stress and an irreversible part due to other contributions to hardening. The reversible part (back stress) provides a natural explanation to the phenomena of Bauschinger Effect. The magnitude of the back stress depends generally on: volume fraction and shape of barriers, amount of plastic strain and degree of plastic relaxation.

(2.2) Factors Influencing the B.E.

Factors that may affect the size of the B.E. are:

Amount of prior strain,

Temperature of deformation,

Volume fraction of second phase particles,

Shape of the particles,

Grain size, and
Stacking fault energy.


It may be worth noting that the degree of influence of each of these factors on the B.E. depends generally on the parameter or parameters defined to account for the effect. Section (2.3) will deal with the different methods used to measure the B.E. The influence of prior strain and temperature will be treated in Section (5).

Effect of Volume Fraction

The experimental data of Wilson (1965) shows that the magnitude of the back stress increases with the addition of increasing volume fraction of rigid particles. He shows that the back stress is directly proportional to the volume fraction of particles for a given size, shape and prior strain. Brown and Stobbs' theory predicts such proportionality. From Wilson's data the effect of particle spacing is much less marked. Janiche et al. (1965) found a larger B.E. in steels with high pearlite content than with low pearlite contents, but the effect was not sensitive to lamellar spacing.

Effect of Particle Shape

If the particle is not spherical, the internal stress field in a specimen will be varied not only by its shape but also by the relative orientation of the



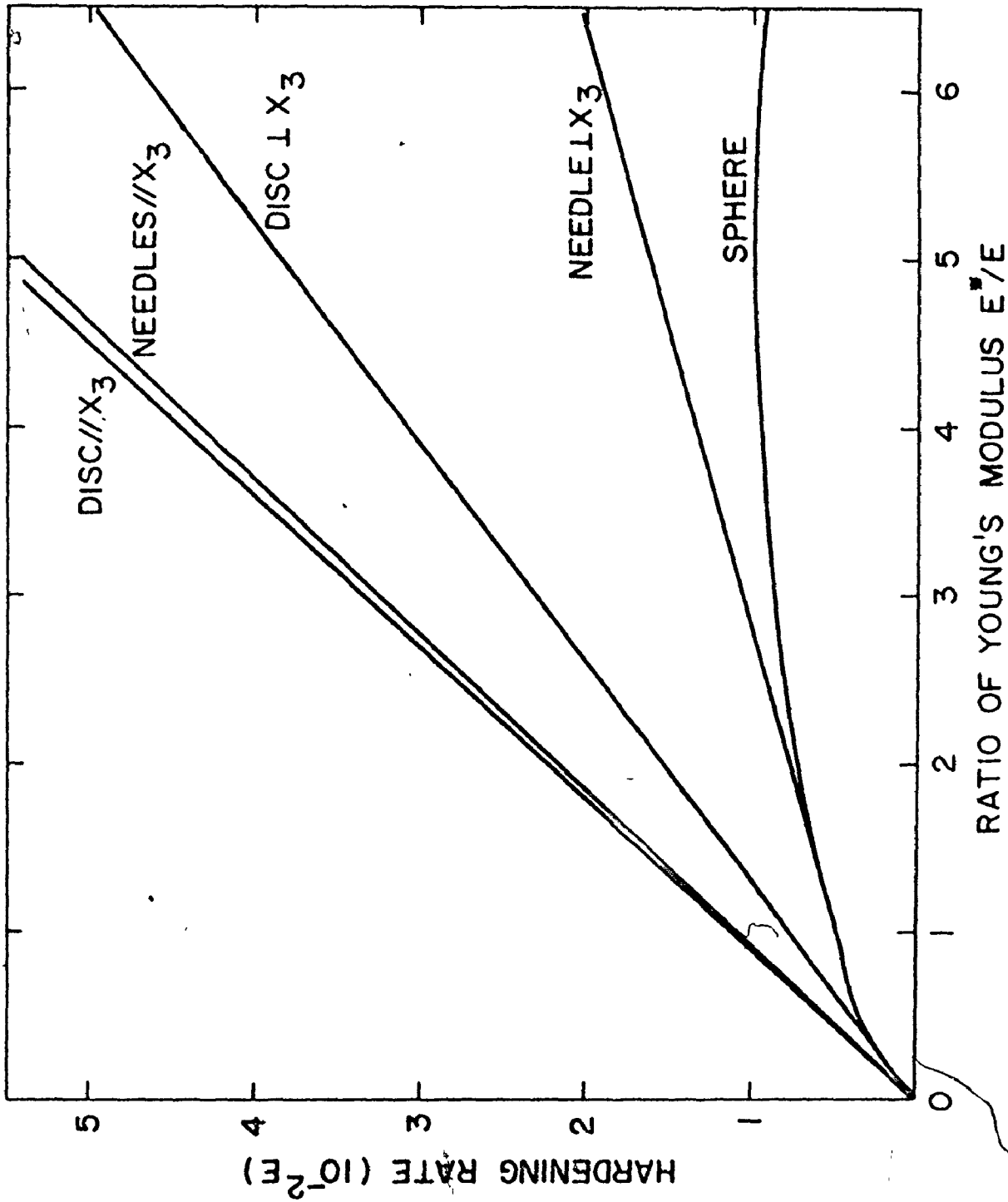


Fig. 1: Effect of the shape of the inclusion on the hardening rate, $f=0.01$, x_3 is the tensile axis, E^* is Young's Modulus of inclusion, E is Young's Modulus of matrix (after Tanaka and Mori 1970)

particles to the direction of plastic flow. Tanaka and Mori (1970) have treated this problem and found that the work-hardening behaviour can be affected by both the form and orientation of particles. Figure 1 shows the results of their calculation.

Kumakura (1968) observed that the B.E. is smaller in the C-steel of spheroidized pearlite than in the same steel of lamella pearlite.

Wilson (1965) found that alloys with closely spaced irregular shaped particles, such as pearlitic steels and Al-Cu alloy with θ' precipitates, show the largest back stress while material with coarse round particles, such as spheroidized steel, show the smallest effect. Among the structures examined by Wilson, the most effective barriers were the cementite lamellae in pearlitic steels. These results clearly indicate that in materials containing plate-like particles or fibers (composite materials) the back stresses can account for a major portion of the work-hardening and are expected to have a large B.E.

Effect of Grain Size

Woolley (1953) found that the B.E. is nearly independent of grain size for a wide range of pure metals. The same independence was observed by Harrison et al. (1972) in C-Mn steels (see also Figure 7). Jamieson and Hood (1971) also showed that grain size does not contribute

significantly to the magnitude of the B.E. in high-strength low-alloy steels.

A possible explanation to the above observations is that, after a small amount of plastic deformation, the main contribution to the back stress comes from the microstructure (dislocation walls) rather than grain boundaries. Thus, in planar-slip mode materials in which the formation of dislocation walls is less favourable, the grain boundaries may act as the major source for back stresses; Schankula and Embury (1971).

Effect of Stacking Fault Energy (SFE)


It is well known that the cross slip of dislocations in high SFE materials is easier than that in materials with low SFE. Cross slip, as shown in Section (2.1), is an important process in plastic relaxation at the barriers. Thus, low SFE materials may develop higher back stresses during deformation, hence suffer larger softening effects when deformation is reversed, as compared to materials with high SFE.

On the basis of experimental evidence (Fig. 8), brass shows a larger softening effect compared to pure copper. Also, the work of Abel and Muir (1972) clearly indicates that in fcc materials the SFE has a major effect on the ability to produce reversible deformation, i.e., the Bauschinger Effect is larger in low SFE materials.

(2.3) Methods of Measuring the B.E.

There have been several proposals in the literature to account for the B.E., some of which are, the difference in yield stresses between forward and reverse deformation (Polakowski 1951), the Bauschinger Strain (Buckley and Entwistle 1959), and the Bauschinger Effect Factor (Janiche et al. 1965). The Bauschinger Strain was defined as, the amount of strain required to raise the stress level in the reverse direction to that of the forward direction. (Fig. 2(a)).


Woolley (1953) and Kumakura (1968) proposed a technique that involves the measurement of Bauschinger Strain (B-strain) " γ " at a specified stress level. Woolley defined a parameter, " ρ " as the ratio between the reverse strain at $3/4$ of the stress level ($\sigma_{3/4}$) divided by that strain at zero stress (γ_0). For a wide range of single phase materials the parameter ρ is independent of prior strain, temperature or grain size. Woolley's technique was tested by Janiche et al. (1965) for unalloyed steels with different carbon content. Their results indicate that the independence of the parameter ρ on prior strain is only valid for practically homogeneous ferrite but not for iron containing carbide particles. Janiche et al. suggested another expression, usually called the Bauschinger Effect Factor (BEF) in the form: $\frac{\tau_F - \tau_R}{\tau_F}$ where τ_F is



the flow stress after certain amount of prestrain, and τ_R is the yield stress corresponding to 0.2% offset in the reverse direction. They showed that the BEF is independent on prior strains larger than 10% shear. For prior strains less than 10% the BEF was found to increase continuously from zero.

The different proposals for measuring the B.E. gave rise to some confusion in comparing different experimental results. Working on Zinc Single Crystals, Edwards and Washburn (1956) obtained a high value of the B-strain, accompanied by a relatively small yield stress lowering. Abel's (1965) results for Al - 4% Cu crystals show a relatively small B-strain accompanied by very large yield stress lowering. If the B-strain is used as a criterion, one may describe the Zinc Crystals as having a larger B.E. compared to the Al - Cu alloy, but in terms of yield stress lowering, the Al - Cu alloy exhibits the larger B.E.. Moreover, both the yield stress difference and the B-strain depend on the amount of prior strain and can hardly be used to compare different materials.

The X-ray work of Wilson (1965), and Wilson and Konnan (1964) provides the best available measurement of the B.E.. The X-ray line peak shifts detected by diffractometry were used to calculate the residual back stress: $\tau_x = \epsilon_x \left(\frac{E}{1-\nu} \right)$; where ϵ_x is the residual



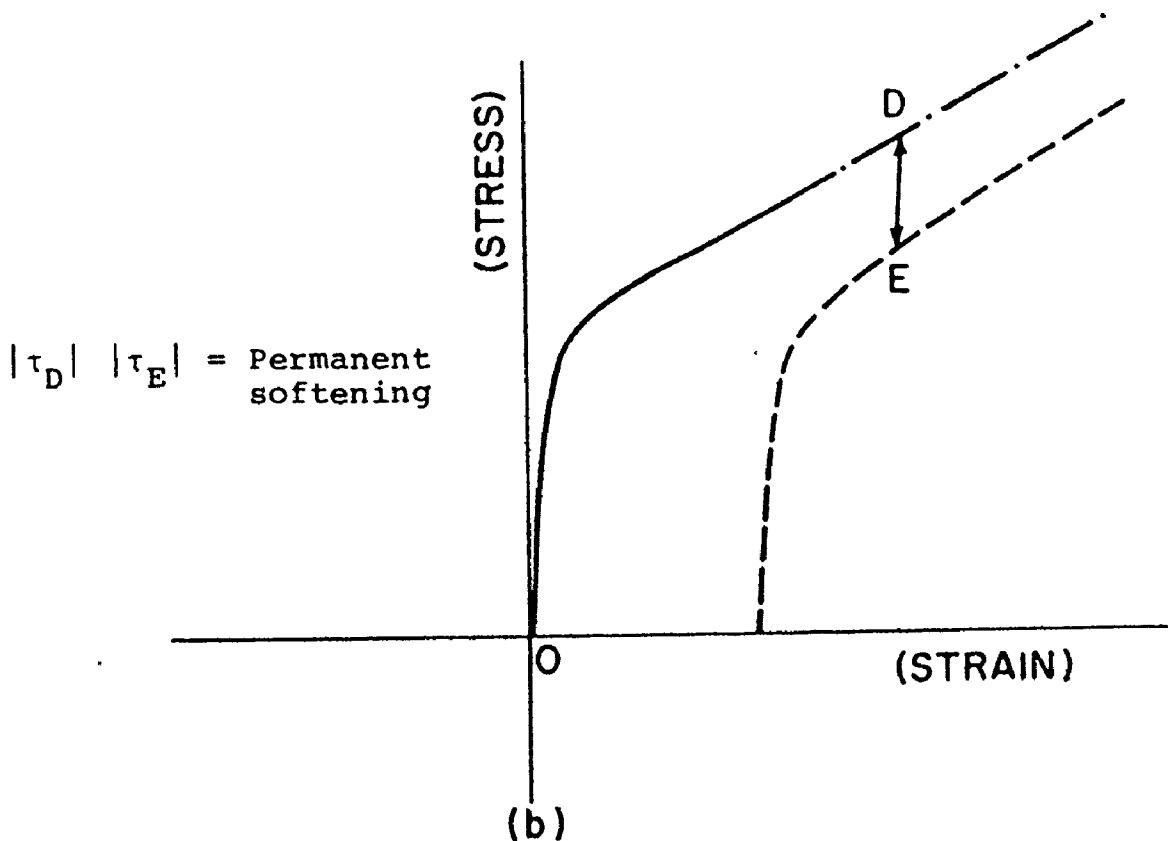
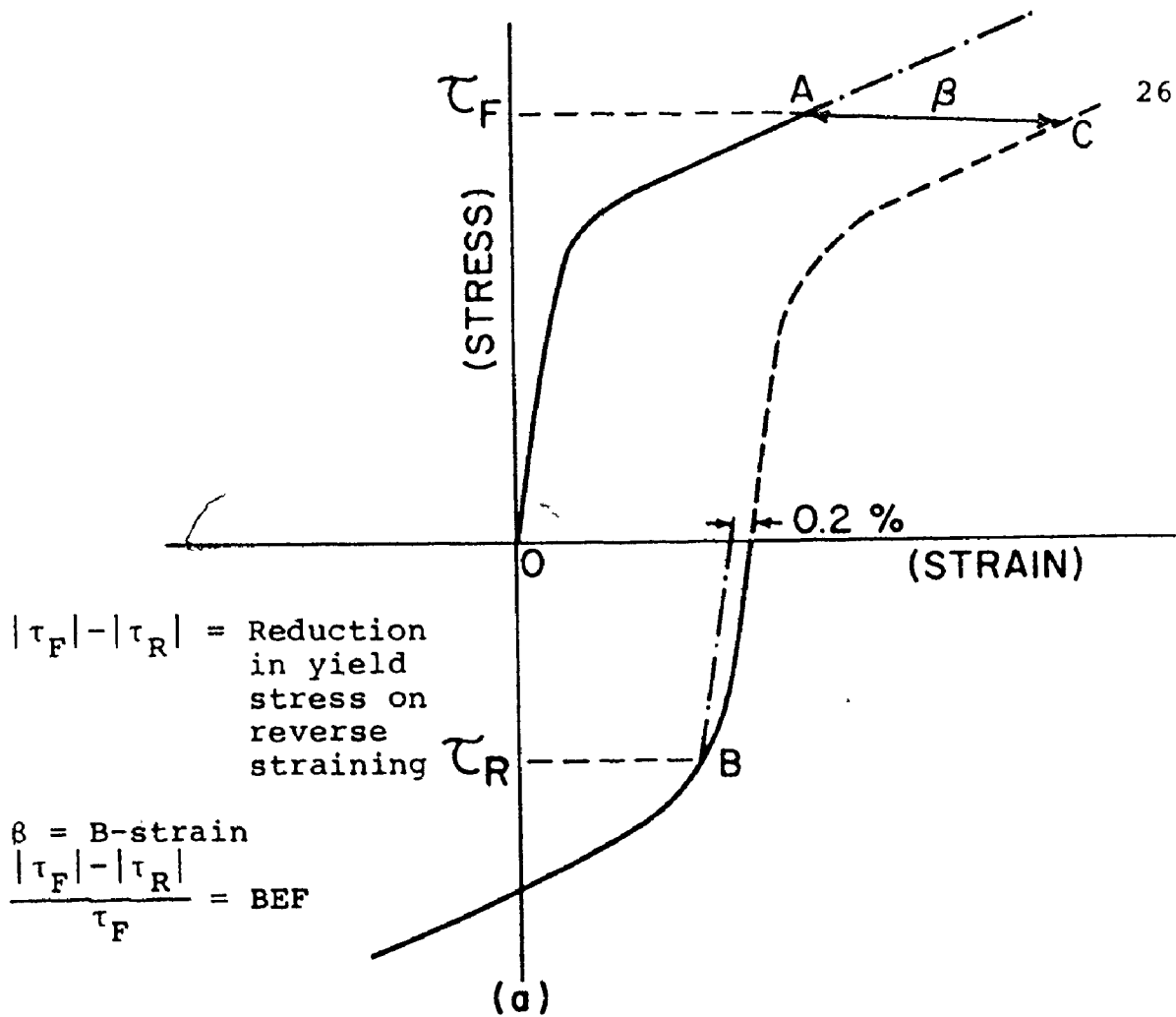



Fig. 2: Schematic illustration of methods commonly used to account for the Bauschinger effect

lattice strain measured by the line shift after certain amount of prior strain. E and ν are the Young's modulus and Poisson's ratio respectively. Their back stress was found to be about half the amount of permanent softening. The permanent softening was defined by McClintock and Argon (1966), as, the difference in the (absolute) values of flow strength, for continued forward and for reverse straining, measured at the same total strain and beyond the point at which the two flow stress curves become approximately parallel (Fig. 2(b)). The main characteristics of the B.E., as normally used, are shown diagrammatically in Fig. 2.



SECTION (3)

EXPERIMENTAL DETAILS(3.1) Materials and Testing Procedure

In order to study the effects of prior strain and deformation temperature on the size of the Bauschinger Effect in bcc single-phase metals, specimens of Armco iron and zone-refined Niobium of compositions given in Table 1 were used.

The as received Armco iron was in the form of rods 3/4 inch diameter. The material was swaged to 1/2 inch diameter rods from which specimens of the dimensions 1/4 inch diameter and 1/2 inch gauge length were machined. The specimens were annealed at 900°C in a vacuum furnace (10^{-5} torr.) for two hours and the average grain size obtained was in the order of 50 microns.

In order to eliminate any surface damage due to machining, a layer of about 0.002 inch thickness of the specimen surface was removed by chemical and electrolytical polishing. A solution of 5% hydrofluoric acid, 15% distilled water and 80% hydrogen peroxide was used for chemical polishing. Following chemical polishing the specimens were electrolytically polished in a solution

TABLE 1
CHEMICAL COMPOSITION

Material	Chemical Composition (wt. %)				
	C	Mn	S	N	O
Armco Iron	0.018	0.037	0.013	0.003	0.072
Zone Refined	Total interstitial content \approx 0.008				
Niobium	Total substitutional content \approx 0.1				

5% perchloric acid and 95% acetic acid using DC current of 10 volts and current density of 150 m. amp./cm².

A similar procedure was used to prepare the Niobium specimens.

All tests were performed on 901-77 Model of the Material Testing System (MTS) machine as described in Chapter III. A range of reversed strains from 0.005 to 0.08 was achieved in tension-compression at two temperatures 195 and 298°K. Tests at 195°K were made by immersing the specimens in a bath of dry ice and methanol and care was taken to ensure that the entire system was at constant temperature prior to the initiation of the test. Each specimen was maintained to within $\pm 2^{\circ}\text{C}$ of the desired temperature for 10 minutes before testing. All tests were performed under a strain rate of $4 \times 10^{-4} \text{ sec}^{-1}$.

The mechanical response of the specimens to reversed straining was measured by X - Y recorder connected to the machine. The recorder was recalibrated using external voltage supply and the error was better than $\pm 3\%$.

The effect of volume fraction of second phase particles on the B.E. was studied on a variety of steels containing various volume fractions of tempered carbides and pearlite. This was achieved by using available data from the literature to calculate different terms involved

TABLE 2

CHEMICAL COMPOSITION

Reference	Material Condition	Chemical Composition (wt. %)							
		C	Mn	P	Si	S	Cr	Ni	V
Wilson (1965)	Recrystallized at 650°C	0.11	0.47	0.03	0.08	0.03			
Jamieson & Hood (1971)	Normalized 1000°C/1 hr	0.21	1.59		0.05				
Harrison et al. (1972)	Treated at 950 to 1250°C to obtain a range of grain sizes - Furnace cooled	0.22	0.88	0.017	0.04	0.03			0.018
Wilson (1965)	Quenched 820°C & tempered 650°C/2 hrs	0.74	0.29	0.015	0.19	0.01			
Milligan et al. (1966)	Austinitized 850°C/1 hr & annealed 650°C/24 hrs (Pearlitic Structure)	0.33	0.62	0.007	0.27	0.008	1	2.62	0.17
Wilson (1965)	Quenched 900°C & tempered 650°C/2 hrs	1.14	0.32	0.03	0.01	0.01			
Wilson & Konnan (1964)	Quenched 950°C & tempered 650°C/2 hrs	1.14	0.32	0.01	0.01	<0.01	<0.01	<0.01	

in measuring the Bauschinger Effect parameter as defined in Section (3.2). The chemical composition of the materials studied is given in Table 2.

(3.2) Measurements and Variables Investigated

It appeared from Section (2) that the elastic back stresses which build-up in the material due to local plastic inhomogeneity provides a physical explanation to the phenomenon of Bauschinger Effect in materials. Thus, measurements of the B.E. must reflect the magnitude of these back stresses. An attempt is made here to define "a parameter" which involves the back stress, to account for the size of the B.E. in single- and two-phase materials.

(3.2.1) The Bauschinger effect parameter

For both single- and two-phase materials we can approximate the forward flow stress σ_F as the linear sum of three terms

$$\sigma_F = \sigma_0 + \sigma_{\text{for}} + \sigma_B \quad (1)$$

where σ_0 is an initial yield stress which can be taken as a friction stress in bcc single-phase materials, or



an Orowan stress in two-phase alloys, σ_{for} is the contribution of forest hardening to the flow stress, and σ_B is a back stress due to elastic stresses supported by the obstacles (e.g., dislocation tangles in single-phase metals, or hard particles in two-phase alloys) which tends to aid reverse plastic flow.

To a first approximation we can assume that σ_0 and σ_{for} are not polarised, i.e., are symmetrical in their action with respect to both forward and reverse deformation. Thus, when the sense of deformation is reversed only σ_B will act to help reverse flow so that the reverse flow stress σ_R can be expressed as

$$\sigma_R = \sigma_0 + \sigma_{\text{for}} - \sigma_B \quad (2)$$

From Eqs. (1) and (2), we have

$$\sigma_F - \sigma_R = 2\sigma_B \quad (3)$$

$(\sigma_F - \sigma_R)$ is the reduction in flow stress due to reverse deformation which can be measured directly from the mechanical response of the material.

One of the important results of Wilson's (1965) is that $(\sigma_F - \sigma_R)$ is nearly ^{twice} the magnitude of the

residual back stress measured by X-rays which indicates that Eq. (3) is practically justifiable. Dividing both sides of Eq. (3) by the total amount of work hardening $(\sigma_F - \sigma_0)$; thus

$$\frac{\sigma_F - \sigma_R}{\sigma_F - \sigma_0} = \frac{2\sigma_B}{\sigma_F - \sigma_0} \quad (4)$$

Let us call this the Bauschinger Effect Parameter (BEP) which is defined as "the reversible fraction of work hardening", i.e., twice the fraction of total work hardening due to the back stress. This parameter will be used throughout this investigation to account for the size of the B.E. in all the materials studied.

(3.2.2) Method of measuring σ_R and σ_0

σ_R was determined in this investigation by extrapolating the part of the reverse curve, which is parallel to the forward curve, back to zero strain as illustrated in Fig. 3.

Wilson (1965) measured the reverse flow stress at certain amount of reverse strain ϵ_n which he defined as the amount of reverse strain required to reduce the average value of the residual back stress in the matrix

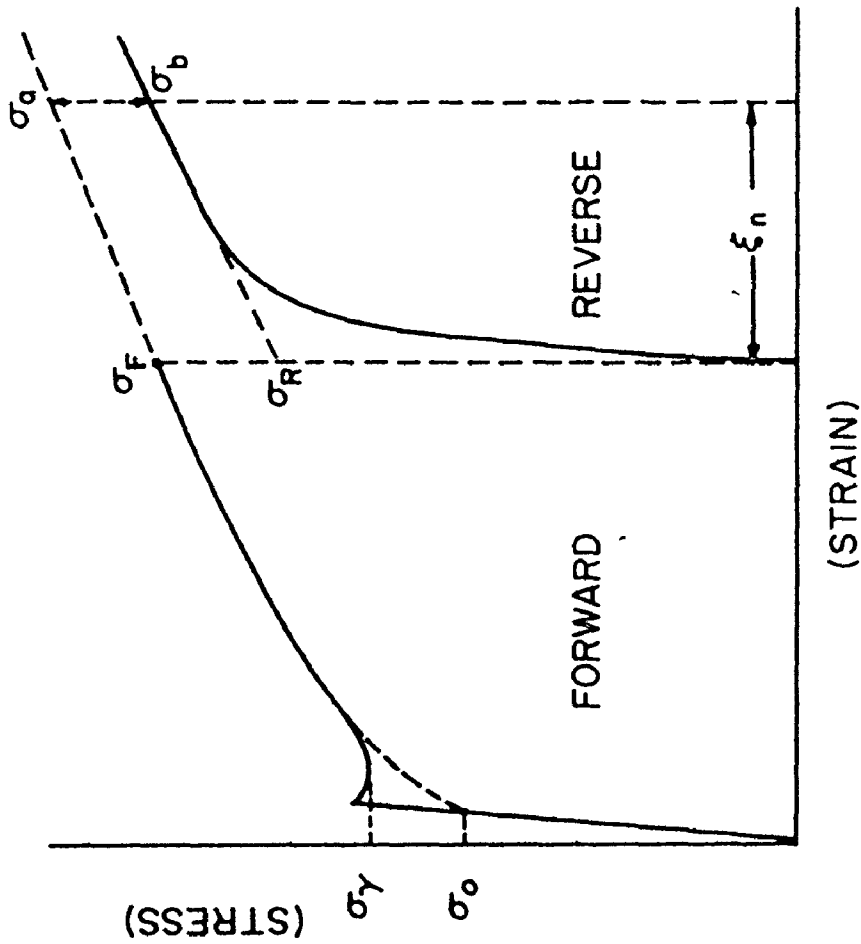



Fig. 3: Schematic diagram showing the method used to evaluate BEP. " σ_0 " was estimated by extrapolating the part of the stress-strain curve corresponding to homogeneous deformation back to zero plastic strain using a log-log plot"

to zero. The BEP according to Wilson's definition of σ_R can be expressed (Fig. 3) as,
$$\text{BEP (Wilson)} = \frac{\sigma_a - \sigma_b}{\sigma_a - \sigma_0}.$$
 The difference in the values of BEP calculated by Wilson's method and the method used here is less than 10%. This was found by applying the method used in this investigation to Wilson's data and comparing the calculated values of BEP to those of Wilson's.

In order to avoid problems of inhomogeneous initial yielding a technique was used to estimate σ_0 by extrapolating the part, of the stress-strain curve, corresponding to homogeneous deformation back to zero plastic strain using a log-log plot. σ_0 was defined by Wilson⁴ as the value of the "unlocked" yield stress. He has indicated that, it is misleading to use the initial macroscopic yield stress σ_y as a measure of σ_0 because σ_y is generally affected by transient strengthening effects associated with initial dislocation locking.

The above treatment provides a new approach to the phenomenon of B.E. based on the recent advances in understanding the detailed mechanisms of dislocation accumulation in materials. The BEP defined here should provide a suitable basis for comparison of the contributions of back stress hardening to total hardening in different materials.



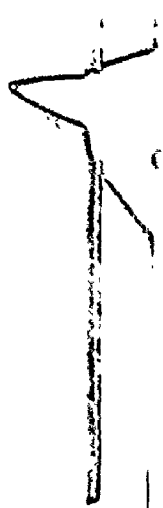
SECTION (4)

EXPERIMENTAL RESULTS

For clarity the experimental results are divided into two sections dealing (a) with the B.E. in single-phase bcc metals and (b) with the B.E. in a range of steels containing various volume fractions (f) of tempered carbides and pearlite.

(4.1) B.E. in Single-Phase Armco Iron and Niobium

Although the magnitude of the B.E. in single-phase materials is much smaller than that in duplex structures, it is pertinent to consider the microstructural factors which control its magnitude. In the present study attention was given to the effect of dislocation arrangement and amount of prestrain on the BEP. Single-phase Armco iron and Niobium were chosen because of the pronounced temperature dependence of dislocation arrangement in such bcc materials. The studies of reverse flow were performed at both 195 and 298°K in the two materials in order to obtain different types of dislocation distribution.



It is well known in bcc materials, that deformation at low temperatures is associated with large amplitudes of effective stresses which prevents dislocations from grouping into tangles or cell walls. (Chapter III will deal with the effect of deformation temperature on dislocation distribution in more details.) Thus, at 195°K dislocations are accumulated in a fairly uniform arrangement with no cell walls formed, at strains of less than 0.15, whereas at 298°K the dislocation substructure consists of well defined clusters of cell walls. These structures are illustrated in Fig. 23 for decarburized iron.

The response of the material to various amounts of prestrain followed by reverse straining was measured at each temperature and magnitudes of the BEP were calculated as mentioned in Section (3.2.2). Figure 4 shows a comparison for the effect of the two temperatures on the magnitude of the BEP in Armco iron. The figure indicates that the BEP is essentially unaffected by the deformation temperature, and consequently by the arrangement of dislocations. The figure also shows that the BEP is independent of the amount of forward strain.

In order to determine how general the dependence of the BEP on deformation temperature, zone-refined Niobium specimens were tested under the same conditions and the

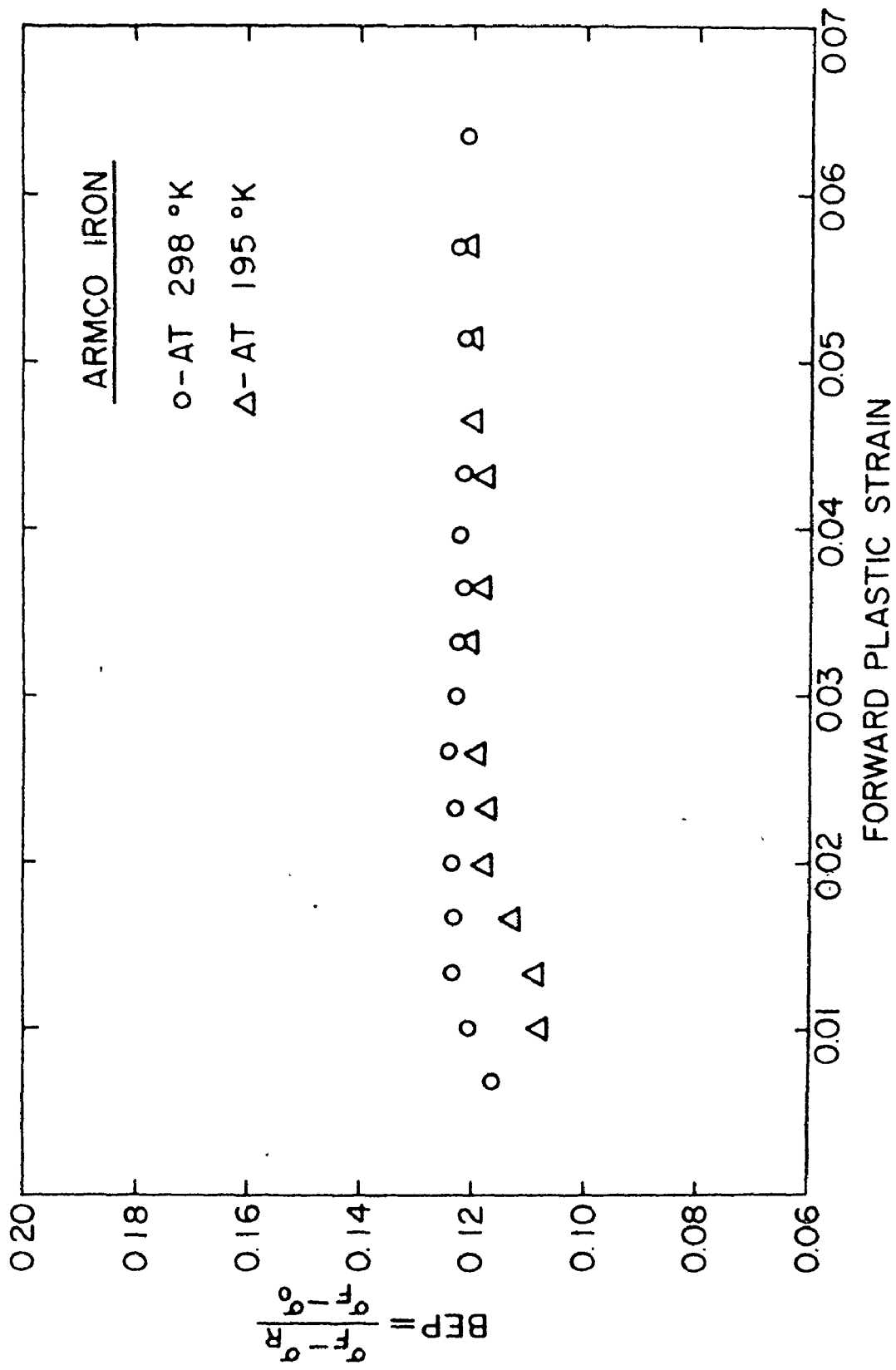


Fig. 4: Effect of temperature and forward strain on the BEP in Armco Iron



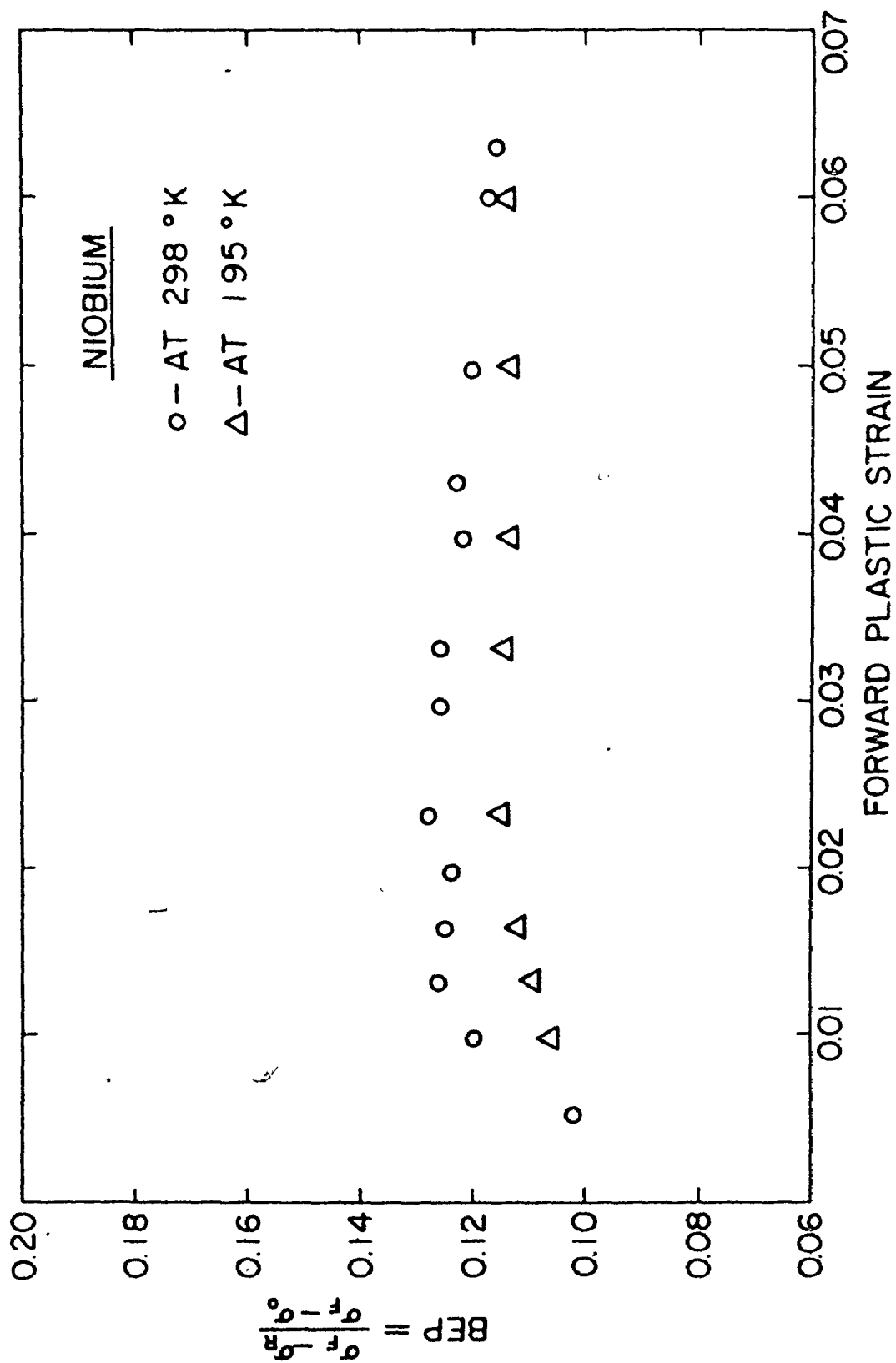


Fig. 5: Effect of temperature and forward strain on the BEP in Niobium



results obtained are illustrated in Fig. 5. The figure shows that the BEP in Niobium is also independent of deformation temperature and amount of forward strain.

The data indicates two important features of the deformation process in single-phase bcc materials: firstly, there is no, or very little, increase in the fraction of total hardening due to back stresses associated with tangles of dislocations, and secondly, the elastic back stress increases in proportion to the total hardening during unidirectional plastic deformation.

(4.2) Effect of Second-Phase Particles on the B.E. in Steels

It has been emphasised in Section (2) that the size of the B.E. may be significant in materials containing hard particles due to the large elastic back stresses supported by these particles during plastic deformation. In order to study the effect of second-phase particles on the Bauschinger Effect, values of the BEP were calculated from data in the literature for the range of steels shown in Table 3.

Figure 6 shows the BEP as a function of forward strain for various volume fractions of second-phase particles. Results obtained in Armco iron are included for comparison. Two salient features emerge from Fig. 6:

TABLE 3
BEP IN STEELS CONTAINING DIFFERENT VOLUME
FRACTION OF SECOND-PHASE PARTICLES

Reference	Vol. Fraction f	Calculated BEP
Wilson (1965)	0.016	0.18
Jamieson & Hood (1971)	0.05	0.52
Harrison et al. (1972)	0.056	0.6 (Average)
<u>Grain Size</u>		
15 μ		0.57
26 μ		0.59
32 μ		0.62
40 μ		0.62
73 μ		0.59
Wilson (1965)	0.11	0.75
Milligan et al. (1966)	0.15	0.80
Wilson (1965)	0.17	0.86
Wilson & Konnan (1964)	0.17	0.84

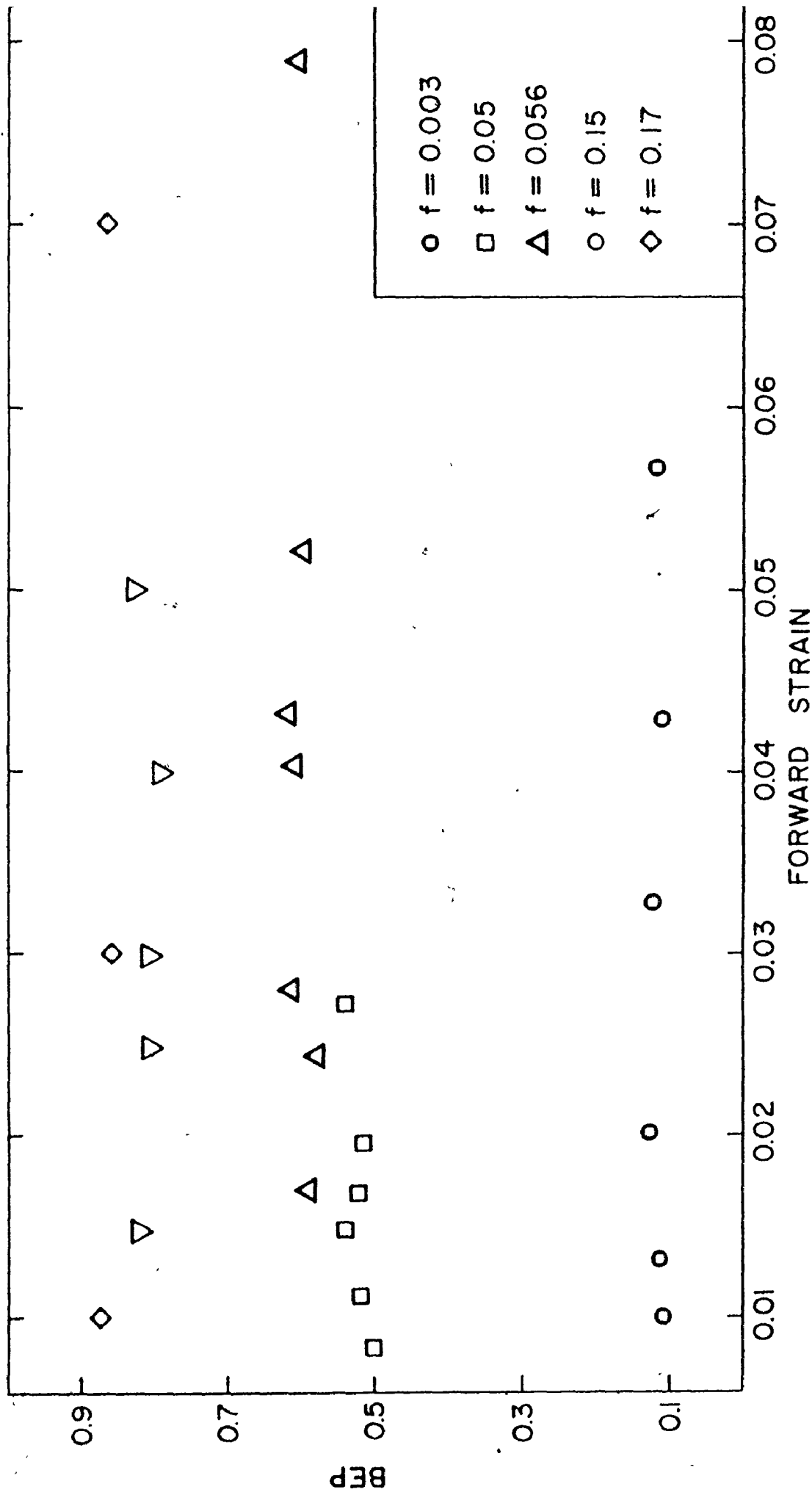


Fig. 6: Effect of volume fraction of second-phase particles on the BEP in steels

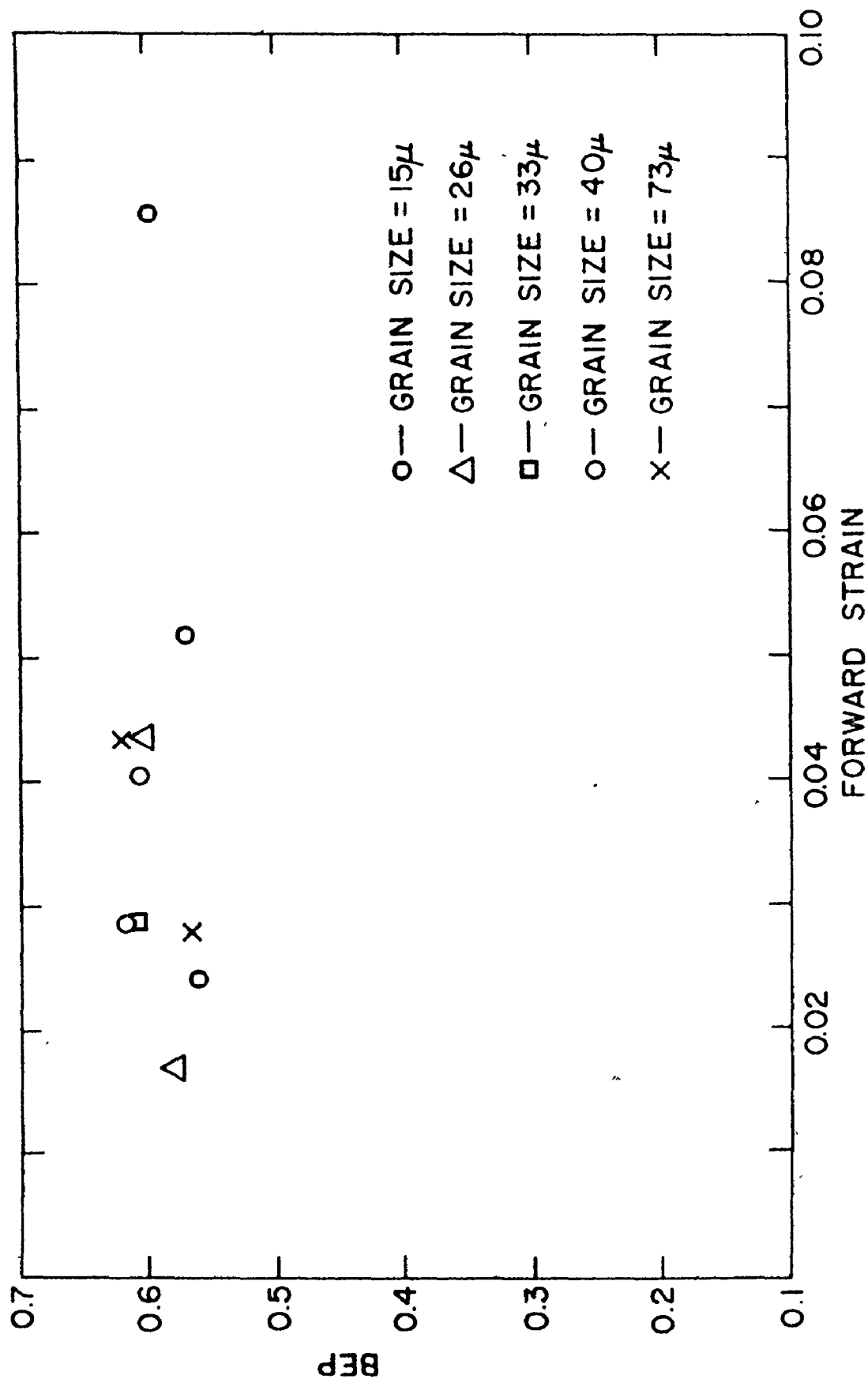
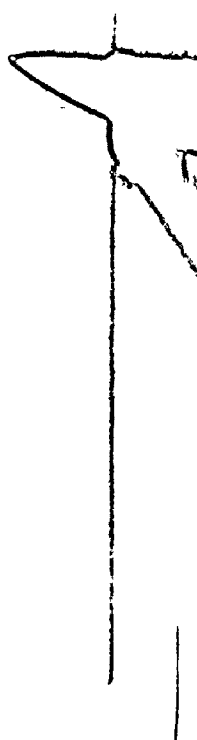


Fig. 7: Effect of grain size on the BEP calculated for the furnace cooled C-Mn steel of Harrison et al. (1972)

Firstly, the magnitude of the BEP increases by increasing volume fraction of particles, and secondly, for the range of the steels studies, the BEP is essentially independent of the degree of forward plastic strain.

In order to determine whether the grain size effects the magnitude of the BEP in two-phase materials, data from Harrison et al. (1972) were analysed for furnace cooled C - Mn steel and the BEP was calculated for the range of grain size (15 μ - 73 μ) included in Table 3. The results are shown in Fig. 7 which illustrates the grain size independence of the BEP. The figure also indicates that grain size has essentially no effect on the strain independence of the BEP. The work of Jameson and Hood (1971) on structural steels and Woolley (1953) on single-phase metals also indicates that the magnitude of B.E. is independent of grain size.



SECTION (5)

DISCUSSION OF RESULTS(5.1) Summary of Experimental Results

The results obtained in Section (4) may be summarized as follows:

(1) The B.F. associated with single-phase low-carbon iron is relatively small compared to that associated with steels containing second-phase particles.

(2) In bcc single-phase metals, the BEP is independent of the deformation temperature and amount of prior strain.

(3) In steels containing second-phase particles the BEP is independent of the amount of prior strain but increases with increasing volume fraction of particles.

The discussion is divided into two parts. In the first part, results obtained in single-phase bcc

iron and Niobium are discussed. The second part discusses the B.E. in two-phase iron-based alloys.

(5.2) The BEP in Single-Phase bcc Materials

It appeared from Section (2) that the B.E. and the microstructural arrangements accompanying it can be better understood in terms of the unrelaxed back stresses which build-up in the material due to local plastic inhomogeneity. In single-phase materials it is possible to think of back stresses as being caused by arrays of shear loops supported by the dislocation tangles. Unfortunately, the detailed nature (shape, size, and dislocation interactions) of these tangles is not well understood which makes it difficult to calculate quantitatively the contribution of back stress to the overall work hardening. Moreover, it is difficult to separate the effects of back stress and forest hardening because tangles are "permeable" barriers to slip, i.e., cannot be treated as rigid particles embedded in a ductile matrix. However, the approach given in Section (3.2) helps to calculate values of back stresses from the magnitudes of flow stresses in forward and reverse deformation, i.e., $2\sigma_B = \sigma_F - \sigma_R$.

It was suggested that relatively small back stresses develop in single-phase materials at dislocation tangles as

deformation proceeds in one direction. Measurements of the BEP in Armco iron predict a back stress of $\sim 6\%$ of the overall work hardening increment. The back stress calculated from $\frac{\sigma_R}{\sigma_F}$ values of Wilson's (1965), more accurate, measurements in low-carbon iron is in the order of 5 - 8% of the overall hardening which is in accord with data presented in this work.

The observed strain independence of the BEP suggests that, as deformation proceeds the back stress rises in proportion to the total hardening, i.e.,

$$\sigma_B \propto \sigma_F - \sigma_0 = \sigma_{\text{for}} + \sigma_B \quad (5)$$

Thus,

$$\sigma_B \propto \sigma_{\text{for}} \quad (6)$$

or,


$$\frac{\sigma_B}{\sigma_{\text{for}}} = C = \frac{\text{BEP}}{2 - \text{BEP}} \quad (7)$$

where C is a constant independent of forward strain.

Equation (7) implies that forest hardening increases during deformation at the same rate as the general level of back stress increases. This can be rationalized in the

following way During plastic deformation of a single-phase bcc material two interrelated processes may occur: firstly, the line length of dislocations increases which gives additional contribution to forest hardening, and secondly, stronger tangles develop progressively which impose increasing resistance to the dislocation movement and act to support more dislocation loops that give rise to additional back stress. This implies that the back stress, like the forest hardening contribution, is related to the total dislocation density.

The observed temperature independence of the BEP for Armco iron and Niobium suggests that, in single-phase bcc materials, the ratio between back stress and forest hardening contribution is independent of dislocation arrangement, i.e., C in Eq. (7) is independent of both forward strain and deformation temperature. The temperature independence of the B.E. was also observed by Woolley (1953) in a wide range of fcc and bcc metals. A possible explanation can be given as follows: during plastic deformation at 298°K dislocation tangles are formed and act as obstacles of increasing strength. However, mechanisms of plastic relaxation, such as cross



slip of shear loops, which tends to lower elastic back stresses supported by the tangles, are more favourable at this temperature because such mechanisms are thermally activated. Now, in case of deformation at 195°K the formation of tangles is less pronounced, but plastic relaxation is more difficult. Thus, the maximum number of dislocations held-up by a single barrier at a certain applied stress is larger at the lower temperature. Stroh (1955), for example, argues that as the temperature of deformation is lowered the time of relaxation of internal stresses at obstacles becomes larger.

According to this view, it can be seen that additional back stresses are not necessarily associated with the presence of dislocation tangles or cell walls. Thus, in single-phase bcc materials, the back stress and the forest hardening contribution are proportional to each other and independent of the arrangement of dislocations.

It should be emphasised, at this point, that the Stacking Fault Energy (SFE) has a major effect on the ability of the material to produce reversible deformation. In general, the B.E. is larger in low SFE materials. A comparison of back stresses in Brass and Copper, calculated from data of Kishi and Gokyu (1972), is given in Fig. 8 as a function of forward shear strain (γ). It can be



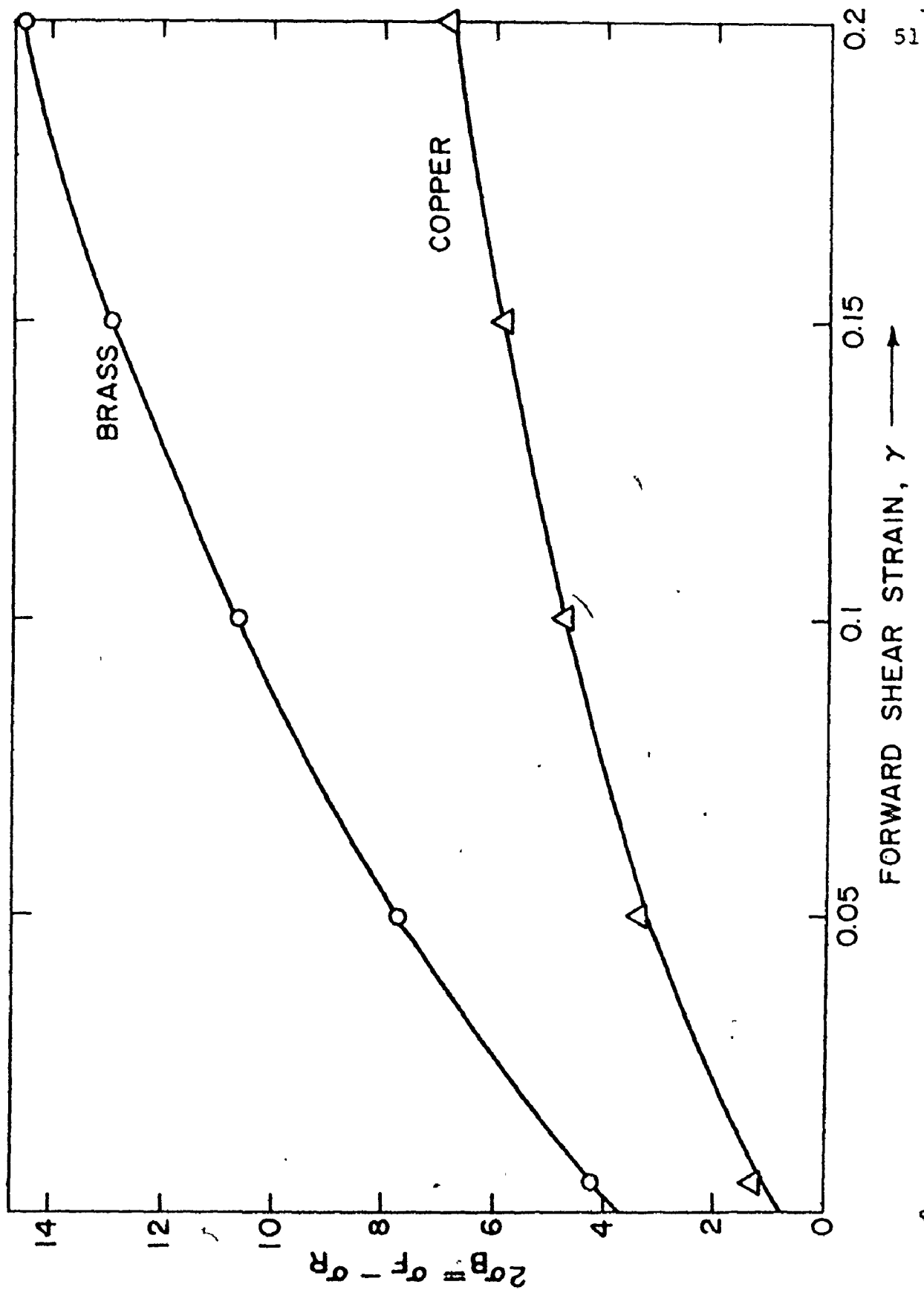



Fig. 8: Effect of forward strain on the back stress in Brass and Copper

clearly seen that, as deformation proceeds, much larger values of back stresses develop progressively in Brass (low SFE) compared to Copper (high SFE). This is probably because grain boundaries, in low SFE materials, may act as a major source for back stresses. Similar results were found by Abel and Muir (1972) in fcc materials.

(5.3) The BEP in Steels Containing Strong Particles

In general, the magnitude of the BEP should be much higher in a material strengthened by rigid nondeforming particles than by dislocation tangles, because the stress needed to promote plastic relaxation will be higher in the vicinity of a rigid particle than at a tangle or cell wall. Data of Fig. 6, for example, show a BEP of ~ 0.12 for Armco iron compared to ~ 0.8 for a pearlitic steel containing 0.15 volume fraction of cementite particles.

Brown and Stobbs (1971) have pointed out that, as plastic deformation proceeds the particles are increasingly elastically deformed to provide the locally high stresses for the relaxation process and a strong plastic zone containing a high density of secondary dislocations builds up in the neighbourhood of the particles. The presence of such a plastic zone contributes, not only to forest hardening, but also acts to prevent full plastic relaxation



and gives rise to a localized elastic stress field with its accompanying image stress which acts as a back stress.

Results obtained in a range of steels containing different volume fractions of carbide particles (Fig. 6) show that the BEP is independent of the amount of forward strain, i.e., back stress is proportional to forest hardening. This can be rationalized in the following way: Brown and Stobbs' (1971) treatment to the problem of hard spherical particles in a soft matrix predicts values for σ_B and σ_{for} in the form

$$\sigma_B = \left(\frac{8\pi b}{\alpha^2 \epsilon_p R} \right)^{\frac{1}{8}} \alpha \mu f \sqrt{\frac{8b\epsilon_p}{\pi R}} \quad (8)$$

$$\sigma_{for} = \sqrt{3} \alpha \mu f^{1/2} \sqrt{\frac{8b\epsilon_p}{\pi R}} \quad (9)$$

where α is a constant ($\frac{1}{3} \sim \frac{1}{5}$), b is the Burger's vector, ϵ_p is the symmetrical plastic shear strain, R is the particle radius and the term $(8\pi b/\alpha^2 \epsilon_p R)^{1/8}$ is in the order of 1 - 1.4. Substituting for σ_B and σ_{for} from Eqs. (8) and (9) in Eq. (4) gives

$$BEP = \frac{2\sigma_B}{\sigma_{for} + \sigma_B} \approx \frac{f^{1/2}}{C_1 + C_2 f^{1/2}} \quad (10)$$

or

$$\frac{1}{BEP} = C_2 + \frac{C_1}{f^{1/2}} \quad (10a)$$

where C_1 and C_2 (calculated for values of $\alpha = 0.3$, $\epsilon_p = 0.1$, and $R/b = 500$) are in the order of 0.62 and 0.5 respectively. The ratio between back stress and forest hardening contribution can be written as

$$\frac{\sigma_B}{\sigma_{for}} = C_3 f^{1/2} \quad (11)$$

where C_3 is in the order of 0.7 to 0.9 for spherical particles.

Equations (10) and (11) demonstrate two important features: firstly, Eq. (10) shows that the BEP is independent of forward strain as observed experimentally in this work. It also predicts a linear relationship between $\frac{1}{BEP}$ and $\frac{1}{f^{1/2}}$, and secondly, Eq. (11) predicts a ratio between back stress and forest hardening contribution of about 0.7 to 0.9 $f^{1/2}$ during plastic deformation of two-phase materials containing hard spherical particles.

In order to examine the validity of Eqs. (10) and (11) for the structures investigated, data from Table 3 were analyzed and results are shown in Figs. 9 and 10. Two observations emerge from Fig. 9: firstly, a linear relationship between $\frac{1}{BEP}$ and $\frac{1}{f^{1/2}}$ in the form of Eq. (10a) can be seen for steels containing nonspherical particles of roughly the same lamellar shape. Values of C_1 and C_2 are found to be 0.35 and 0.4 respectively. Secondly, with $C_1 = 0.62$ and $C_2 = 0.5$ (as predicted from Brown and Stobbs'

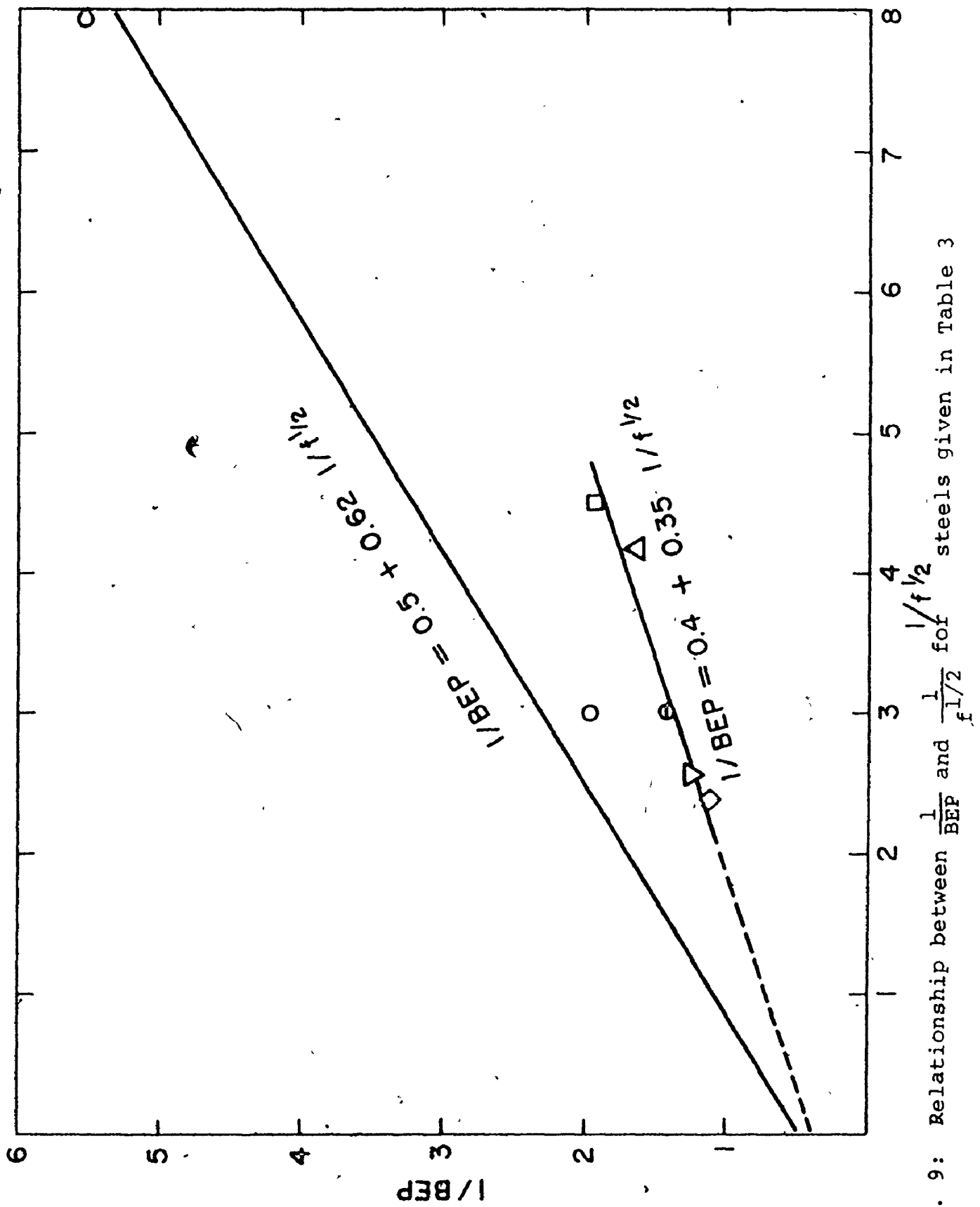


Fig. 9: Relationship between $\frac{1}{BEP}$ and $\frac{1}{f^{1/2}}$ for steels given in Table 3

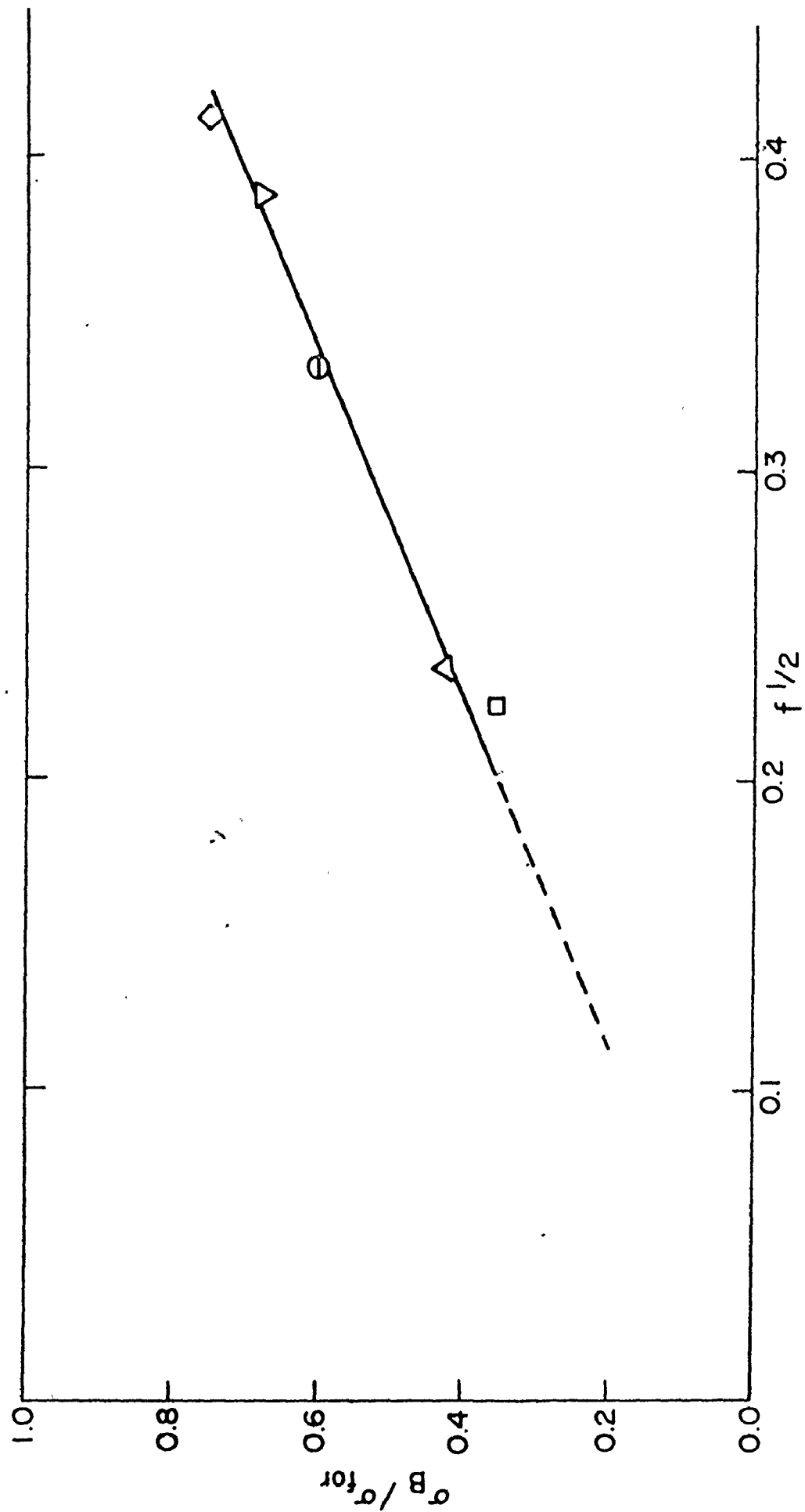


Fig. 10: Relationship between σ_B / σ_{for} and $f^{1/2}$ for various steels given in Table 3

treatment) Eq. (10a) seemed to be valid for steels containing spheroidized particles.

Thus, Fig. 9 demonstrates the importance of particle shape in studying the reverse flow in two-phase materials as indicated by Tanaka and Mori (1970). Values of BEP calculated from Wilson's data (1965), for example, show that the BEP increases from 0.55, in carbon steel ($f = 0.11$) containing spheroidized particles, to 0.86 in the same steel containing lamellar particles.

The ratio $\sigma_B/\sigma_{\text{for}}$ is plotted in Fig. 10 as a function of $f^{1/2}$ and a linear relationship in the form of Eq. (11) is found but with $C_3 = 1.8$. Thus, the ratio of back stress to forest hardening contribution, during unidirectional straining of steels containing lamellar carbide particles, is almost twice that value for steels containing spherical carbides.

It becomes clear from the foregoing discussion that the results obtained, in a wide range of two-phase iron-based alloys, confirm the general validity of Brown and Stobbs' treatment and emphasize the importance of particle shape in characterizing work hardening in the structures examined.

Recently, Kishi and Gokya (1973) have carried out a series of reversible torsion tests on a range of carbon steels and found that the back stress can be related to the forward plastic strain (ϵ_p) through an empirical power relationship in the form

$$\sigma_B = K_1 \epsilon_p^m \quad (12)$$

where K_1 and m are characteristic constants of a given material.

It is interesting to note that such relationship can be reached directly from the observed strain independence of the BEP. Also, their experimentally calculated values of m for a wide range of steels (from 0.1 to 0.9% carbon) lie between 0.44 and 0.55. Comparing these values with the value $m = 0.5$, quoted from Brown and Stobbs' treatment and used in this investigation, a good agreement can be seen.

(5.4) Summary and Conclusions

The Bauschinger effect provides a mechanism for studying the dislocation accumulation process in materials. The present investigation had two aspects: the study of the influence of dislocation distribution on the magnitude of the Bauschinger effect in single-phase bcc materials, and the study of the Bauschinger effect in two-phase iron-based alloys as a function of both forward strain and volume fraction of second-phase particles.

The Bauschinger effect has been explained in terms of the unrelaxed back stresses which build up in the material due to local inhomogeneity. A Bauschinger effect parameter (BEP) (defined as the reversible fraction of work hardening)

was used to account for the effect in the materials examined. The most significant results have been summarized in Section (5.1). The increased understanding of the process of reverse flow, which evolves from these observations, had led to the formulation of two new basic concepts of the deformation process in bcc materials:

(1) In single-phase bcc materials, as deformation proceeds, the back stress rises in proportion to the forest hardening contribution, independent of the temperature of deformation, i.e., the back stress and the forest hardening contribution are proportional to each other and independent of the arrangement of dislocations.

(2) In both single-phase and two-phase bcc materials, the ratio between back stress and forest hardening contribution is independent of the amount of forward strain but increases with increasing volume fraction of second-phase particles.

CHAPTER III

FATIGUE SOFTENING IN LOW-CARBON IRON

SECTION (1)

OBJECTIVES

One of the important processes in fatigue is the establishment of a microstructure in which localized plasticity and fracture can occur. The establishment of this microstructure involves changes in the character of the response as fatigue proceeds.

During cyclic straining, materials may harden or soften depending upon their prior thermomechanical history. Initially soft or annealed materials, usually, exhibit hardening under cyclic straining. This process of fatigue hardening is characterized by a rapid hardening stage, usually observed during the first few percentage of life, followed by a saturation stage, where almost no hardening is observed. Cyclic hardening is quite different from uniaxial hardening (where deformation occurs in one direction only, as in an ordinary tension test). Under the latter conditions, hardening increases monotonically (except at high temp.) such that no saturation takes place. The rate of cyclic hardening depends on the applied strain amplitude but, in general, is lower than that of uniaxial work hardening (Shinozaki and Embury 1969). On the other hand, initially cold worked materials, usually soften under subsequent cyclic straining. This process is characterized by a period of rapid softening,

followed by a leveling off or saturation of the effect. Materials of high stacking fault energy were found to attain the same saturation stress level in both hardening and softening, when subjected to the same controlled cyclic strain.

The process of cyclic hardening has been thoroughly examined and reported for many metals and alloys, although, to date, no adequate theoretical treatment is available. However, there is less information in the literature on the process of fatigue softening of prestrained materials, specially the microstructural aspects of this process in bcc metals. The present investigation deals particularly with the phenomena of fatigue softening in low carbon polycrystalline iron. This material was chosen because of the extensive literature on the dislocation arrangements produced by tensile straining at various temperatures, and because the concepts developed in such a model system can be readily extended to materials of current technological interest.

The study had two main objectives: first, an attempt was made to characterize, from a microstructural viewpoint, the changes occurring in single-phase bcc materials during cyclic softening, i.e., changes in dislocation arrangements, the scale of substructure, etc.; and second, to delineate the microstructural features which control the rate and extent of fatigue softening. This may be useful from the viewpoint of alloy design particularly in regard to the utilization of thermo-mechanical treatments for strengthening.

In order to accomplish these objectives, a variety of experiments were performed to study the following:

(1) The Overall Response. This was achieved by: studying the mechanical response in uniaxial tension prior to fatigue, following the fatigue response under controlled cyclic strain, and comparing, on a macroscopic scale, the uniaxially deformed structure with the fatigue softened structure. For such comparison, a back reflection X-ray experiment was conducted before and after cyclic softening.

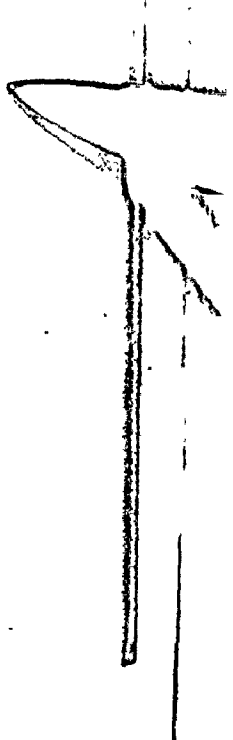
(2) The Detailed Response, in terms of dislocation arrangements. Such a study is complicated in bcc metals because dislocation arrangements vary with temperature of deformation, strain rate, and presence of solute atoms. Thus, a series of decarburized iron specimens were prestrained at different temperatures to establish different arrangements of dislocation substructure for the process of fatigue softening. Also, specimens of Armco iron were prestrained at the dynamic strain ageing temperature to study the effect of induced microstructure on subsequent cyclic straining.

Transmission electron microscopy was performed before fatigue, as well as after different stages of cyclic softening, in order to

provide a detailed characterization of the microstructure.

(3) A Comparison Between Thermal Recovery and Fatigue Softening Processes. The removal of the strength increment due to work hardening, by subsequent fatigue suggests that, it would be useful to compare this process with the thermal recovery of prestrained specimens. Thus, a limited range of experiments on thermal recovery were conducted to make such comparison.

Finally, in an attempt to rationalize the kinetics of softening, simple models were developed and are described in the final section of this chapter.



SECTION (2)

LITERATURE REVIEW

The study of the deformation of bcc metals is made difficult by the variability of slip systems, the pronounced effects of certain solutes (particularly interstitials), and the strong dependence of the flow stress on temperature and strain rate.

In dealing with a complex phenomena like the removal of work hardening increment by subsequent fatigue, it is unnecessary to attempt a complete review of all work concerning work hardening and fatigue softening in bcc materials. Thus, for reasons of brevity, reference is made to more general reviews (Nabarro et al. 1964, Christian 1970) on dealing with mechanical and structural aspects of work hardening in these materials. In the present study, some specific works of special importance to the problem under investigation will be reviewed.


(2.1) Effect of Deformation Temperature on Dislocation
Distribution

Transmission electron microscopy investigations on deformed iron have revealed that: although there is essentially no temperature dependence for the overall

density of dislocations at a given strain (except in the dynamic strain ageing region), there is a marked temperature dependence for the distribution of dislocations. The strain only determines the dislocation density of a given material, but the distribution of dislocations becomes more uniform as the temperature of straining decreases.

During deformation of iron at room temperature tangles of dislocations and cell walls are usually observed (Keh and Weissmann 1963). The majority of dislocations are arranged in complex cell walls separated by regions of low dislocation density. Lowering the temperature of deformation, decreases the tendency of cell formation and most of the dislocations are distributed uniformly throughout the matrix.

Arsenault and Lawley (1966) have related the dislocation distribution to the associated thermal stress component (τ^*) of the flow stress. They found that, when Niobium single crystals were deformed at temperatures where τ^* is nearly zero, a complex dislocation network and tangle structure were developed. They also found that samples deformed to the same strain but at lower temperature (larger τ^*) tend to develop a uniform substructure which was dominated by straight screw segments of dislocations. Similar observations were reported by Orava et al. (1968) and Schankula (1970) on polycrystalline iron. Arsenault and



Lawley have attributed the observed predominance of screw dislocations to the difference in mobilities of edge and screw components as a result of difference in Peierl's stress associated with each component at low temperature. Since deformation at low temperature is associated with large thermal stress component, a small variation in the internal stress would not act as barrier to the edge component. Thus, edge components would move out of the sample rapidly leaving behind straight screw segments. Embury (1971) has, also, indicated that when the amplitude of the thermal stress needed to overcome lattice obstacles is large, it will prevent dislocations from grouping in tangles or cell walls and the probability of dislocations becoming uniformly distributed in the matrix is increased. Thus, by increasing the temperature, dislocations will move easily between interactions with other dislocations and will spend most of their time in the vicinity of other dislocations. By further deformation, dislocation multiplication takes place and dislocations tend to aggregate into groups. This will result in exceedingly non-uniform distributions. Figure 11 illustrates schematically the above viewpoint.

From the foregoing it can be seen that deformation at low temperature is associated with a larger component of thermal stress, and a lower mobility of screw dislocations which result in uniform distribution of screw segments of dislocations. On the other hand, deformation at higher

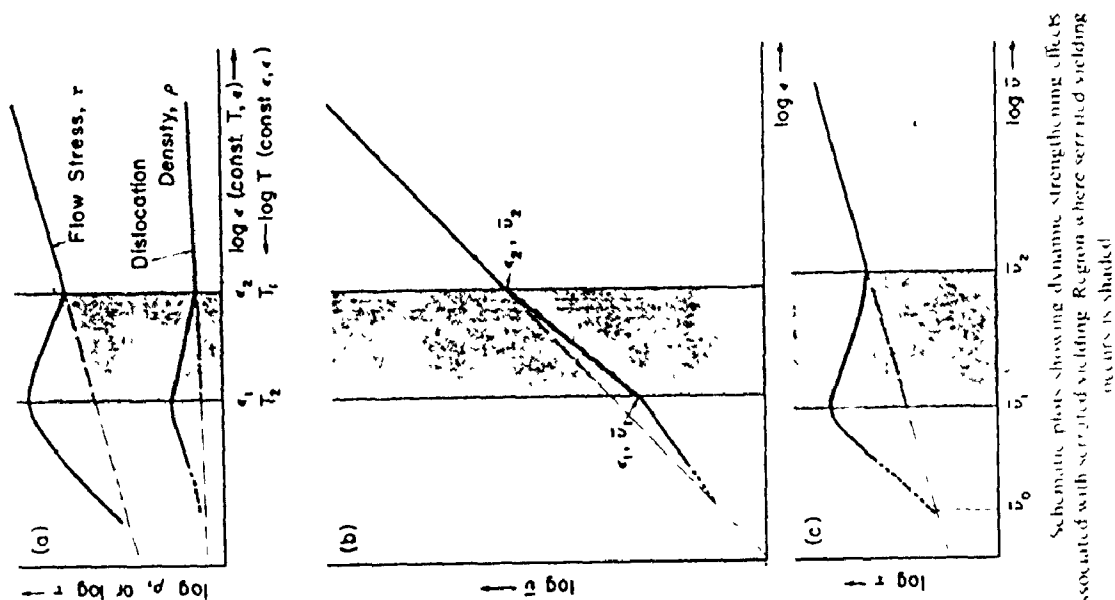
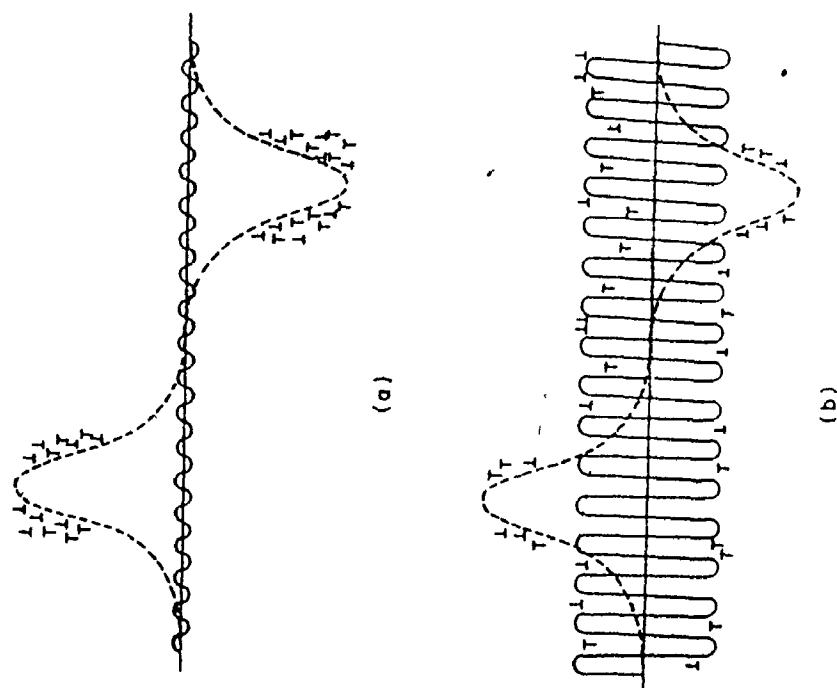
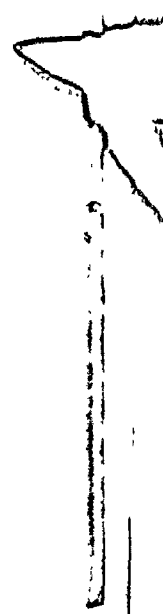


Fig. 12: (After Wilcox and Rosenfield (1971))



A schematic diagram illustrating the effect of (a) a low amplitude periodic frictional stress, and (b) a high amplitude periodic frictional stress on the distribution of dislocations during deformation. The frictional stress is represented by the solid lines and the internal stress distribution associated with the substructure by the broken lines

Fig. 11: (After Embury (1971))



temperature is associated with a smaller thermal stress which leads to a non-uniform structure of tangles and cell walls.

(2.2) Effect of Dynamic Strain Ageing

Dynamic strain ageing is important from the viewpoint of utilizing interstitial solutes in bcc metals to "stabilize" the cold worked state. It is commonly assumed that a dynamic strengthening process is associated with the phenomena of the Portevin-Le Chatelier effect (i.e., serrated stress-strain curves), which depends on the strain rate and temperature of deformation. The observed serrations during dynamic strain ageing suggest that deformation is non-uniform under these conditions. This was interpreted by Sleeswyk (1958) in terms of the dynamic instability of plastic flow. However, to account for the general increase in work hardening rate observed during serrated flow, Simon et al. (1964) have suggested that some general homogeneous deformation must occur in addition to plastic localization.

The work of Edington and Smallman (1964), Baird and MacKenzie (1964), and Wilcox and Rosenfield (1966) has revealed two important features of the deformation process under conditions of dynamic strain ageing: first, at a given

strain (ϵ), both the dislocation density (ρ) and flow stress (τ) decrease with increasing either strain rate ($\dot{\epsilon}$) or deformation temperature (T), and second, the average distance travelled by dislocations (mean free path) is decreased during serrated flow. Wilcox and Rosenfield (1966) have shown that when serrated flow occurs, there exists an instability in the average dislocation velocity (\bar{V}) - stress relationship (Fig. 12) which leads to negative values of $\partial \log \tau / \partial \log \bar{V}$ and consequently a negative strain rate sensitivity* (r). Figure 12 predicts, also, the following relations in the dynamic strain ageing region

$$(\partial \log \rho / \partial \log \dot{\epsilon})_{\epsilon, T} < 0 ,$$

$$-(\partial \log \rho / \partial \log T)_{\epsilon, \dot{\epsilon}} > 0 ,$$

$$(\partial \log \tau / \partial \log \dot{\epsilon})_{\epsilon, T} < 0 ,$$

and

$$(\partial \log \tau / \partial \log T)_{\epsilon, \dot{\epsilon}} > 0 .$$

* $r = (\partial \log \tau / \partial \log \dot{\epsilon})_{\epsilon, T}$ and $\dot{\epsilon} = \rho b \bar{V}$ where ρ is the mobile dislocation density and b is the burgers vector.

The observed stress peaks associated with dynamic strain ageing can be attributed to: a drag stress due to segregation of solute atmospheres to moving dislocations which assists in impeding dislocation motion, plus a stress increment due to enhanced work hardening rate. Wilcox and Rosenfield have pointed out that at very low strains ($< 0.2\%$) the stress peaks are mainly due to the drag stress, but as deformation proceeds the stress increment due to enhanced work hardening increases continuously with strain and gives rise to increasing peak height.

Keh et al. (1968) have observed that the rate of dislocation multiplication in low carbon iron at dynamic strain ageing is about 3 times greater than that observed at room temperature. Electron microscopic observations of Edington and Smallman (1964) show that the increased rate of dislocation multiplication during dynamic strain ageing gives rise to a fine uniform dispersion of dislocations rather than a cell structure.

(2.3) Cyclic Strain Softening

Cold working has long been recognized as one of the important strengthening mechanisms in metals and alloys. Attempts to improve fatigue properties by cold working are hindered by the phenomenon of cyclic softening. A rapid

decrease in the flow stress of prestrained materials are usually observed during subsequent cyclic straining (Coffin and Read 1956, Morrow 1965).

This phenomenon of cyclic softening was defined by Forsyth and Stubbington (1961) as structural instability. Wood (1962) has indicated that a considerable part of internal stresses, introduced into aluminium specimens by uniaxial tension, is unstable under subsequent cyclic straining. He observed a rapid decrease in the tensile flow stress but a relatively little change in the reverse proof stress as cycling proceeds, so that both stresses converge quickly to a common symmetrical value. He argued that cycling disperses the initial asymmetry of internal stresses so that a state of symmetrical stresses will develop. Such a state is associated with an intrinsic strain hardening which is stable and independent of direction of strain.

Wood's argument is based on the phenomena of the Bauschinger effect, i.e., if the metal is prestrained in one direction, it will have a lower "proof" stress in the reverse direction (see also Chapter II). This argument is supported by Huggard's (1970) observation in copper single crystals which shows that the Bauschinger effect induced by prestrain could be reduced by cyclic softening. Embury (1971) has suggested that this is probably because reverse deformation disperses any piled up groups of dislocations of like sign from the cell walls.

A number of experiments have been advanced to study changes associated with cyclic straining as compared with uniaxial deformation. Clarebrough et al. (1957) have compared the released stored energy for unidirectionally and cyclically deformed copper at low annealing temperatures. They found that the stored energy associated with the recovery of fatigued structure is much smaller than that associated with uniaxially deformed structure. Other changes associated with cyclic strain softening include a sharpening of Debye-Sherrer X-ray reflections and an increase in temperature required for complete recrystallization (Kemsley 1958).

The above macroscopic observations suggest that the structure developed by cyclic straining is in a lower energy state compared with that developed by uniaxial tension.

Many other characteristic features of the fatigued structure have been revealed by transmission electron microscopy. Feltner and Laird's (1967) detailed investigation on high stacking fault energy materials showed that cell boundaries of the fatigued structure consist mainly of twist boundaries in addition to some tilt and mixed networks. Very small misorientations were associated with the cell boundaries, which may suggest that such boundaries are comprised mainly of dislocation dipoles. Huggard (1970) observed the production of dipoles and the conversion of primary dislocations into dipoles during cyclic softening

of prestrained copper single crystals. These observations imply that dislocations produced by uniaxial deformation are originally in high energy configurations and undergo rearrangement to a lower energy configuration during cyclic straining.

Feltner and Laird (1967) have argued that fatigue softening will only occur if the equilibrium cell size reached at saturation is larger than that existing in the prestrained material. Thus, fatigue softening may be achieved by dislocation annihilation, rearrangement of dislocations, or by dipole formation.

The mode of slip and cyclic plastic strain amplitude were found to have pronounced influence on the induced fatigued structure in metals and alloys. The detailed microstructural analysis of Feltner and Laird (1967) demonstrates such influence. Wavy slip mode materials were found to develop dislocation debris of dipoles when subjected to low cyclic strain amplitude. However, at higher amplitudes cell structure was observed in these materials. On the other hand, when the slip character was planar, the substructure consisted, primarily, of debris of multipoles at low cyclic strain amplitudes but uniform distributions of dislocations at higher amplitudes.

Similar observations were reported by Klesnil and Lukás (1965), McGrath and Bratina (1965), and Wei and Baker

(1965) on cyclic hardening of iron.

The influence of temperature on fatigued structure of polycrystalline copper was studied by Pratt (1967). She observed that the cyclic cell size developed at 78°K is smaller than that developed at 295°K. However, the basic dislocation arrangements in the cell boundaries appeared to be similar at both temperatures.

(2.4) Cyclic Saturation Behaviour

The saturation stage after either cyclic softening or hardening is characterized by a "steady state" cyclic stress-strain curves and stabilized hysteresis loops.

Results of Feltner and Laird (1967) on copper indicate that the strain rate sensitivity of both fatigue softened and hardened structures are the same for equal values of stress and strain. Kemsley (1958) has, also, shown that the saturation stresses of both fatigue hardened and fatigue softened specimens of copper are identical functions of the temperature of subsequent anneal. These observations, together with the microstructural features at saturation, have led Feltner and Laird to suggest that a wavy slip mode material would attain identical cell sizes and cell wall structures, in both cyclic hardening and softening, at saturation, if tested under similar conditions of temperature and cyclic strain amplitude.

The fact that stabilized hysteresis loops are observed at saturation suggests that the dislocation structure undergoes only minor changes during one cycle and virtually no net change from cycle to cycle. Results of Halford (1966) on the stored energy changes during cyclic straining of copper supports this view. He has shown that there is a storage-release-storage-release of energy as a stable hysteresis loop is traversed but the net stored energy change in a complete cycle is zero. This observation also indicates that there is no net change in dislocation density during the saturation stage.

A number of models have been proposed to explain the steady state behaviour under cyclic straining. Alden (1962) suggested that saturation may result from some sort of balance between hardening and softening similar to the "dynamic recovery" process observed during Stage III in uniaxial deformation. Thus, the large accumulated plastic strain at saturation presumably would allow the eventual establishment of a dynamic balance between annihilation and formation of dislocations. Cross-slipping of screw dislocations was suggested as a mechanism for annihilation.

There has been at least two objections to Alden's argument: first, if such argument is correct, the saturation stress should exhibit the same temperature dependence as that for Stage III in uniaxial deformation.

Broom and Ham (1957) and Wadsworth and Hutchings (1964) showed that the temperature dependence of the flow stress of copper after fatigue was very much greater than after tensile straining, suggesting point defect contribution in fatigue. Moreover, Kocks et al. (1966) indicated that if true stress were plotted against strain, during Stage III in uniaxial deformation, the stress level will not reach "saturation" (like the case in fatigue) but instead will continue to increase with strain. Second, Alden's model was inadequate to explain the saturation behaviour in low stacking fault energy materials where cross slipping of dislocations is less favourable.

Avery and Backofen (1963) suggested an alternative model applicable to low stacking fault energy materials. They proposed that reversible plastic strain due to dislocation bowing back and forth may contribute importantly to the establishment of saturation. According to this view, saturation may set in if the reversible plastic strain becomes increasingly large relative to the total strain as cycling progresses. In the limit if all the plastic strain were reversible, the net hardening should go to zero.

Feltner (1965) has argued that unless some hardening mechanism is involved in Avery and Backofen's model, bowing dislocations should relax along the same stress-strain curve along which bowing occurred and consequently no hysteresis

loops should be produced. Feltner, instead, suggested another model for saturation under low cyclic strain amplitudes in which an attempt was made to relate the mechanical behaviour directly to the observed microstructure. In this model, the strain is derived from the flip-flop motion of elongated prismatic loops (dipoles) and the saturation flow stress is developed by the resistance of these dipoles to flipping. The response of the loop to reverse cyclic stress is to flip from one equilibrium position to the other.

Feltner's model is based on the observations that most of the defects produced during low amplitude cyclic hardening are in the form of prismatic dislocation loops. It requires that the density of dislocations and the scale of cell structure should stay constant during saturation stage.

Watt (1967) showed that the flipping mechanism can only produce a very small amount of strain, thus, cannot account for the total imposed strain amplitude. Moreover, it does not take into consideration the role of persistent slip bands (PS bands), usually associated with the saturation state. (The role of PS bands will be discussed with more details in Chapter IV dealing with instability of plastic flow during cyclic deformation.)

Feltner and Laird (1967) have developed another model to account for saturation behaviour under high

amplitude fatigue. According to this model, the saturation stress is controlled by the reaction of free mesh lengths of dislocations (ℓ') at the cell wall, against bowing out. The stress required to bow out a length of dislocation ℓ' beyond its critical radius was found to have the same order of magnitude as the saturation stress. Thus, a loop will be emitted from a link ℓ' , and can move freely through the clear volume between cell walls. Segments of the loop will experience both attractive and repulsive interactions as they enter the stress fields of the cell walls, as well as destruction by annihilations. The attractive interactions and annihilations entangle the loop in the walls and its free mesh length is again about ℓ' . The process repeats itself when the stress is reversed. This model was found to apply for both wavy and planar slip mode materials.

(2.5) Factor Influencing the Cyclic Saturation State

The salient factors which may influence the saturation stress level in materials are:

slip mode of the material,
testing temperatures,
cyclic strain amplitude,

cyclic strain rate, and
grain size of the material.

Feltner and Laird (1967) have predicted that the cyclic saturation stress response of wavy slip mode materials, (i.e., high SFE materials such as copper and iron) is independent of the material history. Results reported by Ham and Broom (1962) on single crystals of copper, and by Coffin (1967) on a wide range of ferrous and non-ferrous materials support this prediction. On the other hand, the saturation stress response of planar slip mode materials (i.e., low SFE materials such as Cu-7.5% Al and Fe-3% Si) was found to depend markedly on the initial pre-cyclic state of the material.

From results obtained in a wide range of materials, Feltner and Laird (1969) have concluded that: wavy slip mode materials would have a unique saturation stress (i.e., reach the same saturation stress level in both hardening and softening) where as planar slip mode materials would not.

The influence of temperature on the cyclic saturation stress was studied by Pratt (1967) on polycrystalline copper and aluminium. She observed that the saturation stress level of specimens fatigued at 78°K was higher than that of specimens fatigued at room temperature. The increase in saturation stress was associated with a decrease in cell size.

An inverse relationship between saturation stress and cell size was found to hold for both temperatures, providing the temperature dependence of rigidity modulus is taken into account. Pratt, also, found that the saturation cell size is reversible, i.e., by changing strain amplitude, cell size changes from one size to the other and back to the first: Temperature was found to have no effect on the uniqueness of cyclic saturation stress response in wavy slip mode materials.

The cyclic plastic strain amplitude was found to have a pronounced effect on the saturation stress level. Increasing the cyclic strain amplitude has the effect of raising the saturation stress level. A power relationship in the form: $\sigma_s = \sigma_c (\Delta \epsilon_p / 2)^n$ was found, by Feltner and Laird (1967), to hold for copper specimens fatigued at 78°K. (σ_s = saturation stress, $\frac{\Delta \epsilon_p}{2}$ = plastic strain amplitude, σ_c = strength coefficient and n = cyclic strain hardening exponent).

Grain size was found to have a negligible effect on the saturation stress in copper, however, an appreciable effect was observed in the low stacking fault energy Cu-7.5% Al (Feltner and Laird 1967).

The influence of deformation rate on saturation stress was studied by Abdel-Raouf and Plumtree (1971) in polycrystalline iron. They have shown that increasing the

cyclic frequency has the effect of raising the saturation stress level and decreasing the associated cell size.

SECTION (3)

EXPERIMENTAL DETAILS(3.1) Introduction

An important aspect of this work was to delineate the microstructural features which control the rate and extent of fatigue softening. With this objective in mind, the experimental scheme was carried on as follows:

- (a) Materials were swaged, machined and annealed before mechanical testing.
- (b) Polished specimens were pulled in tension at three temperatures; 195, 298, and 473°K in order to start the fatigue process with different dislocation arrangements.
- (c) Prestrained specimens were fatigued in tension-compression under controlled stroke amplitude, and their cyclic stress response was measured.
- (d) Electron microscopy investigations were performed after both tensile and fatigue testing in order to correlate the mechanical response to the microstructural changes.

- (e) Back reflection X-ray Laue patterns were obtained from coarse grained specimens in an attempt to compare the macroscopic lattice distortions associated with uniaxially deformed structure with those developed after subsequent fatigue softening.
- (f) A range of recovery anneals were, also, performed before and after fatigue softening.

(3.2) Material Preparation

(a) Decarburised Ferrovac-E

Specimens were produced from one inch diameter rods obtained through Crucible Steel Company. The carbon and oxygen contents of the original composition were 120 ppm and 60 ppm respectively. The Ferrovac-E rods were reduced from the bulk by swaging to 1/2 inch diameter rods from which the material was machined to fatigue specimens (Fig. 13 (a) of the dimensions 1/4 inch diameter and 1/2 inch gauge length in order to minimize buckling during fatigue.

To obtain the desired grain size, the material was annealed at 900°C in a vacuum furnace (10^{-5} torr) for 2 hours. The grain size determination was made by the linear intercept method. Six different traces were made in the

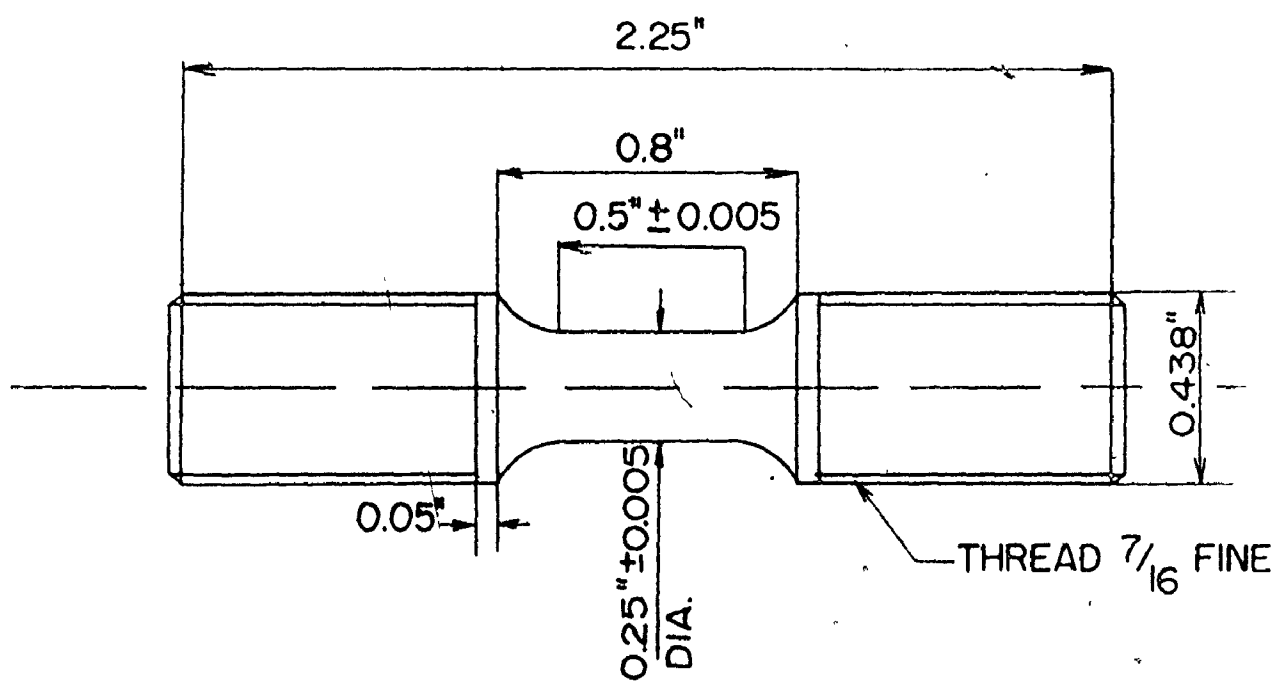
FATIGUE SPECIMEN

Fig. 13(a)

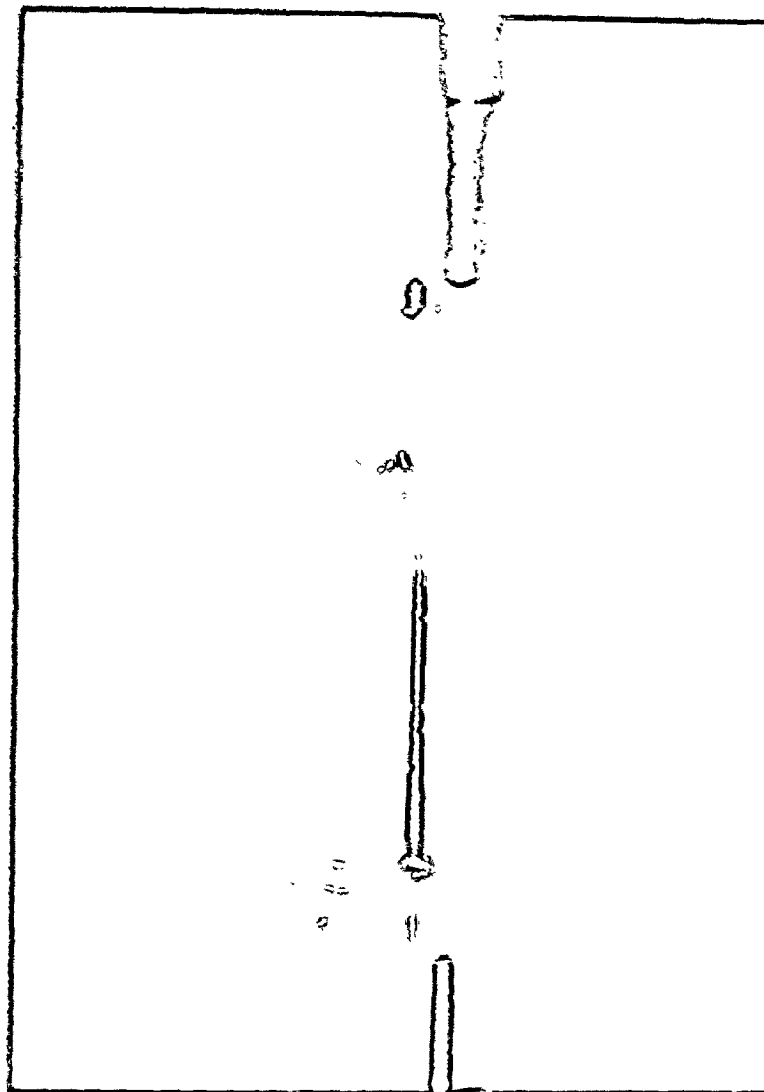


Fig. 13(b)

THE FATIGUE GRIPPING SYSTEM

horizontal and vertical directions across the total section of the specimen, in order to obtain a representative grain size. The results were then averaged to express the mean grain size. The average grain size obtained was 50 μ .

Some coarse grained specimens were prepared for the X-ray experiment using a strain-anneal technique in which specimens were given 3% tensile plastic strain, followed by 20 hours anneal at 1050°C. A uniform grain size (0.3 mm average) was obtained by this method.

In order to remove the large yield drop and the Lüders elongation which complicate the mechanical behaviour, the Ferrovac-E specimens were decarburised in wet hydrogen at 650°C for 72 hours, followed by 48 hours in dry hydrogen. There was no change in grain size as a result of the decarburising treatment. The carbon and oxygen contents after decarburisation were 50 and 60 ppm respectively.

Note: When specimens were decarburised in wet hydrogen for more than 90 hours, grain boundary embrittlement was observed due to the relatively high oxygen content in the original material. For further details, see McMahon (1966), Low (1969) and Papzian and Beshers (1971). This difficulty was eliminated by shortening the time of decarburisation to 72 hours, controlling the hydrogen flow rate and by increasing the time of flow of dry hydrogen to 48 hours.

(b) Armco Iron

Armco iron was supplied by Corey Steel Co. of Chicago, in the form of rods 0.75 inch diameter. The chemical composition is given in Table 1. Swaging, machining and annealing treatments were as described above for Ferrovac-E.


The Armco iron specimens were used to study the fatigue softening behaviour of structures developed at 473°K by uniaxial tension.

(3.3) Mechanical Testing

Prior to mechanical testing, about 0.002 inch thick of the specimen surface was removed by chemical and electrolytical polishing in order to remove any surface damage due to machining.

(3.3.1) Tensile testing

All tensile tests were performed in Universal Instron machine using a cross head speed of 0.02 inch per minute, corresponding to a strain rate of $6.7 \times 10^{-4} \text{ sec}^{-1}$. The specimens were screwed from the top to a stainless steel grip connected to the load cell through a universal joint, while the bottom of the specimens were screwed to a lower grip




connected to the movable cross head frame through a hemispherical ball joint. This assembly assured accurate alignment of the specimens in the grips and tests at different temperatures.

The testing machine was equipped with an x-y servo drive system and the strains were measured using a 1/4 inch transverse extensometer. The strain gauges were calibrated at each test temperature by imposing a fixed movement to a calibrating jig and adjusting the chart travel to give the required extension. The load weighing system was simply calibrated by hanging small weights to the upper grip and adjusting the sensitivity. The accuracy of the overall load weighing system was normally better than $\pm 0.5\%$.

Tests at 195°K were achieved by immersing the specimens in a bath of dry ice and methanol, which gave a uniform and constant temperature. Care was taken to ensure that the entire system was at constant temperature prior to the initiation of the test. Tests at 473°K were achieved by using oil bath heated by electric power and the temperature was kept constant and uniform by controlling the power supply and by using a pre-calibrated Chromel-Alumel thermocouple to detect any temperature variations.

Each specimen was maintained to within $\pm 2^{\circ}\text{C}$ of the desired temperature for 10 minutes before testing.



(3.3.2) Fatigue testing

All the fatigue tests were performed on 901-77 model of the Materials Testing System (MTS) machine, Fig. 14(a).

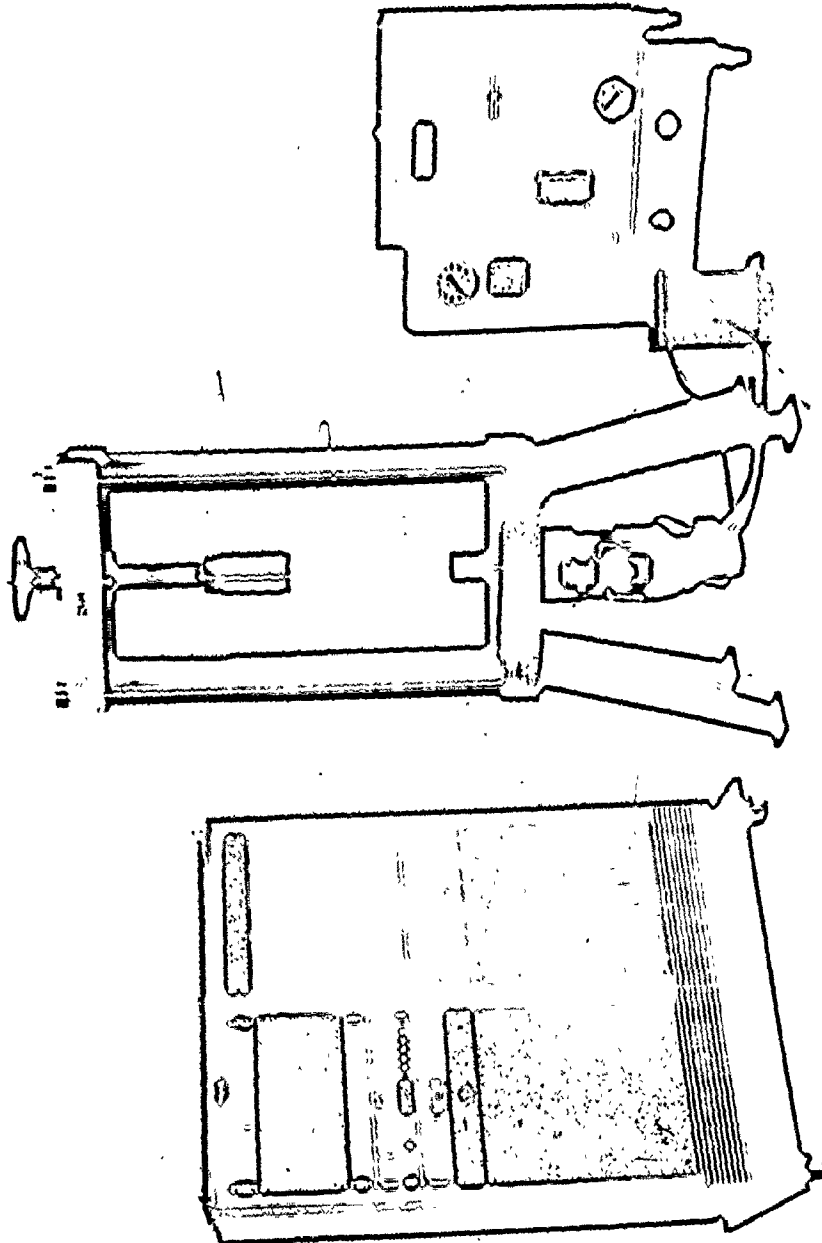
A closed-loop materials test system utilized for these tests generally involves three basic elements: a load frame, control console, and hydraulic power supply.

The load frame contains an electro-hydraulic actuator by which the force is imposed upon the specimen. The control console contains the closed-loop electronic controller, associated programmers, and read-out equipment. The hydraulic power supply, provides high-pressure fluid for activating the actuator in the load frame.

The operating mechanisms of an MTS closed-loop control system is the comparison of the desired condition of a controlled parameter, (the stroke in this work), with the actual condition of the parameter and the resultant generation of correction signals that causes the actual condition to equal the desired condition. Implementation of this idea is accomplished by using electronic signals to represent the desired condition (command), the actual condition (Feed-Back) and the correction signal (Difference). Figure 14(b) shows a simplified model of the servac control system.

A pre-set electrical signal, applied to a hydraulic actuator, operates a moving ram against a specimen attached to a moving ram, and to a fixed ram. The transducer records

FIGURE 14(a) MODEL 901.77 MATERIALS TESTING SYSTEM



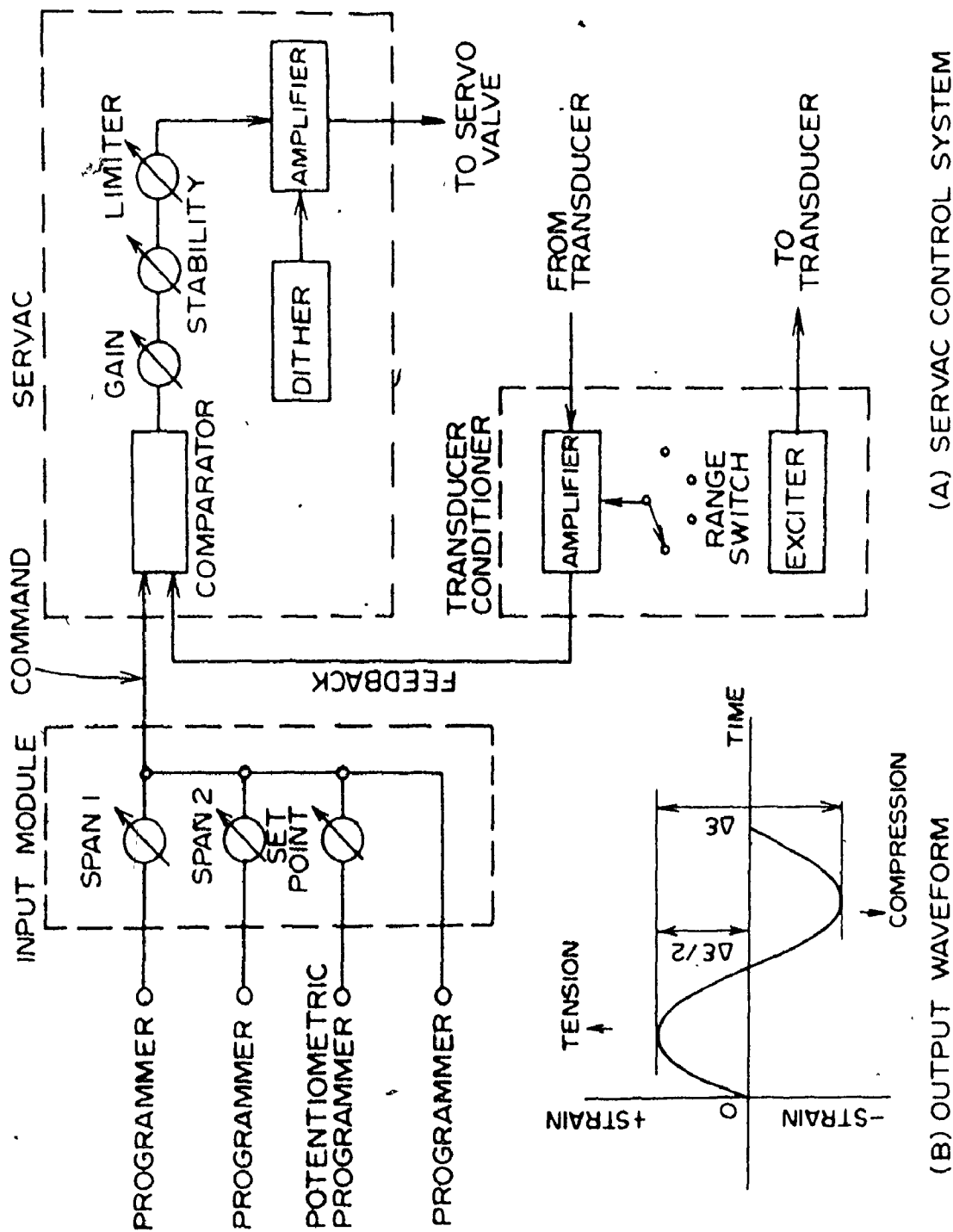



Fig. 14(b): Schematic illustration of (A) Servac Control System and (B) Output Waveform in MTS machine

the output due to the specimen or ram response, and transmits a signal to a comparator, which modifies continually the input signal to the actuator to maintain the set point.

The equipment is capable of simple sequences of programmed commands and possesses multiple output capacity for recording devices and for calibration. Error detection devices are provided. A linear variable differential transducer (L.V.D.T.) was used to monitor the movement of the ram, which for rigid systems closely approaches the total extension in the specimen. This parameter was controlled during fatigue to well within the manufacturers stated accuracy of $\pm 2\%$. For the purpose of the present investigation, the L.V.D.T. had been put at its lowest total stroke range of ± 0.25 inches. The cyclic load amplitude and the applied stroke amplitude were taken from filtered output and recorded continuously on a two-pen chart recorder with response time 0.2 sec.

Alignment of the upper and lower ram was carried out carefully by adjusting the bearings supporting the upper ram. An off-axiality of less than 0.002 inches was obtained. The misalignment was measured by a concentricity variation on a dial gauge mounted on the lower ram reading off the upper ram. The fatigue specimens were mounted in an upper rigid threaded grip bolted on the load cell, and the lower gripping fixture consisting of an internally threaded inner grip cylinder with a keyed surface, which was embedded in an outer hollow



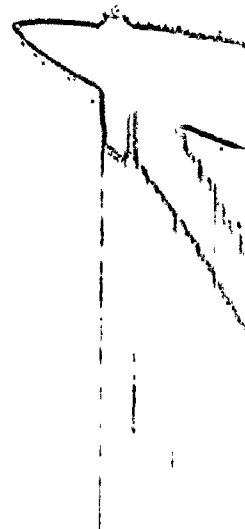
cylindrical grip with a small diametrical clearance about 0.15 inches, bolted to the moving ram (Fig. 13(b)). Woods metal was used to minimize the misalignment and was casted into the lower grip at about 90°C. Specimen cooling was effected by using precooled compressed air-blast. The surface temperature was measured by a flat thermocouple attached to the centre of the grip section of a thin specimen never exceeded 40°C.

A sinusoidal wave form supplying a tensile signal followed by a compressive signal was selected for all the fatigue tests.

The testing programme was carried out at a controlled stroke amplitude equivalent to $(\Delta\epsilon_p/2) = 0.0025$ (unless otherwise stated), where $(\Delta\epsilon_p/2)$ is the plastic strain amplitude, and the peak stresses were recorded as a function of cycles. All the fatigue tests were performed at room temperature, under a cyclic frequency of 1 cps.

(3.4) Transmission Electron Microscopy

Foils for electron microscopy were prepared in the following way: Discs of about 1/16 inch thickness were cut from the test specimens perpendicular to the tensile axis by means of a fine-toothed jeweller's saw, then mechanically polished on 200 grit Emery paper to about 0.01 inches. The mechanically thinned sections were then chemically thinned



to about 0.003 inches using a solution of 80 ml hydrogen peroxide (30%) + 15 ml distilled water + 5 ml hydrofluoric acid, maintained at a temperature of about 10°C. Final thinning was achieved electrolytically in a mixture of 10 ml perchloric acid and 90 ml acetic acid at 15°C, using DC current of 10-12 volts and current density of 150 m.amp/cm². The thinned slices were washed in acetic acid followed by dry methanol. This method was found to produce good thin foil specimens.

All foils were examined at an operating voltage of 100 KV, in a Siemens Elmiskop 1 microscope. A few observations were made using a Phillips EM300 instrument. The Siemens microscope was fitted with a double-tilt stage capable of tilts of $\pm 10^\circ$ about two perpendicular axes. The existing calibrations, for both the rotation of the image relative to the diffraction pattern and the variation of true magnification with indicated magnification, were employed during this investigation.


In an endeavour to describe representative behaviour, information was derived from as many different areas of the foil as possible, or from more than one foil, wherever possible.

(3.5) Laue Back-Reflection X-ray Photographs

The development of Laue asterism during deformation was studied using a Hilger & Watts back-reflection X-ray unit as described by Schankula (1970). A 100 μ collimator was used with unfiltered silver radiation and a specimen to film distance of 3 cm.

(3.6) Thermal Recovery

A range of recovery anneals from 360 to 470°C were performed in a molten salt bath. The specimens were wrapped in steel foil and annealed for increasing intervals of time up to 30 hours. For all the recovery tests, the bath temperature was controlled to within $\pm 4^\circ\text{C}$.



SECTION (4)

EXPERIMENTAL RESULTS(4.1) Introduction

For clarity the results are reported in 4 sections as follows:

(4.2) Overall Response: The mechanical response during cyclic softening and hardening of decarburised ferrovac-E specimens are presented. Observations of X-ray asterism obtained after tensile straining as well as after subsequent fatigue softening are included.

(4.3) Detailed Microstructural Changes: The dislocation structure developed after cyclic softening for various numbers of cycles is presented together with the characteristic features of the microstructure at saturation.

(4.4) Kinetics of Fatigue Softening: The cyclic responses of specimens prestrained in tension at different temperatures are compared in order to elucidate the effect of dislocation arrangements on rate and extent of cyclic softening.

(4.5) Thermal Recovery of Fatigued Structure: The effect of recovery treatment on various temperatures on the flow stress of both prestrained and fatigued specimens is compared.

N.B. All the fatigue tests were performed at room temperature under a cyclic frequency of 1 cps and a total strain amplitude equivalent to $(\Delta\epsilon_p/2) = 0.0025$, except where otherwise stated.

(4.2) Overall Response

Figure 15 shows cyclic flow stress as a function of number of cycles for initially annealed and initially prestrained specimens of decarburised ferrovac-E. The prestrained specimens were given 10% tensile strain at 298°K prior to the cyclic process and their stress-strain curve is included with Fig. 15. It is clear that under cyclic straining, initially annealed specimens undergo hardening, while initially prestrained specimens undergo softening. It appears that over 50% of the work hardening increment introduced by uniaxial deformation is quickly removed by subsequent cyclic straining. The figure, also, shows that after only a few cycles (200-400 cycles) the rates of both fatigue hardening and softening become comparable and a steady state or saturation condition is achieved at a stress level of about 22,000 psi.

It should be noted that the saturation level obtained after cyclic hardening is approximately equal to that obtained on cyclic softening. This result demonstrates

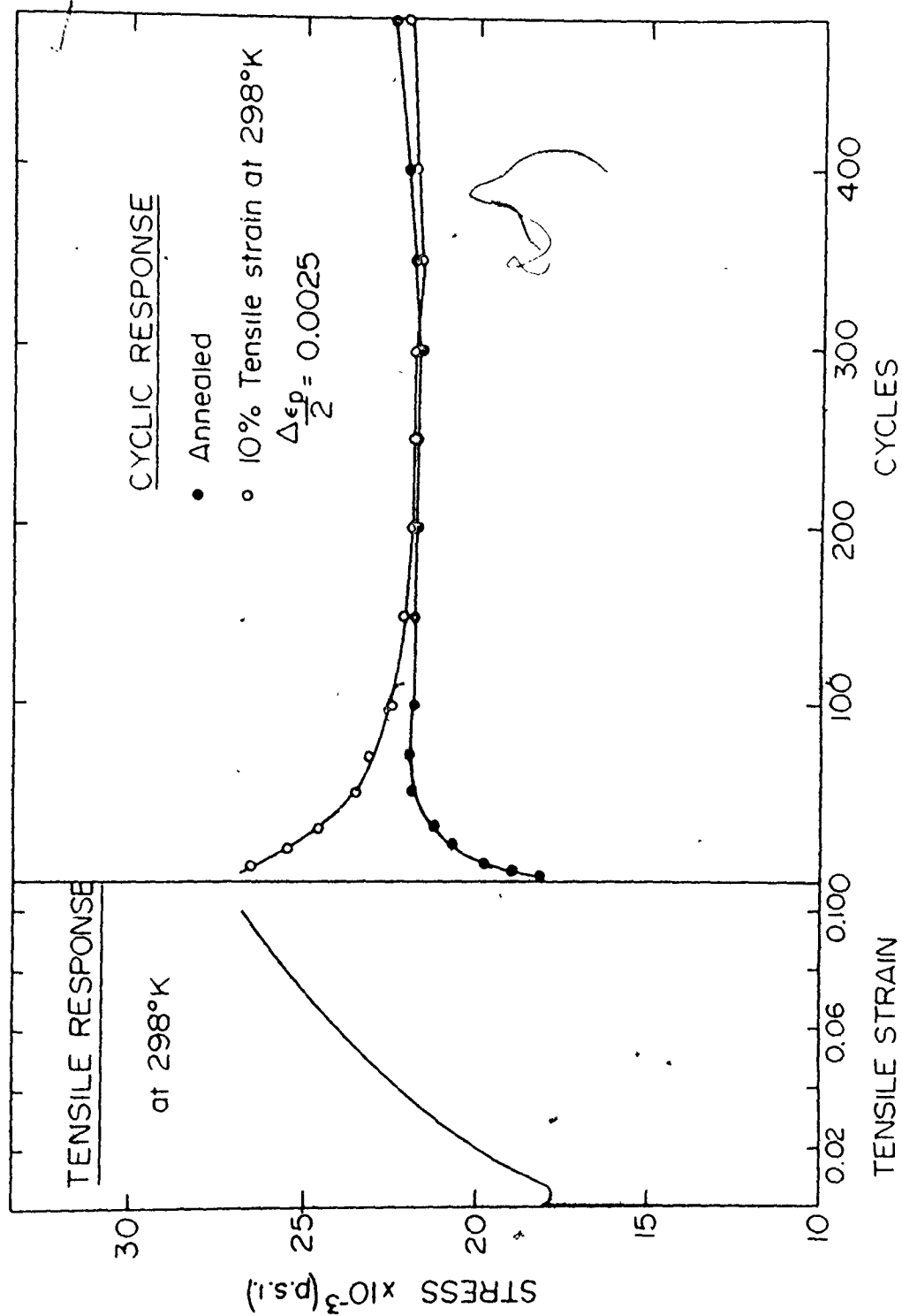


Fig. 15: Tensile and cyclic response of decarburized iron specimens

that decarburised ferrovac-E behaves in a manner similar to high SFE materials (Feltner and Laird 1969) and establishes during cyclic straining a structure which is independent of pre-history. A period of "subsequent hardening" was observed following the saturation stage. More details about this period are given in Appendix B.

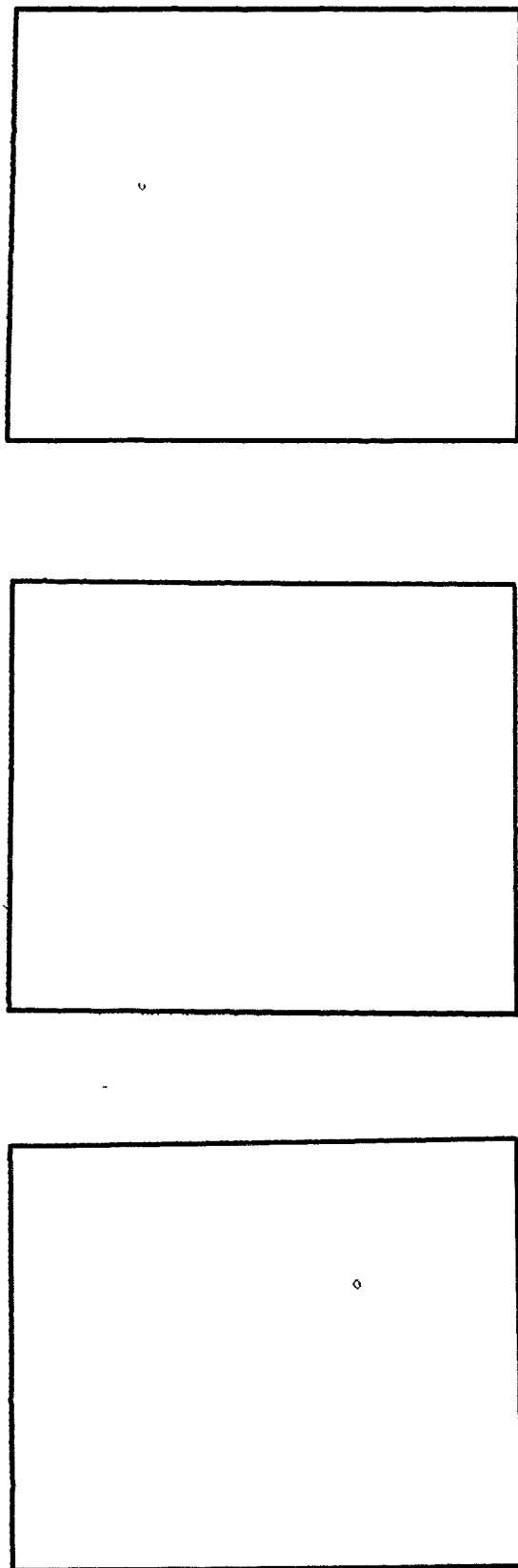
Figure 16 shows a series of back-reflection X-ray Laue photographs obtained for coarse grained iron specimens at various states: a) annealed, b) prestrained 7% in tension at 298°K, and c) fatigue softened. The Laue spots were sharp for annealed material but developed asterism as a result of tensile straining. On subsequent cycling a marked decrease in asterism was observed.

It would appear that most of the asterism observed in iron is due to the small lattice rotations associated with tangles of dislocations and cells formed within the grains. The apparent lack of asterism after cyclic softening suggests that the fatigued structure is associated with smaller gradients of plastic strain.

4.3 Detailed Microstructural Changes

4.3.1 Microstructural changes during softening

To follow the microstructural changes during cyclic softening, specimens of decarburised iron were prestrained



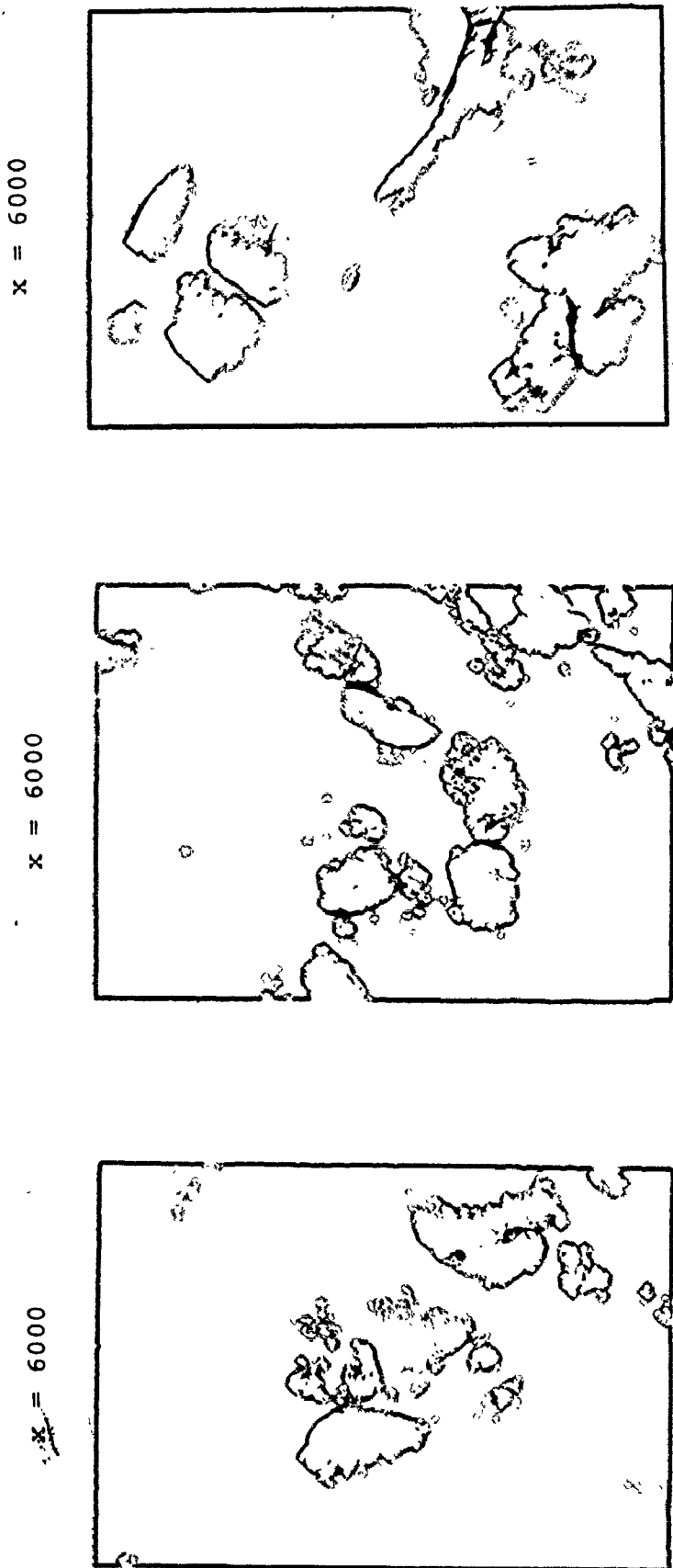
(a) Annealed (b) Prestrained 7% (c) Fatigue Softened

Fig. 16: Back-reflection X-ray Laue patterns obtained from the surface of a decarburized iron specimen:
 (a) annealed, (b) prestrained 7%, and (c) fatigue softened

10% at 298°K, then fatigued and the dislocation arrangements evolved after successive intervals of cycles were examined in transmission electron microscopy. Figure 17 includes a series of micrographs showing the substructure as a function of the number of cycles (N). Figure 17 shows that the initial dislocation structure (N = 0) consisted of complex tangles and irregular boundaries enclosing areas of relatively low dislocation density, but, as cycling proceeds significant changes in the microstructure take place. These changes can be summarised as follows:

- (1) The shape of the cells tend to be more regular and the cell walls become progressively sharper and well defined with smaller number of dislocations observed in the interior of cells.
- (2) A continuous, but relatively small, increase in cell size is associated with cyclic softening. Figure 18 shows the cell size as a function of cycles. It appears from Fig. 18 that the average cell size has increased from $\sim 1.2 \mu$ at the beginning of cycling, to $\sim 1.8 \mu$ at the onset of saturation*. During the saturation

* It should be emphasized that the large scatter in the measurements of cell size, observed in Fig. 18 at initial stages of cycling, is due to the effect of irregularity and nonuniformity of the cell structure at these stages.



(a) $N = 0$ (b) $N = 10$ (c) $N = 100$

Fig. 17: Microstructural development during fatigue softening in decarburized iron prestrained at 298°K: (a) initial microstructure, (b) microstructure after 10 cycles, and (c) microstructure after 100 cycles

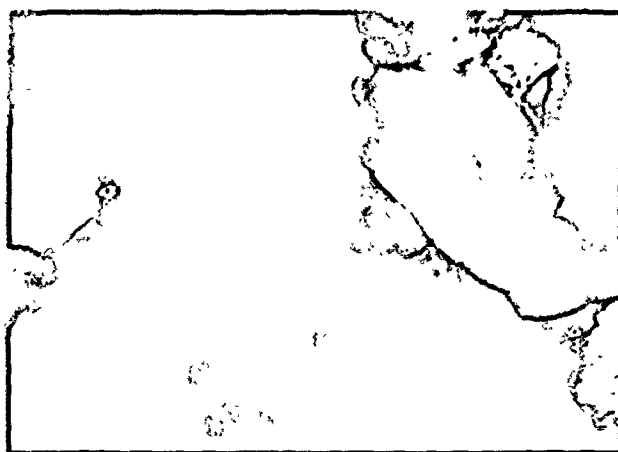
x = 6000



(d)

N = 500

x = 6000



(e)

N = 1000

Fig. 17 (continued): (d) microstructure after 500 cycles,
and (e) microstructure after 1000
cycles

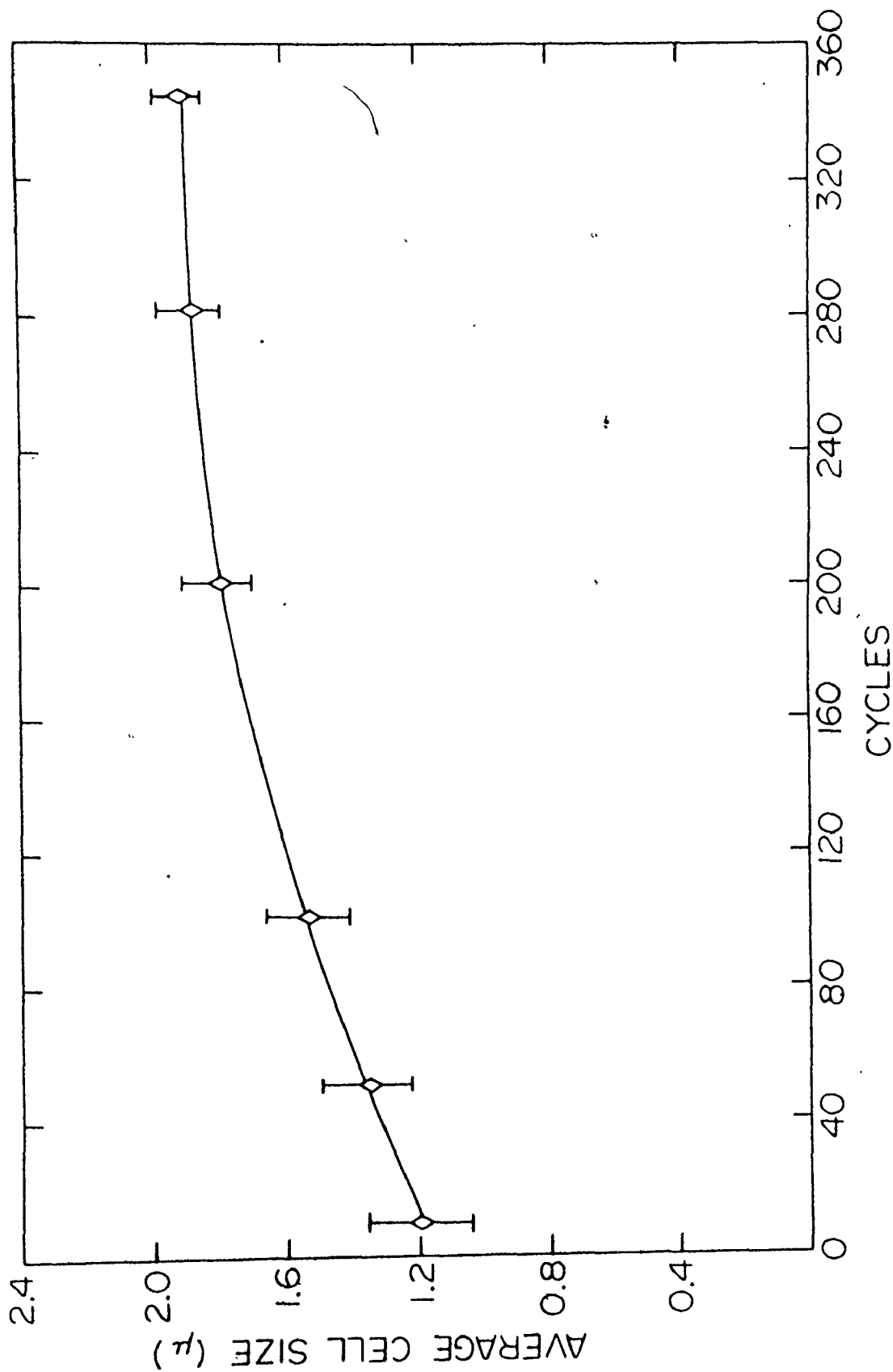


Fig. 18: Change in cell size with number of cycles during fatigue softening in decarburized iron

stage no change in cell size or cell shape was observed. A detailed analysis of the substructure at saturation is given in the following section.

(4.3.2) The substructure at saturation

In general, the substructure at saturation is characterized by the presence of two types of cells: an equiaxed type and a rectangular-shaped type of cell. This is illustrated in Figs. 19(a) and 19(b). The rectangular cells have an average width of $\sim 1.6 \mu$ and an average length of $\sim 3.5 \mu$ in the plane (111) (Fig. 22).

The dislocation aggregations in the cell walls are generally not as tangled or irregularly mixed together as are those observed by uniaxial deformation. The structure of a typical wall is illustrated in Fig. 20 which shows that the dislocations are arranged with some degree of regularity. This seems to suggest that the process of cyclic softening is associated with some dislocation rearrangement. Laufer and Roberts (1966), for example, observed that cell walls developed in copper single crystals, after fatigue, are mainly twist boundaries which indicates that dislocations tend to form lower energy configurations under cyclic straining.

From careful examination of many fields in foils including large number of cells two salient features emerge:

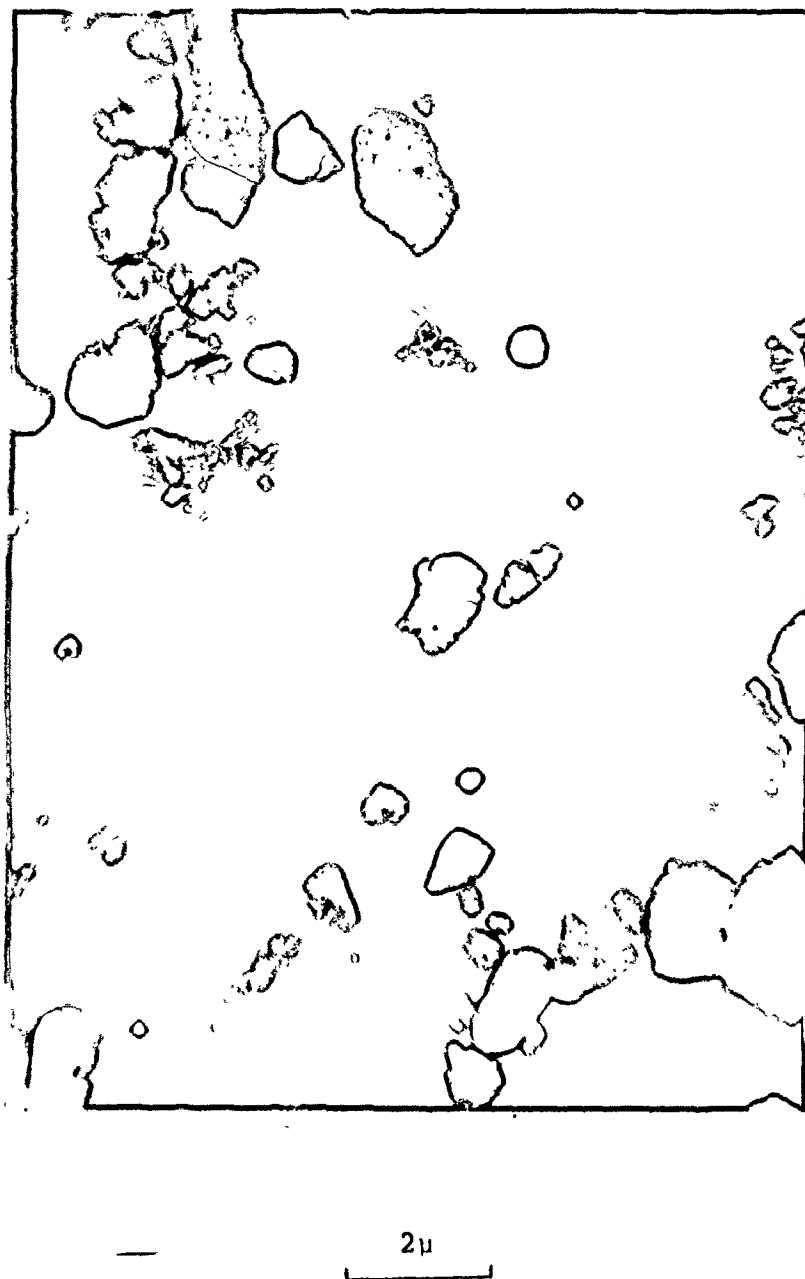
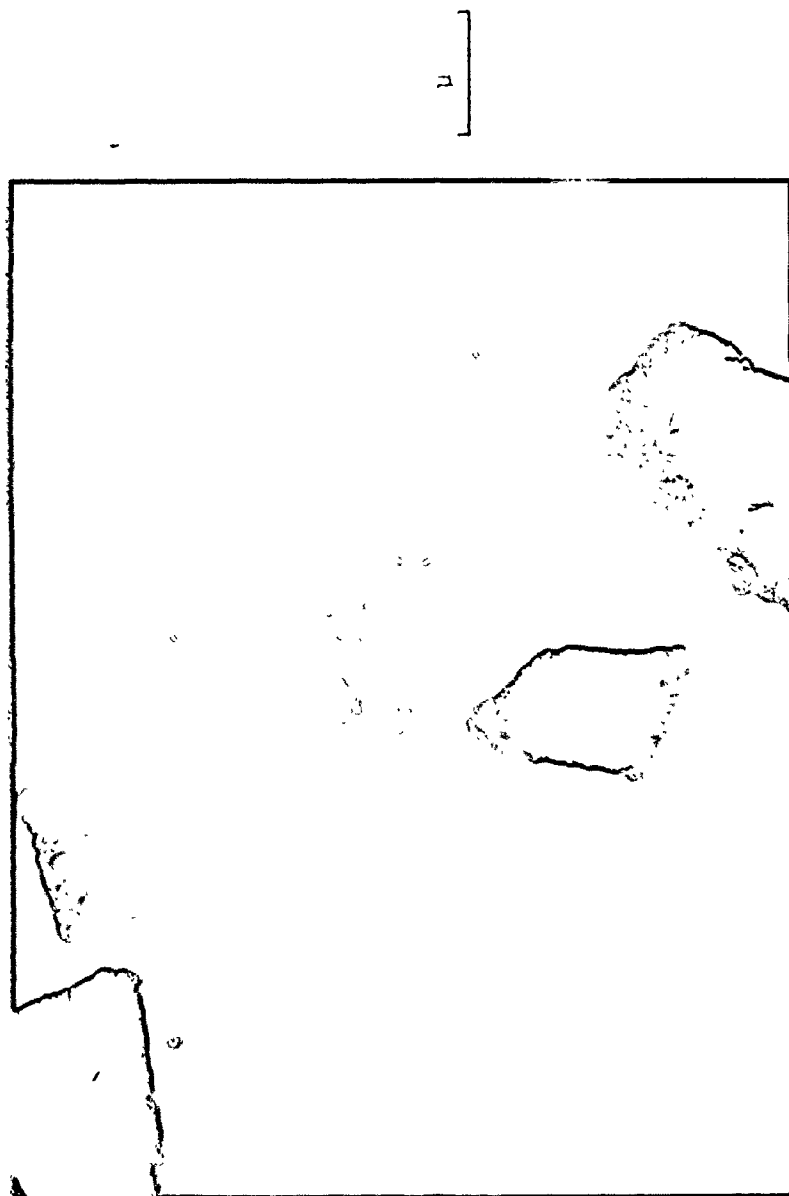


Fig. 19(a): The general features of the substructure after fatigue softening in decarburized iron prestrained at 298°K



·F 19(b): Dislocation cell structure at fatigue saturation
in decarburized iron prestrained at 298°K



Fig. 20: Structure of a cell wall at fatigue saturation in decarburized iron

firstly, the misorientations associated with cell walls are very small (of the order of $1/4 - 3/4$ of a degree) and from a map of the misorientations between cells it appears that these small misorientations are compensated at adjacent or neighbouring walls. (Misorientations across cell walls were measured from shifts in Kikuchi line patterns as indicated by Hirsch et al. (1965).) An example is illustrated by the composite micrograph in Fig. 21 and the related Table 4 of measured misorientation

The observed lack of misorientations associated with cell walls suggests that some walls are composed mainly of dislocation dipoles and that positive and negative edge dislocations must be present in approximately equal number. Similar observations were reported by Laufer (1969) in copper single crystals after fatigue saturation. It should be noted that the above misorientations, measured after fatigue, are very small compared to those ($2 - 3^\circ$) reported for iron after unidirectional deformation (Keh and Weissman 1963). Secondly, the dislocation arrays become more compact and regular in form with a tendency to alignment along low index crystallographic planes of the form $\{110\}$ and $\{112\}$ planes as shown in Fig. 22. This was determined by stereographic projection of the traces of walls intersecting reciprocal lattice sections from a number of foils of different orientations.



111

111
111

seven
f dec

1-111
e-sot

1:

TABLE 4

ANGLES OF MISORIENTATION ACROSS CELL WALLS OF FIG. 21

Cell Wall	Angle of Misorientation (degrees)
1 - 2	0.8
1 - 3	0.4
1 - 4	0.3
1 - 5	0.7
1 - 6	0.6
1 - 7	0.6
2 - 3	0.4
3 - 4	0.7
4 - 5	1.0
5 - 6	0.1
6 - 7	0.1
7 - 2	0.2

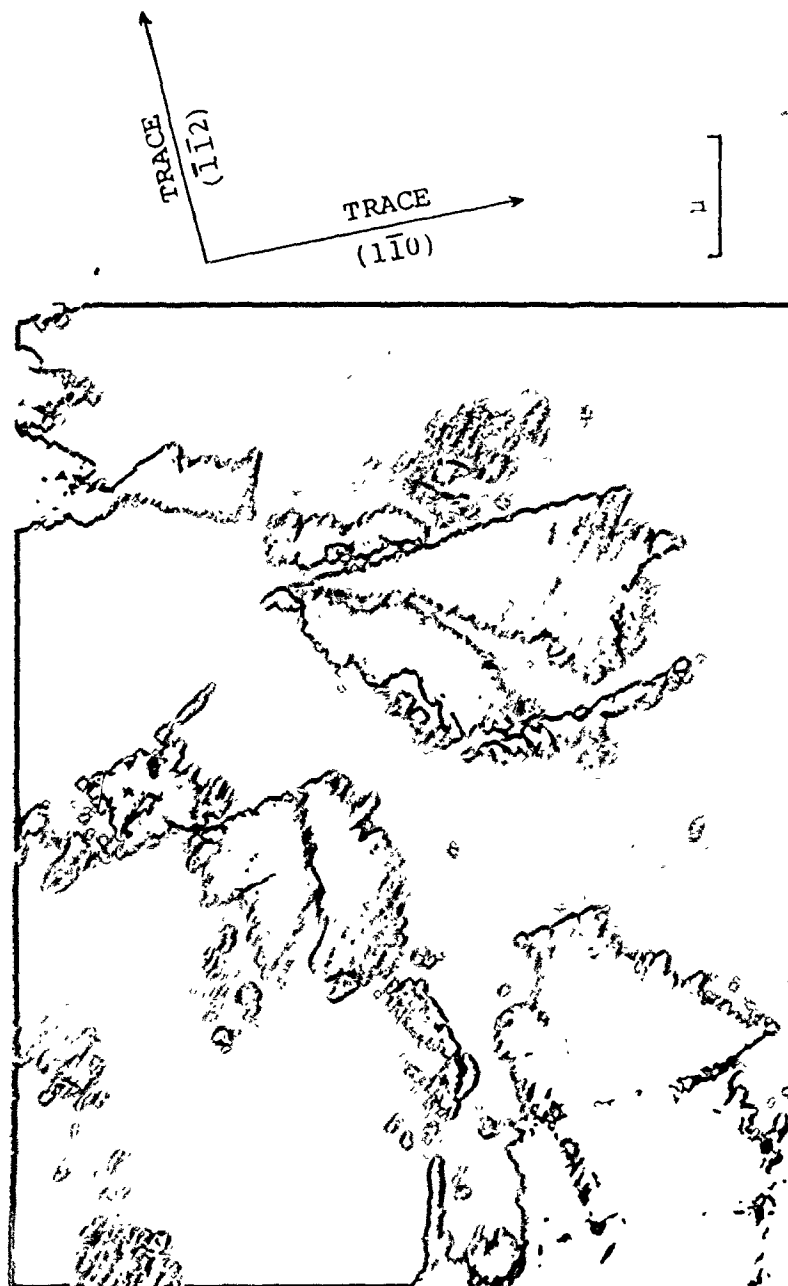


Fig. 22: Regular cell walls developed at fatigue saturation in decarburized iron. Plane of the foil (111)

This observation together with the above observations suggests that during cyclic softening of prestrained iron specimens, the dislocations tend to rearrange themselves into a lower energy configuration.

(4.4) Effect of Initial Dislocation Arrangements on the Kinetics of Cyclic Softening

In order to start the fatigue softening process with different dislocation arrangements, specimens were pulled 10% plastic strain at three different temperatures: 195, 298 and 473°K. Decarburised iron was used for the cases of prestraining at 195 and 298°K, while Armco iron was used for the 473°K case. The values of yield stress and flow stress after 10% strains at each temperature are given in Table 5. All the fatigue tests were performed at room temperature under a cyclic frequency of 1 cps and a total stroke amplitude equivalent to $(\Delta\epsilon_p/2) = 0.0025$.

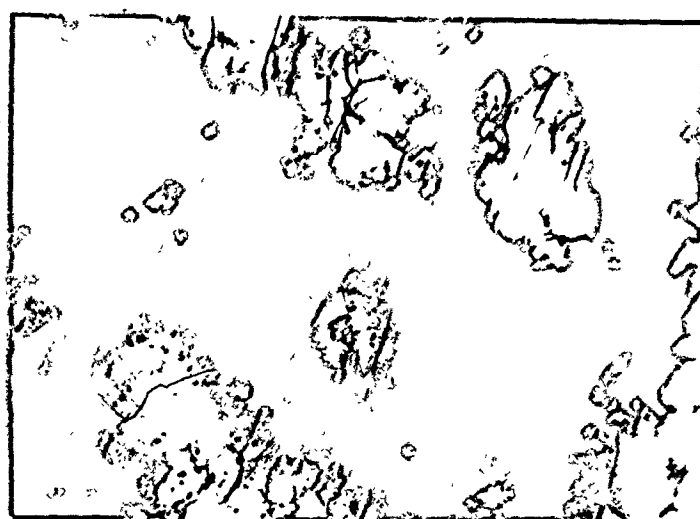
(4.4.1) Initial dislocation arrangements

After 10% tensile deformation at 298°K, the dislocation structure consisted, mainly, of complex tangles and cell walls of high density of dislocations separated by regions of low dislocation density (Fig. 23(b)). The observed cell

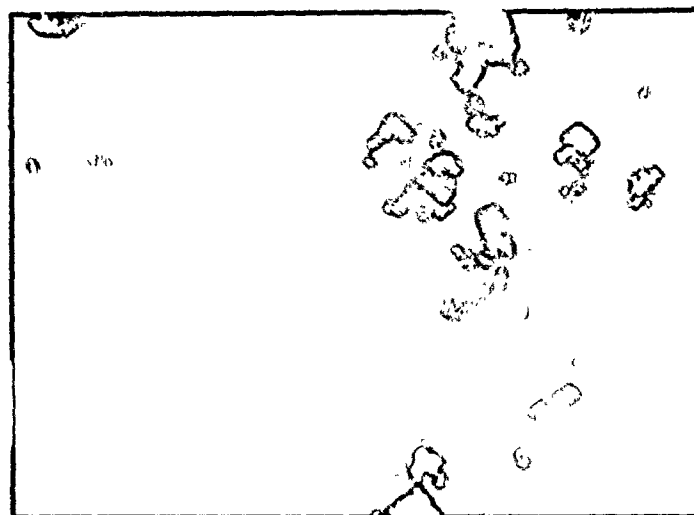
TABLE 5

VALUES OF YIELD STRESS (σ_y) AND FLOW STRESS AFTER 10%
TENSILE STRAIN (σ_f) FOR SPECIMENS OF DECARBURISED IRON
AND ARMCO IRON PRESTRAINED AT 195, 298, AND 473°K

Deformation Temp.	195°K		298°K		473°K	
Stress $\times 10^{-3}$ psi	σ_y	σ_f	σ_y	σ_f	σ_y	σ_f
Dec. Ferrovec-E	35	46	16	32	-	-
Armco Iron	40	51	20	36	22	42



(a)



(b)

Fig. 23: Dislocation structure in decarburized iron:

(a) after 10% tensile strain at 195°K

(b) after 10% tensile strain at 298°K

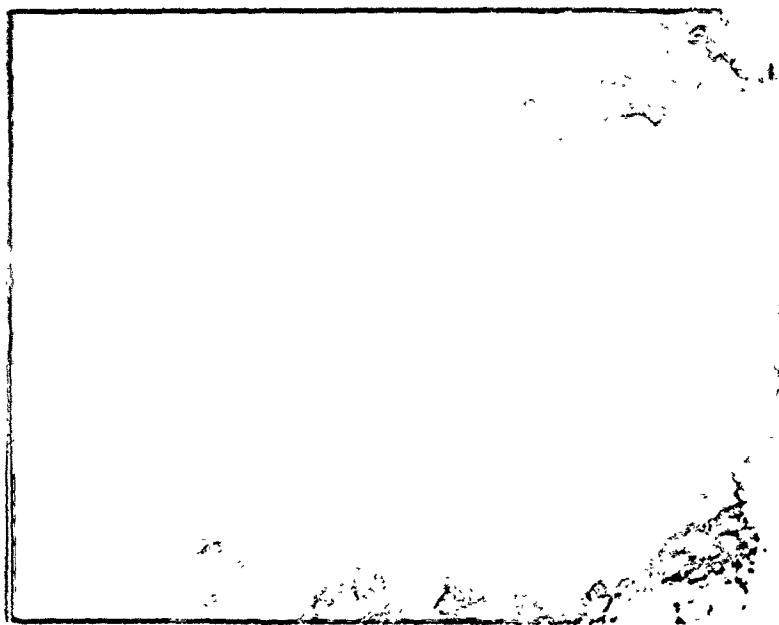


Fig. 23: (c) Dislocation structure in Armco iron
after 10% tensile strain at 473°K

structure is, generally, irregular in shape and shows a rather nonuniform size distribution throughout the matrix.

In contrast with the tangled dislocation structure after deformation at 298°K, the dislocation structure resulting from 10% tensile strain at 195°K is much more uniform. Figure 23(a) shows that the tendency for cell formation at 195°K is less pronounced and that the dislocation structure is characterized by the presence of long straight segments of screw dislocations and small loops. These observations are in accord with previous observations of Keh and Weissman (1963), Keh and Nakada, (1967), and Taylor and Christian (1967) on the temperature dependence of the dislocation structure in bcc materials.

Figure 23(c) shows the dislocation structure in Armco iron resulting from 10% tensile deformation at 473°K. Due to migration of solute atoms at this temperature, dislocations are pinned by solute atoms and the general feature of the microstructure is a fine uniform dispersion of dislocations. No evidence for cell structure was observed.

(4.4.2) Kinetics of cyclic softening

Figure 24 shows a comparison of the rates of cyclic softening for specimens which have been prestrained at 195, 298, and 473°K. Three important results can be drawn from Fig. 24.

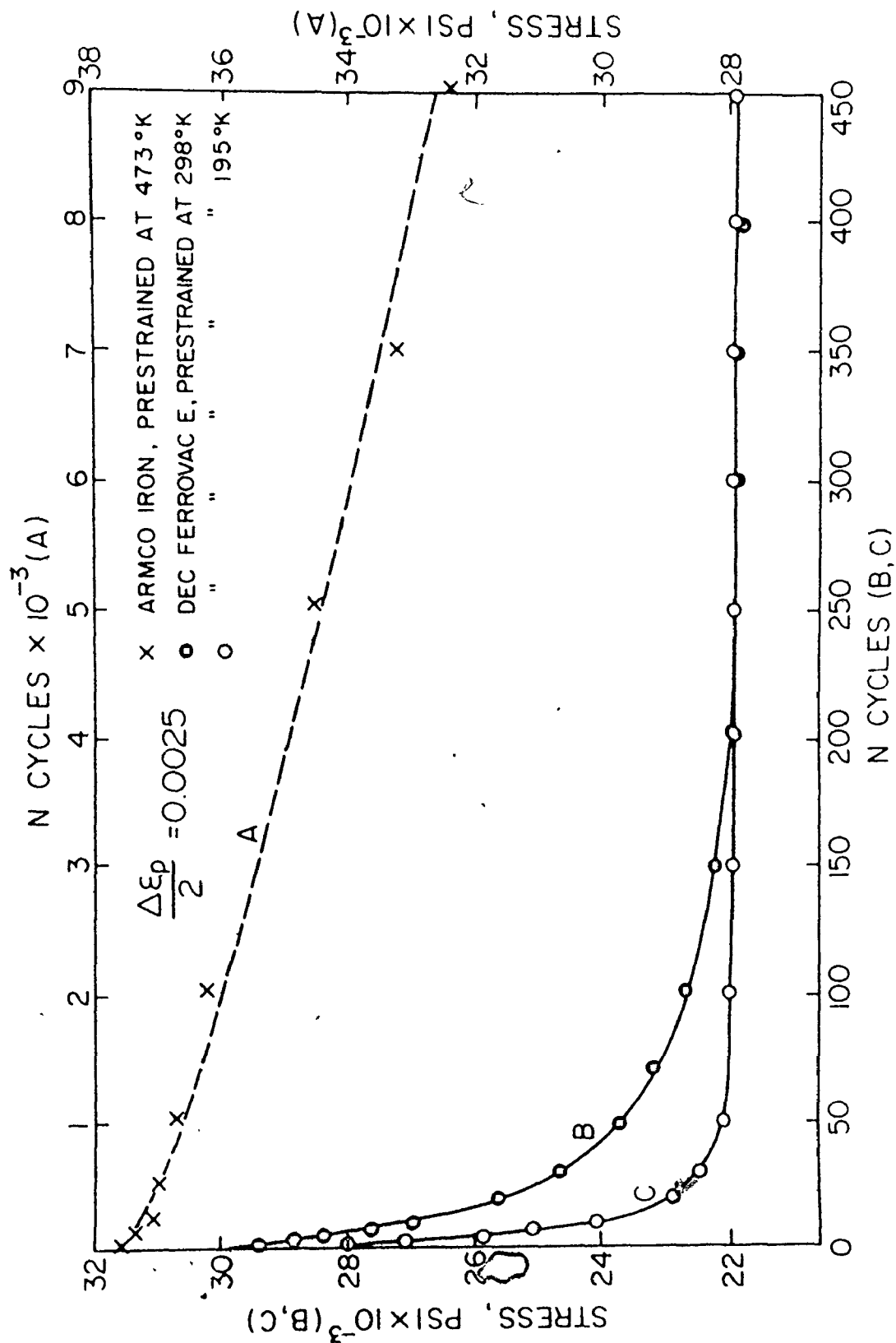


Fig. 24: Change in cell size with number of cycles during fatigue softening

of decarburized iron

Firstly, the rate of cyclic softening of specimens prestrained at 195°K is much higher than that of specimens prestrained at 298°K while specimens prestrained at 473°K show the lowest softening rate.

Secondly, the cyclic flow stress of specimens prestrained at 195°K decreased very rapidly in the initial stages of cycling and reached the saturation stress level after only a few cycles (100 to 150 cycles), whereas specimens prestrained at 298°K show much lower rates of softening to reach the same saturation level after about 300 to 400 cycles as illustrated in Fig. 25. It must be noted that almost the same saturation level is, also, reached during fatigue hardening. In both cases, a period of "subsequent hardening" was observed following the saturation period and continued until near fracture. This period will be discussed with more details in Appendix B.

Thirdly, the cyclic response of specimens prestrained at 473°K shows neither saturation nor subsequent hardening. A continuous, but very slow, decrease in flow stress was observed till fracture.

Figures 19, 26, and 27 show the microstructures developed after cyclic softening. Similar structures were formed in specimens prestrained at either 195°K or 298°K. The fatigued structure in specimens prestrained at 473°K (Fig. 27) was characterised by a cell structure in which

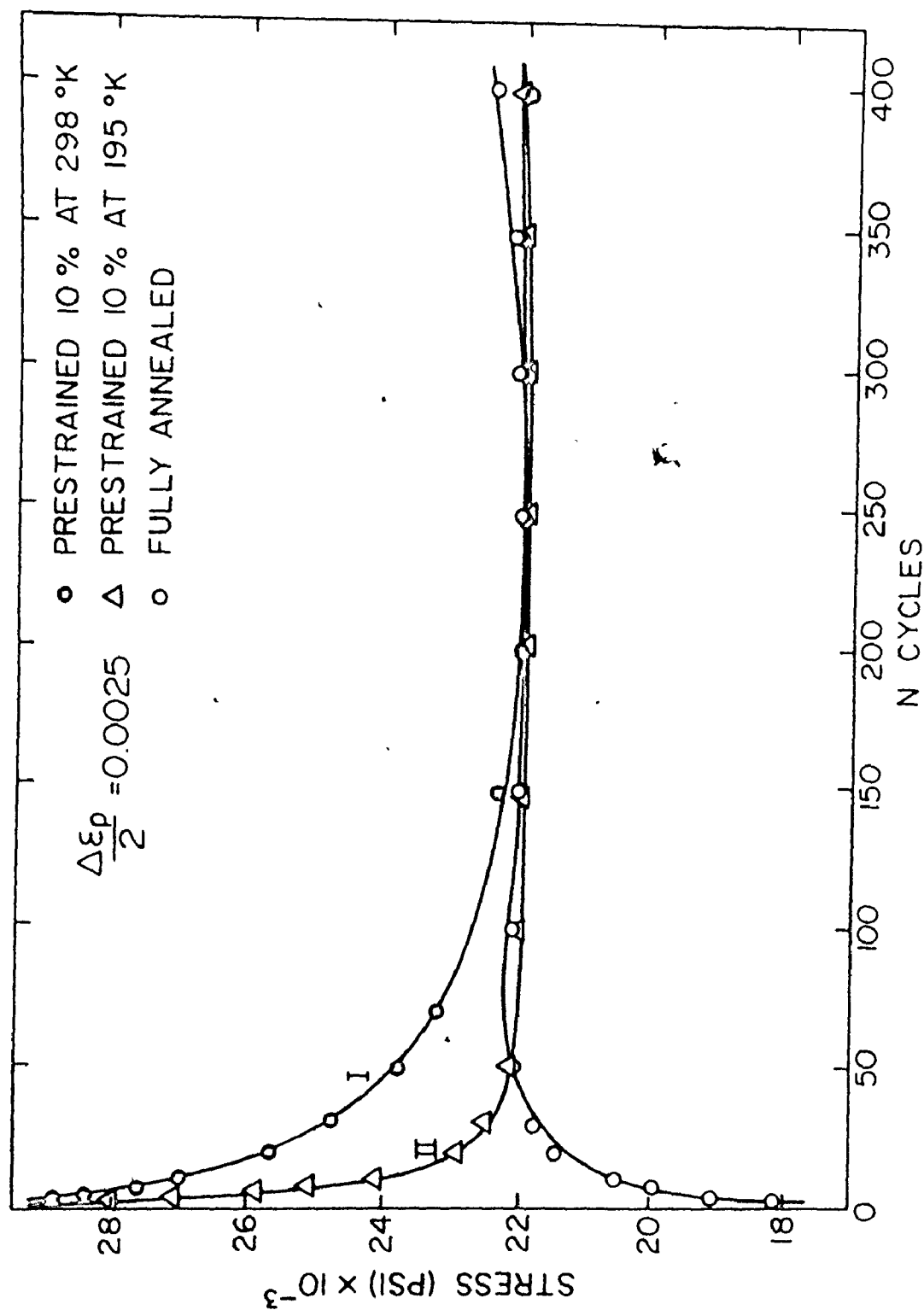
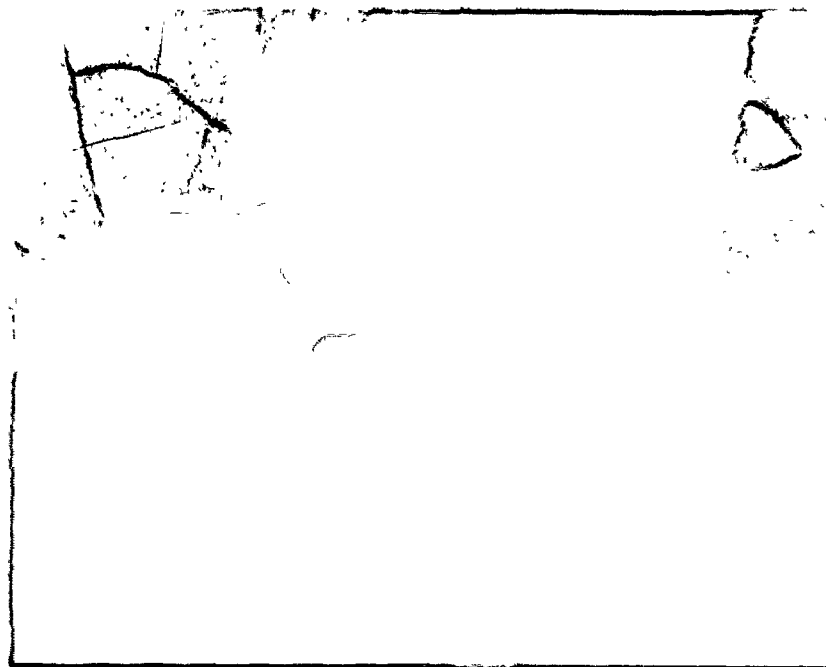


Fig. 25: Fatigue softening and hardening in decarburized iron



(a)



(b)

Fig. 26: Substructure after fatigue softening of decarburized iron specimens prestrained at 195°K: (a) equiaxed cells and (b) rectangular cells



Fig. 27: Fatigued structure in Armco iron
prestrained at 473°K

the cell walls were associated with dense and more complex dislocation structure. The cell walls were not as sharp or well defined as those observed in specimens prestrained at either 195°K or 298°K. Also, the interior of cells was not as free of dislocations.

The effect of cyclic strain amplitude on the rate of softening was studied on specimens which have been prestrained 10% in tension at 195°K. Figure 28 demonstrates this effect on a normalized scale. The data is plotted in the form $(1 - \frac{\sigma_1 - \sigma_N}{\sigma_1 - \sigma_S})$ versus N where σ_1 is the peak stress at the first cycle, σ_N is the flow stress after N cycles and σ_S is the saturation stress level. The term $(\sigma_1 - \sigma_N)$ represents the amount of softening reached after N cycles, while the term $(\sigma_1 - \sigma_S)$ represents the total amount of softening reached till saturation. It can be clearly seen that in the range of amplitudes studied, increased strain amplitude results in an increasing rate of softening. The saturation stress was also found to increase with increasing plastic strain amplitude. Similar observations were reported by Pratt (1967) on copper.

Feltner and Laird (1967) have shown that the rate of softening in copper increases with increasing strain amplitude, reaching a maximum value and then begins to decrease at higher plastic strain amplitudes. They found that the maximum rate occurs for amplitudes which result in lives of the order of 10^4 cycles.

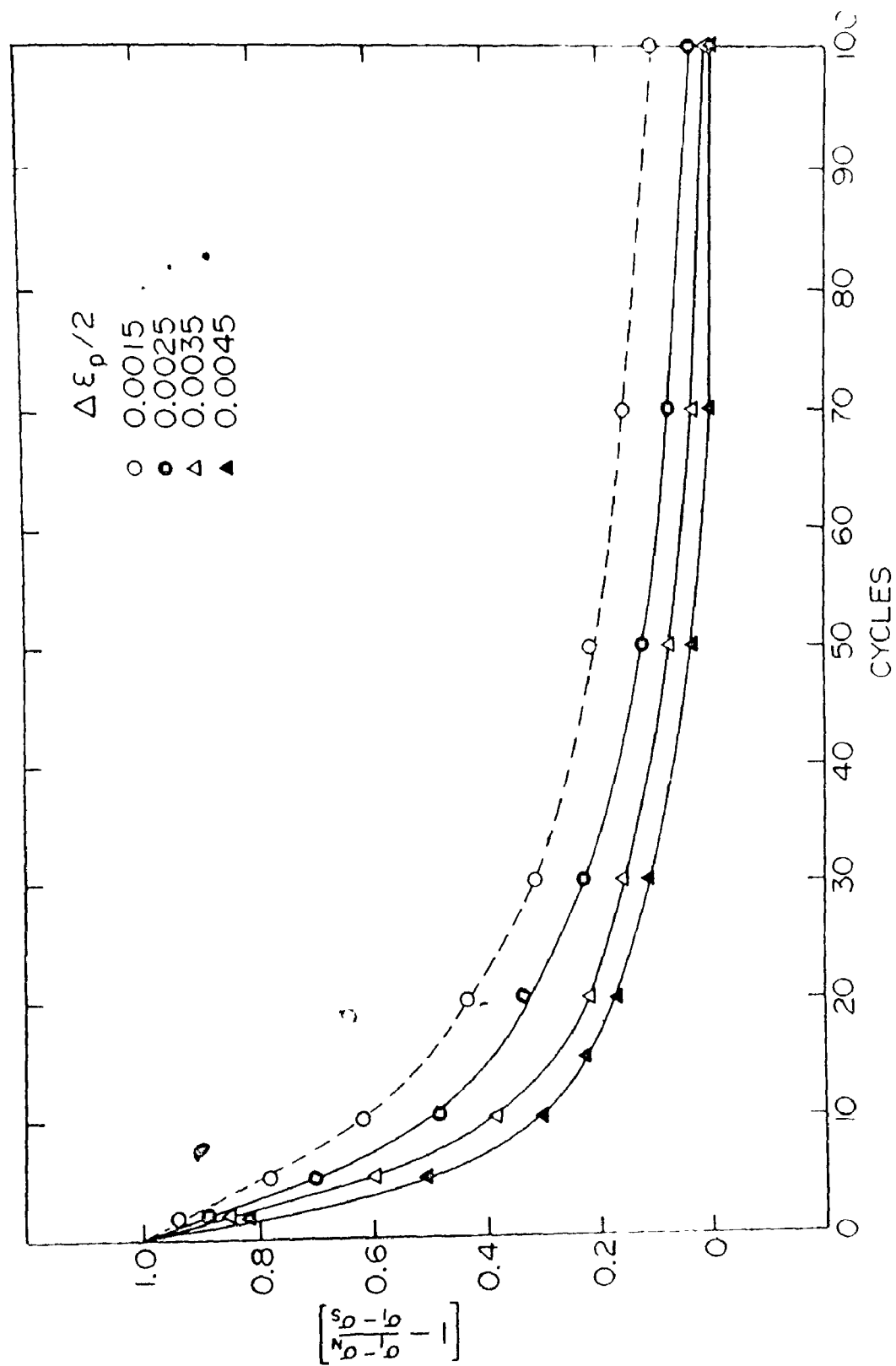


Fig. 28: Cyclic softening of decarburized iron specimens
prestrained 10% at 195°K

A log-log plot of saturation stress (σ_S) versus plastic strain amplitude ($\Delta\epsilon_p$) is shown in Fig. 29 for decarburised iron. Data of Fig. 29 suggests that a power law of the form: $\sigma_S = \sigma_C (\Delta\epsilon_p/2)^n$ may hold for decarburised iron. Similar relationships were found by Feltner and Laird (1967) for copper and by Abdel-Faouf (1972) for ferrovac-E. The cyclic strength coefficient (σ_C) and the cyclic strain hardening exponent (n) have been calculated from data of Fig. 29 for decarburised iron and found to be 40,000 psi and 0.1 respectively. Thus the relationship between saturation stress and plastic strain amplitude for decarburised iron may be written as

$$\sigma_S = 40,000 \left(\frac{\Delta\epsilon_p}{2} \right)^{0.1} \quad (1)$$

(4.5) Thermal Recovery of Fatigued Structure

The thermal recovery experiment was designed to fulfil two objectives: first, to compare the process of fatigue softening with the thermal recovery of prestrained specimens, and second, to study the effect of thermal recovery treatment on the saturation stress and dislocation structure following fatigue softening or hardening of decarburised iron specimens.

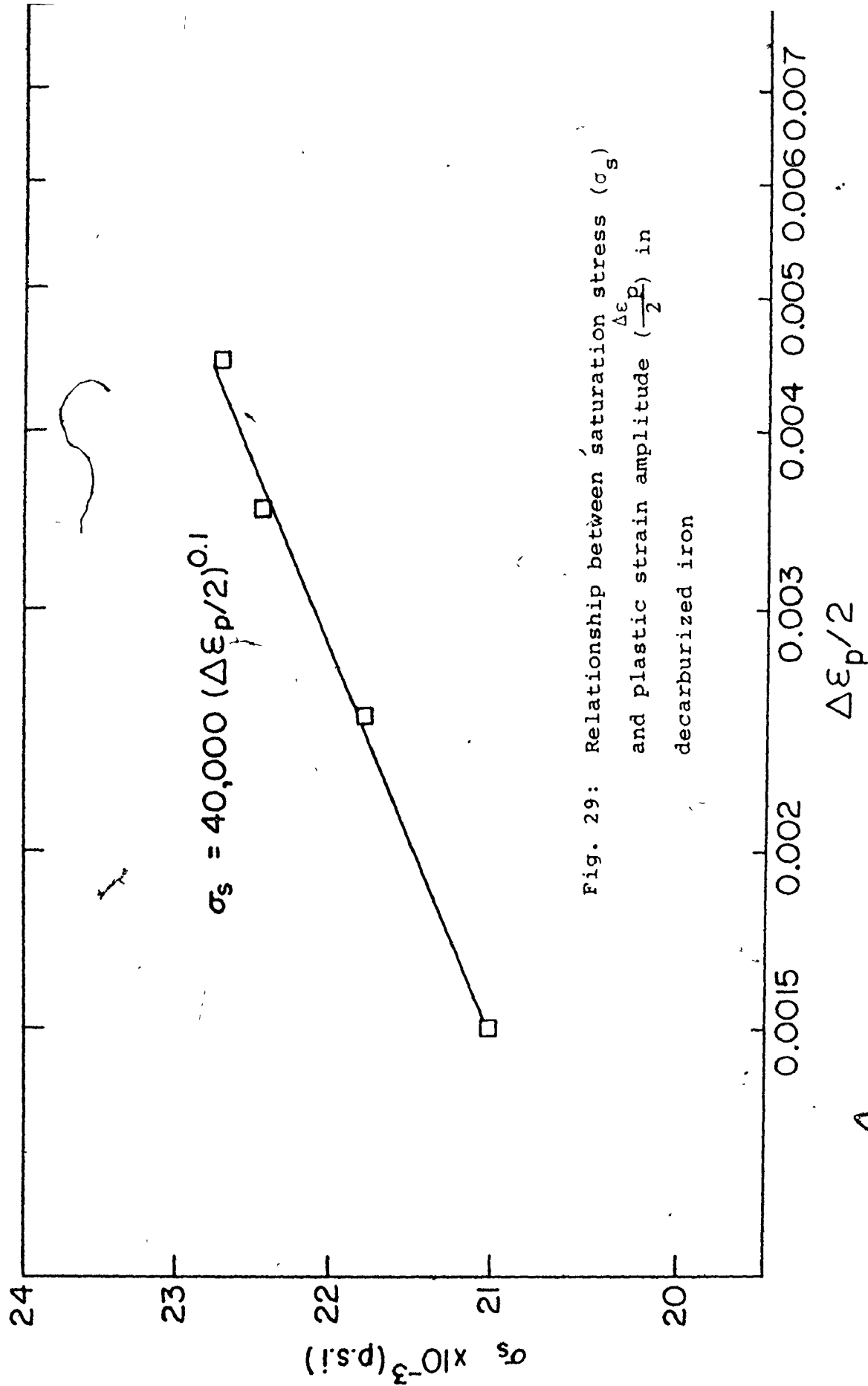


Fig. 29: Relationship between saturation stress (σ_s) and plastic strain amplitude ($\frac{\Delta \epsilon_p}{2}$) in decarburized iron

The testing scheme was performed according to the schedule included in Table 6. Specimens marked R_1 and R_2 were prestrained 12% in tension at 298°K and 195°K respectively prior to the thermal recovery treatment at 410°C. Specimens marked R_3 , R_4 , and R_5 were prestrained 12% in tension at 298°K and fatigue softened before thermal recovery treatments at 360, 410, and 470°C respectively. Specimens marked R_6 , R_7 , and R_8 were prestrained 12% in tension at 195°K and fatigue softened before thermal recovery treatments at 360, 410, and 470°C respectively. Specimens marked R_9 were fatigue hardened prior to the thermal recovery treatment at 410°C.

The degree of recovery was evaluated in terms of fractional softening (F_R) defined as

$$F_R = \frac{\sigma_I - \sigma_r}{\sigma_f - \sigma_y} \quad (2)$$

where σ_I = initial flow stress measured in tension at room temperature before starting the thermal recovery treatment (for R_1 and R_2 , $\sigma_I = \sigma_f$),

σ_r = proof stress (at 0.02% off set) measured at room temperature after a recovery anneal,

σ_f = flow stress after 12% tensile strain measured at room temperature, and

σ_y = yield stress at room temperature of fully annealed specimens.

TABLE 6
SPECIMEN IDENTITIES AND USAGE

Series	Pre-Treatment	σ_I (psi)	Temperature of Recovery
R ₁	Strained 12% at 298°K	27500	410°C
R ₂	Strained 12% at 195°K	26900	410°C
R ₃	Prestrained 12% at 298°K + Fatigue softened	21600	360°C
R ₄	Prestrained 12% at 298°K + Fatigue softened	21600	410°C
R ₅	Prestrained 12% at 298°K + Fatigue softened	21600	470°C
R ₆	Prestrained 12% at 195°K + Fatigue softened	21500	360°C
R ₇	Prestrained 12% at 195°K + Fatigue softened	21500	410°C
R ₈	Prestrained 12% at 195°K + Fatigue softened	21500	470°C
R ₉	Fatigue hardened	21700	410°C

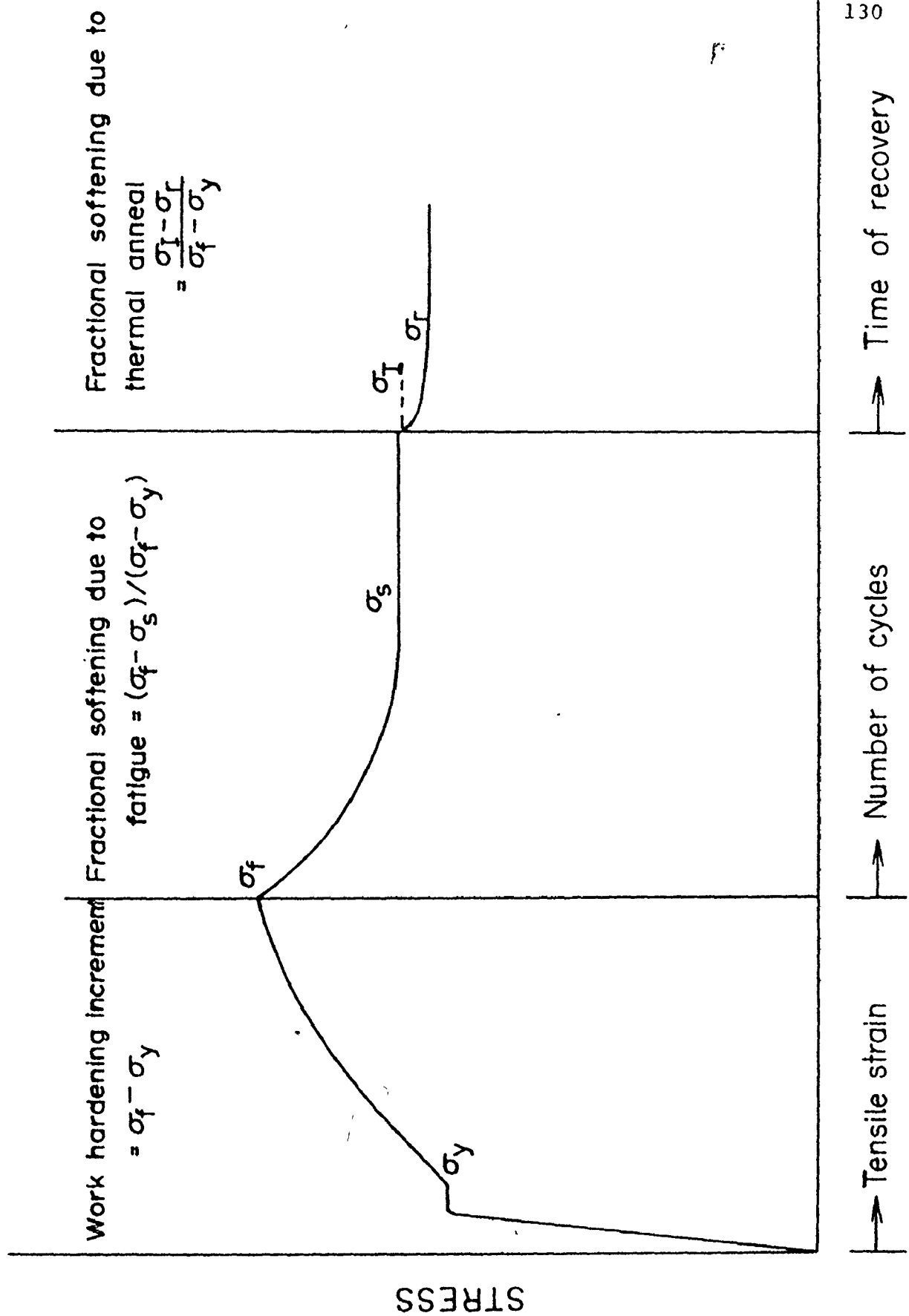


Fig. 30: Schematic diagram showing the method used to evaluate the degree of recovery

Figure 30 shows schematically the method used to evaluate the degree of recovery.

(4.5.1) Thermal recovery of prestrained specimens

The fractional softening F_R is shown in Fig. 31 as a function of annealing time at 410°C for specimens R_1 and R_2 . The resulting curves show a rapid rate of recovery in the initial stages and a decreasing rate as the time increases till a "saturation" value of recovery is attained. The figure indicates that decreasing the temperature of prestrain has the effect of increasing both the rate and extent of recovery. Similar observations have been reported by Leslie et al. (1961) and Schankula (1970) on iron. This result emphasises the importance of initial dislocation arrangement on subsequent thermal recovery of prestrained material. Thus, in both fatigue softening and thermal recovery, of prestrained iron specimens, the rate of softening is greatly influenced by the initial dislocation arrangement.

From the foregoing it appears that the uniformly distributed arrays of dislocations introduced by uniaxial straining at 195°K are less stable, both mechanically (under subsequent fatigue) and thermally (under subsequent recovery) compared to the cell structure developed by uniaxial straining at 298°K. An example is illustrated in

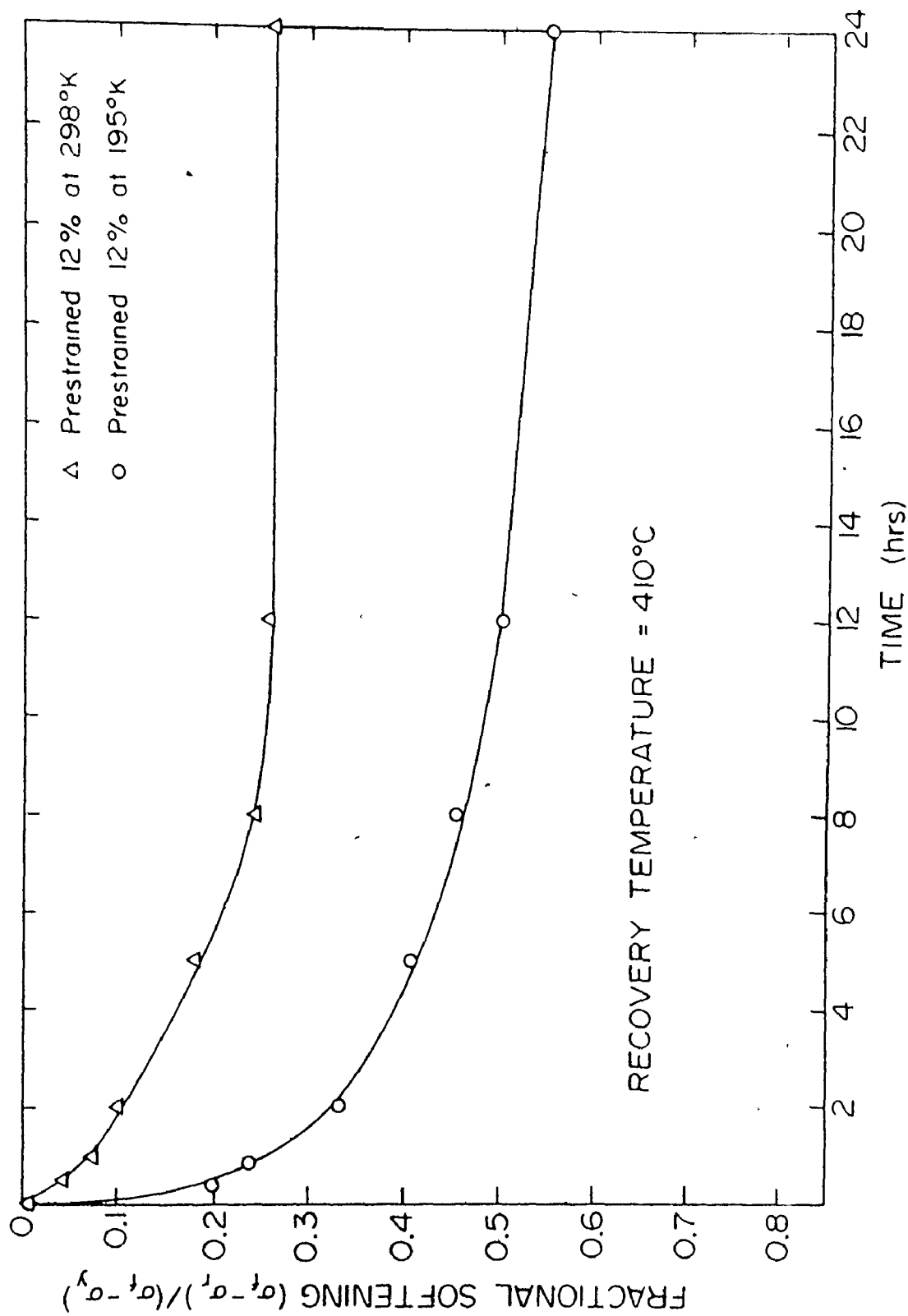


Fig. 31: Progress of thermal recovery in decarburized iron prestrained at 298°K and 195°K

195°K

V.

Table 7 which shows that specimens prestrained at 195°K have lost about 34% of their work hardening increment after only 10 cycles in fatigue, and about 32% after 2 hours recovery at 410°C. On the other hand, the loss of work hardening increment, by similar treatments, in specimens prestrained at 298°K is only 10-12%.

(4.5.2) Thermal recovery of fatigued specimens

Figure 32 shows the effect of thermal recovery at 410°C on the saturation stress of fatigue hardened specimens. It can be seen that less than 8% of the total cyclic hardening increment was recovered after 30 hours at 410°C. This seems to indicate that stored internal stresses associated with the recovery of fatigued structure is much smaller than that associated with specimens deformed in tension (Fig. 31). This suggests that the substructure produced in fatigue is in a lower energy configuration compared to that developed by uniaxial straining.

Data on the release of stored energy of unidirectionally (Bailey 1963) and cyclically (Hargreaves et al. 1963) deformed fcc materials at low annealing temperatures indicate that a large release of stored energy without a significant change in dislocation density is associated with recovery of unidirectionally deformed material, whereas this stage is not observed for cyclically

TABLE 7
A COMPARISON OF FRACTIONAL SOFTENING
IN DECARBURISED IRON SPECIMENS
PRESTRAINED AT 195 AND 298°K

Series	Total Work Hardening Increment ($\sigma_f - \sigma_y$) psi	Fractional Softening $\frac{\sigma_I - \sigma_r}{\sigma_f - \sigma_y}$	
		After 10 Fatigue Cycles	After 2 hrs Recovery at 410°C
R ₁	11200	-	0.10
R ₂	11800	-	0.32
R ₄	11000	0.12	-
R ₇	11100	0.34	-

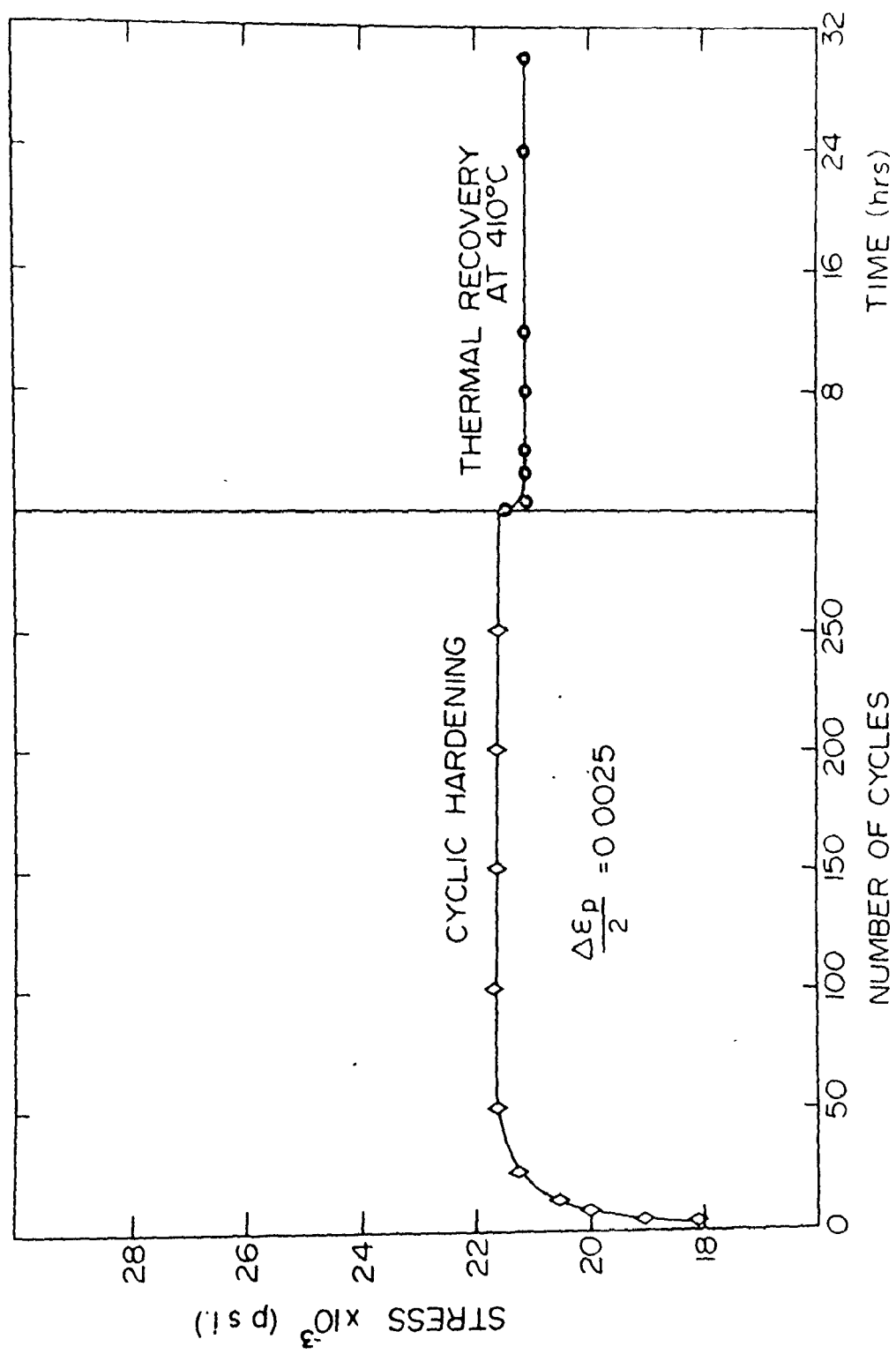


Fig. 32: Effect of thermal recovery on the fatigue-hardened structure in decarburized iron



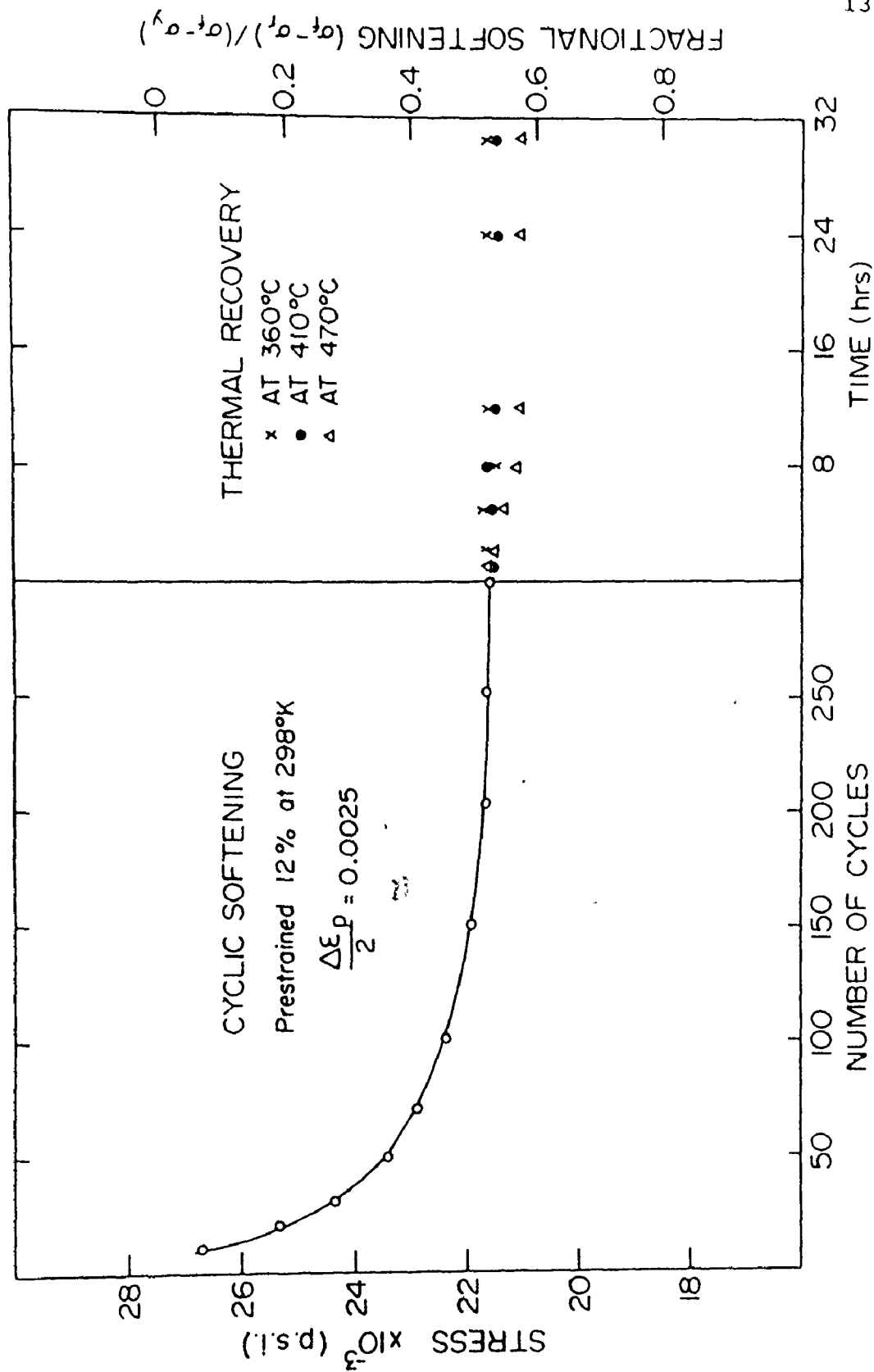


Fig. 33: Effect of thermal recovery on the fatigue-softened structure in decarburized iron prestrained 12% at 298°K

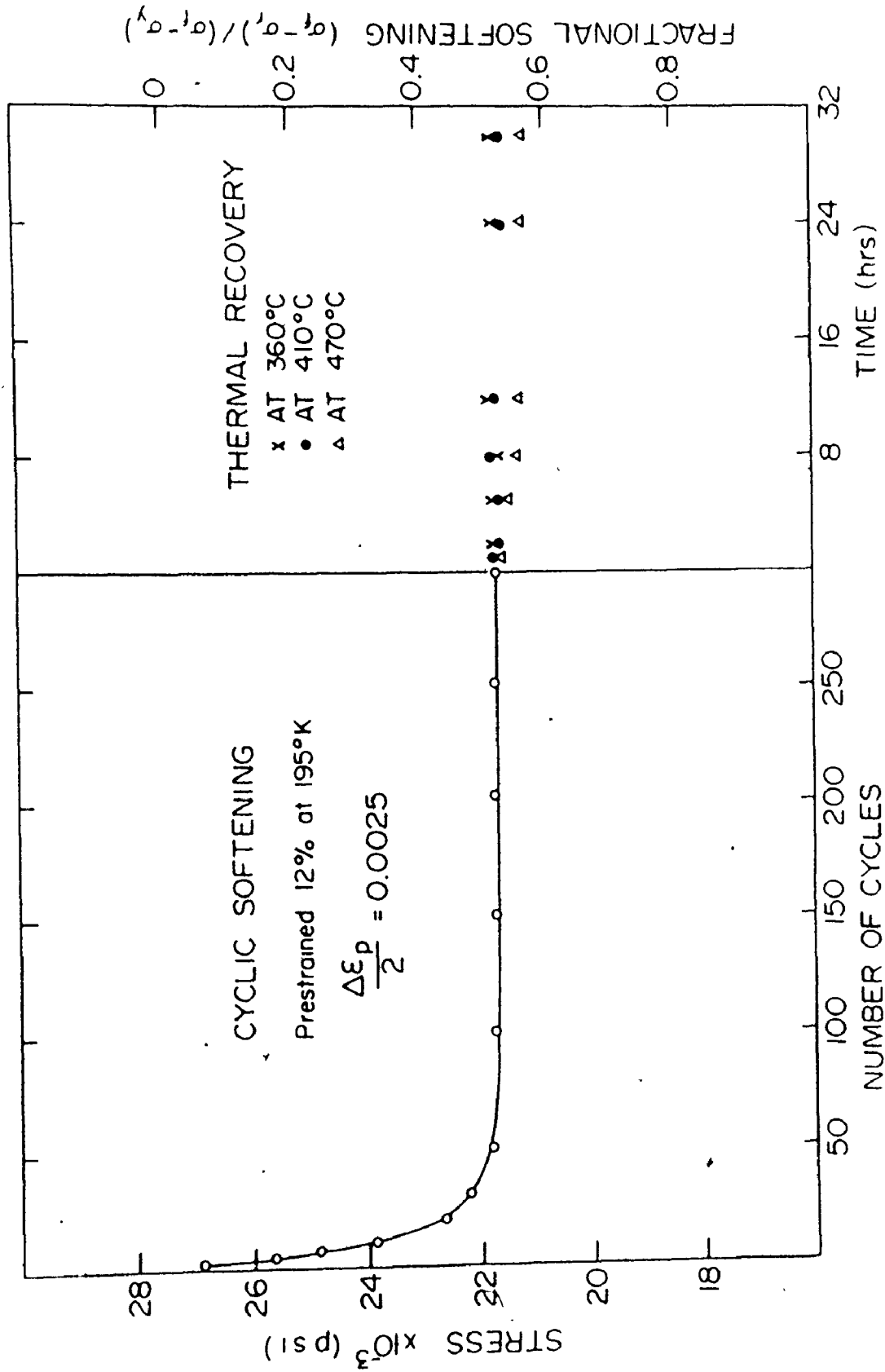


Fig. 34: Effect of thermal recovery on the fatigue-softened structure of decarburized iron prestrained 12% at 195°K

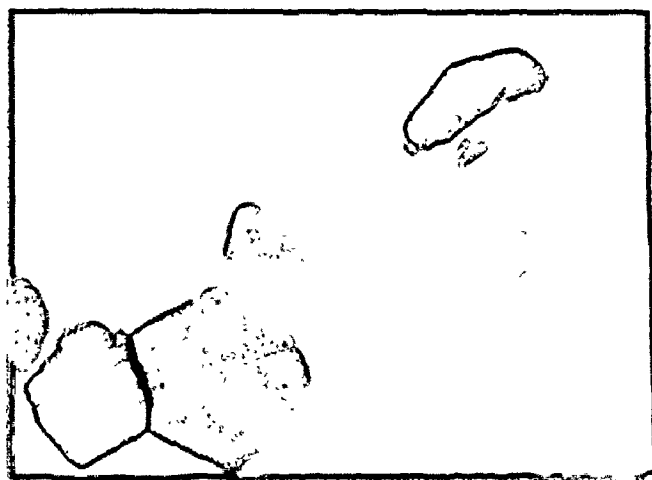
deformed material. This annealing stage is bypassed in cyclically deformed materials, possibly because cyclic deformation is associated with dislocation rearrangement in lower energy configurations.

The effect of thermal recovery on previously fatigue softened specimens is shown in Figs. 33 and 34. Again, very little decrease in saturation stress was achieved by subsequent thermal recovery. Even after 30 hrs anneal at 470°C the fractional softening is less than 0.06.

Figures 35 and 36 include micrographs showing the dislocation structure evolved, after thermal recovery at different temperatures, in previously fatigued specimens. Except for minor changes in cell size and cell shape, the fatigued structure is basically the same before and after recovery. After 18 hrs at 470°C a polygonized structure was observed and is shown in Fig. 37.

The data presented in this section seems to suggest that in iron the substructure formed by fatigue is thermally more stable than that formed by uniaxial deformation.

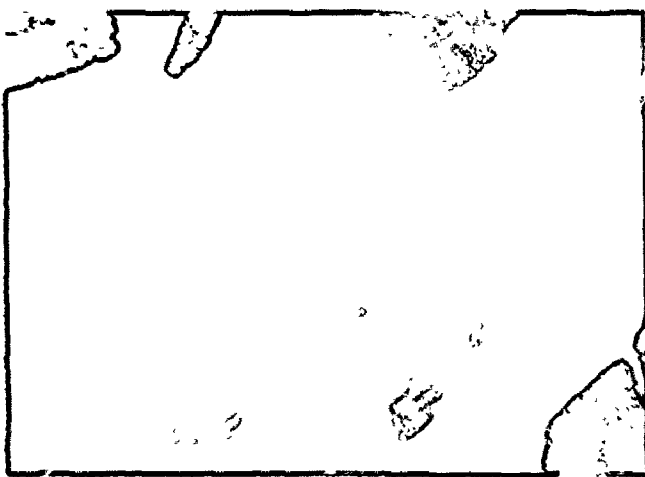
x = 7000



(a)

After 100 min. at 360°C

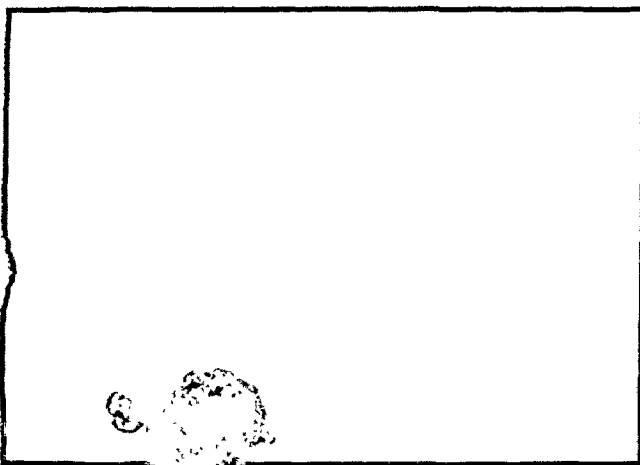
x = 7000



(b)

After 100 min. at 410°C

x = 7000



(c)

After 100 min. at 470°C

Fig. 35: Effect of thermal recovery on fatigue-softened structure in decarburized iron prestrained at 298°K

x = 10000

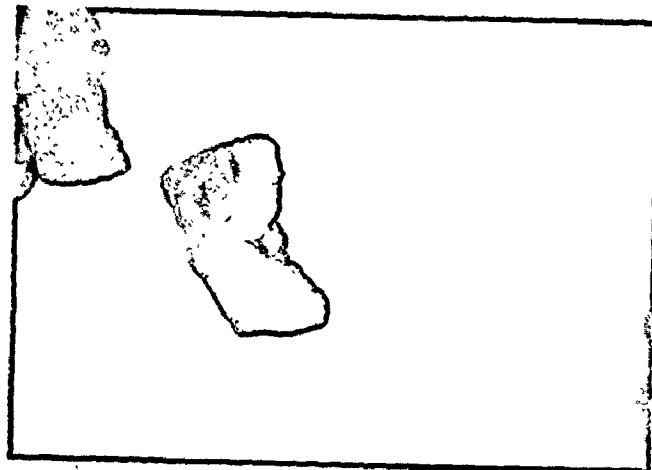
x = 10000

x = 10000



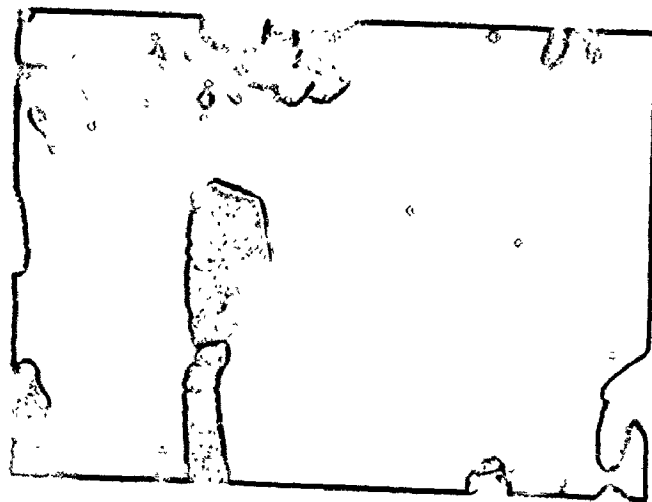
(a)

After 100 min. at 3. °C



(b)

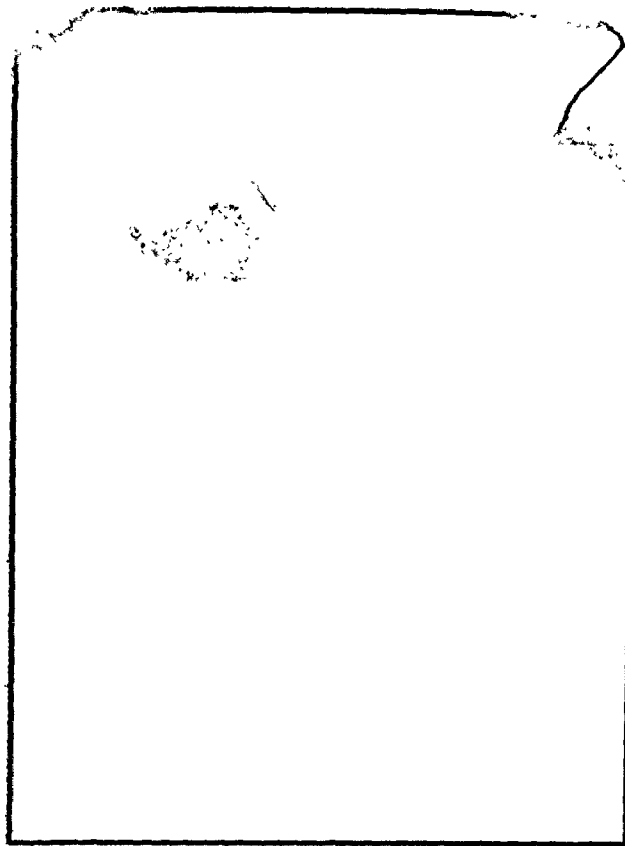
After 100 min. at 410°C



(c)

After 100 min. at 470°C

Fig. 36: Effect of thermal recovery on fatigue-softened structure in decarburized iron prestrained at 195°K



μ

Fig. 37: Polygonized structure evolved after 14 hours recovery at 470°C in fatigued specimens of decarburized iron

SECTION (5)

DISCUSSION OF RESULTS(5.1) Summary of Experimental Results

The results obtained in Section (4) may be summarized as follows:

- (1) Decarburised iron specimens reach a unique saturation stress level both in cyclic hardening and softening.
- (2) The X-ray asterism associated with prestrained specimens decreases appreciably by subsequent cyclic straining.
- (3) During cyclic softening, the salient microstructural changes are:
 - a) The shape of the dislocation cells tend to be more regular and become progressively sharp and well defined with a tendency to alignment along low index crystallographic planes of the form $\{110\}$ and $\{112\}$.
 - b) There is an observable increase in cell size with cyclic softening.
 - c) The substructure at saturation is characterized by the presence of two types of cells: an equiaxed type and a rectangular shaped type. Within the cell

walls, dislocations are arranged with some degree of regularity.

- d) Very small misorientations are associated with cell walls at saturation.
- (4) In order to study the influence of initial dislocation arrangement on subsequent fatigue softening, specimens were prestrained in tension at 298, 195, and 473°K. At 298°K, the substructure consists of complex tangles and cell walls separated by regions of relatively low dislocation density. At 195°K, a uniform distribution of long straight screw segments of dislocations and small dislocation loops are formed. At 473°K, under the conditions of dynamic strain ageing, a fine dispersion of dislocations rather than cell structure is formed.
- (5) The rate of cyclic softening in specimens prestrained at 195°K is much higher than that in specimens prestrained at 298°K whereas specimens prestrained at 473°K show the lowest rate of softening.
- (6) In the range of amplitudes studied, both the rate of cyclic softening and the saturation stress level increase with increasing the

plastic strain amplitude. A relationship between saturation stress and plastic strain amplitude is found for decarburised iron as:

$$\sigma_S = 40,000 \left(\frac{\Delta \epsilon_p}{2} \right)^{0.1}$$

- (7) In prestrained specimens of decarburised iron, the dislocation structure developed at 195°K is less stable, both mechanically (under subsequent fatigue) and thermally (under subsequent recovery), compared to the cell structure developed at 298°K.
- (8) The fatigued structure of decarburised iron resists thermal recovery for several hours at 470°C and is thermally more stable than the structure developed in uniaxial tension.

(5.2) General Characteristics of the Fatigue Softening Process in Decarburised Iron

It appears from the foregoing observations that work hardening increments, introduced by unidirectional deformation, are quickly removed under subsequent cyclic straining. Thus, the prestrained material must go through a process of reverting the initial deformation structure to the new

structure which characterizes the cyclic state.

On the basis of microstructural observations, associated with fatigue softening, the reduction of flow stress may be assigned to: the dipole formation, dislocation annihilation, and/or rearrangement of dislocations into lower energy configurations such as twist boundaries and simple tilt boundaries.

In the present study indications of structural reversion during cyclic softening are apparent on two scales: first, on a macroscopic scale, from the observed resistance of the fatigued structure to thermal recovery and the lack of X-ray asterism following cyclic softening; and second, on a microscopic scale, from the observed increase in cell size, lack of misorientations across cell boundaries, regular arrangement of dislocation arrays within cell walls and from the observed tendency of those walls to lie on low index crystallographic planes.

These property changes correspond to changes in the arrangement and density of dislocations in order to decrease the overall energy. In a wavy slip mode material such as iron, where cross-slip is an easy process, the dislocations are capable of moving in three dimensions which allow such changes to take place during cyclic straining.

The observed small misorientations across cell walls suggest that the dislocation structures which constitute those walls are associated with relatively small amplitude

of long range stresses. A macroscopic confirmation of this can be seen from the lack of X-ray asterism which suggests a dissolution of the strain gradients, associated with the prestrained structure, under subsequent cyclic straining.

The well defined and sharp appearance of the cell walls, and their tendency to lie on low index crystallographic planes, indicate that their configurations are of relatively low energy. This is consistent with the strong resistance of the fatigued structure to thermal recovery which implies that most of the dislocation structures developed in fatigue are thermally stable.

Microstructural studies of Feltner and Laird (1967) and Laufer and Roberts (1966) on high SFE materials, fatigued under intermediate cyclic strain amplitudes (as the case in this work), suggest that the cell boundaries consist mainly of twist configurations. Such configurations, as indicated by Li (1963), are thermally stable. Combining this with our observations, on thermal recovery and misorientations across cell boundaries, lead to the probable conclusion that cell walls, at saturation, consist mostly of low angle twist boundaries and dipole structures.

The observed increase in cell size during cyclic softening suggests that the fatigue softening process is, also, associated with some dislocation annihilation.

(5.3) Kinetics of Fatigue Softening

The marked differences in the initial microstructure, after unidirectional prestrains at 195°K and 298°K, reflect the increasing lattice friction forces at lower temperatures. These result in decreased mobility of screw components and the tendency for dislocations to be trapped either singly or in pairs rather than accumulated in more complex groups due to the interactions between dislocations as observed at 298°K.

Although the structures developed on cyclic softening are similar, at saturation, regardless of the temperature of prestrain, the rate of cyclic softening is much greater in the material prestrained at 195°K.

This can be rationalised in the following simple kinetic model: consider the nature of dislocation arrangement after deformation at 195°K. Dislocations are trapped as long screw segments and pairs of dislocations of opposite sense. When the temperature is raised to 298°K, the lattice friction forces, inhibiting the mobility of dislocations, decrease and when the specimen is cycled at 298°K dislocations are able to move and mutually annihilate, under the action of the applied stress, by cross slip.

Thus, the rate of decrease of dislocation density with number of cycles can be expressed as

$$\frac{d\rho}{dN} = -K\rho^2 \quad (3)$$

where K is a rate constant which describes the annihilation probability and involves the area swept out by a dislocation and the activation energy for cross slip.

We assume that the saturation level represents a constant structure condition with dislocation density ρ_S and flow stress σ_S . Thus, if after N cycles the flow stress is σ_N and dislocation density is ρ_N , we can write

$$\rho_N = \rho_R + \rho_S \quad (4)$$

where ρ_R represents an "excess" dislocation density to be annihilated according to Eq. (3).

Thus, Eq. (3) can be integrated to yield

$$\frac{1}{\rho_R} - \frac{1}{\rho_0} = KN \quad (5)$$

where ρ_0 is the initial value of ρ_R . Using the well known relation between dislocation density and the square of the flow stress, Eq. (4) yields

$$\frac{1}{\rho_R} = \frac{(\alpha\mu b)^2}{\sigma_N^2 - \sigma_S^2} \quad (6)$$

where α is a constant and μ is the shear modulus.

Substituting in Eq. (5), gives

$$\frac{1}{\sigma_N^2 - \sigma_S^2} = \frac{K}{(\alpha \mu b)^2} N + \frac{1}{\rho_0 (\alpha \mu b)^2} \quad (7)$$

Figure 38 shows the softening kinetics of the decarburised Ferrovac-E, predeformed at 195°K, plotted in the form of Eq. (7).

The rate constant K was found to be proportional to the plastic strain amplitude $\Delta \epsilon_p$ as expected from a simple model in which the annihilation occurs due to dislocations being swept to within some initial collision distance during cyclic straining. Figure 39 shows a linear relationship between K and $\Delta \epsilon_p/2$.

The agreement between the data and the model is good. However, a more quantitative appraisal of the rate constant requires a careful study of the temperature dependence of the softening rate which is difficult in the present context due to the problem of the simultaneous action of both an effective stress component and an internal stress component in determining the overall stress level. Similar difficulties arise in considering the frequency dependence of cyclic softening.

Let us now consider the situation in specimens deformed at 298°K. Unlike the uniform arrangement of dislocations developed at 195°K, deformation at 298°K results in the formation of a cell structure which when

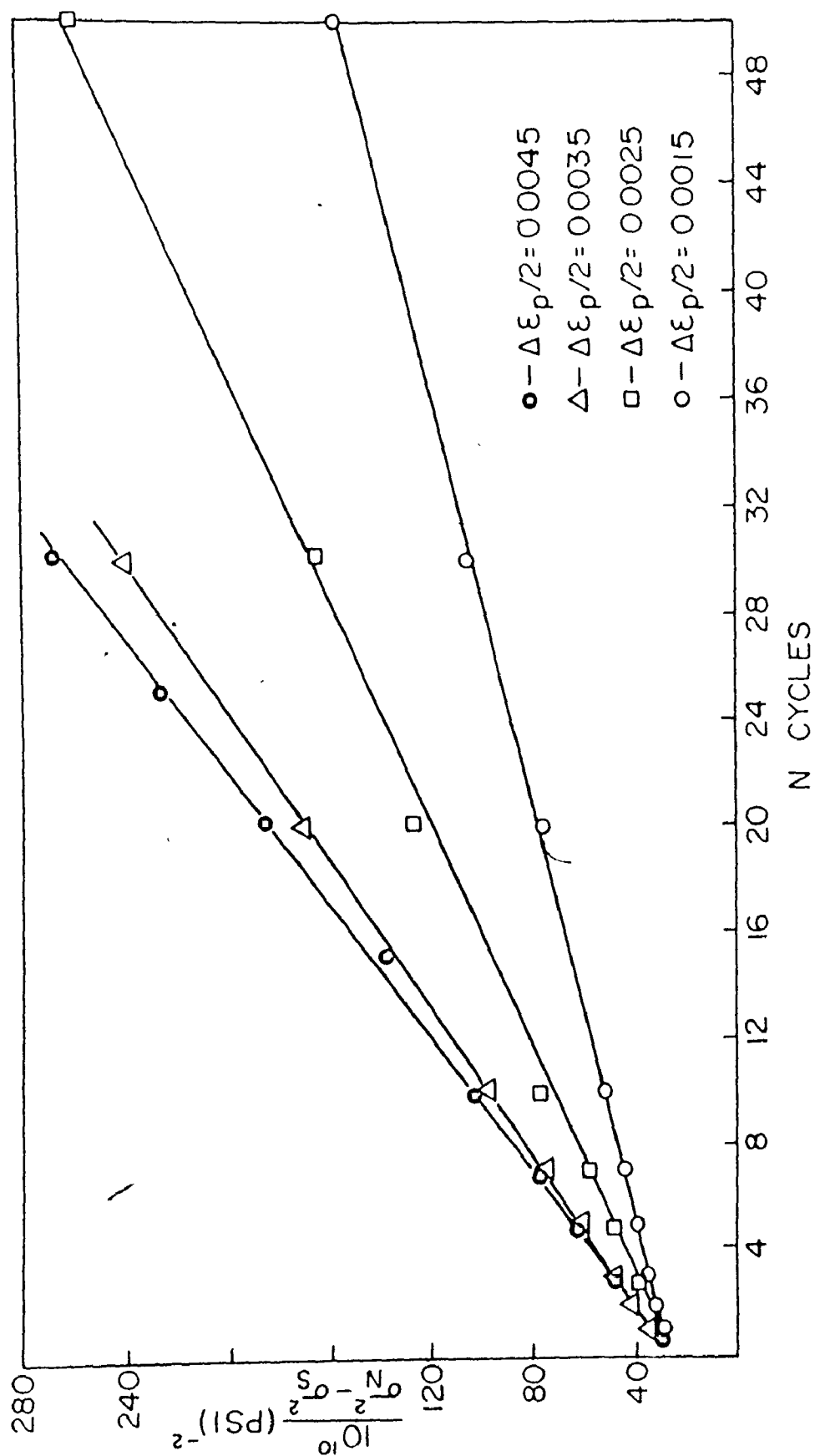
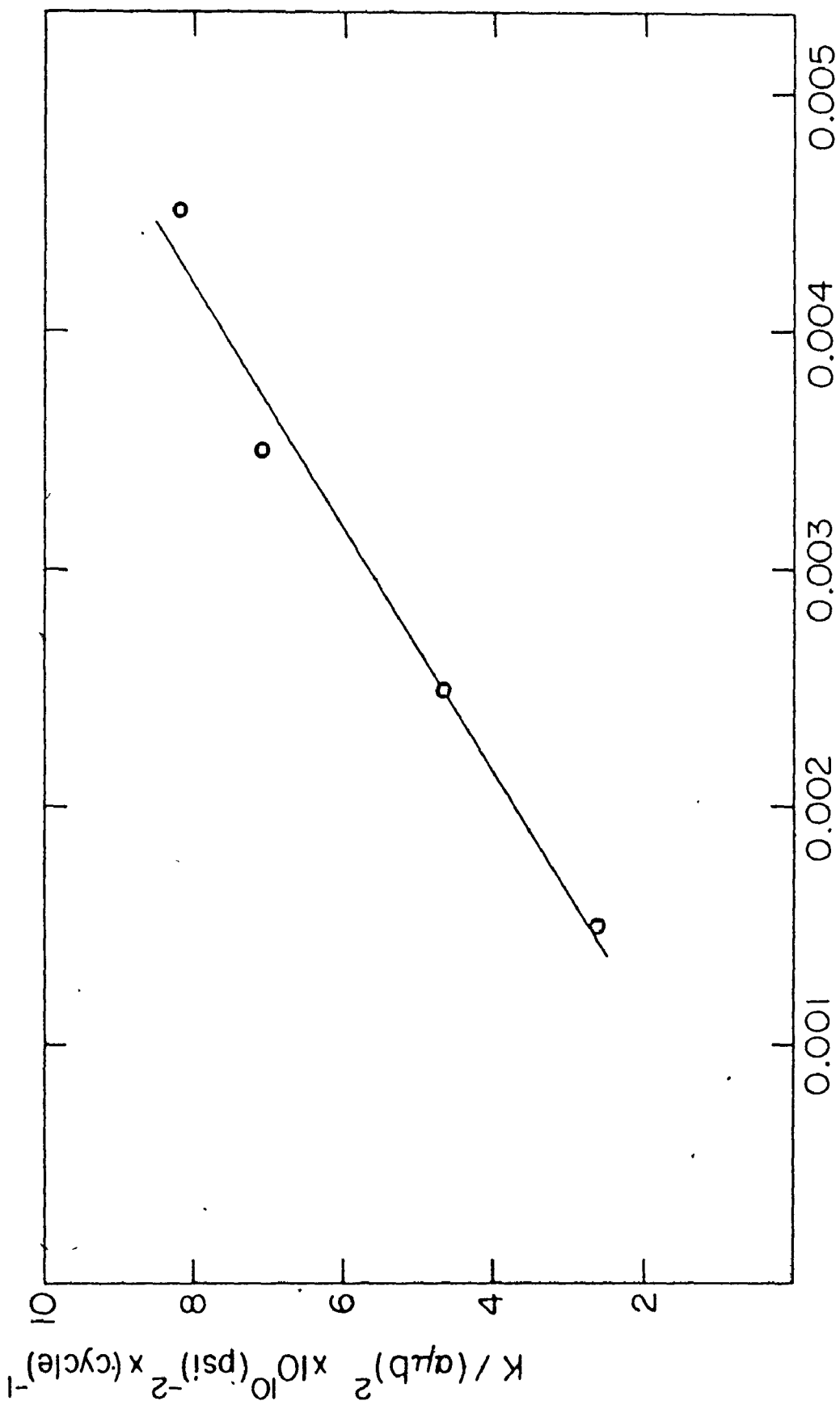


Fig. 38: Kinetics of fatigue softening in decarburized iron specimens prestrained

10% at 195°K





151

Fig. 39: Effect of plastic strain amplitude ($\Delta \epsilon_p / 2$) on reaction rate constant (K) in decarburized iron specimens prestrained 10% at 195°K

[Handwritten signature]

cycled, requires only a change in the "degree" or "intensity" of the structure, not of kind, to achieve complete softening.

Because of the favourable conditions for cross slip at 298°K, it is possible that part of the dislocation rearrangement can take place during prestraining. Thus, some relatively stable dislocation configurations are expected to be associated with the prestrained structure developed at 298°K. The work of Keh and Weissman (1963) on uniaxial deformation in iron, and Li (1963) on work hardening in bcc materials, support this viewpoint. In this case, the tangles of dislocations are not able to disintegrate spontaneously under the action of the applied stress during subsequent cycling. Thus, additional resistance to the annihilation process will be imposed by the initial microstructure. Such resistance may act to decrease the probability of dislocation annihilation and consequently the magnitude of the rate constant K in Eq. (3).

Data for specimens prestrained at 298°K is plotted in Fig. 40 in the form of Eq. (7). It can be seen that the experimental data is again in good accord with the theory.

It is significant to note that the values of $K/(\alpha\mu b)^2$, calculated at $\Delta\epsilon_p/2 = 0.0025$, for specimens prestrained at 195 and 298°K, are: 4.7×10^{-10} and 2.2×10^{-10} (psi)⁻²/cycle respectively. This indicates clearly the higher rates of softening associated with specimens prestrained at 195°K.

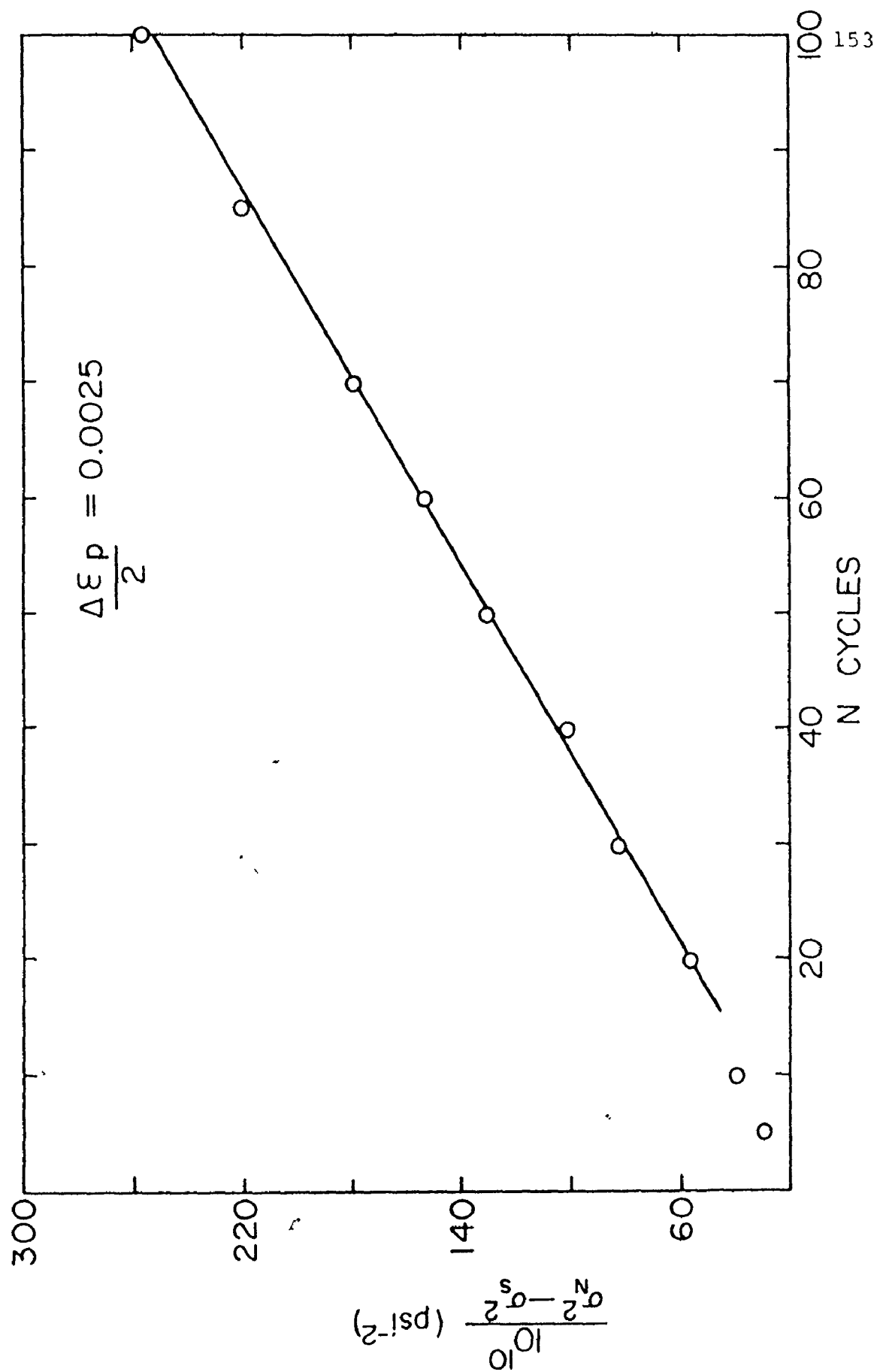


Fig. 40: Kinetics of fatigue softening in decarburized iron specimens prestrained
10% at 298°K



We now consider the case of Armco iron predeformed at 473°K. After uniaxial deformation at this temperature, dislocations are pinned by solute atoms and are assumed to be relatively immobile during cycling. Let us assume that on each cycle each immobilised dislocation has a probability A of being annihilated by a mobile dislocation of opposite sign, then one can write a first order kinetic reaction in the form

$$\rho_R = \rho_0 A^N \quad (8)$$

where ρ_R and ρ_0 are defined as in Eq. (4). Then, by reasoning applied above regarding the relationship of the dislocation density and the flow stress we have

$$(\sigma_N^2 - \sigma_S^2) = (\alpha \mu b)^2 \rho_0 A^N$$

Thus,

$$\log(\sigma_N^2 - \sigma_S^2) = \log(\alpha \mu b)^2 \rho_0 + N \log A \quad (9)$$

A reasonable agreement with Eq. (9) is shown in Fig. 41 from the softening data for Armco iron prestrained at 473°K.

It can be seen from the foregoing discussion that the nature and scale of the substructure play an important

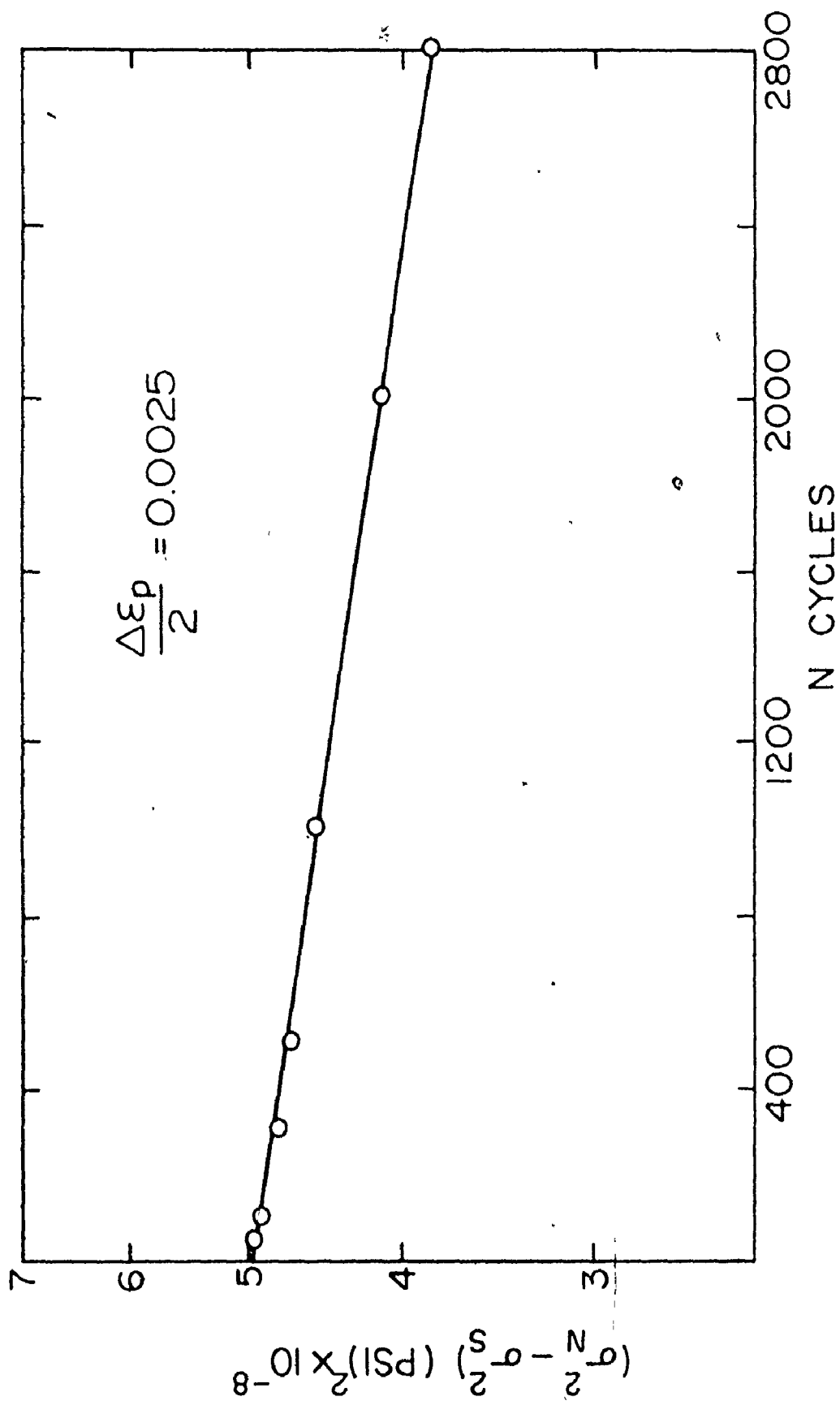


Fig. 41.: Kinetics of fatigue softening in Armco iron specimens prestrained

10% at 473°K



role as a strengthening mechanism in fatigue. The model presented above gives a preliminary account of the kinetics of cyclic softening and illustrates that the rate of softening is dependent on the initial dislocation distribution. This emphasises the importance of mechanical-thermal history of the microstructure on subsequent cyclic straining. It is of interest to note that the rate of thermal recovery is also dependent on the initial distribution in a similar fashion to that reported above.

(5.4) Summary and Conclusions

The problem of cyclic softening is an important one in that it concerns to the degradation of load bearing capacity developed by previous cold work. In the present chapter, two basic aspects of this problem were studied in iron: first, the structural changes associated with the softening process and, second, the microstructural features which control the rate of softening.

The most significant results have been summarized in Section (5.1). On the basis of these observations the following conclusions can be made:

- (1) During cyclic softening, dislocations undergo annihilation and rearrangement, to a lower energy configuration such as dipoles and twist

boundaries, in order to decrease the overall energy. Also, the cell boundaries become sharp and well defined and tend to align along low index crystallographic planes. Macroscopic observations confirm that the structure developed by cyclic straining is in a lower energy state compared to that developed by uniaxial tension.

- (2) The rate of cyclic softening is governed by the initial arrangements of dislocations.
- (3) A model, based on mutual annihilation of dislocations, is proposed to account for the kinetics of cyclic softening after prestraining at different temperatures. For specimens prestrained at 195 and 298°K, the rate of decrease of dislocation density with number of cycles can be described as a second order process evidenced by the observed linear relationship between $1/(\sigma_N^2 - \sigma_S^2)$ and N . This behaviour is explained in terms of a pairwise annihilation of dislocations. For specimens prestrained at 473 K, the rate equation describes a first order process, giving straight line on a $\log(\sigma_N^2 - \sigma_S^2)$ versus N plot. In this case a fixed resistance to the dislocation

motion is assumed.

- (4) The data suggests that in order to inhibit the cyclic softening process, some form of effective pinning of the prestrained dislocation structure must be utilized as in the dynamic strain ageing and thermal mechanical working as reported in Chapter IV.

CHAPTER IV

STABILITY OF PLASTIC FLOW
IN FATIGUE

SECTION (1)

OBJECTIVES

In the past decade efforts have been directed toward utilizing work hardening and precipitation hardening processes to increase the strength of engineering materials. Dislocation substructure, precipitation hardening and solid solution hardening are usually regarded as effective mechanisms for uniaxial strengthening. Unfortunately, strength in uniaxial loading is an unreliable guide to fatigue performance. In Chapter II, for example, it appeared that some of the work hardening increment introduced by uniaxial deformation is removed by subsequent cyclic straining; a behaviour which imposes limitations on the exploitation of dislocation structure as a strengthening mechanism in fatigue applications. Also, cyclic strain hardening in two phase materials is limited compared to that in uniaxial deformation because in reversed cyclic straining there is no, or very little, build-up of long-range back stresses from the particles as one would predict from data presented in Chapter I. Moreover, very fine precipitates that provide effective barriers in uniaxial loading may dissolve locally under the influence of cyclic straining. Such behaviour can impose another limitation on the utilization of uniaxial strengthening mechanisms in fatigue

applications. Thus, it is important not only to develop materials that are strong under uniaxial loading, but also to understand how they perform under cyclic loading.

The influence of microstructure on fatigue is felt in the initiation and propagation of cracks. From a metallurgical viewpoint, it appears that the most important parameter which governs the development of fatigue induced cracks is the nature of the plastic deformations which occurs at the crack tip. Previous studies on microstructural aspects of the fatigue process suggested that the localization of plastic flow, such as the formation of persistent slip bands (P.S. bands) is pre-requisite to the growth of fatigue fracture nuclei (Broom and Ham 1962). This emphasises the importance of the stability of plastic flow under cyclic deformation and the connection between plastic instability and crack growth.

As outlined by McClintock (1963), the low work hardening rate leads to the ability of the material to undergo localized plastic deformation and consequently higher rates of fatigue crack propagation. Localization of plastic flow, usually, occurs when the rate of doing external work exceeds the rate of internal dissipation. Thus, as the rate of work hardening decreases, the rate of internal dissipation will be decreased and inhomogeneous deformation can occur in which large local strains are permissible.

During the fatigue process of simple systems such as single-phase materials, the saturation state is shown to be pre-requisite to the onset of strain localization into active bands. As outlined in Chapter II saturation occurs when no hardening is observed macroscopically, i.e., when the rate of dislocation production due to strain hardening is balanced by some recovery process such as cross-slip.

In the more complex structures such as materials containing fine particles, localization of plastic flow can be greatly intensified by dissolution of particles during fatigue. Several authors (Broom et al. 1957, McGrath and Bratina 1967, and Wilson and Mintz 1972) have observed that localized softening, during cyclic straining of aged ferrous and non-ferrous alloys, is associated with an attendant dissolution of fine particles in localized regions.

Local instabilities, in general, must arise from the nature of the microstructure at the onset of plastic strain localization. Thus, one of the objectives of this chapter is to delineate the characteristic microstructural features developed in fatigue which lead to the condition where the work hardening characteristics of the material are unable to prevent the localization of plastic flow and thus the onset of fatigue cracks.

The present study was performed on quench-aged low carbon iron containing various dispersions of iron carbides

in order to utilize a well characterized model system which is of direct relevance to current engineering materials.

The study had two objectives: firstly, to develop an overall understanding of the problem of plastic instability in fatigue, and secondly, to delineate the role of substructure on plastic instability in dispersion-hardened materials subjected to cyclic straining.

In order to accomplish these objectives it was necessary to study the following:

- (a) The overall responses of the materials under both uniaxial and cyclic straining,
- (b) The influences of: strain rate, interrupted strain rate changes, temperature, interrupted temperature changes, and interrupted static ageing on the cyclic responses of the materials, and
- (c) The detailed microstructural features before and after fatigue.

SECTION (2)

EXPERIMENTAL DETAILS

The experimental scheme consisted of thermal pre-treatment of the material to produce different dispersions of carbide particles in ferrite. Polished specimens were fatigued in tension-compression under controlled strain amplitude, and their cyclic stress response measured. The observed mechanical properties were correlated with substructural changes revealed by transmission electron microscopy.

The study was performed on Armco iron of the composition shown in Table 1 and of grain size approximately 50 μ .

In order to vary the distribution of second-phase particles, specimens were austenitized at 900°C for two hours, cooled slowly through the austenite-ferrite transformation to 725°C, water quenched, and then aged at two temperatures; 25°C and 240°C.

In addition, some comparative tests were made on furnace-cooled Armco iron specimens prepared as in Section (3.2) of Chapter III.

The procedures for specimen preparation, machining and polishing were as described in Section (3) of Chapter III.

All the fatigue testing was completed using a closed-loop M.T.S. machine and all the tensile tests were performed in Universal Instron machine.

The main fatigue testing programme was carried out at a controlled stroke amplitude equivalent to a plastic strain amplitude $\frac{\Delta \epsilon_p}{2} = 0.008$ at room temperature and under a cyclic frequency of 0.1 cps.

In order to investigate the influence of particle dispersions on the mechanical response during the fatigue history, some strain rate change tests and interrupted temperature change tests were conducted at various times during the course of the fatigue test. Changes in strain rate were, simply, achieved by changing cyclic frequency during the test. In order to change the temperature, the test was stopped, temperature changed to 4°C and then, cycling continued at the new temperature. The change in temperature was achieved by surrounding the specimen and the entire gripping system with a bath of cooled water and ice cubes. Care was taken to ensure that the system was at constant temperature by using two thermometers attached to the specimen and grips.

The microstructure of each material was studied by transmission electron microscopy both prior to and subsequent to the cyclic deformation, in order to establish the detailed microstructural changes which occurred.

All the details concerning testing equipment, precautions and accuracy measurements were as described previously in Chapter III and will not be considered further in the present chapter.

SECTION (3)

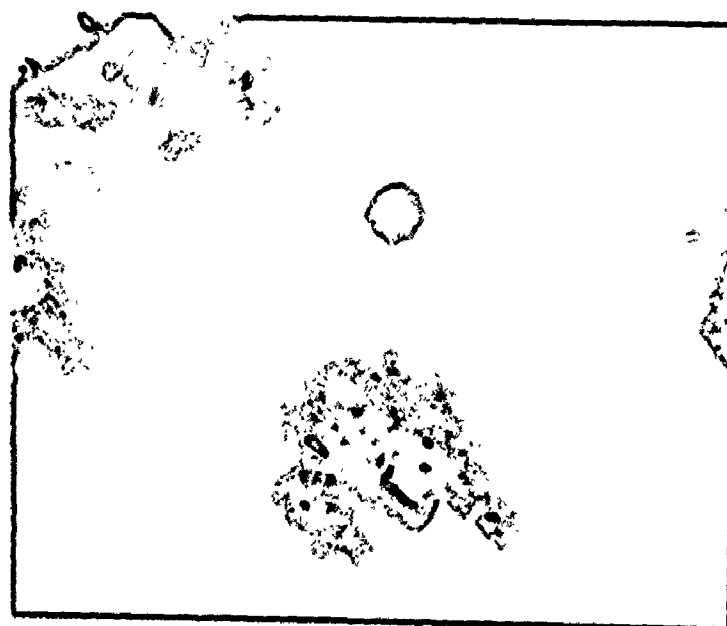
EXPERIMENTAL RESULTS

For clarity the results are reported in four sections. The first describes the detailed microstructures observed prior to fatigue. The second concerns the overall mechanical response to cyclic deformation. The third describes the dislocation microstructures produced by the cyclic deformation and the fourth section compares fatigue and tensile properties.

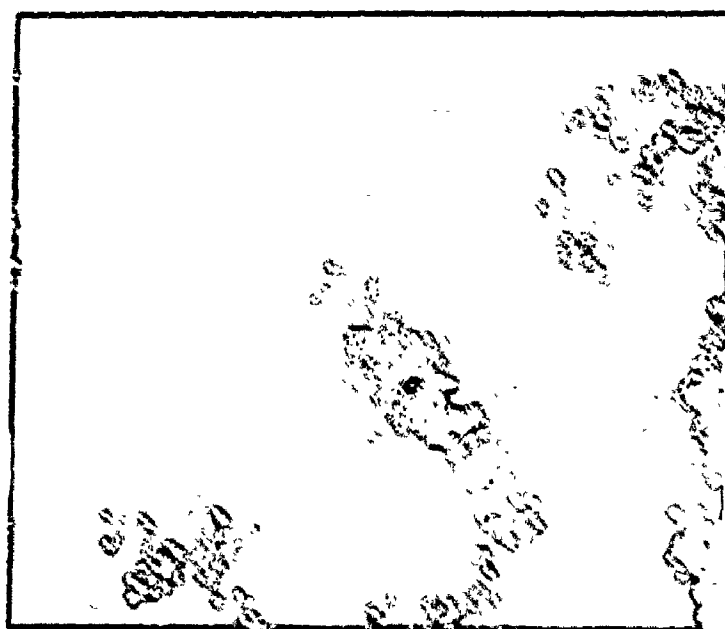
(3.1) Initial Microstructure

After ageing at 240°C for 5 hours, an irregular distribution of dendritic particles was formed. Figure 42 shows transmission electron micrographs of the microstructure at low and high magnifications. The particles observed in these micrographs are consistent with the appearance of cementite (Kelly and Nicholson 1963). The spacing of the particles was in the range 1-3 μ , with a mean of about 1.7 μ ; and the particle size was in the order of 4000 Å.

After ageing at 25°C for four weeks a much more regular distribution of much finer particles was produced. The precipitates can be resolved, at high magnification, as

 $x = 4000$

(a)

 $x = 15000$

(b)

Fig. 42: Carbide particle distribution in Armco iron

platelets of (100) habit plane (Fig. 43). The platelet average diameter is about 500 Å and the thickness of the plates is in the order of 100 Å. The disc like morphology of these particles and their habit plane correlates with similar observations of ϵ -carbides made by Brown and Embury (1972).

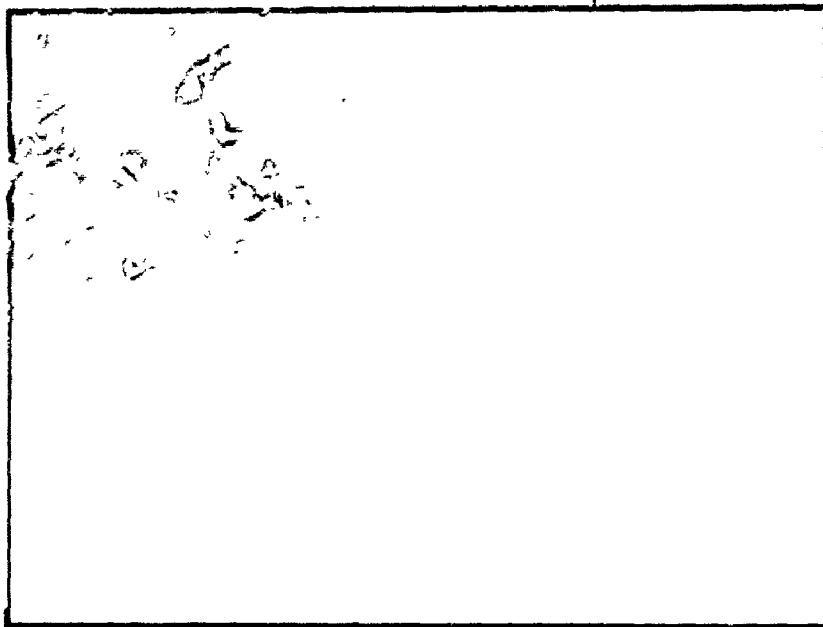
(3.2) Overall Mechanical Response

Table 8 summarises tensile properties of all the materials investigated.

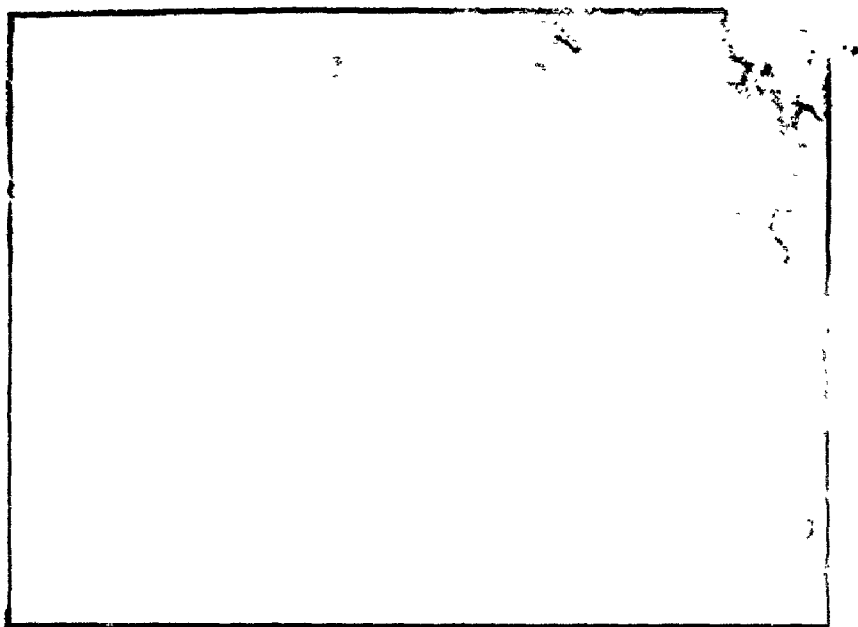
In order to provide a basis for comparison, all the specimens were fatigued at room temperature under the same plastic strain amplitude ($\frac{\Delta \epsilon_p}{2} = 0.008$) and frequency (0.1 cps).

In case of material quenched-aged at 25°C to produce a fine dispersion of particles, the cyclic response was characterized by a period of low hardening rate in the first few cycles, followed by a continuous softening behaviour as shown in Fig. 44.

In contrast, the material aged at 240°C to produce a coarse dispersion of particles showed a short period of saturation followed by a period of gradual hardening (Fig. 44). The type of cyclic behaviour in this material was similar to that observed for furnace-cooled material (Fig. 45).



(a)



(b)

Fig. 43: Carbide particle distribution in Armco iron
quenched-aged at 25°C

TABLE 8
TENSILE PROPERTIES

Material	σ_Y PSI	σ_U PSI	% R.A. to Failure	ϵ_f
Furnace Cooled	22300	43100	82%	1.71
As-Quenched	16200	36000	80%	1.61
Q-A (25°C)	46000	60700	69%	1.33
Q-A (240°C)	32500	44000	78%	1.49

σ_Y = Yield Stress, σ_U = Ultimate Tensile Stress,

% R.A. = Percentage Reduction in Area and

ϵ_f = True Tensile Strain to Fracture.

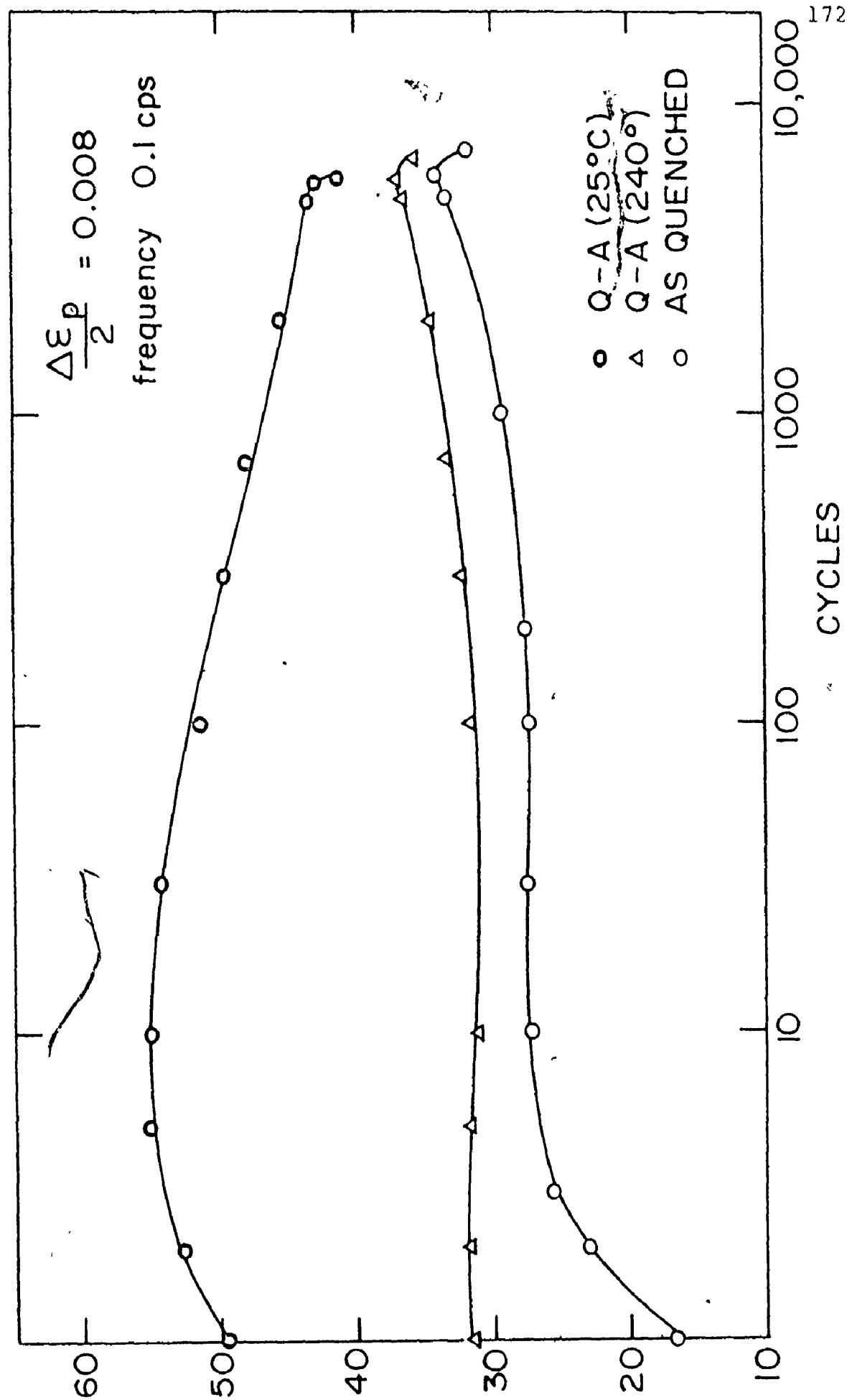


Fig. 44: Cyclic response in As-quenched, Q-A (25°C) and Q-A (240°C) Armco iron

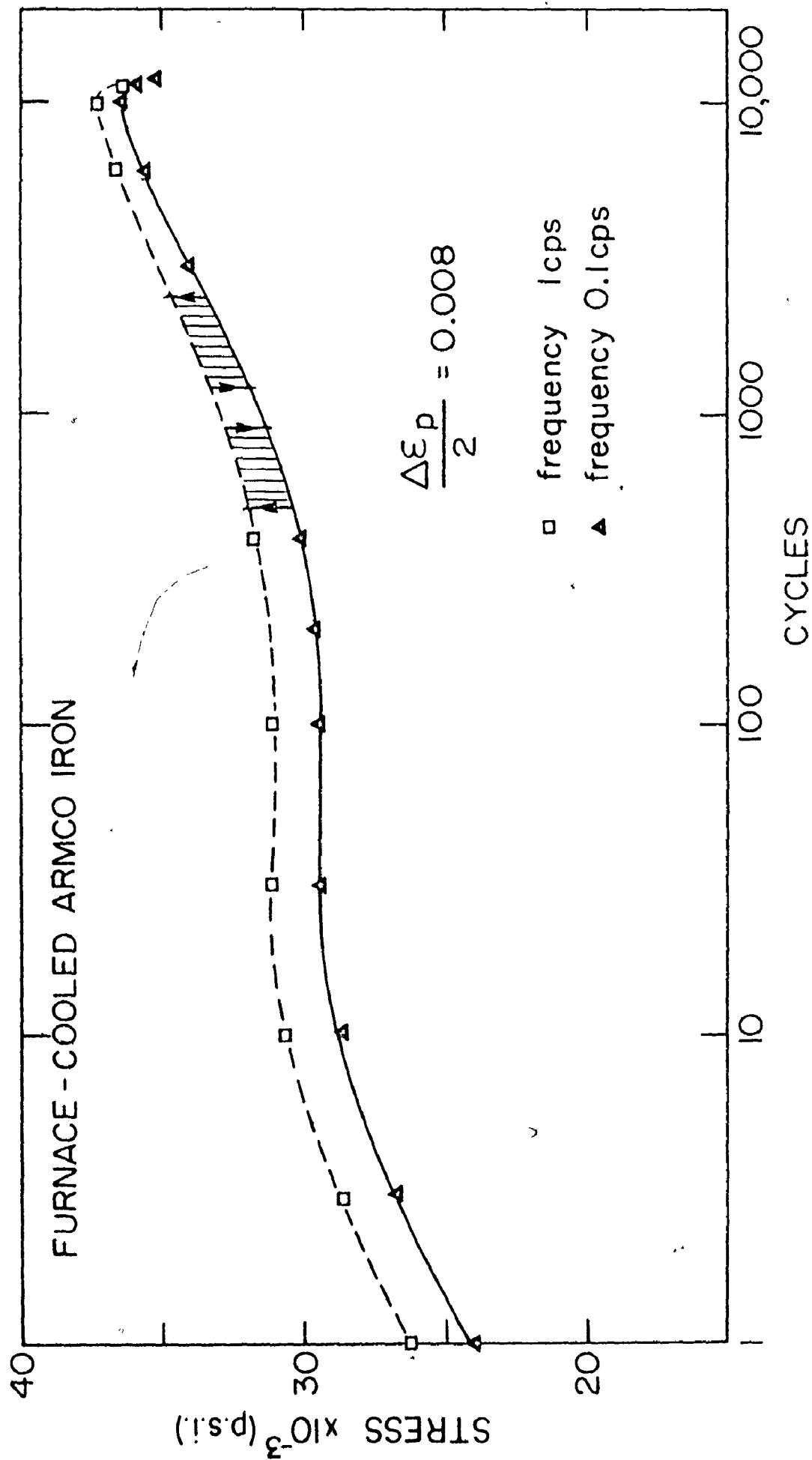


Fig. 45: Effect of strain rate and strain rate changes on cyclic response of furnace-cooled Armco iron

cooled Armco iron

[Handwritten signature]

The cyclic response of the material in the As-quenched condition is included with Fig. 44 for comparison. This material exhibited high rates of hardening in the primary region. Such behaviour was attributed by McGrath and Bratina (1969) to the excess carbon in ferrite matrix.

In the present study more emphasis is placed on the softening behaviour associated with the fine dispersion of particles. Such behaviour is an indication of structural instability which limits the utilization of fine particles as a strengthening mechanism in fatigue applications. Thus, to obtain a more comprehensive understanding of the influence of particle dispersions in fatigue, three sets of experiments were conducted at various times during the course of the fatigue test. These experiments involved strain rate change tests, temperature change tests and, static ageing tests.

Note: For reasons of brevity, specimens quenched-aged at 25°C to produce a fine dispersion of particles will be identified as Q-A (25°C) while, specimens quenched-aged at 240°C to produce a coarse dispersion of particles will be identified as Q-A (240°C).

(a) Strain rate change tests

During the cyclic softening period, in specimens Q-A (25°C), it was observed that increasing the test frequency resulted in a decrease in flow stress. On the contrary, the material Q-A (240°C) and the furnace-cooled material both showed conventional increase in flow stress by increasing the cyclic frequency. This is illustrated in Fig. 46. The data indicates two important features: firstly, the cyclic softening behaviour in material Q-A (25°C) is associated with a negative strain rate sensitivity. Thus, it is possible that such behaviour is associated with a dynamic strain ageing effect similar to that described by Mintz and Wilson (1965) for the case of quenched materials containing excess carbon in solid solution.

Secondly, the cyclic response of both the Q-A (240°C) material and the furnace-cooled material, is associated with positive strain rate sensitivity. More important is that the subsequent hardening behaviour, in both materials, is associated with a positive strain rate sensitivity. This result seems to suggest that the subsequent cyclic hardening behaviour (usually observed in ferrous systems) is not necessarily due to a strong dynamic strain ageing effect. This aspect will be considered further in Appendix B.

It appears from Fig. 46 that the structures of both materials, Q-A (25°C) and Q-A (240°C), exhibit a gradual

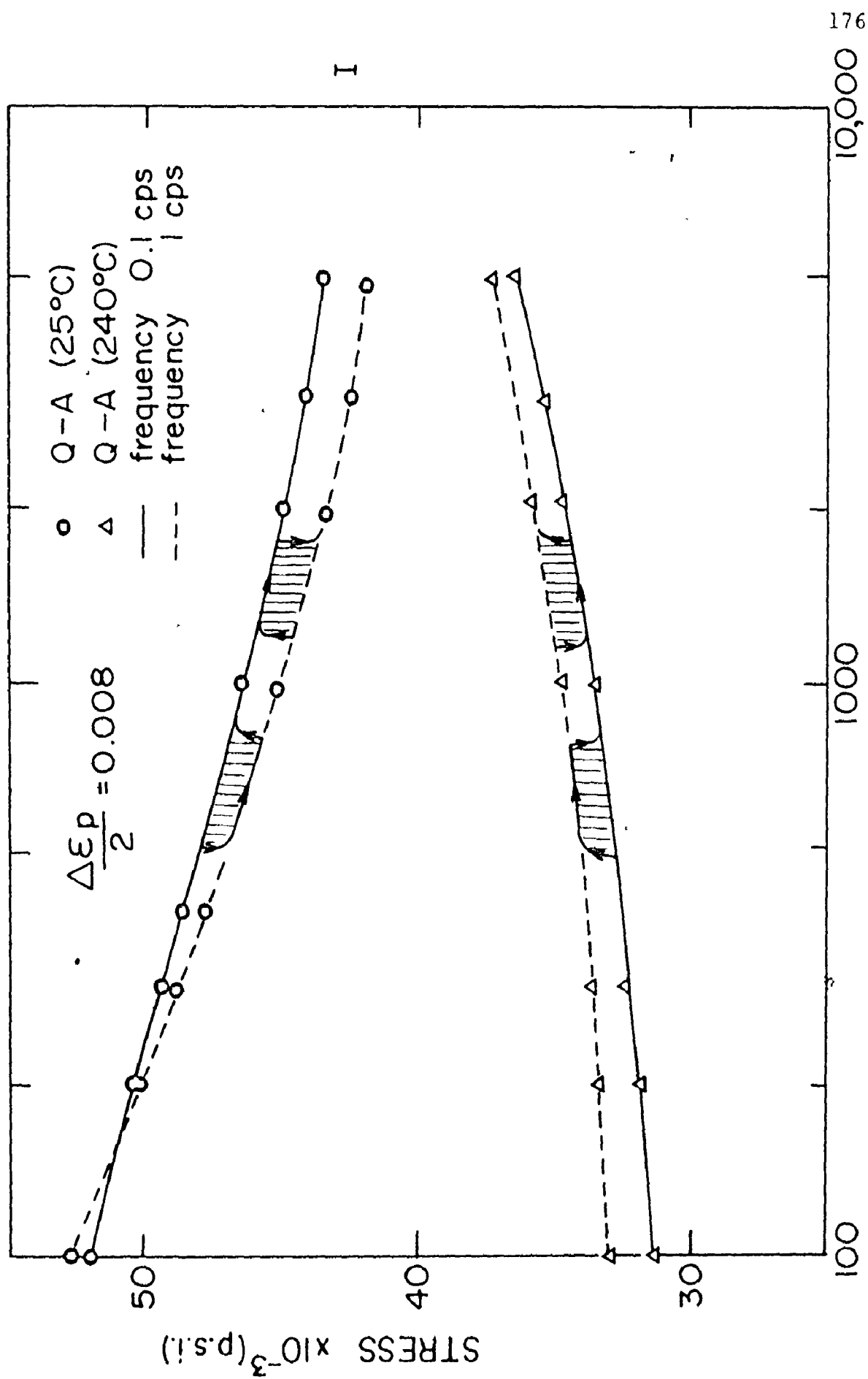


Fig. 46: Effect of strain rate and strain rate changes on cyclic response of Q-A (25°C) and Q-A(240°C) Armco iron

(rather than instantaneous*) response to sudden changes in cyclic frequency. In both materials (after 10 - 30 cycles under the new frequency) the stress response approached the envelope which characterizes the cyclic state of each material at the current frequency.

(b) Interrupted-temperature change tests

This experiment was designed to determine whether a decrease in the deformation temperature can slow-down the softening process in the Q-A (25°C) material.

The fatigue tests of some Q-A (25°C) specimens were interrupted by a slight change in temperature from $\sim 26^{\circ}\text{C}$ (room temperature) to 4°C . A typical set of results are shown in Fig. 47. The decrease in temperature from 26°C to 4°C resulted in an immediate increase in cyclic flow stress which corresponds to the difference in thermal components of flow stress at the two temperatures. This increase was followed by much lower rates of softening which correspond to an adjustment in the structure with continued cycling to a structure which is characteristic of the current deformation temperature.

It is interesting to note that - unlike the behaviour at room temperature - the cyclic behaviour of the material at

* as observed for furnace-cooled material, Fig. 45.

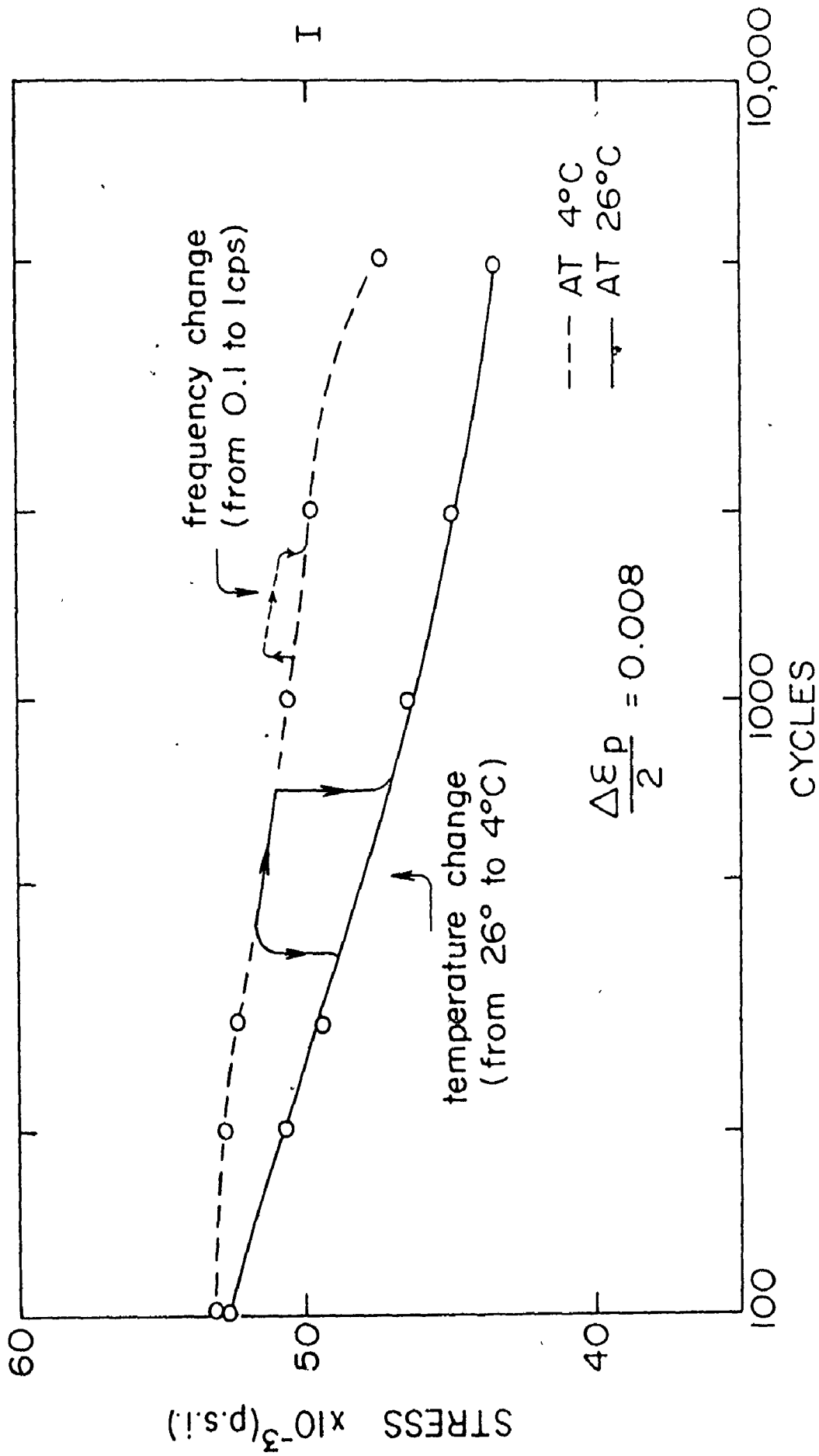


Fig. 47: Effect of cyclic temperature on softening behaviour in O-A (25°C) Armco iron

178

4°C is characterized by a positive strain rate sensitivity. Figure 47 illustrates changes in cyclic response at 4°C due to changing cyclic frequency.

(c) Static ageing tests

It was indicated by several authors (McGrath and Bratina 1967, and Wilson and Tromans 1970) that ferrous systems containing fine particles will suffer particle dissolution in localized regions if subjected to cyclic straining. This suggests that such localized regions must contain a supersaturation of carbon from the dissolved particles. To examine this hypothesis on the Q-A (25°C) material, the fatigue tests of some specimens were interrupted after ~ 4500 cycles by a static ageing process for 12 hours at room temperature under zero stress. Restarting the test resulted in a considerable increase in flow stress which decayed back after about 1000 cycles to nearly the stress level that was reached before static ageing. Selected results are shown in Fig. 48. It can be clearly seen that the interrupted static ageing process resulted in about 17% initial increase in cyclic flow stress and about 20% increase in fatigue life. This seems to emphasise the importance of interrupted static ageing processes in improving the fatigue life of dispersion-hardened materials which suffer particle dissolution in fatigue.

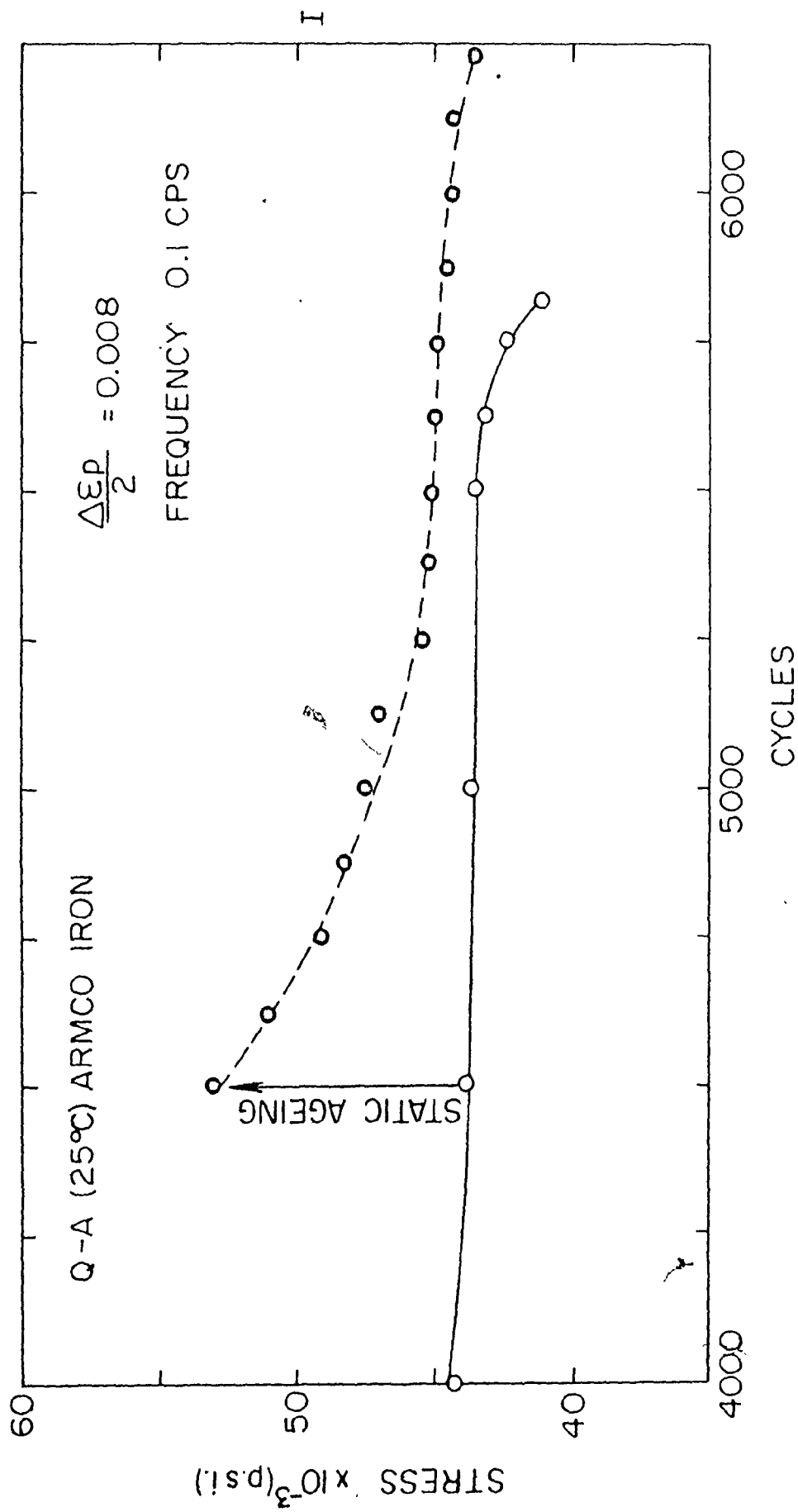
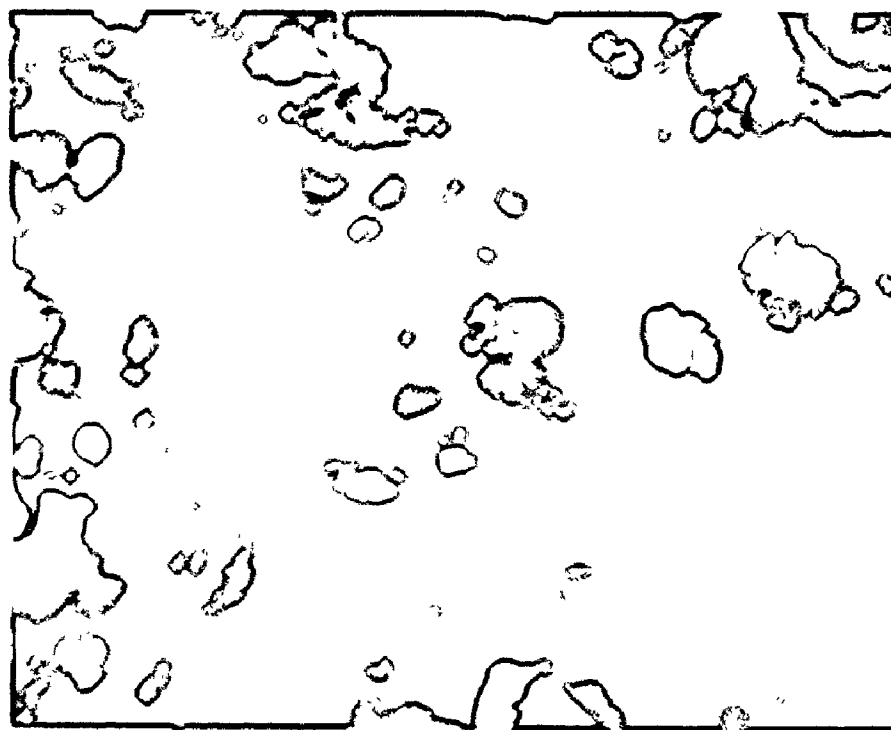


Fig. 48: Effect of static ageing for 12 hours at room temperature on cyclic response of Q-A (25°C) Armco iron

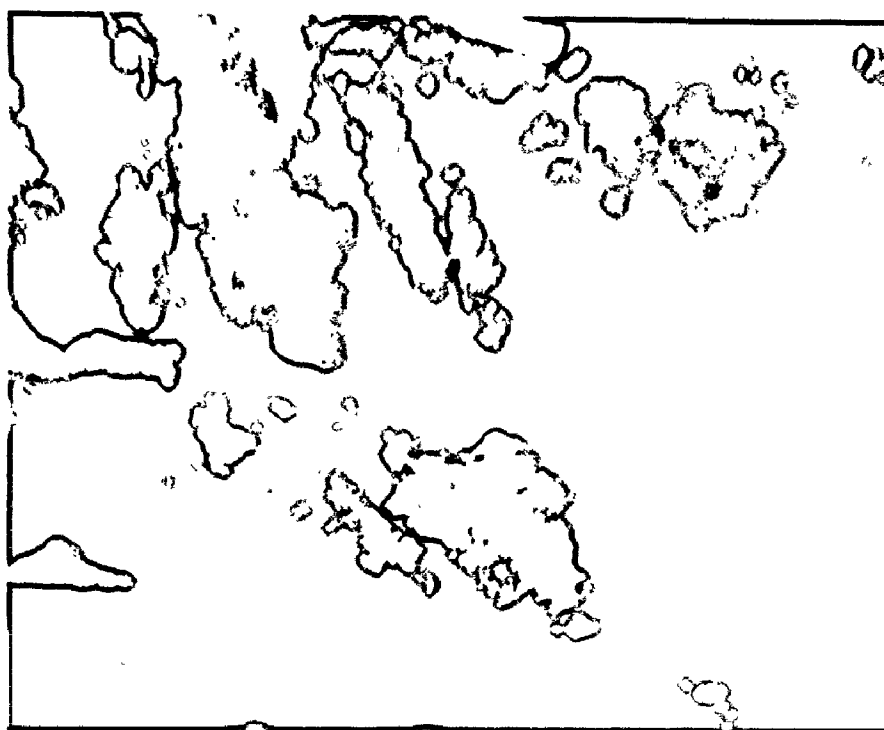
The above result may be interpreted as a consequence of solute atoms condensing to or diffusing back to the particle-free channels which block the motion of dislocations and cause the flow stress to be temporarily raised. With continued cycling, any small precipitates that could have been formed during static ageing may redissolve again causing the flow stress to gradually decay back to its original level.

(3.3) Microstructures After Fatigue

In the specimens Q-A (240°C) which contain coarse distribution of cementite particles, it was observed, after 4000 cycles, that a cell structure was formed which was similar in scale to that produced in a furnace-cooled material as shown in Fig. 49. No evidence of narrow active slip bands was observed, probably because the increased interparticle spacing allows dislocations to move freely in the lattice and give rise to diffused slip. This is consistent with the surface observations made by McGrath and Bratina (1967) on an iron-carbon alloy that was quenched-aged at 200°C. However, in some regions the material exhibited a more regular coarse rectangular cell structure with walls lying on {110} and {112} planes. It should be emphasised that similar features have been observed in



(a)



(b)

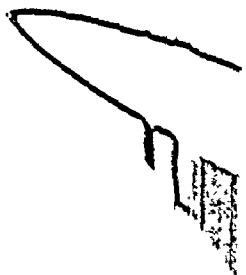
Fig. 49: Dislocation structure in Q-A (240°C) material after fatigue: (a) general features of the substructure
(b) regular cell walls

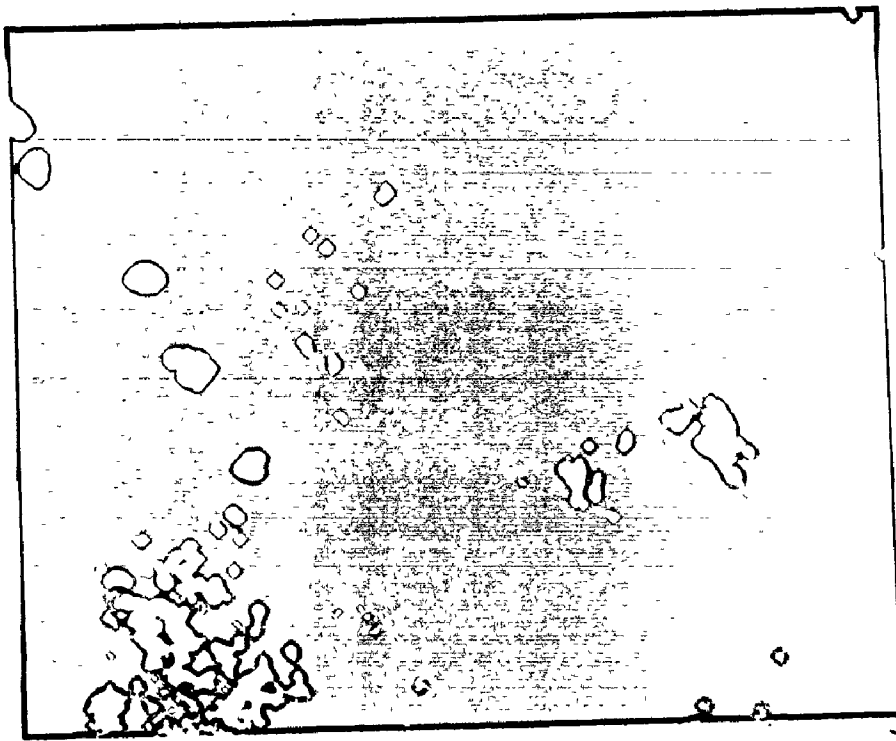
Chapter III associated with the fatigued structure of decarburized iron.

The average cell size was of the order of 1.5 μ , i.e., of the order of the interparticle spacing.)

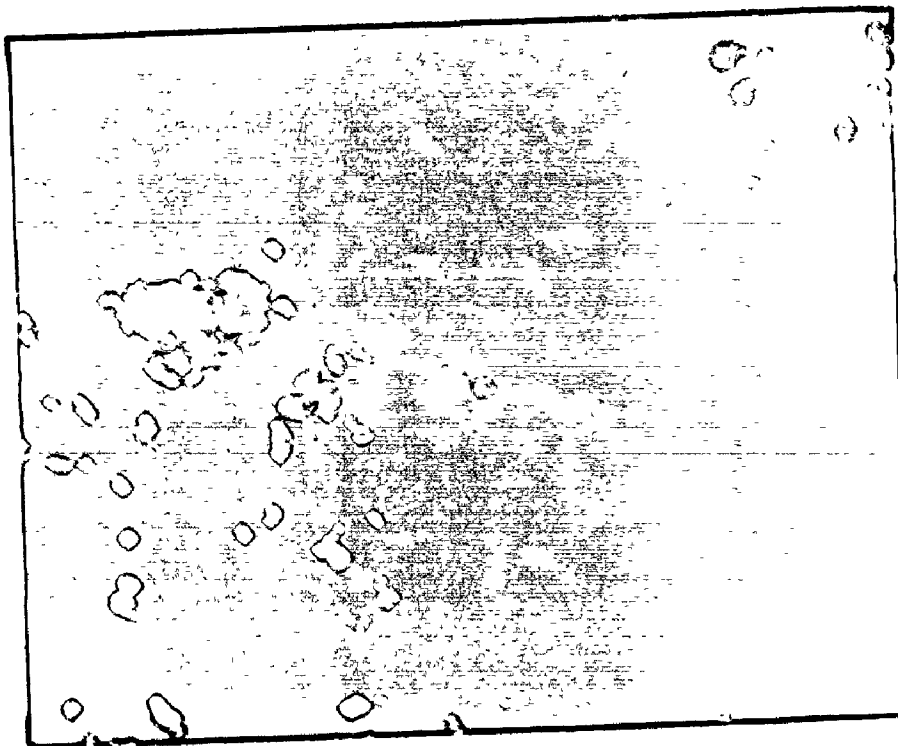
In the material containing fine dispersions of ϵ -carbide, narrow active slip bands denuded of particles were observed after 4000 fatigue cycles. This material produced clear evidence of localized slip bands and particle dissolution which suggest that deformation was highly localized. Precipitate-free channels were developed in regions of strain localization but, the degree to which particles were being sheared by dislocations was not discernible. No evidence of cell structure was observed. The characteristic features of microstructure are shown in Fig. 50. These features are essentially similar to the observations made by McGrath and Bratina (1967) and Wilson and Mintz (1972) on fatigued structures, of carbon-iron systems that were aged at 60°C to produce fine dispersions of carbide particles.

Moreover, careful Kikuchi line analysis of the matrix and slip band orientations revealed that the slip bands were misoriented some 2-3 degrees with respect to the matrix. This misorientation is taken up by a complex arrangement of dislocations at the slip band matrix interface as shown in Fig. 51 which clearly indicates that



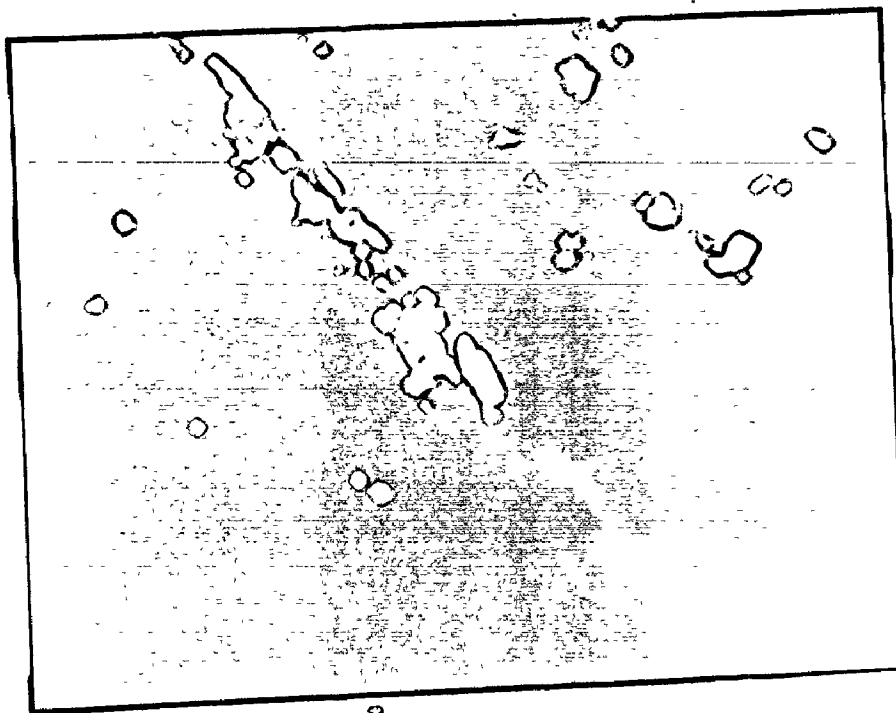


(a)

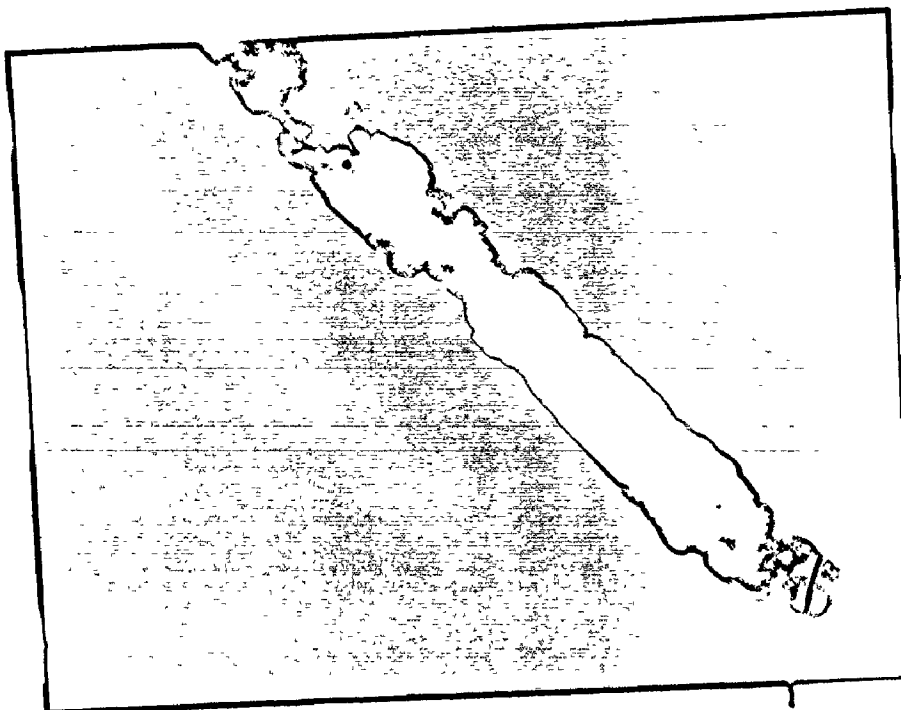


(b)

Fig. 50: Localized slip bands in Q-A (25°C) material,
after fatigue



(a)



(b)


Fig. 51: Localized slip bands in Q-A (25°C) material illustrating (a) marked difference in contrast between bands and matrix and (b) complex dislocation structure at the band-matrix interfaces

the channels differ markedly in contrast from the matrix.

It is unlikely, that these arrangements of dislocations are stress free and this correlates with the observations reported in the literature (Wilson 1973) that on annealing fatigued specimens recrystallization commences at the active slip bands.

The complex dislocation structure at the slip band interface may also serve as a site for the nucleation and growth of large carbides during fatigue. This aspect is illustrated in Figs. 52 and 54 which show clear evidence of large cementite particles in the region of an interaction between two active slip bands and also along the interface between slip bands and matrix. These observations correlate with the observations made by Wilson (1973) on a quenched steel that was subsequently fatigued at 60°C.

It was also observed that the active slip bands contain a relatively low density of dislocations suggesting that such bands are relatively free from dislocation barriers. Thus, local conditions within the bands and along their interfaces may enhance the process of transporting dissolved carbon (originally present in the active bands) to the band matrix interfaces where particle coarsening can take place. No evidence of particle growth was observed in the matrix regions more remote from the bands. This confirms the conclusion made by Wilson and Troman (1970) that strain



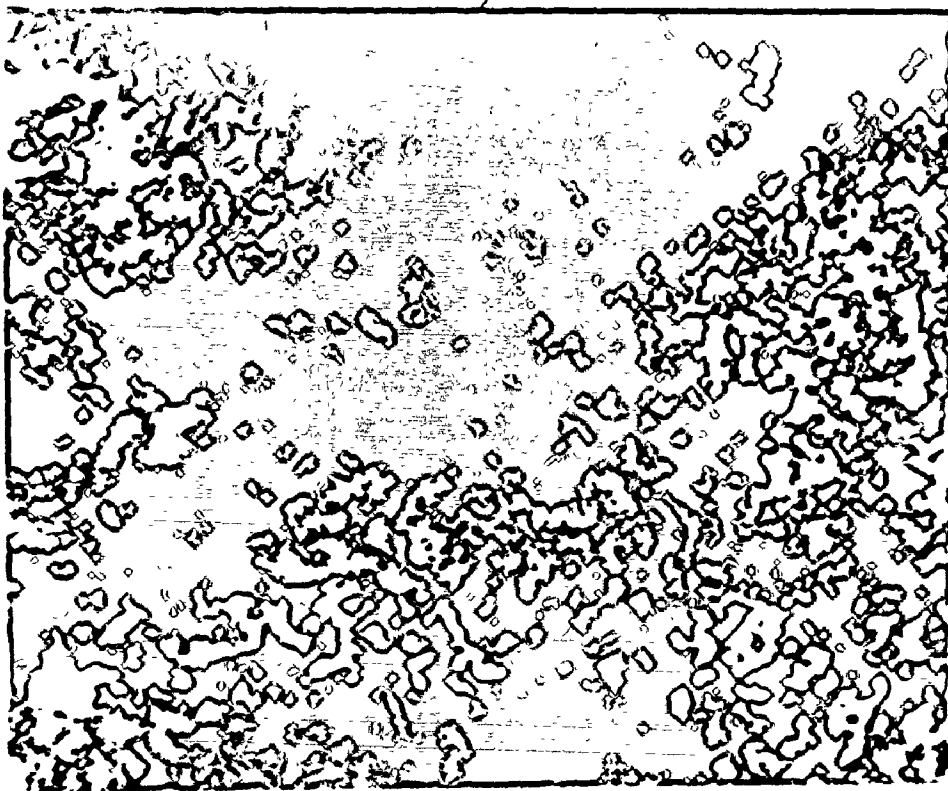


Fig. 52: Micrograph showing large carbide particles at the band-matrix interfaces in Q-A' (25°C) material after fatigue

ageing would strengthen the fatigue-hardened matrix between active slip bands and would promote strain concentration within the bands. However, another possibility exists that is that the presence of fine particles tend to suppress the activity of secondary slip systems and thus reduce the rate of creation of dislocation tangles. This is in essence similar to effects of radiation hardening discussed by Ono and Meshii (1966).

The observed active slip bands are likely to be supersaturated with carbon, due to dissolution of particles as outlined in the previous section. Thus it becomes feasible that an interrupted static ageing during fatigue would result in the re-precipitation of carbides within those bands. This seems to be the reason for the observed high increase in cyclic flow stress by the interrupted ageing experiments described in Section (3.2).

In specimens subjected to prolonged cycling, the active slip bands were sharply defined and often extended right across grain boundaries. Evidence of void formation was also clear in regions of intersection between bands and also along band matrix interfaces. This can be seen from the micrographs of Figs. 53 and 54. This observation seems to indicate that precipitate-free regions are weak spots and potential areas for crack nucleation. It is also consistent with the data of Broom et al. (1957) on aluminum alloys that

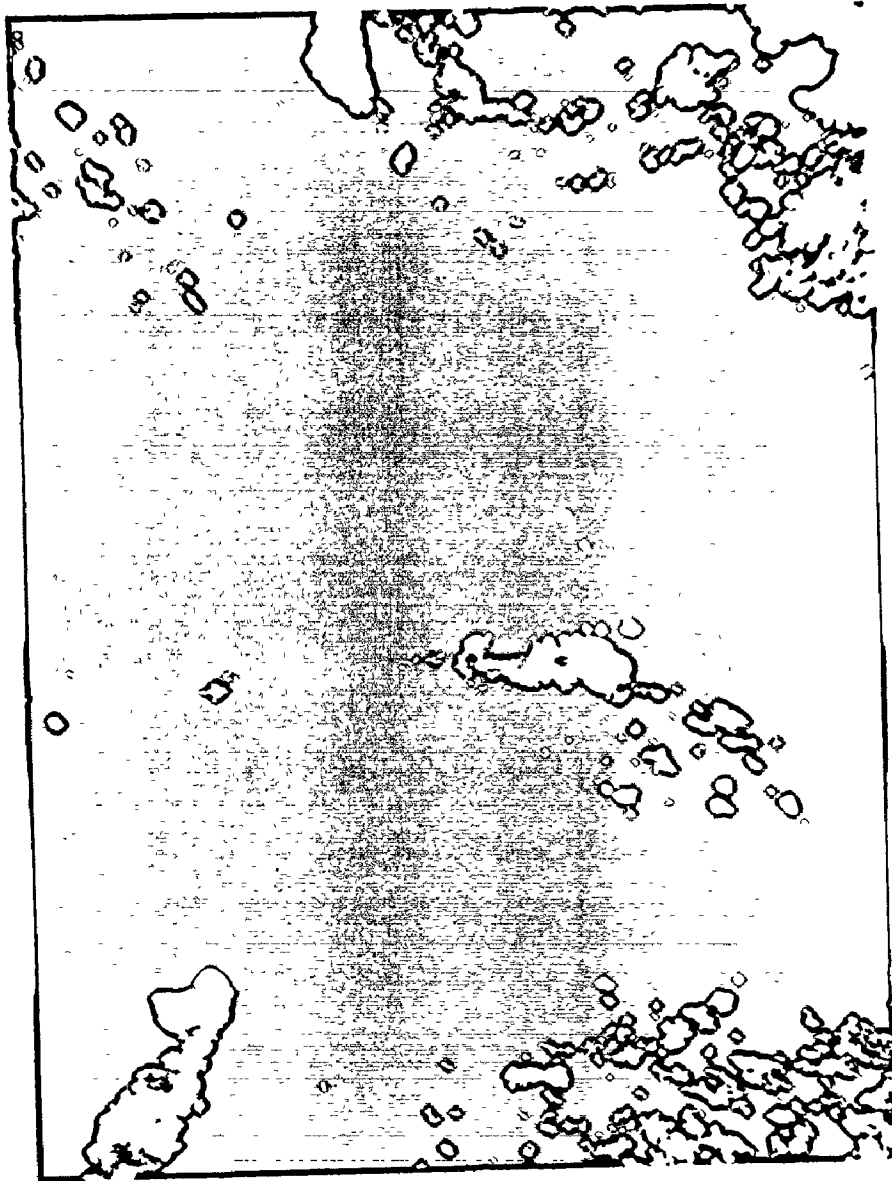


Fig. 53: Micrograph showing localized slip bands extending across a grain boundary



Fig. 54: Localized slip traces (110) and (112) parallel to the traces of both (110) and (112) (foil surface 001)

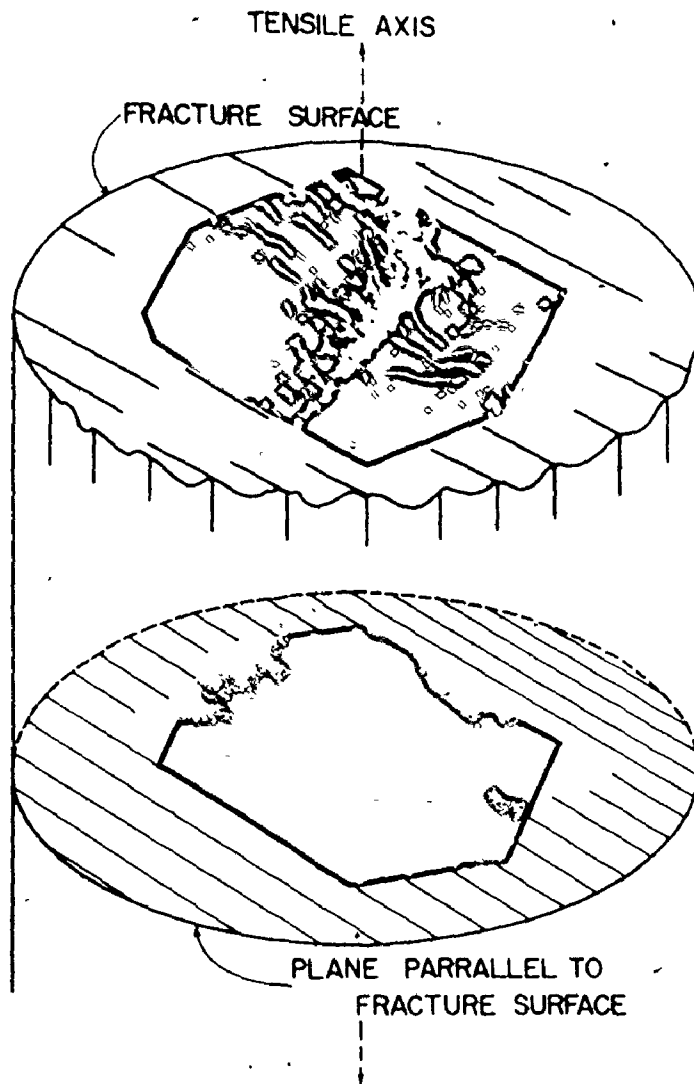



Fig. 55: Composite micrograph showing fatigue striations (on fracture surface) and localized slip bands (on plane parallel to fracture surface) in Q-A (25°C) material

the resolution of fine precipitates in local areas leads to a poor fatigue resistance.

A careful stereographic analysis of diffraction patterns taken from a large number of regions in thin foils indicated that the slip bands lie nearly parallel to the traces of both $\{110\}$ and $\{112\}$ glide planes. An example is illustrated in Fig. 54. The width of these bands is about 0.3μ and the interband spacing averages about 1.5μ measured on (001) foil plane.

Scanning electron microscopy was performed on fractured specimens to study the topography of the fracture surface. Results showed that the scale of the fatigue striations on the fracture surface and the scale of the localized slip bands are similar in form. This is illustrated by the composite micrograph of Fig. 55. A correlation between the two features would, undoubtedly, help to formulate a better understanding of the role of microstructure on the problem of fatigue fracture. However, in order to establish a meaningful correlation it is necessary to make a more extensive study on crack growth rates, nature of plastic zones, surface topography, etc., which is beyond the scope of this thesis.



(3.4) Comparison of Fatigue Data and Tensile Properties

Selected specimens from all the materials studied were tested to failure in tension. The mechanical properties determined from the tests are listed in Table 8.

Results of Table 8 show that a maximum strength accompanied by low ductility is associated with the fine dispersion of precipitate particles in the material Q-A (25°C). As the particle size and interparticle spacing became greater with increasing ageing temperature to 240°C the strength became less and the ductility increased. The tensile properties obtained for the material in the furnace-cooled condition are included with Table 8 for comparison. Table 9 summarizes results obtained in fatigue.

As a basis for comparison, the ratio $\frac{\sigma'_F}{\sigma_U}$ was calculated for each material and results are included in Table 9. σ'_F is cyclic flow stress near fracture and σ_U is ultimate tensile stress. (Note that σ'_F is the cyclic flow stress under a controlled plastic strain amplitude of $\frac{\Delta \epsilon_p}{2} = 0.008$ and not the usual fatigue endurance limit.)

Results show that the $\frac{\sigma'_F}{\sigma_U}$ ratio has decreased considerably from 0.88 for furnace-cooled material to 0.69 for Q-A (25°C) material while, a slight decrease was observed for Q-A (240°C) material. For material in as-quenched condition the $\frac{\sigma'_F}{\sigma_U}$ ratio was slightly higher than that for furnace-cooled material.

TABLE 9
FATIGUE PROPERTIES

Material	σ_S $\times 10^{-3}$ psi	σ'_F $\times 10^{-3}$ psi	N_f	σ'_F/σ_U
Furnace-Cooled	27	38	9800	0.88
As-Quenched	28	34	6800	0.94
Q-A (25°C)	No Sat.	43	6000	0.69
Q-A (240°C)	44	37	6700	0.84

σ_S = saturation stress

σ'_F = cyclic flow stress near fracture

N_f = number of cycles to failure

σ_U = ultimate tensile stress

The data indicates that the fine carbides, while substantially increasing the tensile strength do not improve the fatigue properties. In general, it appears that tensile properties do not provide reliable guidance to performance in fatigue. The same conclusion was reached by Wilson and Mintz (1972) on quench-aged steels.

At this point, it seems appropriate to examine whether the results obtained in the present investigation correlate with the well known Manson-Coffin relation which relates fatigue life to plastic strain amplitude.

In terms of the plastic strain amplitude $\frac{\Delta \epsilon_p}{2}$ the Manson-Coffin relation is

$$\Delta \epsilon_p = N_f^{1/2} = \text{constant}$$

where N_f = number of cycles to failure. This relation has alternatively been stated as

$$(2N_f)^C \frac{\Delta \epsilon_p}{2} = \epsilon_f \quad (1)$$

where C is a constant = 0.545, calculated from fatigue data of the materials studied, and ϵ_f is the true strain to failure in tension which can be related to the percentage reduction in area (% R.A.) as

$$\epsilon_f = \ln \left(\frac{100}{100 - \% \text{ R.A.}} \right)$$

The predicted values of N_f , calculated from the Manson-Coffin relation, for the two materials Q-A (25°C) and Q-A (240°C) are ~ 6300 and 7400 cycles respectively. Comparing those values with corresponding values of Table 9, a fair agreement to within $\sim 10\%$ can be seen.

At first sight it appears that the Manson-Coffin relation correlates reasonably well with the data. However, from a microstructural viewpoint it appears that an important feature of fatigue plasticity is not incorporated into the Manson-Coffin equation. As it stands, the equation does not reflect the localized nature of fatigue plasticity. That is to say that $\frac{\Delta \epsilon_p}{2}$ is not uniformly accommodated in the material, but is rather localized in narrow active regions. This process of strain partitioning is an important feature of fatigue plasticity and must be recognized in making predictions for fatigue life because it is basically related to the problem of crack initiation and propagation. Moreover it is evident from the microstructural observations that plasticity in fatigue is a unique property and not a simple extension of tensile plasticity. However, these objections should not discredit the fact that the relationship holds surprisingly well for quite a number of materials. The form of the Manson-Coffin relationship does, of course, immediately suggest some mechanism of statistical accumulation of strain. For this reason, May (1960) has suggested a mathematical model for the interpretation of Coffin's relationship. The

model used by May is not too detailed but it assumes that slip becomes concentrated in specific regions within which the surface displacement takes place statistically by equal increments per cycle.



SECTION (4)

DISCUSSION OF RESULTS(4.1) Summary of Experimental Results

The salient features of the results reported in the previous section may be summarized as follows:

- (1) In case of material quenched-aged at 25°C to produce a fine dispersion of carbides, the cyclic response was characterized by a continuous softening behaviour associated with a negative strain rate sensitivity. A decrease in temperature of deformation resulted in a slower rate of softening. Interrupting the fatigue test by a static ageing process resulted in an appreciable increase in fatigue life. After fatigue, the material produced clear evidence of localized slip bands and particle dissolution. The microstructure had the following characteristics:

- (a) the localized active bands were nearly denuded of particles and contained a relatively low density of dislocations,
- (b) large cementite particles were observed in the regions of intersection between bands and also along the interface between slip.

bands and matrix,

- (c) the bands were nearly parallel to $\{110\}$ and $\{112\}$ slip planes and were misoriented some 2-3 degrees with respect to the matrix,
 - (d) after prolonged cycling, the bands were sharply defined and often extended across grain boundaries. Some voids were observed in regions of intersection between bands and also along band-matrix interfaces, and
 - (e) no cell structure was observed.
- (2) The material aged at 240°C to produce a coarse dispersion of cementite particles and the furnace-cooled material both showed a period of saturation followed by a gradual hardening until near fracture. These materials showed cell structures with no evidence of narrow slip regions. Further, on increasing the test frequency both materials showed conventional positive strain rate sensitivity.
- (3) The ratio $\left(\frac{\sigma'_F}{\sigma_U}\right)$ (σ'_F = cyclic flow stress near fracture and σ_U = ultimate tensile stress) was lower for material containing fine particles than that for material containing coarse particles or that for furnace-cooled material.

(4.2) Nature of Localized Flow in Fatigue

It appears generally recognized at present that fracture in metals occurs as the result of plastic flow. The main requirement for fracture is the localization of plastic flow referred to here as plastic instability. The intense localization of flow is a required event to produce conditions necessary for fracture.

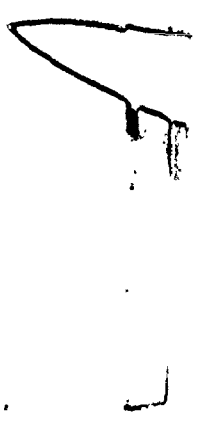
In order to approach this problem in fatigue, it must be recognized that in cyclic deformation the mean strain is zero and thus there is very little build-up of internal stresses from the second-phase particles. Therefore, in cyclic deformation, the hard particles do not promote rapid work hardening as in unidirectional deformation. This is important because the low work hardening rate leads to the ability of material to undergo localized plastic deformation as indicated by McClintock (1963).

As described in the previous section, both the mechanical response and the basic dislocation microstructures differ for materials containing either fine dispersions of carbides or a coarse dispersion of cementite particles. Let us first consider the case of material containing coarse cementite particles: this material, like the furnace-cooled material, produced a conventional cell structure with no evidence of narrow active slip bands. It is possible that the increased interparticle spacing allows dislocations to move more freely in the matrix giving rise to a more diffuse

slip. The observed cell size was comparable to the interparticle spacing. This is expected in two-phase materials with large particles which are not by-passed by dislocations.

Now the question arises to which microstructural features determine the critical conditions for localization of plastic flow in Q-A (240°C) material subjected to cyclic straining? In unidirectional deformation, hard particles can promote local instabilities due to build-up of localized strain in the vicinity of particles leading, in many cases, to void-formation. However, the role of particles in fatigue seems to be different. The fact that no voids were observed at particles - after fatigue - suggests that the particles do not promote local instabilities in fatigue as they usually do in unidirectional deformation. This is possible (specially during initial stages of cycling) because any localized flow which may occur in the vicinity of the particles on the first tensile half stroke will be dissipated in subsequent cycles as indicated by Stobbs et al. (1971).

However, a salient feature of the microstructure, after prolonged cycling, was the presence of a more regular coarse rectangular cell structure ("tidy" regions) with walls lying on {110} and {112} slip planes. Similar features were also observed in the decarburised iron of Chapter III. It is proposed that these regions may serve as sites for localization of cyclic plastic strain. This



proposal is supported by the microstructural observations of Wei and Baker (1965) in iron, that the intense damage bands formed in fatigue correspond to $\{110\}$ and $\{112\}$ planes.

It should be emphasised that under low amplitude fatigue, dislocations can accumulate at the particles in the form of dipoles as observed by Brown and Embury (1972), however, under the higher strain amplitude ($\frac{\Delta \epsilon}{2} = 0.008$) used for the present study, a complex cell structure has been observed. Thus, it appears that the detailed nature of fatigue substructure can vary considerably with strain amplitudes.

The fatigue behaviour, in materials containing fine dispersion of ϵ carbides, is much more complicated. In this case, the fatigue response is associated with a process of localized plastic instability in regions where gradients of plastic strain occur. There are also the interrelated problems of particle dissolution and particle growth. Thus, an attempt will be made, in the following sections, to rationalize such behaviour in a rather detailed manner.

However, it should be emphasised that the development of instability must be considered in terms of local competition between the factors promoting hardening (such as dislocation accumulation, solid solution strengthening, influence of hard particles, etc.) and those promoting softening (such as recovery, dissolution of particles,

adiabatic heating, local decrease in volume fraction of particles, etc.). Thus, instability develops when the work hardening characteristics of the material are unable to prevent the localization of plastic flow and thus the onset of crack propagation. If slip can be dispersed due to a high work hardening rate, the local strain at any point on the localized region will decrease and the tendency to fracture will be reduced. This appears to be of importance in regard to a comparison of the behaviour of the Q-A (25°C) material and the Q-A (240°C) material. A comparison of both the surface slip line observations of McGrath and Bratina (1967) and the evidence of the form of slip bands observed in the transmission electron microscopy of the present investigation indicates that slip is more localized in the material containing fine dispersion of particles. Thus, the presence of small particles and their tendency to dissolve locally appear to promote localization by lowering the work hardening capacity of the material and allowing for local softening to occur.

It appears, therefore, that the form of precipitate distribution and the local conditions at the localized regions have a great influence on the tendency to localize plastic flow under cyclic deformation. Thus, we recognize that, among the factors promoting local instabilities are: local increase in temperature, localization of strain rate and local dissolution and growth of particles. This is the

reason for the emphasis placed on these aspects in the present study.

(4.3) The Mechanical Equation of State

Let us first consider the more macroscopic approach to the problem of instability on the basis of the mechanical equation of state.

Following Holloman (1946), the mechanical equation of state can be represented as

$$\sigma = \sigma(\epsilon, \dot{\epsilon}, T) \quad (1)$$

where σ is the flow stress, ϵ is the strain, $\dot{\epsilon}$ is the strain rate and T is the temperature. An infinitesimal change in stress at any instant of deformation can then be written by differentiating the expression (1) as

$$d\sigma = \frac{\partial \sigma}{\partial \epsilon} d\epsilon + \frac{\partial \sigma}{\partial \dot{\epsilon}} d\dot{\epsilon} + \frac{\partial \sigma}{\partial T} dT \quad (2)$$

Thus,

$$\frac{d\sigma}{d\epsilon} = \frac{\partial \sigma}{\partial \epsilon} + \frac{\partial \sigma}{\partial \dot{\epsilon}} \frac{d\dot{\epsilon}}{d\epsilon} + \frac{\partial \sigma}{\partial T} \frac{dT}{d\epsilon} \quad (3)$$

The term $\frac{d\sigma}{d\varepsilon}$ corresponds to the apparent (or total) strain hardening which is a consequence of three contributions namely; the true work hardening of the material $\frac{\partial \sigma}{\partial \varepsilon}$, the effect of strain rate $(\frac{\partial \sigma}{\partial \dot{\varepsilon}} \cdot \frac{d\dot{\varepsilon}}{d\varepsilon})$, and the effect temperature $(\frac{\partial \sigma}{\partial T} \cdot \frac{dT}{d\varepsilon})$.

Thus, in order to spread slip and minimize strain gradient, the term $\frac{d\sigma}{d\varepsilon}$ needs to be positive. (If $\frac{d\sigma}{d\varepsilon}$ is zero, the material will behave as a rigid plastic solid.)

The process of dislocation accumulation, the effect of hard particles, etc. have positive contributions to the true work hardening of the material $\frac{\partial \sigma}{\partial \varepsilon}$. On the other hand, the decrease in dislocation accumulation (e.g., by recovery), the removal of obstacles (e.g., particle dissolution), etc. can exert negative effects on $\frac{\partial \sigma}{\partial \varepsilon}$ during deformation.

Changes in both strain rate and temperature are in many cases associated with plastic instability which might modify the total strain hardening behaviour. Thus, the larger the $\frac{\partial \sigma}{\partial \varepsilon}$ in comparison to negative effects of both strain rate and temperature, the more gradual the loss of instability is expected to be.

At this point it should be emphasised that, as strain becomes localized the above quantities need to be defined for the material state at the localized regions. This is important because the macroscopic quantities (i.e., stress, strain, strain rate and temperature which refer to the overall specimen plus the loading system) may differ in

magnitude and even in sign from the real values at the localized regions.

In case of instability and development of localization by shear, there is no first order change of stress due to area reduction and instability may develop either: due to strain softening (e.g., removal of obstacles or recovery, etc.), due to adiabatic heating, or due to negative strain rate effect.

The fundamental equation for the deformation process was developed by Argon (1973) and can be expressed, at constant pressure, as

$$\frac{d\dot{\epsilon}}{d\dot{\gamma}} = m \frac{\dot{\epsilon}}{\dot{\gamma}} - \dot{\gamma} \left[\frac{m}{\tau} \frac{\partial \tau}{\partial \dot{\gamma}} - \theta \right] \quad (4)$$

where $m = \left(\frac{\partial \ln \dot{\epsilon}}{\partial \ln \dot{\gamma}} \right)_T$ = the stress exponent in the strain rate - stress expression, $\theta = \frac{\Delta H}{kT} \left(\frac{\beta \sigma \dot{\gamma} h^2}{K_t \dot{\gamma} T} \right)$ = the adiabatic heating term, σ = the applied stress, τ = the plastic resistance (shear stress of the material at 0°K), ΔH = activation enthalpy, β = the fraction of the deformation work converted to heat, h = the localized band thickness, K_t = the thermal conductivity, k = Boltzmann's constant and γ = the shear strain.

Localization occurs when $\dot{\epsilon} \leq 0$, thus at the onset of instability,

$$\frac{d\dot{\gamma}}{d\dot{\gamma}} = - \dot{\gamma} \left[\frac{m}{1} \frac{\partial \tau}{\partial \dot{\gamma}} - \theta \right] \quad (5)$$

Thus, localization of shear strain can occur by the gradual transfer of the uniform deformation into a few inhomogeneity sites so that the strain can concentrate in the form of active slip bands on the expense of the matrix and instability develops.

At this stage we can proceed by considering the effects of both adiabatic heating and localization of strain rate and their relevance to the problem of instability in fatigue.

(4.3.1) Adiabatic heating effect

Adiabatic heating instabilities are favoured in materials with large plastic resistance and low thermal conductivity at high deformation rates. Thus, when a local region undergoes plastic deformation, only a small portion of the deformation work is stored and produces strain hardening while a major fraction (θ) of it is converted into heat.

The rate of increase of temperature $\left(\frac{dT}{dt}\right)$ in a localised slip band of thickness h was given by Argon (1973) as

$$\frac{dT}{dt} = \left(\frac{\dot{\gamma}_b^2 h^2}{K_t \dot{\gamma}_b} \right) \dot{\gamma}_b \quad (6)$$

where the subscript b refers to bands.

A rough estimate for the temperature rise in the slip bands of a Q-A (25°C) material subjected to fatigue may be obtained as follows.

The strain rate within bands can be estimated from a simple relationship of the form

$$f \dot{\gamma}_b + (1-f) \dot{\gamma}_m = \dot{\gamma}_0 \quad (7)$$

where f is the volume fraction of bands and $\dot{\gamma}_0$ is the average imposed strain rate $\sim 2 \times 10^{-3} \text{ sec}^{-1}$.

A value of ~ 0.01 was obtained for f from the density and width of bands. Thus, from Eq. (7), $\dot{\gamma}_b \sim 2 \times 10^{-1} \text{ sec}^{-1}$. Taking $\rho \sim 0.9$, $\sigma \sim 50,000 \text{ psi}$, $h \sim 0.3 \times 10^{-4} \text{ cm}$, $K_t = 0.2 \text{ cal/cm} \cdot \text{sec} \cdot ^\circ\text{K}$, $\gamma_b \sim 2 \times 0.008$ per cycle and substituting those values in Eq. (6) gives the rate of increase of temperature within the band $\sim 5 \times 10^{-3} \text{ }^\circ\text{C}$ per cycle. This shows that the increase in local temperature at the bands after ~ 4000 cycles will be of the order of 15 to 30 degrees above ambient. This indicates that although $\frac{\partial \sigma}{\partial T}$ in Eq. (3) is generally steep for bcc materials (Basiniski and Christian 1960), the contribution of such slight increase in temperature is less than 10% of the overall observed cyclic softening in Q-A (25°C) material.

It appears from the above crude estimate that the adiabatic heating term in Eq. (4) is too small to be

responsible for the apparent negative work hardening in Q-A (25°C) material.

(4.3.2) Development of instability and localization of strain rate

By ignoring the effect of adiabatic heating then, the rate at which the material deforms can be taken to be a function of both the strain in the material and the applied stress. This function can be represented in three dimensions as a surface relating the flow stress of a material to changes in strain and strain rate. For contours of constant stress, the change in strain rate with strain can be illustrated schematically as shown in Fig. 56.

A criteria for inhomogeneous deformation can be developed by considering the stability of a region of inhomogeneous strain at the nucleation stage.

Following Bowden (1970), let us consider that the strain in the localized bands, at the onset of softening, is larger than that in the rest of the material by a small amount $\Delta\gamma$. Consider further that the stress is uniform, then the situation is unstable and the sequence of events will be as shown in Fig. 56. The points m and b correspond to the strain in both matrix and bands, respectively, at an initial strain rate $\dot{\gamma}_0$ so that $mb = \Delta\gamma$ and $\frac{mA}{\Delta b} = \frac{f}{1-f}$ where f is the volume fraction of bands.

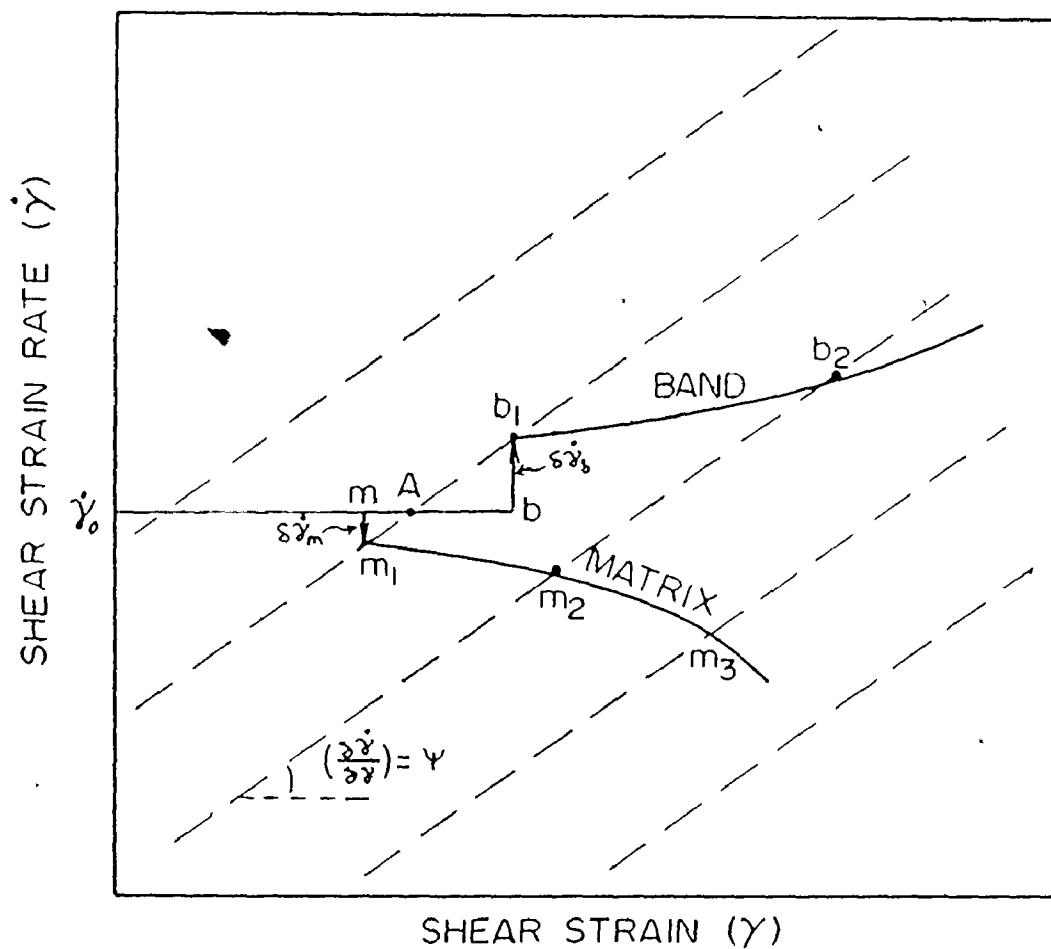


Fig. 56: Schematic illustration of the development of strain and strain rate in matrix and bands. The broken lines are contours of constant stress on the stress-strain-strain rate surface (after Bowden 1970)

$$\frac{mA}{mb} = f$$

$$\delta \dot{\gamma}_m = -mm_1 = -\psi \times mA = -\psi f(\dot{\gamma}_b - \dot{\gamma}_m)$$

$$\delta \dot{\gamma}_m = -\psi f(\dot{\gamma}_b - \dot{\gamma}_m) \delta t$$

also,

$$\delta \dot{\gamma}_b = \psi(1-f)(\dot{\gamma}_b - \dot{\gamma}_m) \delta t$$

Since the stress is uniform, the strain rate in bands will increase instantaneously from b to b_1 and the strain rate of the matrix will decrease from m to m_1 according to Eq. (7) so that both regions fall on the same stress contour. The strain rates of bands and matrix are now different and will diverge still further as deformation proceeds. As seen from Fig. 56, the bands are deforming faster than the matrix and will draw ahead in strain by an amount $(\dot{\gamma}_b - \dot{\gamma}_m) \delta t$. Thus, the change in strain rate at a small interval of time δt can be given as

$$\delta \dot{\gamma}_b = \psi(1-f)(\dot{\gamma}_b - \dot{\gamma}_m) \delta t$$

and

$$\delta \dot{\gamma}_m = -\psi f(\dot{\gamma}_b - \dot{\gamma}_m) \delta t$$

where the subscripts b and m refer to bands and matrix, respectively, and ψ is taken to be constant $= \frac{\partial \dot{\gamma}}{\partial \gamma}$. Thus,

$$\frac{d\dot{\gamma}_b}{d\gamma_b} = \psi(1-f)(\dot{\gamma}_b - \dot{\gamma}_m)/\dot{\gamma}_b \quad (8)$$

and

$$\frac{d\dot{\gamma}_m}{d\dot{\gamma}_m} = - \psi f (\dot{\gamma}_b - \dot{\gamma}_m) / \dot{\gamma}_m \quad (9)$$

In Fig. 56, as deformation proceeds, the matrix will follow the path $m_1 m_2$... while the bands will follow the path $b_1 b_2$ Thus, it appears that there is a general tendency for the strain rate in the matrix to reduce to zero and for the strain of the band to increase. The strains in both the matrix (γ_m) and the bands (γ_b) were given by Bowden (1970) as

$$\gamma_m = \frac{1}{\psi} [\dot{\gamma}_m - \dot{\gamma}_0 + \dot{\gamma}_0 \ln(\frac{\dot{\gamma}_0 - \dot{\gamma}_m}{\psi f \dot{\gamma}})] \quad (10)$$

and

$$\gamma_b = \frac{1}{\psi} [\dot{\gamma}_b - \dot{\gamma}_0 + \dot{\gamma}_0 \ln(\frac{\dot{\gamma}_b - \dot{\gamma}_0}{\psi(1-f)\dot{\gamma}})] \quad (11)$$

It can be clearly seen, from Eq. (11), that the localized strain in bands increases by increasing either the initial strain inhomogeneity, $\Delta\gamma$ or, the volume fraction of localized bands. Bowden has also suggested a parameter γ_b^D in order to predict whether inhomogeneous deformation is likely to develop and produce a significant increase in the strain rate within the bands. This parameter is the strain in the band required for its strain rate to become double the matrix strain rate. Assuming a very small volume fraction of bands ($f \ll 1$), then Eq. (11) can be written as

$$\dot{\gamma}_b^D = \frac{\dot{\gamma}_0}{\dot{\gamma}} \left[1 + \ln \frac{\dot{\gamma}_0}{\dot{\gamma} \dot{\gamma}} \right] = \dot{\gamma}^* \left[1 + \ln \left(\frac{\dot{\gamma}^*}{\dot{\gamma}} \right) \right] \quad (11)$$

where $\dot{\gamma}^*$ is a characteristic strain rate = $\frac{\dot{\gamma}_0}{\dot{\gamma}}$. Also, substituting for $(\dot{\gamma}_0 - \dot{\gamma}_m)$ in Eq. (10) by $f(\dot{\gamma}_b - \dot{\gamma}_m)$ from Eq. (7) and taking $\dot{\gamma}_m = \dot{\gamma}_0$ for $f \ll 1$, gives

$$\dot{\gamma}_m^D = \dot{\gamma}^* \ln \left(\frac{\dot{\gamma}^*}{\dot{\gamma}} \right)$$

This means that the strain in the matrix will be less than $\dot{\gamma}_b^D$ by the quantity $\dot{\gamma}^*$. Thus, the overall strain that has to be applied to the specimen as a whole before the band strain rate doubles is

$$\dot{\gamma}^D = \dot{\gamma}^* \ln \left(\frac{\dot{\gamma}^*}{\Delta \dot{\gamma}} \right) \quad (12)$$

The two parameters that control the instability are now the characteristic strain rate ($\dot{\gamma}^*$) and the initial strain inhomogeneity ($\Delta \dot{\gamma}$).

In terms of linear deformation, Eq. (12) can be written as

$$\epsilon^D = \epsilon^* \ln \frac{\epsilon^*}{\Delta \epsilon} \quad (12')$$

It should be noted that when the characteristic strain rate $\dot{\gamma}^*$ and the initial strain inhomogeneity $\Delta \dot{\gamma}$ are equal, then $\dot{\gamma}^D = 0$. This means that the inhomogeneity is already large

enough to deform at twice the matrix strain rate.

In order to examine the above criterion for the fatigue behaviour of Q-A (25°C) material, the parameters ϵ^D and ϵ^* were determined as follows (the reciprocal of the characteristic strain can be written as shown below)

$$\frac{1}{\epsilon^*} = - \frac{\partial \dot{\epsilon} / \dot{\epsilon}_0}{\dot{\epsilon}_0} = \frac{-1}{\dot{\epsilon}_0} \left(\frac{\partial \dot{\epsilon}}{\partial \dot{\epsilon}_0} \right) \left(\frac{\partial \dot{\epsilon}}{\partial \dot{\epsilon}_0} \right) \quad (13)$$

where $\left(\frac{\partial \dot{\epsilon}}{\partial \dot{\epsilon}_0} \right)_\epsilon$ is the slope of the stress-strain curve determined at constant strain rate. It would be reasonable to take it as the maximum negative slope of the stress - cumulative strain curve (Fig. 44), as it is in this region that the tendency for inhomogeneous deformation will be greatest. From data of Fig. 44 we have $\left(\frac{\partial \dot{\epsilon}}{\partial \dot{\epsilon}_0} \right)_\epsilon = -4 \times 10^3 \text{ lb/in}^2$.

The term $\frac{1}{\dot{\epsilon}} \left(\frac{\partial \dot{\epsilon}}{\partial \dot{\epsilon}_0} \right)_\gamma$ can be expressed as

$$\frac{1}{\dot{\epsilon}} \left(\frac{\partial \dot{\epsilon}}{\partial \dot{\epsilon}_0} \right)_\gamma = \left(\frac{\partial \ln \dot{\epsilon}}{\partial \ln \dot{\epsilon}_0} \right)_\gamma$$

and can be deduced from a plot of the flow stress against the logarithm of the strain rate measured under conditions which cause the material to deform homogeneously. This was calculated from a tensile test in which a series of strain rate changes were performed at a specific constant strain. This strain was taken as the one at which the flow stress in tension equals the cyclic flow stress at the onset of softening. Figure 57 shows the relationship between tensile

stress and strain rate in Q-A (25°C) material. From Fig. 57

$$\frac{\partial \ln \dot{\epsilon}}{\partial \ln \dot{\sigma}} : 1.1 \times 10^{-3} \text{ sec}^{-1} \cdot \text{psi}^{-1}$$

Thus, the characteristic strain ϵ^* is about 0.25. Equation (12') can then be written for the Q-A (25°C) material as

$$\epsilon^D = 0.25 \ln \frac{0.25}{\Delta \epsilon} \quad (14)$$

By reference to Fig. 44, it can be seen that the cyclic softening behaviour in Q-A (25°C) material started after ~ 50 to 60 cycles, i.e., 0.4 to 0.5 cumulative strain. Taking $\epsilon^D = 0.5$ in Eq. (14) gives: $\Delta \epsilon \sim 0.03$.

The above criteria predicts that in order for instability to develop in Q-A (25°C) material subjected to a cyclic strain amplitude $\frac{\Delta \epsilon}{2} = 0.008$, an initial inhomogeneity ($\Delta \epsilon$) of only ~ 0.03 must exist in the material at the onset of instability. This demonstrates that a small inhomogeneity developed locally in the material should, according to the above considerations, be capable of producing macroscopic instability. This is in essence similar to McClintock's model (1963) for the stability in a plastic zone ahead of a growing fatigue crack. McClintock's model also demonstrates on a macroscopic scale the basic fact that

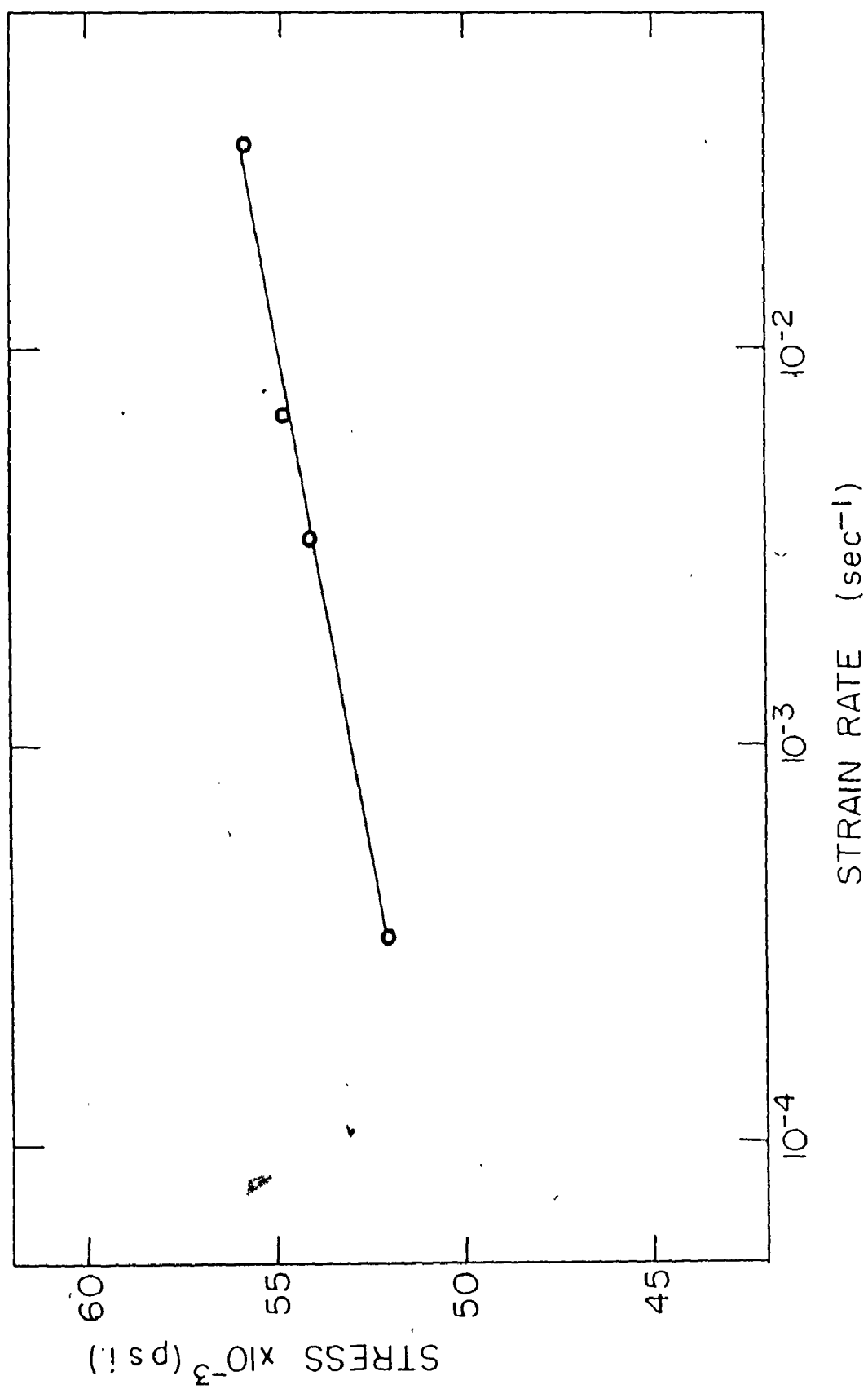


Fig. 57: Relationship between tensile stress and strain rate in Q-A (25°C) material

any material which possesses little strain hardening capacity will not resist fatigue crack propagation.

(4.4) Microstructural Aspects of Instability

The two salient features of the fatigue behaviour in Q-A (25°C) material are the tendency for softening and the associated process of localization of plastic flow in the active slip bands within which the material suffers dissolution and growth of particles. Thus a question arises as to how does the microstructure enter into strain localization and tendency to softening?

Firstly, it should be emphasised that the overall material strength is due to two main contributions: one from the dislocation accumulation and another from second-phase particles. Assuming, at the onset of softening, that the rate of dislocation accumulation is unchanged then, the softening must be essentially due to the precipitate contribution by dissolution or coarsening.

In the following sections an attempt is made to rationalize, in a semi-quantitative way, problems of particle-dissolution and particle-growth in relation to fatigue softening and localization of plastic flow.

Let us first consider briefly how particles are likely to be dissolved during fatigue?

(4.4.1) Mechanistic views on particle dissolution

At present most of the mechanisms advanced to explain particle dissolution are limited to the concept of particles which are cut by dislocations to below a "critical size" and thus dissolve.

Broom et al. (1957), for example, have suggested a mechanism which involved the shearing of the coherent particles, in aluminum alloys, by glide dislocations, to a size smaller than the critical size of the stable precipitate under the conditions imposed. However, they did not observe particle shearing.

Recently, Sargent and Purdy (1974) have suggested a similar approach in which a critical nucleus size was defined as that particle size in equilibrium with the matrix composition. According to this viewpoint any size above or below that equilibrium size will tend to dissolve. This mechanism was supported by microstructural evidences in alloys with cuttable precipitates subjected to tensile straining. Boyd and Hoagland (1972), for example, showed clearly both cutting and dissolution of Ti_3Al particles in Ti-Al-Mo alloys after tensile deformation.

However, there exists no evidence to confirm particle shear in alloys with hard particles, such as carbide precipitates in ferrous alloys. (In materials containing small particles it is usually difficult to reveal particle

shear). Thus, it can only be speculated that the concentration of slip within narrow bands results in a large accumulated strain, enough to cut the particles.

However, there are also other possibilities that may lead to particle dissolution. Some of these possibilities are:

- (a) For carbides and nitrides, it can be argued that the interaction energy between dislocations and solutes is greater than the binding energy of the metastable carbides. Dijkstra (1949), for example, showed that the solubility of nitrogen in iron at 300°C was reduced from 0.012 to 0.0025 by cold working.

Thus during cyclic deformation of Q-A (25°C) material it is possible that the binding energy of carbon to carbides is less than the interaction energy with a passing dislocation. Hence dislocations transport carbon, not by cutting but by local attraction. Thus, the local volume fraction of particles decreases and consequently promotes local softening.

For a particle of radius r , the tendency to go into solution is related to the size of the Gibbs-Thomson equation

$$\ln\left(\frac{C_r}{C_\infty}\right) = \frac{\gamma V_m}{2rC_rRT} \quad (15)$$

where C_r is the solubility of a particle radius r , C_∞ is the solubility of a particle of infinite radius, γ is the interfacial energy, V_m is the molar volume for particles, R is the gas constant, T is the absolute temperature, and C_r is the mole volume fraction of solute in the precipitate.

From this, the rate of shrinkage can be expressed as

$$\frac{dr}{dt} = -D\left(\frac{C_r - C_m}{r}\right) \quad (16)$$

where C_m is the average solute concentration.

However, if a dislocation is present and the solubility at the dislocation is greater than C_r , the particle will tend to dissolve at a higher rate.

Thus, as dislocation passes hard carbide particles they can attract solute and cause the particles to shrink, i.e., the volume fraction can be reduced in the shear band and thus promoting localized shear.

The important point to emphasise is that solute atoms could be picked up from

solution by dislocations forcing particles to dissolve. This, of course, does not require particle shearing.

- (b) A possibility, not of much difference from the above, is the case of an alloy which contains a range of size distribution. In this case the fine precipitate has a larger amount of precipitate-matrix interfacial area per unit volume. This area represents a surface free energy, and even without any discussion of specific mechanism, it can be seen that this area will tend to decrease with time. This occurs by diffusion of solute from smaller particles to bigger ones. It should be emphasised that the process of solute transport can be greatly enhanced under concurrent deformation, as will be discussed later. Thus, the smaller particles can dissolve locally leading to softening in localized regions. At the same time, the dissolved carbon will be available for particles adjacent to these local sites to increase their mean particle size.

- (c) Another possibility is to consider cases where adiabatic heating becomes important. In the

range of frequencies used for this study, adiabatic heating was negligibly small.

However, in a situation where the material is subjected to ultra-high frequencies, there is a possibility that slip bands can be heated up due to concentration of high strain rates.

Thus, the thermodynamic solubility of carbon in iron can increase locally forcing particles to dissolve.

It should be emphasised, at this point, that all the above possibilities are, in fact, interrelated and can occur concurrently during cyclic deformation.

(4.4.2) Influence of second-phase particles on cyclic softening

Let us consider that the carbide particles in Q-A (25°C) material are acting as hard obstacles to dislocations, i.e., as Orowan type obstacles. On the basis of Orowan strengthening, the increase in shear stress ($\Delta\tau$) can be given as

$$\Delta\tau = \frac{1.2}{2.4} \frac{\mu b}{\pi \ell} \ln \frac{\bar{d}}{2b} \quad (17)$$

In terms of an applied tensile stress (σ), Eq. (17) can be written as

$$\Delta\sigma \approx \frac{\mu b}{\pi \ell} \ln \frac{\bar{d}}{2b} \quad (18)$$

where μ is the shear modulus of the matrix, ℓ is the interparticle spacing, b is the Burgers vector, and \bar{d} is the average diameter of particles.

Assuming spherical particles we can write

$$\ell = \frac{\pi d}{2f^{1/2}}$$

where f is the volume fraction of particles. Thus,

$$\Delta\sigma \approx \frac{\mu b f^{1/2}}{2.5 \bar{d}} \ln \frac{\bar{d}}{2b} \quad (19)$$

It can be seen from Eq. (19) that local softening, i.e., decrease in $\Delta\sigma$, can occur if either the volume fraction in a slip band decreases or the local distribution coarsens.

Let us examine in a simple manner whether either of these effects can occur during cyclic deformation of Q-A (25°C) material. Firstly, the effects of volume fraction of second-phase particles and particle size on the tensile stress were calculated from Eq. (19) for $\mu = 11 \times 10^6$ psi and $b = 2.8 \text{ \AA}$. The results are shown in Fig. 58 and were found to be consistent with similar data of Gladman et al. (1971). Secondly, the average particle size \bar{d} was calculated from a simple volume balance between a platelet of ϵ carbide (500 \AA diameter and 100 \AA thickness) and an

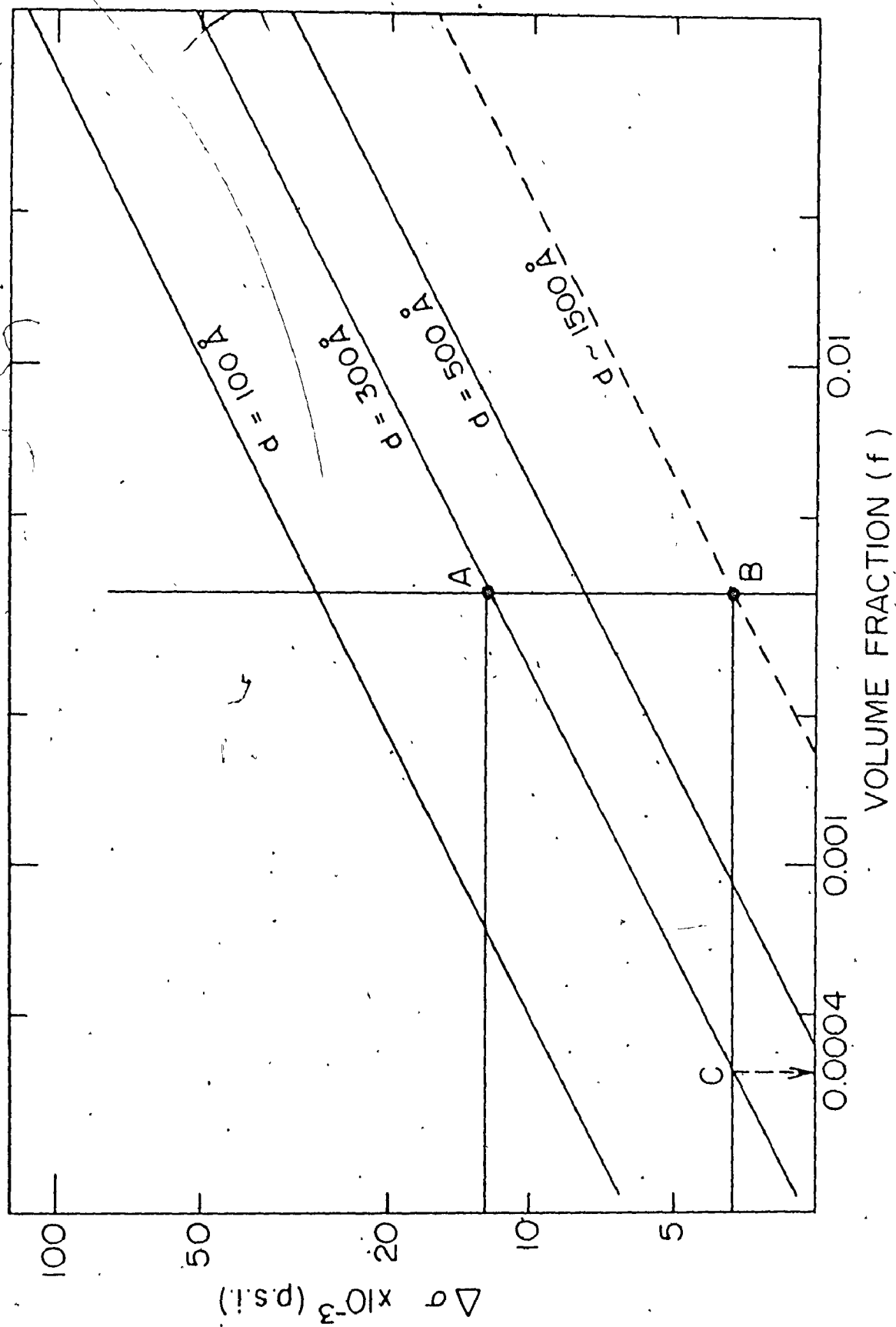


Fig. 58: Effects of volume fraction (f) and particle size (d) on increase in tensile stress ($\Delta \sigma$) in iron

equivalent sphere of diameter \bar{d} . Thus the volume-mean particle size \bar{d} is about 300 Å. Thirdly, we assume for simplicity that during fatigue softening the rate of dislocation accumulation is unchanged and also the contribution due to solid solution hardening is negligible. Thus, softening must be essentially due to precipitate contribution.

For Q-A (25°C) material (Fig. 44), a decrease in cyclic flow stress of about 10,000 psi was observed. Thus, for a volume fraction of 3.3×10^{-3} and a particle size of 300 Å, the initial increase in flow stress from Fig. 58 can be represented by a point such as A.

Now, it can be seen from Fig. 58 that a decrease in flow stress of $\sim 10,000$ psi corresponds to either an increase in particle size from 300 Å to ~ 1500 Å, or a decrease in volume fraction from 3.3×10^{-3} to $\sim 4 \times 10^{-4}$. From the microstructural observations of Section (4.3) it was possible to observe coarse particles of ~ 1000 Å size along localized band-matrix interfaces and in regions of intersection of bands. Also, the localized bands were relatively free of particles, indicating a decrease in volume fraction of particles in those bands. Thus, both processes of particle dissolution and particle growth are associated with the fatigue behaviour in Q-A (25°C) material. This is also consistent with the basic work on aluminum alloys (Clark and McEvily 1964, and Stubbington and Forsyth 1966) which

suggests that both resolution and overageing can occur.

The dissolution of particles will tend to reduce the local flow stress in the active bands. Also, as the average size of particles in the active bands decreases there will be a net flux tendency to coarsen the particles immediately adjacent to the active bands as observed.

The important point to emphasise is that whenever the local rate of softening (due to both particle-dissolution and particle-coarsening) is much faster than the increase in flow stress due to contributions of dislocation accumulation and solid solution strengthening, then the tendency to localize plastic strain in the active bands will increase. This seems to be the case in Q-A (25°C) material.

(4.4.3) Particle coarsening under concurrent deformation

Consider first a simple coarsening model of the type elegantly described by Lifshitz and Sloyozov (1961).

Conventionally, particle coarsening results from the higher solubility of small particles which may tend to dissolve and cause the growth of larger particles. The driving force is provided by the reduction of total interfacial energy. The theoretical predictions of Lifshitz and Sloyozov (1961) give a linear relationship between the cube of the mean particle size and time for a diffusion controlled process as

$$d^3 - d_0^3 = Kt \quad (20)$$

where d is a volume mean particle size at time t and d_0 is the mean size at zero time, and K is the coarsening rate constant.

$$K = \frac{64\gamma DC_0 V_m^2}{9RT}$$

where γ is the interfacial energy per unit area, V_m is the molar volume of particles, C_0 is the equilibrium solubility of carbon, R is the gas constant, T is the absolute temperature, and D is the rate-controlling diffusion coefficient.

For the Q-A (25°C) material, fatigued at room temperature, we have

$$\gamma = 700 \text{ ergs/cm}^2^*$$

$$V_m = 23.4 \text{ cm}^3/\text{mole}$$

$$C_0 = 5 \times 10^{-5} \text{ mole/cm}^3$$

$$R = 8.3 \times 10^7 \text{ ergs/mole}^\circ\text{K}$$

and $T = 300^\circ\text{K}$

* Mukherjee et al. (1969).

Consider also an increase in particle size from $\sim 300 \text{ \AA}$ to $\sim 1000 \text{ \AA}$ during a fatigue cycling period of $\sim 40,000$ seconds and substituting for those values in Eq. (19), thus,

$$D \sim 10^{-10} \text{ to } 10^{-11} \text{ cm}^2/\text{sec}$$

This value of D is about four to five orders of magnitude higher than the volume diffusion of carbon at room temperature.

It should be noted that Eq. (20) was derived for constant volume fraction of particles. However, within a localized band we expect a gradient in the volume fraction, being higher at band-matrix interfaces. Thus, it is recognized that some approximation was involved in calculating the diffusion coefficient (D), however, this should not affect the general approach to the point under discussion.

Now, if we add a static dislocation substructure, we simply increase the effective diffusion coefficient D_{eff} to

$$D_{\text{eff}} = D_v(1-S) + D_p S$$

where D_v is the volume diffusion coefficient, D_p is the dislocation-core diffusion rate and S is the fraction of

short circuit sites. For a static dislocation density of 10^8 cm/cm^3 , S is $\sim 10^{-6}$. Thus, even when $\frac{D_p}{D_v} = 10^6$, the effective diffusion coefficient is only double the value of D_v . Also, if we consider the local high density of dislocations at the active band-matrix interfaces, then the local value of S will be about 10^4 . Thus, D_{eff} is only two orders of magnitude higher than D_v .

However, if deformation occurs concurrently, we consider that in general the dislocations spend most of their time waiting at particles rather than in flight between particles. Thus, each particle is visited by many dislocations and the total time available for flux via the dislocations is much greater.

For fatigue tests of the present investigation, the average strain rate was about 10^{-3} sec^{-1} . If we consider a mobile dislocation density of 10^8 cm/cm^3 , thus, in one second each dislocation will sweep out 10^{-3} cm^2 . Thus, the effective density of sites available for flux is of the order of $2 \times 10^{-3} \text{ cm}^{-2}$, i.e., some 10^3 times greater than for the static case. Hence, for values of $\frac{D_p}{D_v}$ of the order of 10^6 we expect rates of coarsening to accelerate by the order of 10^3 to 10^4 times as observed.

From the foregoing it appears that because plastic flow occurs, all the particles are visited by short circuit diffusion paths and the net flux is greater than that estimated by simple consideration of volume diffusion or static dislocation density.

(4.5) Influence of Particle-Dissolution on Macroscopic Behaviour

Three salient macroscopic features were observed in Q-A (25°C) material during fatigue: firstly, the cyclic softening behaviour at room temperature was associated with negative strain rate sensitivity; secondly, lowering the temperature of deformation resulted in an appreciable decrease in the cyclic softening behaviour and; thirdly, an interrupted static ageing process led to an initial increase in flow stress and a considerable increase in fatigue life.

The observed negative strain rate sensitivity in Q-A (25°C) material, reflects the predominant effect of local obstacles in this material under cyclic straining. It appeared from the previous section that local dissolution of particles is greatly enhanced under concurrent deformation. Thus, it is expected that the carbon atoms from the dissolved particles should be present both as a supersaturation in the localized regions and at dislocations. The microstructural observations of Section (3) showed that extremely dense dislocation clouds were present at the matrix-band interfaces, where strong interactions with solute atoms could have been occurring. This suggests that many of the low-amplitude dislocations were captured and effectively locked by solutes at the band-matrix interfaces.

Thus, it appears that a process similar to a dynamic strain ageing process may occur at these interfaces due to solute locking of dislocations undergoing low-amplitude movement. On these bases, the observed negative strain rate response can be due to the tendency to unlock new dislocation sources.

It should also be emphasised that increasing the density of local obstacles will tend to restrict dislocation activity, during fatigue, to localized regions thus, enhance instability and formation of fracture nuclei as observed in Section (3.3). This is consistent with the observation of McGrath and Bratina (1967) that the fine particles promote coarse slip and bring about embrittlement in the form of surface microcracks. Thus, the localization of slip can be greatly intensified by local dissolution of particles. This seems to be the reason for the observed low $\frac{\sigma_F}{\sigma_U}$ ratio in Q-A (25°C) material. This is also consistent with the conclusion reached by Abel and Ham (1966) that particle dissolution leads to low fatigue ratio.

The effect of lowering the temperature of deformation may be explained, in part, as a consequence of suppressing the dissolution of particles. Since particle dissolution is a thermally activated process, thus lowering the temperature results in lower rates of particle dissolution.

Another possibility is to consider the temperature dependence of both the localized regions (which are

supersaturated with solutes) and the matrix (which contains undissolved particles). McLean (1962) indicated that solid solutions have higher temperature dependence than particle dispersions. Thus, decreasing the deformation temperature may lead to a transfer of slip from the localized regions back to the matrix.

The observed increase in cyclic flow stress after a static ageing process indicates that the soft particle-free regions can be re-strengthened by allowing for the dissolved carbon to condense back to these regions and, consequently, for the local flow stress to be temporarily raised. Also, the fatigue life can be improved by promoting such increases in local stresses and thus reducing the tendency to localized deformation.

It appeared, from the foregoing, that localization of slip is greatly intensified by local dissolution of particles. Such problem limits the fatigue performance for materials containing fine dispersion of unstable particles.

Thus, to improve fatigue resistance, one may think of utilizing either: (a) a coarser dispersion of particles, (b) pre-stabilized dislocation structures, or (c) a fine dispersion of mechanically stable particles.

(a) The results on Q-A (240°C) material showed that it would be desirable in fatigue to use coarse particles. This is based on the fact that, for

larger particle size and particle spacing, the dislocation motion will not be restricted and, therefore, stability will improve because the material is more capable of spreading slip. However, it is known that, as particle size increases, the strength decreases. This, together with the fact that in fatigue the particles do not promote as much hardening as in unidirectional deformation, impose limitation on the exploitation of coarse particles as strengthening mechanism in fatigue. Such limitation has led Wilson and Mintz (1972) to conclude that, "the best choice of structure in a precipitation hardened alloy is essentially a compromise between the conflicting requirements of strong stable particles and the fineness of their dispersion".

(b) Another possibility is to utilize prestabilized dislocation substructures. The data of Chapter III suggests that, in order to inhibit the cyclic softening process, some form of effective pinning of the prestrained dislocation structure must be utilized. Thus, it is possible to enhance resistance to fatigue softening by utilizing a prestabilized dislocation structures in which a solute atmosphere or a series of fine precipitates form along dislocation

lines and exert resistive stresses to fatigue softening.

(c) A third possibility is to utilize a fine dispersion of mechanically stable (non-dissolvable) particles such as the carbides of Vanadium or Chromium in steels. Thus, by using the concepts of both fine dispersion and non-dissolvable particles, one hopes to achieve improvements in the fatigue strength and the stability of plastic flow. This hypothesis was examined on a limited number of Vanadium-steel specimens and results are included in Appendix A. The data indicated that in comparison to Q-A (25°C) material, the fatigue behaviour in quench-tempered Vanadium-steel was associated with much lower rate of softening and better fatigue strength.

(4.6) Summary

The nature of strain localization in fatigue has been investigated in quench-aged low carbon iron containing two different dispersions of carbide particles: a fine dispersion of ϵ carbides (obtained by ageing at 25°C) and a coarse dispersion of cementite particles (obtained by

ageing at 240°C). The material containing fine particles produced clear evidence of localized slip bands within which the material suffered dissolution and growth of particles. On the contrary, the material containing coarse particles exhibited more stable mechanical response and produced conventional cell structure with no evidence of narrow active regions.

The most significant results have been summarized in Section (4.1).

The problem of instability was approached on two levels: a macroscopic level, from the viewpoint of the mechanical equation of state, and a microscopic level, from the viewpoint of the detailed structure of localized regions.

The analysis demonstrated that a basic microscale inhomogeneity should be capable of producing macroscopic instability in materials possessing insufficient strain-hardening capacity to dissipate local partitioning of strain rate. It appeared that the effect of adiabatic heating in the localized bands of Q-A (25°C) material is too small to affect bulk behaviour.

The microstructural rationale showed that the form of precipitate distribution and the local conditions at localized regions both have a great influence on the tendency to localize plastic flow under cyclic deformation. It appeared that local dissolution and growth of particles can be intensified under concurrent deformation.

Thus, instability of plastic flow is influenced by the ability of material to spread slip and the effectiveness of obstacles in promoting better fatigue resistance.

Beneficial effects may be achieved by conventional working and ageing techniques or by utilizing a fine dispersion of mechanically stable particles.

CHAPTER V

CONCLUSIONS

The present thesis has been concerned with both the mechanical behaviour and the microstructural changes preceeding fatigue fracture in ferrous systems subjected to controlled cyclic straining. Attention has been focussed on three basic aspects of the fatigue process, namely, the Bauschinger Effect and the Polarization of Plastic Flow, Fatigue Softening and Hardening in Single-Phase Low-Carbon Iron, and the Stability of Plastic Flow in Quench-Aged Armco Iron.

The increased understanding of the process of cyclic deformation, which evolved from the data presented in this thesis, has led to the formulation of the following conclusions:

(A) On the Bauschinger Effect and the Polarization of Plastic Flow

(1) In single-phase bcc materials, the Bauschinger Effect Parameter (BEP) - defined as the reversible fraction of work hardening - is independent of both the temperature of deformation and the amount of prior strain. This indicates that the back stress

and the forest hardening contribution are proportional to each other and independent of the arrangement of dislocations.

(2) In steels containing second-phase particles, the BEP is independent of the amount of prior strain but increases with increasing volume fraction of particles. For the same volume fraction, the BEP is higher in the materials containing non-spherical particles compared to those containing spherical particles.

(3) In both single- and two-phase iron-based alloys, the ratio between back stress and forest hardening contribution is independent of the amount of forward strain.

(B) On Fatigue Softening and Hardening in Single-Phase
Low-Carbon Iron

(1) Decarburised iron specimens, tested under the same conditions of temperature and plastic strain amplitude, have a unique saturation stress in both cyclic softening and hardening.

(2) The X-ray asterism associated with prestrained specimens decreases appreciably by subsequent cyclic straining.

(3) During cyclic softening, the salient microstructural changes are:

(a) The shape of the dislocation cells tend to be more regular and become progressively sharp and well defined with a tendency to alignment along low index crystallographic planes.

(b) There is an observed increase in cell size with cyclic softening.

(c) The substructure at saturation is characterised by the presence of two types of cells: an equiaxed type and a rectangular-shaped type. The latter type ("tidy" regions) is suggested as possible site for localization of plastic flow and formation of fracture nuclei at latter stages of fatigue:

(d) The cell walls at saturation are associated with very small misorientations.

(4) A power relationship of the form:

$$\sigma_s = 40,000 \left(\frac{\Delta \epsilon_p}{2} \right)^{0.1}$$

(σ_s = saturation stress and $\frac{\Delta \epsilon_p}{2}$ = plastic strain amplitude) was found to hold for decarburized iron.

(5) The rate of cyclic softening is governed by the initial arrangement of dislocations. The rate of cyclic softening in specimens prestrained at 195°K (to produce a uniform arrangement of dislocations) is much higher than that in specimens prestrained at 298°K (to produce a cell structure), whereas specimens prestrained at 473°K (to produce a fine dispersion of dislocations by dynamic strain ageing) show the lowest rate of softening.

(6) A model, based on mutual annihilation of dislocations, is proposed to account for the kinetics of cyclic softening after prestraining at different temperatures. For specimens prestrained at 195°K and 298°K, the rate of decrease of dislocation density with number of cycles can be described as a second-order process in which the softening behaviour is explained as a pairwise annihilation of dislocations. For specimens prestrained at 473°K, the rate equation describes a first-order process in which a fixed resistance to the dislocation motion is assumed.

(7) The data suggests that in order to inhibit the cyclic softening process, some form of effective pinning of the prestrained dislocation structure

must be utilized as in the dynamic strain ageing and the ausforming processes.

(8) The fatigued structure of decarburised iron resists thermal recovery for several hours at 470°C, and is thermally more stable than the structure developed in unidirectional deformation.

(9) The most significant microstructural change, occurring during subsequent cyclic hardening in decarburised iron, is the increase in misorientations across the cell walls particularly those associated with the "tidy" regions.

(C) On Stability of Plastic Flow in Quench-Aged Armco Iron

(1) In fatigue, the form of precipitate distribution and the local conditions at the localized regions both have a great influence on the tendency to localize plastic flow.

(2) The fatigue response in material containing fine dispersion of ϵ carbides - Q-A (25°C) - is characterized by a softening behaviour associated with a process of localization of plastic flow in active slip bands within which the material suffers dissolution of small particles and growth of larger particles.

(3) The localization of slip is intensified by local softening, due to particle dissolution and particle growth, leading to low $\frac{\sigma'_F}{\sigma_U}$ ratio (σ'_F = cyclic flow stress near fracture and σ_U = ultimate tensile stress).

(4) The rates of dissolution and growth of particles are greatly enhanced under concurrent deformation and are expected to increase by increasing either the temperature of deformation or the strain rate.

(5) The active slip bands in Q-A (25°C) material are potential sites for the formation of fracture nuclei.

(6) The local increase in temperature within active slip bands is too small to make a major contribution to the observed fatigue softening behaviour in Q-A (25°C) material.

(7) Local softening can be suppressed by lowering the temperature of deformation.

(8) Improvements in both the local stability and the fatigue life of Q-A (25°C) material, can be achieved by interrupting the fatigue test with a static ageing process.

(9) Stability under cyclic straining can be improved by increasing both the particle size and the

inter-particle spacing. The material containing coarse dispersion of cementite particles - Q-A (240°C) - produces a conventional cell structure with no evidence of narrow active slip bands, and the fatigue behaviour is associated with higher $\frac{\sigma_F}{\sigma_U}$ ratio. In this material, the rectangular shaped cells ("tidy" regions) may serve as potential sites for localization of plastic flow and formation of fracture nuclei at later stages in fatigue.

(10) Low rate of fatigue softening associated with high $\frac{\sigma_F}{\sigma_U}$ ratio was achieved in a quench-tempered Vanadium-steel containing fine dispersion of alloy carbides, but the fatigue life was shorter compared to that of Q-A (25°C) material. Although no localized bands were observed, the fracture surface produced clear evidence of intergranular cracks.

It is pertinent to consider the applicability of these findings to a more general rationale of cyclic deformation.

The Bauschinger effect, for example, may provide a useful method of quantifying the nature of plastic inhomogeneities in both single-phase and two-phase materials. It provides in essence a direct indication of

the magnitude of Brown-Stohbs and Tanaka-Mori type hardening and its relation to the nature, size and volume fraction of obstacles able to support local elastic back stresses. This may also have practical application in regard to many steels where modern rolling and cooling practices result in variation in carbide content (Shewman 1969). Thus, processing variables which intend to raise the yield stress may also increase the Bauschinger effect and thus lead to losses in the strength during subsequent forming processes. The work of Civallero et al. (1973) showed clearly that, in many cases, steel plate suffers considerable loss in yield stress when manufactured into steel pipes.

An important feature of the present work is the role of dynamic strain ageing in stabilizing prestrained structures against cyclic softening. Also, the work of Brown and Embury (1972) demonstrated the importance of thermal-mechanical treatments, such as a quenching - swaging - and ageing process, on producing structures resisting fatigue softening. Thus, it is possible to enhance resistance to fatigue softening by utilizing a prestabilized dislocation structure in which a solute atmosphere or a series of fine precipitates form along dislocation lines and exert resistive stresses to fatigue softening. This may also be applicable to more complex commercial alloys such as ausformed alloy steels.

The investigation of Hahn et al. (1971) on the nature of plastic zone ahead of a propagating fatigue crack has raised the possibility that the instability of fatigue substructure contributes to the crack growth mechanism. Thus, it is of extreme importance, for future studies, to establish the relationship between localization of plastic flow and crack growth rates and to provide a reasonable microstructural rationale for the power law expressions relating crack growth rate to the cyclic stress intensity variations. Such rationale requires more detailed investigation of the plastic zone-size and zone-shape in relation to microstructural aspects of the process. It would also be useful to investigate the influence of both metallurgical variables and working conditions on the form of these plastic zones.

APPENDIX A

CYCLIC BEHAVIOUR IN QUENCH-TEMPERED VANADIUM STEEL

It appeared from data of Chapter IV that localization of plastic flow in fatigue is greatly intensified by local dissolution of particles. Thus, an attempt was made to examine the possibility of minimising particle dissolution and improving fatigue performance by utilizing a relatively stable dispersion of fine scale alloy carbide particles.

The study was performed on a limited number of quench-tempered specimens of Vanadium-steel (Q-Temp. V-steel). The composition of the material is given in Table 10. The material was austenitized at 1100°C for 2 hours, quenched in oil and then tempered at 700°C for 6 hours. Typical micrographs of the obtained martensitic structure, both in the as quenched condition and after tempering, are shown in Fig. 59.

A fine dispersion of elliptical-shaped particles ($\sim 400 \text{ \AA}$ size) were obtained after tempering as shown in Fig. 60. The observations of Fig. 60 are consistent with the detailed investigation of Smith and Nutting (1957) on the tempering of low-alloy steels.

The quench-tempered material was fatigued at a constant strain amplitude, $\frac{\Delta \epsilon}{2} = 0.008$, under the same

TABLE 10

CHEMICAL COMPOSITION OF V-STEEL

C	V	Mn	P	Si
0.22	0.8	0.6	0.002	0.25

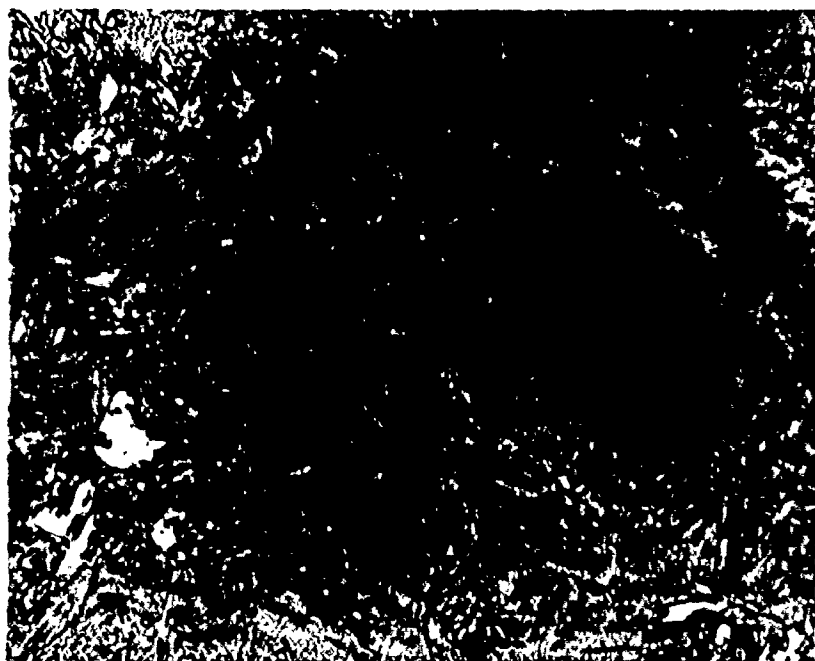
TABLE 11

MECHANICAL PROPERTIES OF Q-TEMP. V-STEEL

σ_Y $\times 10^{-3}$ psi	σ_U $\times 10^{-3}$ psi	σ'_F $\times 10^{-3}$ psi	σ'_F/σ_U
108	126	94	0.75

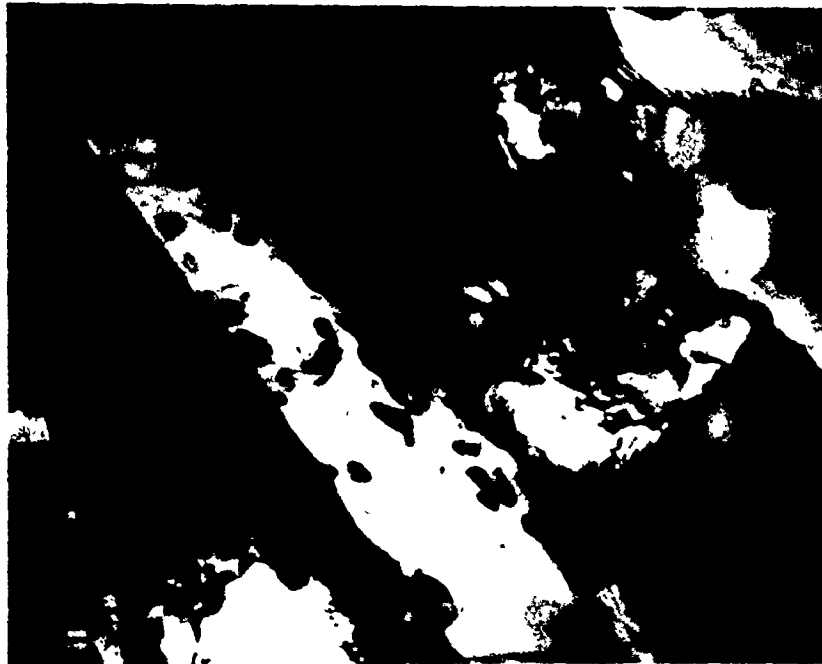


(a) As-Quenched ($x = 750$)



(b) Quenched-Tempered ($x = 100$)

Fig. 59: Optical micrographs of the martensitic structure
in Vanadium-steel: (a) as-quenched
(b) quenched-tempered



0.25 μ

Fig. 60: Transmission electron micrograph of quenched-tempered V-steel

conditions described in Section (4.2) of Chapter IV. Some specimens were also tested in tension and the obtained results are given in Table 11.

Figure 61 shows the fatigue response in Q-Temp. V-steel. It can be seen that the cyclic behaviour is associated with relatively small amount of softening (less than 10% decrease in the initial flow stress). The $\frac{\sigma_F}{\sigma_U}$ ratio is ~ 0.75 .

Two salient results emerge from a comparison of the cyclic behaviour in both Q-Temp. V-steel and Q-A (25°C) Armco iron (Fig. 44): firstly, the fatigue response in Q-Temp. V-steel is associated with lower rate of softening and higher $\frac{\sigma_F}{\sigma_U}$ ratio compared to that in Q-A (25°C) Armco iron. Secondly, the fatigue life in Q-Temp. V-steel is shorter than that in Q-A (25°C) Armco iron.

The microstructure after fatigue showed no evidence of localized slip bands as can be seen from the micrographs of Fig. 62. However, the fracture surface produced clear evidence of intergranular cracks as illustrated in Fig. 63. The formation of these intergranular cracks may be the cause for the observed low fatigue life in quenched-tempered Vanadium steel.

Rollason (1961) has pointed out that tempered alloy steels may suffer from the phenomena of temper brittleness, possibly due to the segregation of solute atoms on grain boundaries.

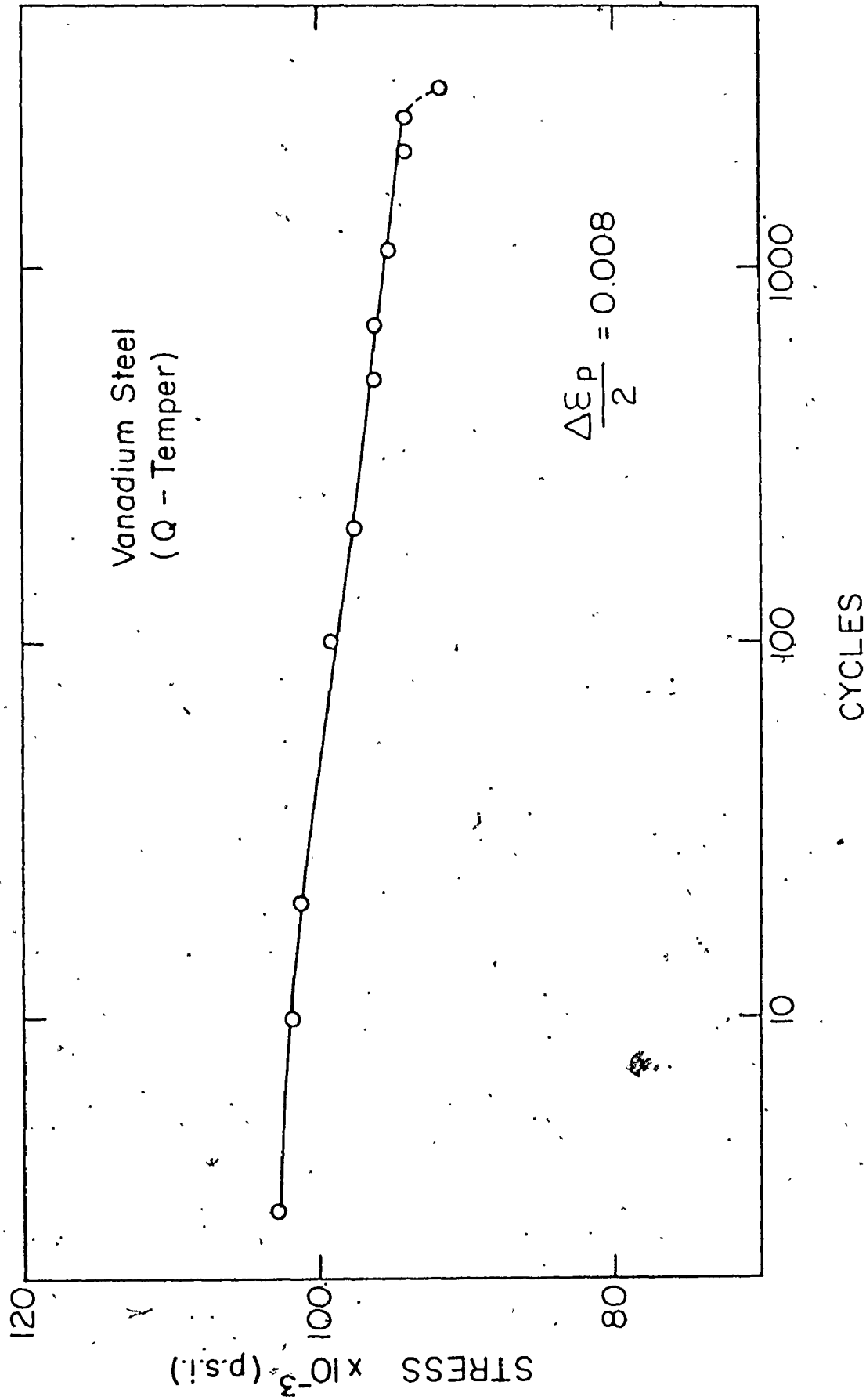
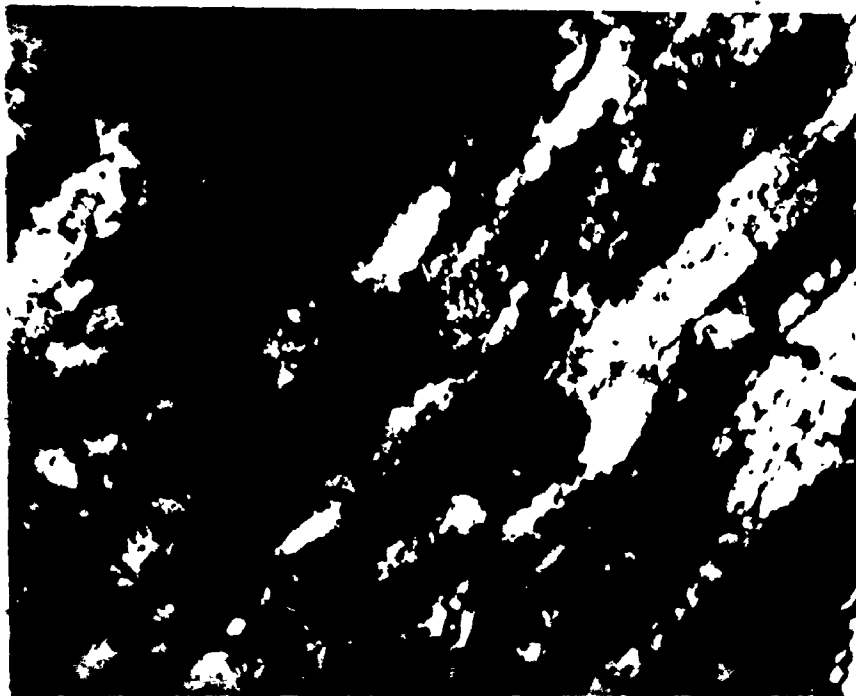
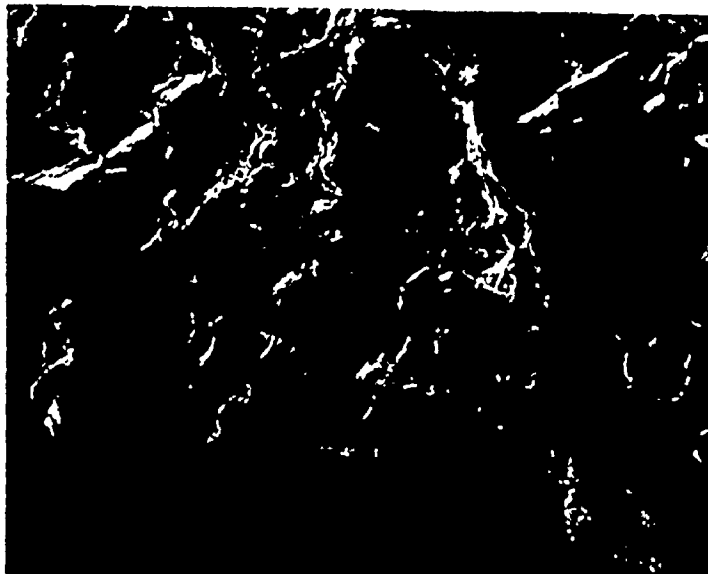


Fig. 61: Cyclic response in Q-Tempered Vanadium-steel

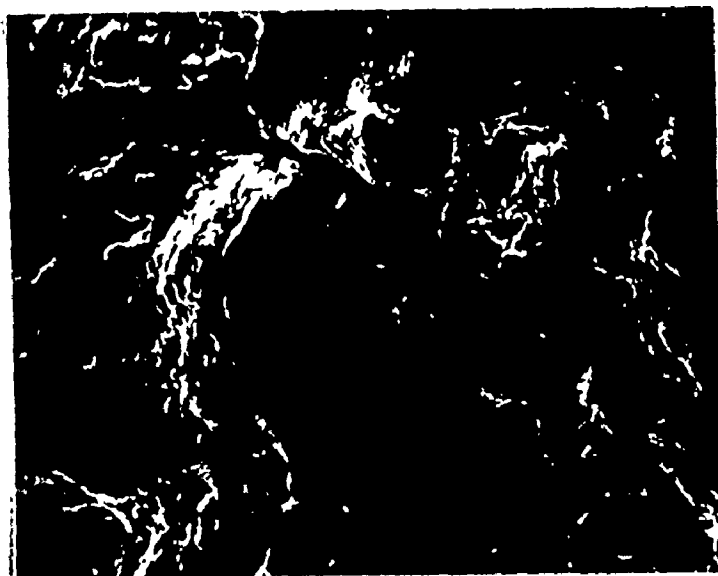


x = 30000

Fig. 62: Fatigued structure in quenched-tempered
V-steel



$x = 100$



$x = 500$

Fig. 63: Fatigue fracture surface of quenched-tempered V-steel

Two salient results emerge from the above experiment: firstly, it is possible to suppress particle dissolution and inhibit fatigue softening by utilizing a fine dispersion of stable alloy carbides in steel, and secondly, in tempered alloy steels, sacrifice in fatigue life may occur as a result of grain boundary embrittlement.

APPENDIX B

SATURATION AND SUBSEQUENT HARDENING IN POLYCRYSTALS SUBJECTED TO CYCLIC STRAINING

(B.1) Relationship Between Saturation Stress and Cell Size

In the past few years a variety of evidence has been accumulated indicating that, in cyclic deformation conducted at constant plastic strain amplitude, a cell structure is developed, the scale of which is uniquely determined by the temperature of deformation and the strain amplitude. It should be noted that in single crystals deformed at low strain amplitudes the dislocation structures are not clearly defined cell structures (Watt 1967) and the only structural feature of well defined size is the ladder structure of the persistent slip bands, the scale of which is essentially independent of strain amplitude. Thus let us consider the more general case of polycrystals fatigued at constant plastic strain amplitude for single-phase fcc materials.

Feltner and Laird (1967) have found that the saturation stress (σ_S) can be related to the plastic strain amplitude ($\frac{\Delta \epsilon_p}{2}$) through a power relationship of the form*

$$\sigma_S = \sigma_C \left(\frac{\Delta \epsilon_p}{2} \right)^n \quad (1)$$

* In the present investigation a similar relationship was found for decarburised iron, (Section (4.4) of Chapter III).

where σ_c = strength coefficient and n = cyclic hardening exponent.

On the other hand, Pratt (1967) has found an inverse relationship between saturation stress and cell size (L) for copper polycrystals, i.e.,

$$\sigma_s = \lambda \left(\frac{1}{L} \right) \quad (2)$$

where λ is a constant. Thus from Eqs. (1) and (2) we can write

$$\left(\frac{\Delta \epsilon_p}{2} \right) = \beta (L)^{-\alpha} \quad (3)$$

where α and β are constants which depend on material and testing conditions (temperature and cyclic frequency). Thus

$$\log \left(\frac{\Delta \epsilon_p}{2} \right) = \log \beta - \alpha \log (L) \quad (4)$$

Equation (4) predicts that at constant temperature and frequency, the cell size at saturation is linear with the strain amplitude on a log-log plot.

It is difficult to explain the temperature dependence of the cell size because the temperature dependence of the cyclic flow stress (Broom and Ham 1957) suggested that many of the obstacles produced in fatigue are short range in character (i.e., point defects). However, the basic

prediction can be compared with existing data in the literature for fcc copper and also for the data obtained in the present investigation for decarburised iron. As shown in Fig. 64 the prediction is in good agreement with the data.

It should be emphasized that in fcc materials, the saturation period extends until near fracture. However, in ferrous systems there is the added complication that under many conditions the system exhibits subsequent hardening after the attainment of saturation. This problem is rationalized in the following section.

(B.2) Subsequent Hardening in Decarburised Iron

Subsequent hardening in ferrous systems is an important phenomena because it occupies over 70% of the fatigue life. Unfortunately, no quantitative study has yet been performed to fully elucidate such phenomena and, at present, ideas are speculative in nature and limited to the concept of a "dynamic strain ageing" effect. However, McGrath and Bratina (1969) have observed a subsequent hardening behaviour in an Fe-0.25% Zr alloy in which the zirconium acts as a getter for interstitials reducing considerably their concentration in the ferrite matrix. Also, in the present study, decarburised iron showed a subsequent hardening behaviour as illustrated in Fig. 65.

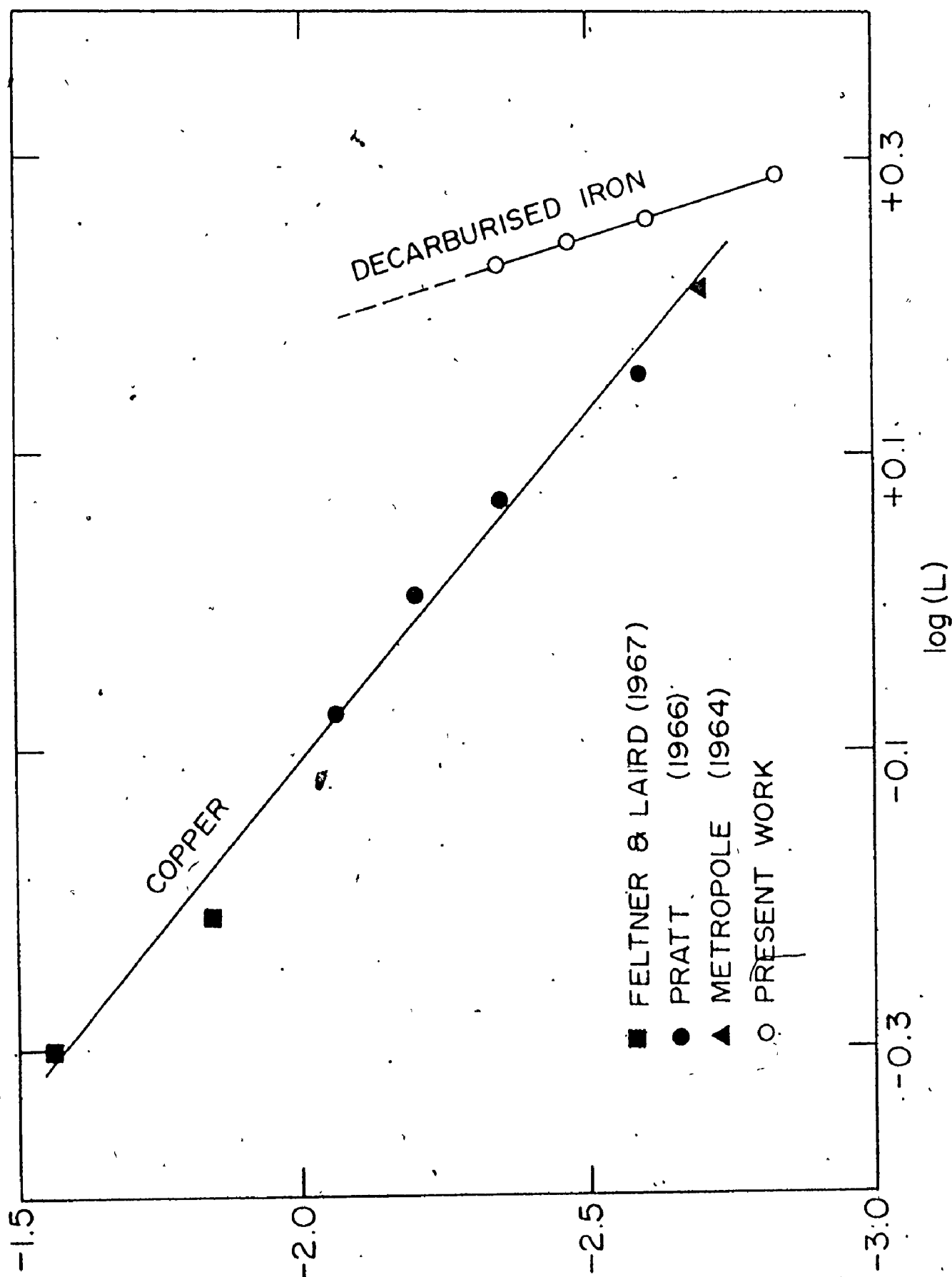


Fig. 64: Relationship between plastic strain amplitude ($\Delta\epsilon_p/2$) and cell size at saturation for Copper and decarburised iron

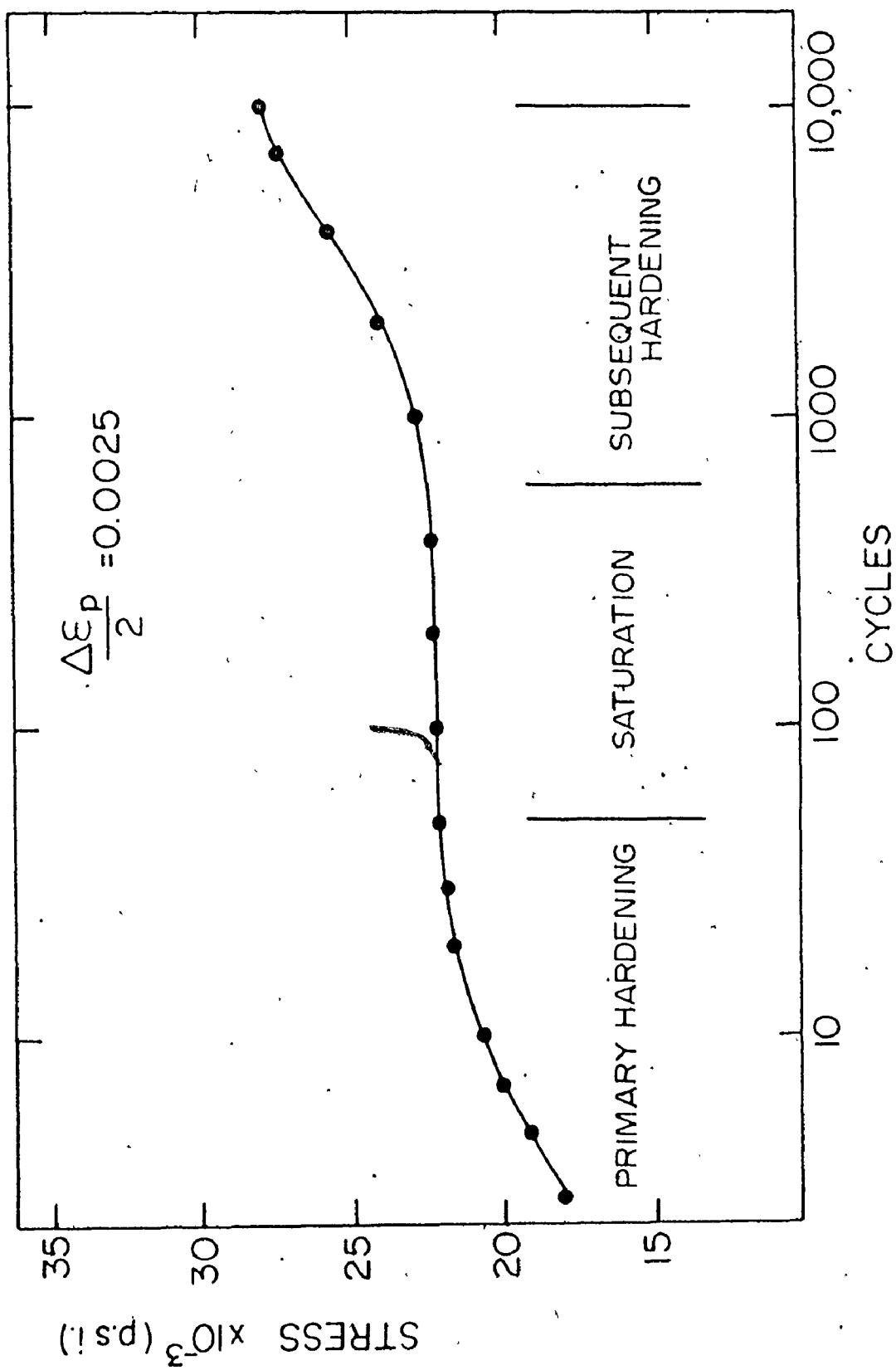


Fig. 65: Fatigue hardening in decarburised iron at room temperature

Thus, it is unlikely that such behaviour is simply due to a conventional dynamic strain-ageing effect in which hardening is enhanced by interaction between dislocations and solute atoms.

However, it should be recognized that subsequent hardening is a period preceeded by saturation and followed by fracture. On this basis, a more quantified view should take cognition of both processes preceeding and following this period of subsequent hardening.

A simplistic view would be that if work hardening resumes plastic flow - after saturation - then deformation should become more homogeneous and thus the tendency to form persistent slip bands and fracture nuclei should decrease. However, it is apparent from both results obtained in the present study and from data in the literature that persistent slip bands still grow during the period of subsequent hardening and result in fracture. By reference to Fig. 66, it can be seen from changes in frequency (ν) that, during the subsequent hardening period the rate of hardening decreases with increasing strain rate. This is a dynamic instability analogous to that discussed in Section (4) of Chapter IV in which the strain tends to become inhomogeneously concentrated into high strain regions.

Thus, let us first examine from a microstructural viewpoint changes occurring during subsequent hardening in decarburised iron fatigued at room temperature under a cyclic

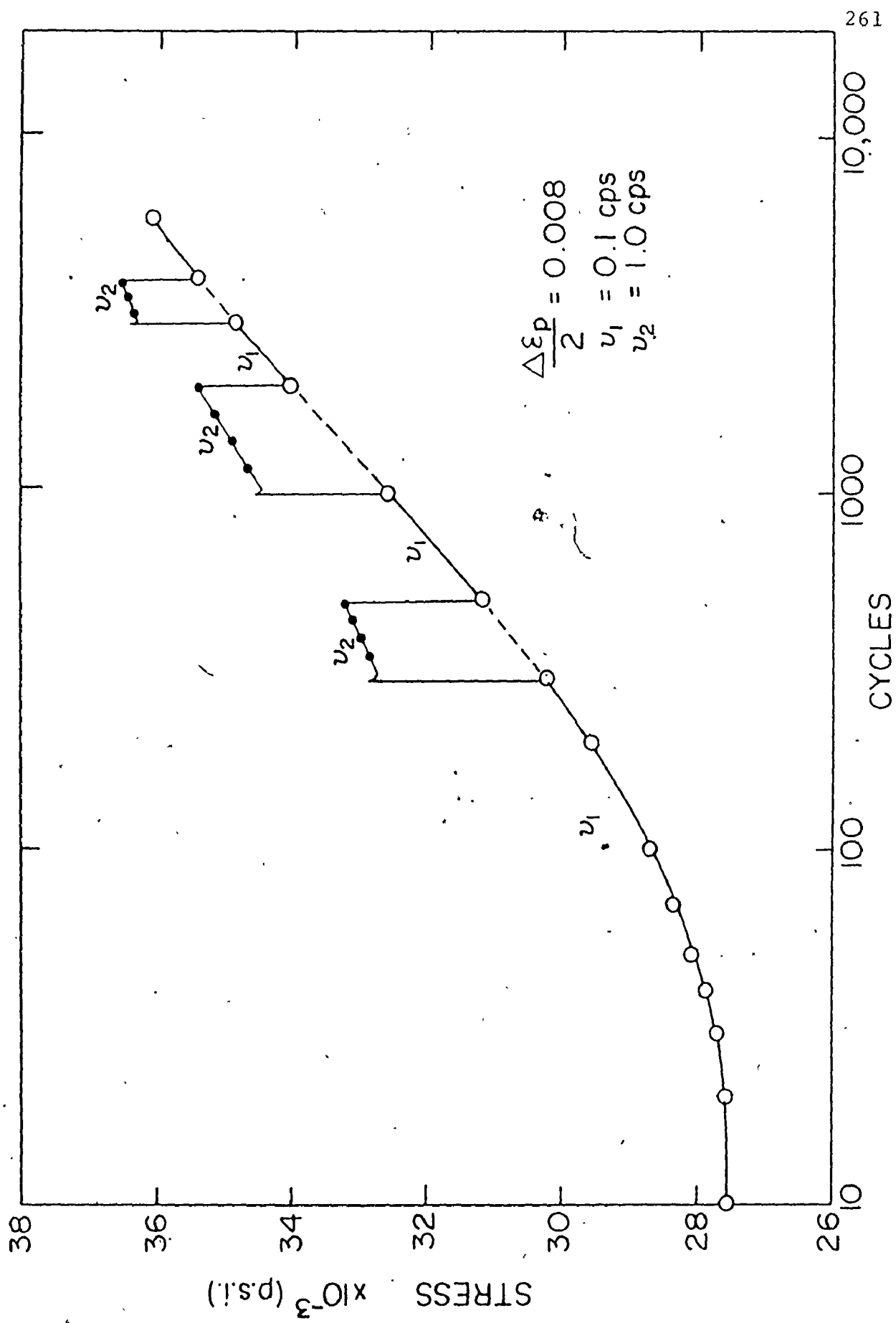


Fig. 66: Effect of strain rate change on subsequent hardening in decarburised iron

strain amplitude of $(\frac{\Delta \epsilon}{2}) = 0.0025$ (Fig. 65). A comparison of the microstructure at saturation to that after 10,000 cycles is shown in Fig. 67. From careful examination of both microstructures the following changes were found: firstly, the average cell size decreased from $\sim 1.8 \mu$ at saturation to $\sim 1.5 \mu$ after 10,000 cycles and, secondly, the average misorientations across cell walls increased from ~ 0.4 of a degree at saturation to ~ 1.1 degrees after 10,000 cycles. It should be emphasised that the maximum increase in misorientations was associated with the walls of the "tidy" regions, i.e., the rectangular-shaped cells.

Let us now estimate approximately the contribution of each of the above microstructural changes to the observed subsequent hardening increment.

Assuming a simple relationship between flow stress (σ) and cell size (L), similar to a Hall-Pitch equation, thus

$$\sigma = \sigma_0 + K_S (L)^{-1/2} \quad (5)$$

where σ_0 is an initial flow stress and K_S is constant. Thus, for a decrease in cell size from L_S at saturation to L_h after 10,000 cycles, the corresponding change in flow stress ($\Delta\sigma$) is

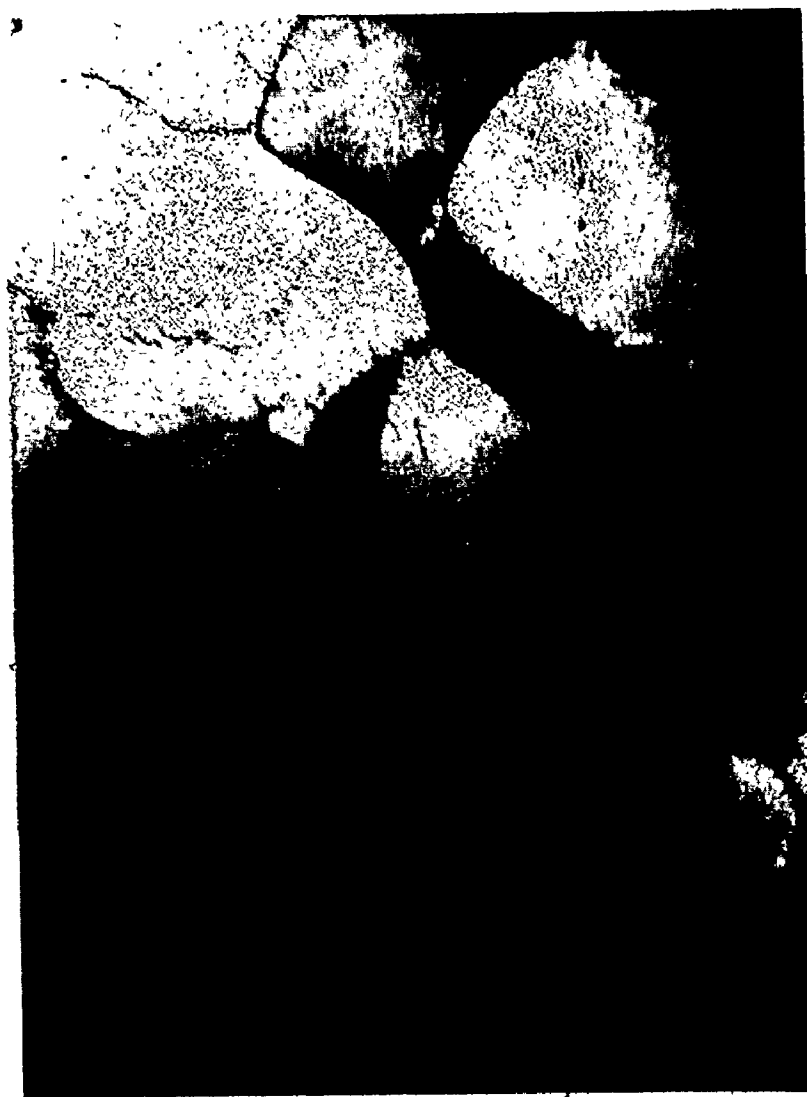


Fig. 67(a): Dislocation structure in decarburised iron
at fatigue saturation

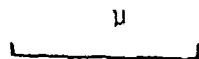


Fig. 67(b): Dislocation structure in decarburised iron
at the subsequent fatigue hardening region
(after 10,000 cycles)

$$\Delta\sigma = (\sigma_S - \sigma_0) [(L_S/L_h)^{1/2} - 1] \quad (6)$$

where σ_S is the saturation stress. Substituting $\sigma_S = 22000$ psi, $L_S = 1.8 \mu$, $L_h = 1.5$ and $\sigma_0 = 14000$ psi in Eq. (6) gives

$$\Delta\sigma \sim 1000 \text{ to } 2000 \text{ psi}$$

which is less than 30% of the observed increase in flow stress (~ 6000 psi) during subsequent hardening (Fig. 65).

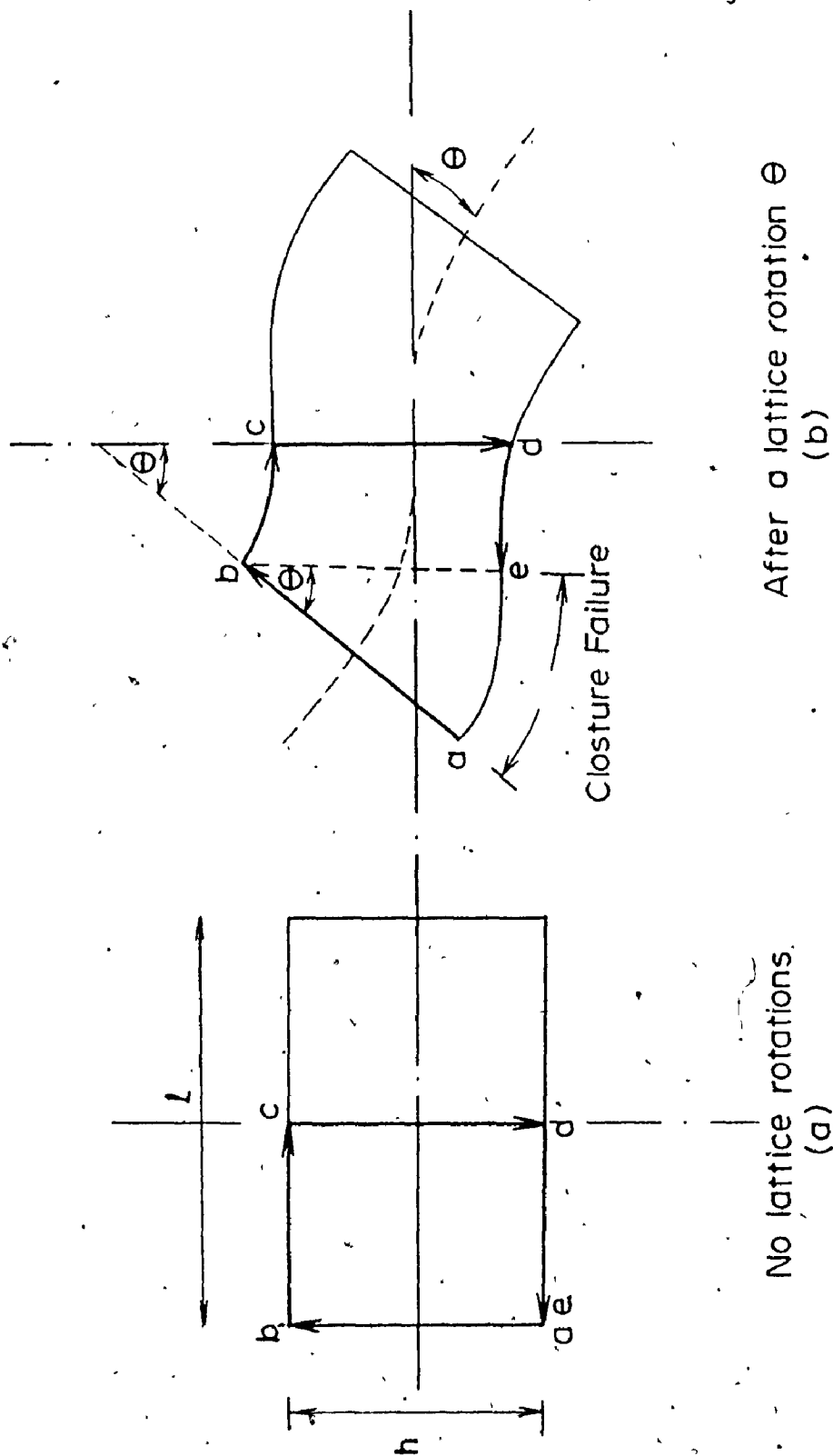
A simple method for calculating increases in flow stress due to lattice rotations is illustrated in Fig. 68 which shows that a lattice rotation (θ) corresponds to an increase in dislocation density $\Delta\rho$ of $2 \frac{\Delta\theta}{Lb}$, where b is the Burgers vector. Thus, the increase in flow stress ($\Delta\sigma_{m.o.}$) as predicted by Ashby (1970) is

$$\Delta\sigma_{m.o.} = \alpha \mu b (\Delta\rho)^{1/2} \quad (7)$$

Substituting for $\Delta\theta = 0.7$ degree $\equiv 0.012$ radians, $L = 1.8 \mu$, $b = 2.8 \text{ \AA}$, $\alpha = 0.3$ and $\mu = 11 \times 10^6$ psi gives

$$\Delta\sigma_{m.o.} \text{ of about } 5000 \text{ psi}$$

i.e., more than 70% of the observed subsequent hardening.



The closure failure $ae = h\Theta$ thus, number of dislocations $= \frac{h\Theta}{b}$ also, area $= \frac{hL}{2}$, thus, the increase in dislocation density ($\Delta\rho$) $= \frac{2\Theta}{Lb}$

Fig. 68: Schematic diagram showing Burgers circuit construction used to calculate $\Delta\rho$ assuming a two-dimensional array of dislocations

Thus, it seems from the above crude estimates that the most important microstructural change during subsequent hardening is the increase in misorientations across the cell walls specially those of the "tidy" regions. This can be rationalized in the following way.

Although it is usually recognized during saturation that the imposed strain amplitude is fully reversible (i.e., no accumulation of strain in the material), the situation is likely to be different when localization of plastic flow occurs. As shown in Chapter IV, the onset of localization of plastic flow takes place at saturation where no hardening is observed macroscopically. Thus as cyclic deformation continues after saturation, a process of partitioning the imposed strain amplitude takes place in the material. The important point to emphasise is that the process of strain partitioning may lead to an increasing irreversibility of the imposed strain amplitude. A confirmation for this was obtained by following the shape of hysteresis loops during and after saturation. It was observed that the loops were symmetrical at saturation (i.e., mean strain = 0), however, as cycling proceeded the loops became progressively asymmetrical with respect to axis of zero strain (i.e., mean strain $\neq 0$).

Thus, it is possible during subsequent hardening that a net accumulation of strain occurs progressively in the

material as a result of an irreversible component of the imposed strain amplitude, leading to the observed hardening behaviour. Also, because of the localized nature of the deformation process, most of the accumulating strain will be concentrated in active slip bands. This may explain the observed higher misorientations at the "tidy" regions which were suggested (Section (3) of Chapter IV) as potential sites for the localization of plastic flow and consequently nucleation of fatigue cracks. This emphasises the importance of the stability of plastic flow in cyclic deformation and the connection between plastic instability and crack nucleation as demonstrated in Chapter IV.

The above rational provides a critical assessment to the subsequent hardening behaviour in ferrous systems, and emphasises the direct connection between such behaviour and the processes of saturation, localization and fracture in fatigue.

The data indicates that the most significant microstructural change occurring during subsequent hardening in low-carbon iron is the progressive increase in misorientations across the dislocation cell walls specially those associated with the "tidy" regions.

REFERENCES

- Abd El Raouf, H. A. (1972) Ph.D. thesis, University of Waterloo, Waterloo, Canada.
- Abd El Raouf, H. A. and Plumtree A. (1971) Metallurgical Trans. 2, No. 7, 1837.
- Abel, A. (1965) M.Sc. thesis, McMaster University, Hamilton, Canada.
- Abel, A. and Ham, R. K. (1966) Acta Met. 13, 807.
- Ibid., Acta Met. 14, 1495.
- Abel, A. and Muir, H. (1972) Phil. Mag. 26, 585.
- Adamson, R. B. (1967) Trans. AIMME 339, 714.
- Alden, T. H. (1962) J. of Metals 14, 828.
- Argon, A. S. (1973) "The inhomogeneity of plastic deformation" ASM. p. 161.
- Arsenault, R. J. and Lawley, A. (1966) "Work Hardening" Met. Soc. Conf. V. 46, 283.
- Ashby, M. F. (1966) Phil. Mag., 14, 1157; (1970) ibid. (1970) 21, 399.
- Avery, D. H. and Backofen, W. A. (1963) Acta Met. 11, 653.
- Bailey, J. E. (1963) Phil. Mag. 8, 223.
- Baird, J. D. and MacKenzie, C. R. (1964) J. Iron & Steel Inst. 202, 427.
- Barnby, J. T. (1972) "Fatigue", M & B technical library TL/ME/4.

Bauschinger, J. (1881) J. Civil Eng. N.F. 27, 289.

Bazinski, Z. S. and Christian, J. W. (1960) Aust. J.

Physics 13, 299.

Bowden, P. B. (1970) Phil. Mag. 22, 455.

Boyd, J. D. and Hoagland, G. (1972) Titanium Science and
Technology 2 (ed. Jaffee, R. I. and Burtle, H. M.)
New York (1972).

Broom, T. and Ham, R. K. (1957) Proc. Roy. Soc. A242, 116.

Broom, T. and Ham, R. K. (1962) Phil. Mag. 7, 95.

Broom, T., Mazza, J. A. and Whittaker (1957) J. Inst.

Metals 86, 17.

Brown, L. M. and Stobbs, W. M. (1971) Phil. Mag. 23,

no. 185, 1185.

Brown, L. M. and Stobbs, W. M. (1971) Phil. Mag. 23,

no. 185, 1201.

Brown, M. J. and Embury, J. D. (1972) Acta Met. 20, 627.

Buckley, S. N. and Entwistle, K. M. (1956) Acta Met. 4,

352.

Christian, J. W. (1970) Second Int. Conf. on the Strength

of Metals and Alloys (ASM) 1, 31.



Civallero, M., Parrini, C. and Pizzimenti, A. (1973)

"Research and Development into pipe steels and pipe
Manufacture", Symposium on Development in Gas
pipeline Technology, Melbourne, Australia.

Clarebrough, L. M., Hargreaves, M. E., West, G. W. and

Hea A. K. (1957) Proc. Roy. Soc. A242, 160.

- Clark, J. B. and McEvily, A. J. (1964) Acta Met. 12, 1359.
- Coffin, L. F. and Read, J. H. (1956) Int. Conf. on fatigue of Metals, London, England.
- Coffin, L. F. (1967) Trans. of ASM Quart. 60, 160.
- Dijkstra, L. J. (1949) J. Metals 1, 252.
- Edington, J. W. and Smallman, R. F. (1964) Acta Met. 12, 1313.
- Edwards, E. H. and Washburn, T. (1956) J. Metals 200, 1239.
- Embury, J. D. (1971) "Strengthening methods in Crystals" (Elsevier, ed. Kelly, A. and Nicholson, R. B.) 348.
- Feltner, C. E. (1965) Phil. Mag. 12, 1229.
- Feltner, C. E. and Laird, C. (1969) Trans. AIME 245, 1372.
- Feltner, C. E. and Laird, C. (1967) Acta Met. 15, 1621; ibid. 15, 1633.
- Fisher, J. C., Hart, E. W. and Pry, R. H. (1953) Acta Met. 1, 336.
- Forsyth, P. J. and Stubbington, C. A. (1961) J. Inst. Metals 90, 347.
- Frost, N. E. and Dugdale, D. S. (1958) J. Mechs. and Phys. of Solids 6, 92.
- Gladman, T., Holmien, B. and McIvor, I. D. (1971) Proceedings of the Iron and Steel Institute, London, p. 68.
- Greenough, G. B. (1952) Progress in Metal Phys. 3, 176 (Pergamon Press, London).
- Hahn, G. T., Hoagland, R. G. and Rosenfield, A. R. (1971) "Local Yielding Attending Fatigue Crack Growth" Technical Report AFML.

- Halford, G. R. (1966) Ph.D. thesis, University of Illinois, Urbana, Illinois.
- Ham, R. K. and Broom, T. (1962) Phil. Mag. 1, 95.
- Hargreaves, M. E., Lorentto, M. H., Clarberough, L. M. and Segal, R. L. (1963) "The Relation Between the Structure and Mechanical Properties of Metals", National Physics Lab., p. 209. 
- Harrison, C. T., Weiner, R. T. and Fearnough, G. D. (1972) J.I.S.I., p. 334.
- Hirsh, P. B. (1957) J. Inst. Metals 86, 7.
- Hirsh, P. B. (1963) "The Relation Between The Structure and Mechanical Properties of Metals", National Physics Lab., p. 39, Symposium No. 15.
- Hirsh, P. B., Howie, A., Nicholson, R. B., Pashley, D. W. and Whelan, M. J. (1965) Electron Microscopy of "Thin Crystals", London, p. 522.
- Holloman, J. H. (1946) Metals Technology, T.P. 2034.
- Huggard, D. (1970) M.Sc. thesis, McMaster University, Hamilton, Canada.
- Jamieson, R. M. and Hood, J. E. (1971) J.I.S.I. 209, 46.
- Jäniche, W., Stolte, E. and Kägler, J. (1965) Tech. Mitt. Krupp, Forschungsber 23, (4), 117.
- Johnson, L. G. (1964) "The Statistical Treatment of Fatigue Experiments".
- Keh, A. S. and Nakada, Y. (1967) Can. J. Phys. 45, 1101.
- Keh, A. S., Nakada, Y. and Leslis, W. C. (1968) "Dislocation Dynamics", McGraw-Hill, p. 381.
- 

- Keh, A. S. and Weissmann, S. (1963) "Electron Microscopy and Strength of Crystals" (ed. Thomas, G. and Washburn, J.) p. 231.
- Kelly, A. and Nicholson, R. B. (1963) Progress in Materials Science 10.
- Kemsley, D. S. (1958) J. Inst. Met. 87, 10.
- Kishi, J. and Gokya, I. (1973) Met. Trans. 4, 391.
- Klesnil, M. and Lukas, P. (1965) J. Iron and Steel Inst. 203, 1043.
- Kocks, U. F., Chen, H. S., Rigney, D. A. and Schaefer, R. J. (1966) "Work Hardening", Metallurgical Society Conf. Vol. 46, p. 151. (ed. Hirth, J. P. and Weertman, J.).
- Kumakura, S. (1968) Bulletin of JSME 11, (45), 926.
- Laufer, E. (1969) Czec. J. of Physics 19, 333.
- Laufer, E. and Roberts, W. N. (1966) Phil. Mag. 14, 65.
- Leslie, W. C., Michalak, J. T. and Aul, F. W. (1961) "Iron and its dilute solutions" (Interscience - New York, p. 119).
- Li, J. C. (1963) The J. Australian Inst. of Metals 8, 206.
- Lifshitz, I. M. and Sloyozov, V. V. (1961) J. Phys. Chem. of Solids 19, 35.
- Low, J. R. (1969) Trans. AIME 245, 2481.
- May, A. N. (1960) Nature (London) 185, 303.
- McClintock, F. A. (1963) Fracture in Solids (ed. Drucker and Gilman, Gordon and Breach, New York) p. 69.
- McClintock, F. A. and Argon, A. S. (1966) Mechanical Behaviour of Metals (Addison-Wesley) p. 185.

- McGrath, J. T. and Bratina, W. J. (1967) Acta Met. 15, 329.
- McGrath, J. T. and Bratina, W. J. (1969) Czec. J. Phys.
B19, 284.
- McGrath, J. T. and Bratina, W. J. (1965) Phil. Mag. 12, 1293.
- McLean, D. (1962) Mechanical Properties of Metals (John Wiley
& Sons, Inc.) p. 164.
- McMahon, C. J. (1966) Acta Met. 14, 839.
- Milligan, R. V. et al. (1966) Trans. ASME 88, No. 2, 480.
- Mintz, B. and Wilson, D. V. (1965) Acta Met. 13, 947.
- Morrow, J. (1965) ASTM, Spec. Techn. Publ. No. 378, p. 45.
- Mukherjee, T., Stumpf, W. E., Sellars, C. M. and Tegart, W. J.
(1969) J.I.S.I. 207, (5), 621.
- Nabarro, F. R., Basinski, Z. S. and Holt, D. B. (1964) Adv.
Phys. 13, 193.
- Ono, K. and Meshii, M. (1966) "Work Hardening" (ed. Hirth,
J. P. and Weertman, J., Gordon and Breach, New York)
p. 227.
- Orava, R. N., Lawley, A. and Conrad, H. V. (1968) Trans.
J.I.M. 19, 489.
- Orowan, E. (1959) Internal Stresses and Fatigue in Metals
(Elsevier) p. 59.
- Papzian, J. M. and Beshers, D. N. (1971) Met. Trans. 2, 497.
- Polakowski, N. H. (1951) J.I.S.I. 169, 337.
- Pratt, J. E. (1967) Acta Met. 15, 319.
- Rice, J. R. (1967) "Fatigue Crack Propagation" ASTM, S.T.P.,
No. 415, p. 301.

- Rollason, E. C. (1961) Metallurgy of Engineers (Edward Arnold, London).
- Sargent, C. M. and Purdy, G. (1974) Scripta Met. 8, 569.
- Schankula, M. H. (1970) Ph.D. thesis, McMaster University, Hamilton, Canada.
- Shewmon, P. G. (1969) "Transformations in Metals" (McGraw-Hill Book Co.) p. 251.
- Shinozaki, D. and Embury, J. D. (1969) Metal Sc. J. 3, 147.
- Simon, J., Caisso, J., Guillot, J. and Violan, P. (1964) Mem. Sci. Rev. Met. 61, 841.
- Sleeswyk, A. (1958) Acta Met. 6, 598.
- Smith, E. and Nutting, J. (1967) J. Iron & Steel Inst. 187, 314.
- Steeds, J. W. (1966) Proc. Roy. Soc. 292, 343.
- Stobbs, W. M., Watt, D. F. and Brown, L. M. (1972) Phil. Mag. 23, 1169.
- Stubbington and Forsyth (1966) Acta Met. 14, 5.
- Stoltz, R. E. and Pelloux, R. M. (1974) Scripta Met. 8, 269.
- Stroh, A. N. (1956) Phil. Mag. 1, 489.
- Tanaka, K. and Mori, T. (1970) Acta Met. 18, 931.
- Taylor, G. and Christian, J. W. (1967) Phil. Mag. 15, 893.
- Tetelman, A. S. and McEvily, A. J. (1967) Fracture of Structure Materials (Wiley & Sons) p. 348.
- Wadsworth, N. J. and Hutchings, J. (1964) Phil. Mag. 10, 195.
- Watt, D. F. (1967) Ph.D. thesis, McMaster University, Hamilton, Canada.

- Wei, R. P. and Baker, A. J. (1965) Phil. Mag. 12, 1005.
- Wilcox, B. A. and Rosenfield, A. R. (1966) Mat. Sci. & Eng. 1, 201.
- Wilson, D. V. (1965) Acta Met. 13, 807.
- Wilson, D. V. (1973) Proceedings of the Third International Conference on Strength of Metals and Alloys, Vol. 1, Cambridge, England.
- Wilson, D. V. and Konnan, Y. A. (1964) Acta Met. 12, 612.
- Wilson, D. V. and Mintz, B. (1972) Acta Met. 20, 985.
- Wilson, D. V. and Tromans, J. K. (1970) Acta Met. 18, 1197.
- Woolley, R. L. (1953) Phil. Mag. 44, 597.
- Wood, W. A. (1962-63) J. Inst. Met. 91, 193.